CHAPTER 1

The Liquid Drop Model

1.1 Introduction

The liquid drop model (LDM) of the nucleus was historically the first model to be proposed as an explanation of the different properties of the nucleus. Since it has regained interest in recent times, we begin with a short outline of this phenomenological model. Some aspects of this model will be taken up in the course of the book and explained from a more microscopic point of view. In this chapter we follow to a large extent the standard representation as given in the texts of, for example, J. A. Eisenberg and W. Greiner [EG 70], A. de Shalit and H. Feshbach [SF 74], and A. Bohr and B. R. Mottelson [BM 75].

The idea of considering the nucleus as a liquid drop originally came from considerations about its saturation properties (see below) and from the fact that the nucleus has a very low compressibility and a well defined surface. However, as we shall see, it is misleading to take this point of view too seriously, since in other respects a nucleus does not bear very much resemblance to an ordinary liquid. For instance, the mean distance of two particles in a liquid is roughly given by the value at which the interparticle force has its minimum value, which for nuclei would be $\sim$0.7 fm. However, nucleons in nuclei are, on the average, $\sim$2.4 fm apart. One reason for this big difference as compared with an ordinary liquid is that the nucleons obey Fermi statistics and a nucleus is thus a quantum fluid. The Pauli principle prevents the nucleons from coming too close to one another. Thus scattering events are very scarce in a quantum fluid, whereas in an ordinary fluid they are predominant.

Consequently, the mean free path of the nucleons inside a ground-state (or moderately excited state) nucleus is of the order of the nuclear dimension and resembles, therefore, apart from the statistics, a non-interacting gas. This fact has some drastic consequences that are absent in droplets of ordinary fluids. For instance, we want to mention that in a vibrating nuclear drop [e.g., (dynamical) quadrupole deformations] the momentum distribution of the nucleons may be influenced by the deformations; i.e., it can be anisotropic, whereas the velocity distribution in an ordinary fluid drop is always isotropic. These peculiarities of a quantum drop will be treated in more detail in Chapter 13. Here, instead, we shall follow the historical development of the LDM idea, since it is very useful in describing overall properties of the nucleus and in introducing many concepts of collective phenomena in nuclear physics in a simple way. This is the main purpose of the first chapter, where we will not bother about the specific differences between an ordinary liquid drop and a quantum drop.

1.2 The Semi-empirical Mass Formula

One quantity that should, according to the discussions above, vary only smoothly with mass number is the binding energy per particle. In fact, the total binding energy $B(Z,N)$, where N and Z are the number of neutrons and protons, respectively, grows with the number of nucleons, A, in such a way that the binding energy per particle $B(N,Z)/A$ stays fairly constant for nuclei with more than twelve nucleons:

$$\left.\frac{B(N,Z)}{A}\right|_{A>12} \simeq -8.5\ [\mathrm{MeV/nucleon}]. \tag{1.1}$$

The explanation for the binding energy per nucleon being approximately constant can be given in the following qualitative way: If the binding of a system of A particles comes from the interaction energy of all possible two-particle pair combinations, then the total binding energy should grow roughly like the number of all possible pairs, namely as $\frac{1}{2}\cdot A\cdot(A-1)$. The binding energy per particle should then be proportional to A. This is the case, for example, for the binding energies of the electrons in an atom.

The completely different behavior of the nuclear binding energy can be attributed to the saturation property of the nuclear forces: one nucleon in the nucleus interacts with only a limited number of nucleons. This has its origin in the short-range nuclear force and the combined effect of the Pauli and uncertainty principles: The total binding energy is a subtle difference effect between the total kinetic energy and the total potential energy; whereas due to the Pauli and uncertainty principles and the hard core [Br 65a], the kinetic energy rises steeply to positive values at decreasing nucleon distances [BM 69, p. 252] (see Fig. 1.1), and the potential energy is lowered to more and more negative energies. For small enough ($d\lesssim 2$ fm) internucleon distances the kinetic energy takes over so that the total

binding energy becomes positive, whereas for large distances ($d\lesssim 3$ fm), there is hardly any potential energy because of the short-range nucleon–nucleon force. Finally, a shallow minimum develops at around 2.4 fm, which is, compared to the strength of the nuclear forces, quite small. From these considerations it becomes clear why there can be only a limited number of nucleons within the interaction range of one nucleon. In this argument we have not taken into account surface effects and the Coulomb force. They have to be treated separately, as we shall see. Neglecting these effects, we expect that the total binding energy rises linearly with A, as in Eq. (1.1).

The saturation property also explains qualitatively the features found experimentally (by, for instance, electron scattering, μ-mesonic x-rays, etc. [FN 76]), that is, the roughly constant density of nucleons inside the nucleus and the nucleus's relatively sharp surface. Describing the nucleus as a sphere with a constant density and a *sharp* surface, we get for its radius

$$R = r_0 A^{1/3}, \tag{1.2}$$

where the parameter r_0 has empirically the value

$$r_0 = 1.2\ [\mathrm{fm}]. \tag{1.3}$$

In Fig. 1.2, we see the dependence of the binding energy per nucleon on the mass number A in more detail.

Up to about $A=12$, we get a steep rise until $B/A\simeq 8$ MeV; at $A\simeq 60$, we obtain the maximum of a little less than 9 MeV. The binding energy per

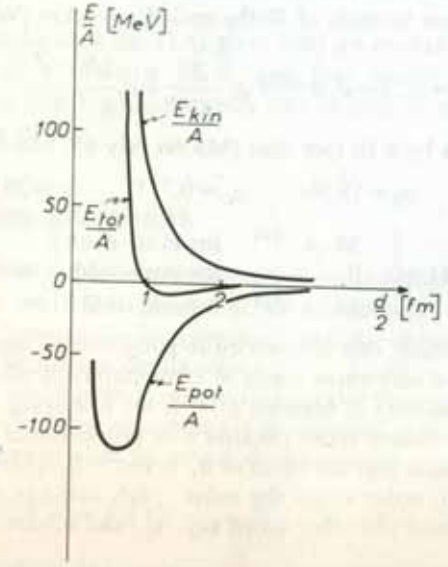

Figure 1.1. Qualitative explanation of nuclear saturation as a subtle difference effect of E_{kin} and E_{pot}.

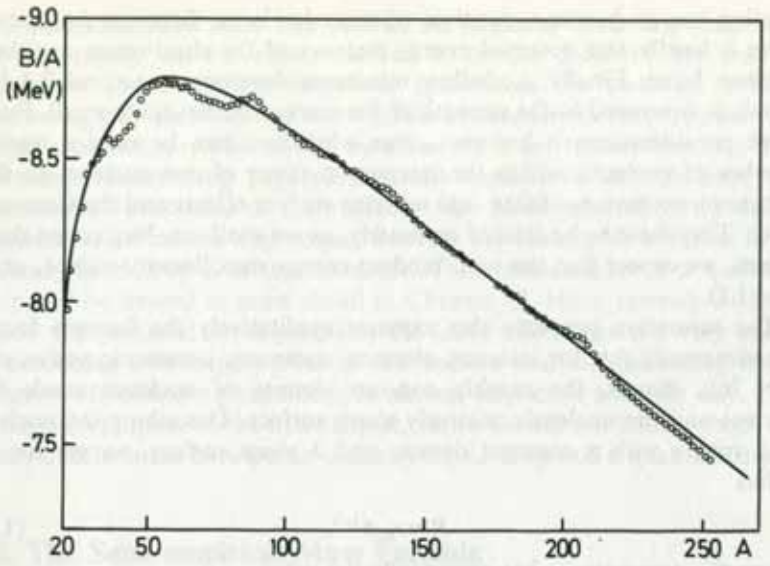

Figure 1.2. Experimental values of B/A for β-stable odd-$A(o)$ nuclei and the calculated curve using a mass formula similar to Eq. (1.4). (From [Ho 75].)

nucleon then drops slightly until at $A=250$ it is about 7.5 [MeV]. This is due to the increasing influence of the Coulomb repulsion of the protons.

There have been many attempts to reproduce the behavior of B/A as a function of N and Z. The best known formula of this kind is the semi-empirical mass formula of Bethe and Weizsäcker [We 35, BB 36]

$$B(N,Z)=a_V A+a_S A^{2/3}+a_C\frac{Z^2}{A^{1/3}}+a_I\frac{(N-Z)^2}{A}-\delta(A), \qquad (1.4)$$

where one obtains by a fit (see also [MS 66, My 69, MS 69]):

$$a_V=-15.68; \quad a_S=18.56; \quad a_C=0.717; \quad a_I=28.1 \quad [\text{MeV}]$$

$$\delta(A)=\left\{\begin{array}{ll} 34\cdot A^{-3/4} & \text{for even–even} \\ 0 & \text{for even–odd} \\ -34\cdot A^{-3/4} & \text{for odd–odd} \end{array}\right\} \text{nuclei.} \qquad (1.5)$$

In Fig. 1.2 we see that one obtains quite good overall agreement with the experimental curve with these kinds of semi-empirical mass formulae.

The physical meaning of formula (1.4) is the following. The first term is usually called the *volume term*, because it is proportional to A [$\propto R^3$ with Eq. (1.2)]. The reason that the value of a_V is not -8.5 [MeV] as in Eq. (1.1) is the following. In order to get the value -8.5, one has to average over a wide range of A, and the other terms (a_S, a_C, and a_I) are positive and not negligible.

The second term is proportional to $A^{2/3}$ ($\propto R^2$), and is therefore called the *surface term*. It results from the fact that the nucleons close to the surface contribute less to the total binding energy. One can calculate from

the parameter a_S a surface tension coefficient σ defined as the surface energy per unit area, and get with Eq. (1.3):

$$\sigma=\frac{a_S}{4\pi r_0^2}=1.03\ [\text{MeV}\cdot\text{fm}^{-2}]. \qquad (1.6)$$

The third term takes into account the Coulomb repulsion of the protons. It can be calculated approximately by assuming the charges to be uniformly distributed over a sphere. The *Coulomb energy* of such a system is proportional to the number of proton pairs ($\propto Z^2$) and inversely proportional to the radius.

Since the protons repel one another, it would be energetically more favorable for a nucleus to have only neutrons—if there were no Pauli principle. A proton decaying into a neutron must enter a state above the neutron Fermi level (see Chap. 2), which is energetically unfavored. The energy balance of the neutron excess $N-Z$ is taken care of in the fourth term of Eq. (1.4), the so-called *symmetry energy*. It cannot depend on the sign of $N-Z$. In the Fermi gas model [SF 74, p. 127 f], one can show that it is proportional to $(N-Z)^2/A$. The quadratic dependence of the binding energy on the proton–neutron mass difference is experimentally very well confirmed. Only the base of the experimental parabola is different according to whether we are considering an even–even, even–odd or odd–odd nucleus. This is due to the so-called *pairing effect*, as we shall see in Chapter 6, and is taken care of by the last term in Eq. (1.4).

Some aspects of the semi-empirical mass formula will be discussed again in Chapter 13 in the context of the Thomas–Fermi approach to nuclear physics.

It should be noted that Eq. (1.4) gives only an overall smooth fit to the binding energy as a function of A, and that locally there are strong deviations from it (see Fig. 2.2), mostly due to shell effects, which will be discussed in Section 2.9.

1.3 Deformation Parameters

Up to now, we have only studied static properties of the liquid drop model. In the following, we will assume that the nucleus has a sharp surface* which must not necessarily be spherical, and we imagine it to undergo dynamical shape or surface oscillations.

Before we can investigate these oscillations, we have to parametrize the surface in some way. One possibility is to describe it by the length of the radius vector pointing from the origin to the surface

$$R=R(\theta,\phi)=R_0\left(1+\alpha_{00}+\sum_{\lambda=1}^{\infty}\sum_{\mu=-\lambda}^{\lambda}\alpha_{\lambda\mu}^{*}Y_{\lambda\mu}(\theta,\phi)\right) \qquad (1.7)$$

where R_0 is the radius of the sphere with the same volume. Such a surface

*Myers and Swiatecki [MS 69, 73] have given up this assumption and introduced a refined liquid drop model with a diffuse surface, the so-called "droplet model" [Ni 72].

is certainly not the most general one* but it is widely used and extremely useful for problems of nuclear structure.

The constant α_{00} describes changes of the nuclear volume. Since we know that the incompressibility of the nuclear fluid is rather high, we require that the volume be kept fixed for all deformations as

$$V=\frac{4}{3}\pi R_0^3. \tag{1.8}$$

This defines the constant α_{00}. Up to second order, we get [EG 70]

$$\alpha_{00}=-\frac{1}{4\pi}\sum_{\lambda>1,\,\mu}|\alpha_{\lambda\mu}|^2. \tag{1.9}$$

The term $\lambda=1$ describes mainly (at least for small deformations) a translation of the whole system. The three parameters $\alpha_{1\mu}$ can be fixed by the condition that the origin coincides with the center of mass

$$\int_V \mathbf{r}\, d^3r=0. \tag{1.10}$$

If the expansion (1.7) contains only even values of λ, this is fulfilled automatically. Otherwise $\alpha_{1\mu}$ starts with second order in the $\alpha_{\lambda\mu}$ ($\lambda>2$). Therefore, in the following we omit both α_{00} and $\alpha_{1\mu}$, since we shall restrict our discussion to small deformations.

It is instructive to look at the shapes of lowest multipolarity in the expansion (1.7), as displayed in Fig. (1.3). The deformations corresponding

*For instance, shapes of two separated fragments in the fission process cannot be represented by (1.7), since R is then multivalued.

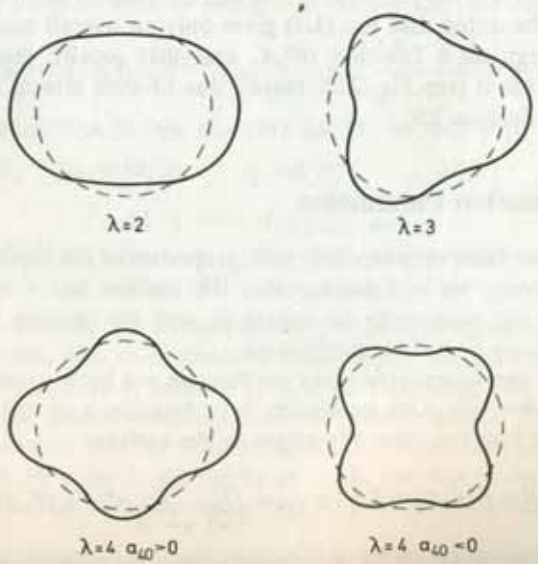

Figure 1.3. Nuclear shapes with quadrupole ($\lambda=2$), octupole ($\lambda=3$), and hexadecupole ($\lambda=4$) deformations.

to $\lambda=2$ look like ellipsoidal deformations. It should be noticed, however, that this is true only up to first order. A pure ellipsoid has non-vanishing $\alpha_{\lambda\mu}$ for all $\lambda\geq 2$.

Another condition on R, and therefore on the parameters $\alpha_{\lambda\mu}$, is the fact that R should be invariant under a reflection of the coordinate system and under a rotation of the coordinate system. In order for this to be the case, the $\alpha_{\lambda\mu}$ must be multiplied by a factor $(-)^\lambda$ under a parity transformation, and must behave like $Y_{\lambda\mu}(\theta,\phi)$ under a rotation of the coordinate system (characterized by the Euler angles $\Omega=(\alpha,\beta,\gamma)$ [Ed 57, Eq. (5.2.1.)]), i.e.,

$$(Y_{\lambda\mu})_{\text{new}}=\sum_{\mu'}D^{\lambda}_{\mu'\mu}(\Omega)(Y_{\lambda\mu'})_{\text{old}}, \tag{1.11}$$

$$a_{\lambda\mu}=\sum_{\mu'}D^{\lambda}_{\mu'\mu}(\Omega)\alpha_{\lambda\mu'},$$

where $D^{\lambda}_{\mu'\mu}(\Omega)$ are the Wigner functions of the rotation and $a_{\lambda\mu}$ are the deformation parameters in the new system.

To make sure that the radius R in Eq. (1.7) is real, we have to use the property $Y^*_{\lambda\mu}=(-)^\mu\cdot Y_{\lambda-\mu}$, and get

$$\alpha^*_{\lambda\mu}=(-)^\mu\alpha_{\lambda-\mu}. \tag{1.12}$$

This will turn out to be the time reversal behavior of the $\alpha_{\lambda\mu}$'s.

Before discussing the surface oscillations of general multipolarity, we mention two special cases:

(i) First are the axially symmetric deformations. Choosing the z-axis as symmetry axis, we find that $\alpha_{\lambda\mu}$ vanishes except when $\mu=0$. The deformation parameters $\alpha_{\lambda 0}$ are usually called β_λ.

(ii) In the case of quadrupole deformations ($\lambda=2$), we have five parameters $\alpha_{\lambda\mu}$. Not all of them describe the shape of the drop. Three determine only the orientation of the drop in space, and correspond to the three Euler angles. By a suitable rotation, we can transform to the body-fixed system characterized by three axes 1, 2, 3, which coincide with the principal axes of the mass distribution of the drop. The five coefficients $\alpha_{2\mu}$ reduce to two real independent variables a_{20} and $a_{22}=a_{2-2}$ ($a_{21}=a_{2-1}=0$), which, together with the three Euler angles, give a complete description of the system. It is convenient to introduce instead of a_{20} and a_{22} the so-called Hill–Wheeler [HW 53] coordinates β,γ ($\beta>0$) through the relation

$$a_{20}=\beta\cdot\cos\gamma,$$
$$a_{22}=\frac{1}{\sqrt{2}}\cdot\beta\cdot\sin\gamma, \tag{1.13}$$

from which we have

$$\sum_{\mu}|\alpha_{2\mu}|^2=a_{20}^2+2a_{22}^2=\beta^2 \tag{1.14}$$

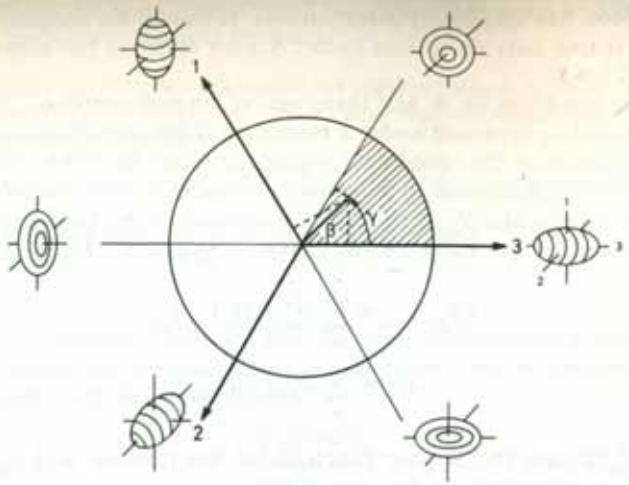

Figure 1.4. Nuclear shapes in the β, γ plane. The projections onto the three axes are proportional to the increments of δR_κ (1.16).

and

$$R(\theta,\phi)=R_0\left\{1+\beta\sqrt{\frac{5}{16\pi}}\left(\cos\gamma(3\cos^2\theta-1)\right.\right.$$
$$\left.\left.+\sqrt{3}\,\sin\gamma\sin^2\theta\cos 2\phi\right)\right\}. \qquad (1.15)$$

In Fig. (1.4) the $\lambda=2$ shapes are represented in the polar coordinates β, γ. We see that

(i) γ values of 0°, 120°, and 240° yield prolate spheroids with the 3, 1 and 2 axes as axes of symmetry;
(ii) $\gamma=180°$, 300°, and 60° lead to the corresponding oblate shapes
(iii) when γ is not a multiple of 60° it corresponds to a triaxial shape;
(iv) there are discrete symmetries, namely, one can interchange all three axes without changing the shape, which means an invariance under the point group D_2. The interval $0<\gamma<60°$ is sufficient to describe all the $\lambda=2$ shapes. All other points in Fig. 1.4 are obtained by suitable exchanges of the different axes.
(v) We can calculate the increments of the three semi-axes in the body-fixed frame as functions of β and γ:

$$\delta R_1=R\left(\frac{\pi}{2},0\right)-R_0=R_0\sqrt{\frac{5}{4\pi}}\;\beta\cos\left(\gamma-\frac{2\pi}{3}\right),$$

$$\delta R_2=R\left(\frac{\pi}{2},\frac{\pi}{2}\right)-R_0=R_0\sqrt{\frac{5}{4\pi}}\;\beta\cos\left(\gamma+\frac{2\pi}{3}\right),$$

$$\delta R_3=R(0,0)-R_0=R_0\sqrt{\frac{5}{4\pi}}\;\beta\cos\gamma,$$

or

$$\delta R_\kappa=R_0\sqrt{\frac{5}{4\pi}}\;\beta\cos\left(\gamma-\frac{2\pi}{3}\kappa\right),\qquad \kappa=1,2,3. \qquad (1.16)$$

We have to remember, however, that the parameters β and γ (with (1.7)) only describe exactly ellipsoidal shapes in the limit of small β-values (see also Eq. 1.88).

1.4 Surface Oscillations About a Spherical Shape

The first kind of excitations are dynamical shape, or surface, oscillations. The dynamical variables are in this case the parameters which describe the surface, i.e., the surface coordinates $\alpha_{\lambda\mu}$ ($\lambda\geqslant 2$) of Eq. (1.7). They are considered to be functions of time: $\alpha_{\lambda\mu}(t)$. For the low-lying excitations one can expect that they produce small oscillations around the spherical equilibrium shape with $\alpha_{\lambda\mu}=0$, and that the classical Hamilton function H_{coll} that describes this process is of a harmonic oscillator form [Bo 52]:

$$H_{\text{coll}}=T+V=\frac{1}{2}\sum_{\lambda,\,\mu}\left\{B_\lambda|\dot\alpha_{\lambda\mu}|^2+C_\lambda|\alpha_{\lambda\mu}|^2\right\}, \qquad (1.17)$$

Here the parameters of inertia B_λ and of stiffness C_λ are real constants. This is, in fact, the only quadratic form which is invariant under rotation and time reversal.*

Following the usual rules of canonical quantization (see for instance, [EG 70, p. 40]), we obtain the quantized form† (see also Appendix C)

$$\hat H_{\text{coll}}=\sum_{\lambda\mu}\hbar\Omega_\lambda\left(B^+_{\lambda\mu}B_{\lambda\mu}+\frac{1}{2}\right) \qquad (1.18)$$

with the frequencies

$$\Omega_\lambda=\left(\frac{C_\lambda}{B_\lambda}\right)^{1/2}. \qquad (1.19)$$

The operators $B_{\lambda\mu}$ obey Bose commutation rules

$$\left[B_{\lambda\mu},B_{\lambda'\mu'}\right]=0;\qquad \left[B_{\lambda\mu},B^+_{\lambda'\mu'}\right]=\delta_{\lambda\lambda'}\delta_{\mu\mu'} \qquad (1.20)$$

and have a corresponding Bose vacuum $|0\rangle$ such that $B_{\lambda\mu}|0\rangle=0$. The Boson operators $B_{\lambda\mu}$ are related to the coordinates $\hat\alpha_{\lambda\mu}$ and corresponding momenta $\hat\pi_{\lambda\mu}$ by

$$\hat\alpha_{\lambda\mu}=\left(\frac{\hbar}{2B_\lambda\Omega_\lambda}\right)^{1/2}\left(B^+_{\lambda\mu}+(-)^\mu B_{\lambda-\mu}\right), \qquad (1.21)$$

$$\hat\pi_{\lambda\mu}=i\left(\frac{\hbar}{2}B_\lambda\Omega_\lambda\right)^{1/2}\left((-)^\mu B^+_{\lambda-\mu}-B_{\lambda\mu}\right).$$

*The time reversal operation is discussed in great detail by Messiah [Me 61] and it is shown that in a system without spin, as we have here, time reversal corresponds to complex conjugation.

†One should not mix up the boson operators $B_{\lambda\mu}$ with the inertia parameters B_λ.

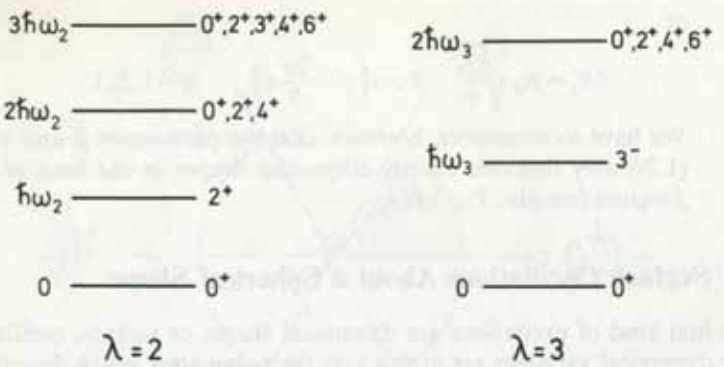

Figure 1.5. Harmonic energy spectra for the quadrupole ($\lambda=2$) and octupole ($\lambda=3$) surface oscillations.

From the above considerations, it follows that for each λ we have a harmonic spectrum of surface vibrations as illustrated in Fig. 1.5.

From the fact that $\alpha_{\lambda\mu}$ and $B^+_{\lambda\mu}$ behave like spherical tensors under rotations of the coordinate system (Eq. (1.11), [Ed 57, Eq. (5.2.1)]) we know the commutation relations of the angular momentum operators with $B^+_{\lambda\mu}$ and find that the one-boson states

$$|\lambda\mu) = B^+_{\lambda\mu}|0) \tag{1.22}$$

have angular momentum $I=\lambda$ and z-component $M=\mu$ with parity $(-)^\lambda$.

To construct multi-boson states we have to use the rules of angular momentum coupling [Ed 57] and also have to take into account that states with more than two bosons are symmetric under the exchange of any two of them. For instance, we get, for the superposition of two quadrupole bosons ($\lambda=2$), the three combinations $I^\pi=0^+,2^+,4^+$

$$|IM) = \frac{1}{\sqrt{2}} \sum_{\mu_1\mu_2} C^{2\,2\,I}_{\mu_1\mu_2 M} B^+_{2\mu_1} B^+_{2\mu_2}|0). \tag{1.23}$$

The states with $I=1,3$ vanish identically because of the behavior of the Clebsch–Gordan coefficients* [Ed 57, Eq. (3.5.14)]

$$C^{2\,2\,I}_{\mu_1\mu_2 M} = (-)^I C^{2\,2\,I}_{\mu_2\mu_1 M},$$

under an exchange of μ_1 and μ_2.

Indeed, many spherical nuclei show in their spectrum a low-lying 2^+ state and, at roughly double the excitation energy, a so-called two-boson triplet $(0^+,2^+,4^+)$ which is, however, usually split up a little (see Fig. 9.4).

The constants B_λ and C_λ can be calculated within the fluid picture; they depend on the flow associated with the surface oscillations. Therefore, it is necessary to postulate the nature of the fluid motion within the drop. At this point we should again discuss what the concept of a nuclear fluid

* We use the symbol $C^{j_1 j_2 j_3}_{m_1 m_2 m_3}$ which is the same as $(j_1 m_1 j_2 m_2 | j_1 j_2 j_3 m_3)$.

implies. In Chapter 13 we will investigate this point in detail and show that the fact that the nucleus is a Fermi liquid and not an ordinary liquid plays an important role. The simplest assumption about the flow pattern of the fluid we can make is that it is irrotational, i.e., $\mathbf{rot}\,\mathbf{v}(\mathbf{r})=0$, where $\mathbf{v}$ is the velocity field. We shall also study the justification of this point in Chapter 13, but for the moment let us take it for granted and thus have:

$$\mathbf{v}(t) = -\nabla\Phi(\mathbf{r}). \tag{1.24}$$

The next assumption is that of *incompressibility*, which is quite well justified for nuclei. It means that the density inside the nucleus is constant ($\dot\rho=0$), and we get from the equation of continuity

$$\nabla\mathbf{v}=0 \tag{1.25}$$

and, from (1.24),

$$\Delta\Phi=0. \tag{1.26}$$

The most general solution of Eq. (1.26) regular at the origin can be written in the form

$$\Phi(\mathbf{r}) = \sum_{\lambda\mu} d^*_{\lambda\mu} r^\lambda Y_{\lambda\mu}(\theta,\phi). \tag{1.27}$$

For small deformations we have the boundary condition that the radial component of the velocity is, in lowest order, given by:

$$v_r = -\frac{\partial}{\partial r}\Phi = \dot R \qquad \text{at} \quad r=R_0,$$

which, with Eq. (1.7), yields the following relation between the coefficients $d_{\lambda\mu}$ and $\alpha_{\lambda\mu}$.

$$d_{\lambda\mu} = -\frac{1}{\lambda} R_0^{2-\lambda}\dot\alpha_{\lambda\mu}. \tag{1.28}$$

The kinetic energy of the surface vibrations is given by

$$T = \frac{m}{2}\rho\int_V \mathbf{v}^2(\mathbf{r})\,d^3r = \frac{m}{2}\rho\int_V |\nabla\Phi|^2\,d^3r = \frac{m}{2}\rho\oint_S \Phi^*\nabla\Phi\,d\mathbf{s},$$

where ρ is the constant density of nucleons with the mass m. Using the gradient formula for spherical harmonics [Ed 57, Eq. (5.9.17)] and [Ed 57, Eqs. (5.9.13) and (5.9.16)] we arrive in the approximation of small deformations (integrating over a sphere), in the following expression for the kinetic energy.

$$T = \frac{R_0^5 m\rho}{2}\sum_{\lambda\mu}\frac{|\dot\alpha_{\lambda\mu}|^2}{\lambda}. \tag{1.29}$$

Comparison with (1.17) yields the mass parameter

$$B_\lambda = \frac{\rho m R_0^5}{\lambda} = \frac{3}{4\pi\lambda} A\cdot m R_0^2. \tag{1.30}$$

For oscillations about a spherical equilibrium shape the mass parameter is not a function of μ; this would not be so for a deformed nuclear drop.

The potential energy of a liquid drop with a surface deformation characterized by the parameters $\alpha_{\lambda\mu}$ can be obtained from the coefficients of the Bethe-Weizsäcker formula (1.4) if we neglect changes of the symmetry and pairing energy with deformation.

Because of the assumption of incompressibility, it is tempting to say that the volume term does not depend on the deformation. This is, however, only true for ordinary fluids, and we will see in Chapter 13 how in quantum fluids the volume term can depend on α in a quite subtle fashion. In the usual treatment of the liquid drop model [BM 53, EG 70], however, the volume term is not taken into account, and therefore the deformation energy has only two parts, resulting from the surface and Coulomb terms in Eq. (1.4). As we will discuss in more detail in Chapter 13 this will be sufficient for the monopole and the dipole resonance but not for resonances of other multipolarities.

The deformation energy is defined as the difference between the energy of the deformed and spherical drop:

$$V(\alpha)=E_S(\alpha)-E_S(0)+E_C(\alpha)-E_C(0). \tag{1.31}$$

The surface energy is given by the product of the surface with the surface tension σ [Eq. (1.6)]. With techniques similar to those used in the derivation of Eq. (1.29), we find up to second order in $\alpha_{\lambda\mu}$ [Wi 64, Chap. 2]:

$$E_S(\alpha)=\sigma\oint_S ds=E_S(0)+\frac{1}{2}\sum_{\lambda\mu}(\lambda-1)(\lambda+2)R_0^2\sigma|\alpha_{\lambda\mu}|^2. \tag{1.32}$$

The Coulomb energy E_C is the sum of interactions between pairs of volume elements d^3r_1 and d^3r_2 [Wi 64]

$$E_C(\alpha)=(Ze)^2\int_V\int\frac{d^3r_1d^3r_2}{|\mathbf{r}_1-\mathbf{r}_2|}=E_C(0)-\frac{1}{2}\sum_{\lambda\mu}\frac{3(\lambda-1)(Ze)^2}{2\pi(2\lambda+1)R_0}|\alpha_{\lambda\mu}|^2. \tag{1.33}$$

From (1.32), (1.33), and (1.17), we thus get the stiffness coefficients ($\lambda>2$):

$$C_\lambda=(\lambda-1)(\lambda+2)R_0^2\sigma-\frac{3(\lambda-1)}{2\pi(2\lambda+1)}\frac{(Ze)^2}{R_0}. \tag{1.34}$$

In principle, we are now able to calculate nuclear spectra from Eq. (1.19) and the coefficients B_λ and C_λ. It turns out, however, that the reproduction of spectra is not the most sensitive test for a nuclear model. A quantum mechanical state is represented by a wave function. Electromagnetic moments and transition probabilities depend strongly on the wave functions and provide a much better test. We therefore first discuss such quantities before comparing the theory with experimental data.

In Appendix B the calculation of the electromagnetic properties of a nucleus is shown. The essential quantities are the electric and magnetic multipole operators.

The electric multipole operators are in the limit of long wavelengths (low transition energies) given by [Eq. (B.18)]

$$\hat{Q}_{\lambda\mu}=e\int_V\rho_p(\mathbf{r})r^\lambda Y_{\lambda\mu}(\theta,\phi)\,d^3r.$$

We can express them by the cordinates $\alpha_{\lambda\mu}$, taking in the integral a constant proton density ρ_p for a shape defined by Eq (1.7) and get

$$\hat{Q}_{\lambda\mu}=\rho_p\cdot e\cdot\int_{4\pi}d\cos\theta\,d\phi\,Y_{\lambda\mu}(\theta,\phi)\frac{1}{\lambda+3}R^{\lambda+3}(\theta,\phi),$$

which is up to second order in $\alpha_{\lambda\mu}$ (with [Ed 57, Eq. (4.6.3)])

$$\hat{Q}_{\lambda\mu}=\frac{3e}{4\pi}ZR_0^\lambda\left\{\hat{\alpha}_{\lambda\mu}+\frac{1}{2}(\lambda+2)\sum_{\lambda_1\mu_1}\sum_{\lambda_2\mu_2}\hat{\alpha}_{\lambda_1\mu_1}\hat{\alpha}_{\lambda_2\mu_2}(-)^\mu\right.$$
$$\left.\cdot\sqrt{\frac{(2\lambda_1+1)(2\lambda_2+1)(2\lambda+1)}{4\pi}}\begin{pmatrix}\lambda_1&\lambda_2&\lambda\\0&0&0\end{pmatrix}\begin{pmatrix}\lambda_1&\lambda_2&\lambda\\-\mu_1&-\mu_2&\mu\end{pmatrix}\right\}. \tag{1.35}$$

The magnetic multipole operators are given by [Eq. (B. 22)]

$$\hat{M}_{\lambda\mu}=\frac{1}{c(\lambda+1)}\int_V(\mathbf{r}\times\mathbf{j}(\mathbf{r}))(\nabla r^\lambda Y_{\lambda\mu})\,d^3r.$$

As in the case of the mass parameters, we could again use the assumption of irrotational flow to define the current density $\mathbf{j}$ and express $\hat{M}_{\lambda\mu}$ by $\alpha_{\lambda\mu}$ and $\dot{\alpha}_{\lambda\mu}$ (see [Da 68, Chap. 6]). However, we will restrict ourselves to the case of $M1$ operators, which form a vector

$$\hat{\mathbf{M}}1=\sqrt{\frac{3}{4\pi}}\;\hat{\boldsymbol{\mu}}.$$

Since we have no spins in the system, we get for the magnetic dipole moment

$$\hat{\boldsymbol{\mu}}=\frac{1}{2c}\int_V(\mathbf{r}\times\mathbf{j})\,d^3r=\frac{Z}{A}\frac{e}{2mc}\int_V(\mathbf{r}\times m\mathbf{v})\,d^3r=\frac{Z}{A}\frac{e\hbar}{2mc}\hat{\mathbf{I}}=g_R\hat{\mathbf{I}}\mu_N \tag{1.36}$$

with the gyromagnetic ratio of the rotor

$$g_R=\frac{Z}{A}. \tag{1.37}$$

The calculation of lifetimes and transition probabilities requires the knowledge of $BE\lambda$- and $BM\lambda$-values [see Eq. (B. 73)] defined by

$$B\left(\begin{Bmatrix}E\\M\end{Bmatrix}\lambda,I_i\to I_f\right)=\frac{1}{2I_i+1}\left|<I_f\|\begin{Bmatrix}\hat{Q}_\lambda\\\hat{M}_\lambda\end{Bmatrix}\|I_i>\right|^2. \tag{1.38}$$

Since the $M1$-operator (1.36) conserves angular momentum, $M1$-transitions are forbidden in this model. The most important transitions are $E2$-transitions.

As an example, we calculate the $BE2$-value for the transition from the one-boson state $B_{2\mu}^+|0)$ to the ground state $|0)$. Expressing $\hat{\alpha}_{2\mu}$ by the operators $B_{2\mu}$ and $B_{2\mu}^+$ (1.21), and using the wave function (1.22), we get to first order in the $\alpha_{2\mu}$'s

$$B(E2,2_1^+\to0^+)=\left(\frac{3}{4\pi}ZeR_0^2\right)^2\frac{\hbar}{2B_2\Omega_2}. \tag{1.39}$$

Before we compare these theoretical results of our model with experimental data, we must discuss which levels in the excitation spectra of nuclei would be appropriate candidates for such surface vibrations. We restrict the following discussion to 2^+ states. For other angular momenta similar considerations apply.

Figure 1.6 shows schematically the structure of the 2^+ spectra. They have a discrete part and a continuum with resonances. Among the discrete lines one 2^+ level is usually very low in energy. With a few exceptions it is the lowest excited state in each nucleus and, as shown in Fig. 1.6, it carries a large $BE2$ value, i.e., it has a high transition probability to the ground state (see Appendix B). The measured $BE2$ values are for spherical nuclei roughly ten to twenty times larger than one would expect from a pure single-particle transition [Weisskopf unit, see Eq. (B. 85)].

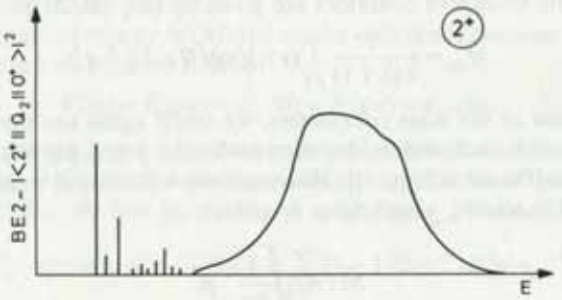

Figure 1.6. Schematic representation of the 2^+ spectra in nuclei. The ordinate gives the $BE2$ values for the discrete levels and the density of the $BE2$ strength in the resonance region. These quantities measure the transition probability to the ground state. The units are arbitrary.

The low-lying 2^+ states therefore have collective character, i.e., many particles contribute and they have very often been interpreted as surface quadrupole vibrations. Figure (1.7) shows the energy E_{2^+} for the lowest 2^+ state in even–even nuclei. One observes large shell effects (see Chap. 2). Only the average trend is given by the liquid drop model with irrotational flow [Eqs. (1.19) (1.30) and (1.34)]. The absolute value is off by a factor of five. The reason for this failure will become clear below.

Experimentally, it has been found that there is a strong correlation between the $BE2$ value of the first 2^+ state and its energy $E_{2_1^+} = \Omega_2$ [Gr 62]:

$$E_{2_1^+} B(E2, 2^+ \to 0^+) \simeq (25 \pm 8) \frac{Z^2}{A} \; [\text{MeV } e^2 \text{ fm}^4]. \tag{1.40}$$

This empirical relation holds for all the nuclei throughout the nuclear table. Equation (1.39) shows the same energy dependence, but the A dependence is different.The strong shell effects in the low-lying 2^+ states indicate that they cannot be pure quadrupole surface oscillations and that there are other states which also have the character of such collective vibrations. From Eqs. (1.22), (1.21), and (1.35) we see that the quadrupole

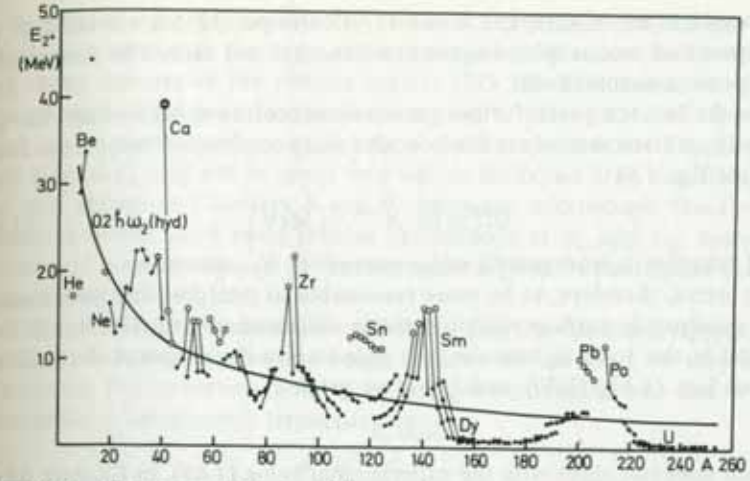

Figure 1.7. The energy of the first 2^+ state in even–even nuclei. The nuclei with closed neutron or proton shells are marked by open circles. (From [NN 65].)

surface vibration can be represented in linear order in α as:

$$|2\mu) = B^+_{2\mu}|0) \propto \hat{\alpha}_{2\mu}|0) \propto \hat{Q}_{2\mu}|0). \tag{1.41}$$

The overlap of an arbitrary state $|\nu\rangle$ with the quadrupole surface vibration is therefore proportional to its $BE2$ value:

$$|\langle \nu | 2\mu \rangle|^2 \propto |\langle \nu | \hat{Q}_{2\mu} | 0 \rangle|^2 \propto B(E2, \nu \to 0), \tag{1.42}$$

and the probability that it can be interpreted as such a vibration is given by the percentage to which it exhausts the sum rule

$$S^0_{2\mu} = \sum_{\nu \neq 0} |\langle \nu | \hat{Q}_{2\mu} | 0 \rangle|^2. \tag{1.43}$$

Only if one state exhausts this sum rule to a large extent is it meaningful to call it a quadrupole surface vibration.

In Section 8.7 we will discuss in great detail the sum rules and how they can be evaluated. It is evident that in a model where the state $\hat{Q}_{\lambda\mu}|0\rangle$ is an eigenstate of the system, like the model we are now investigating, this state exhausts the sum rules completely, because all the other states are orthogonal to it.

Experimentally, it has been found that the low-lying 2^+ state usually exhausts about 10–20% of the sum rule. The major part is exhausted by the resonances in the continuum [see Fig. (1.6)], the so-called giant resonances.

Such giant resonances for different I values have been observed. The most famous is the giant dipole resonance (1^-) which has been well known since more than 30 years and lies at an energy (see Fig. 1.8) (for more details see Chap. 13):

$$\Omega_1^{\text{GR}} \simeq 77 \cdot A^{-1/3 + -1/6} \; [\text{MeV}]. \tag{1.44}$$

As we shall see in Chapters 8 and 13, it corresponds to a vibration of the neutron and proton sphere against one another and cannot be described in the present simple model.

In the last ten years, further giant resonances have been observed. The most important example is the isoscalar giant quadrupole resonance. It lies at (see Fig. 1.8)

$$\Omega_{2^+}^{GR} \simeq 62 \cdot A^{-1/3}\,[\mathrm{MeV}] \tag{1.45}$$

and exhausts in most cases a major part of the S_{2^+} sum rule.

It seems, therefore, to be more reasonable to interpret this resonance as the quadrupole surface vibration mode discussed so far. The liquid drop model in this form is, however, not able to give the proper A-dependence. From Eqs. (1.19), (1.30), and (1.34) we get

$$\Omega_2 \propto A^{-1/2},$$

which does not agree with the experimental value (1.45). In Chapter 13 we will see that the reason for this deviation comes from the fact that the potential energy coefficients C_λ correspond to the total binding energy of the liquid drop [(1.31), (1.34)]. This total binding energy is, however, a sum of intrinsic kinetic and potential energy. The fact that (at least, for small deformations) the intrinsic kinetic energy depends on the deformation has been neglected in (1.34). This can be understood simply as an effect of the long mean free path of the nucleons and the uncertainty principle, which states that in an ellipsoidal shape the nucleons along the short axis have higher momenta than those along the long axis. An ellipsoidal momentum distribution, however, yields a larger kinetic energy than a spherical one. Since all particles are affected, it is a volume effect which dominates in general over the surface dependence given in (1.34). In Chapter 13 we will give a detailed discussion of this point.

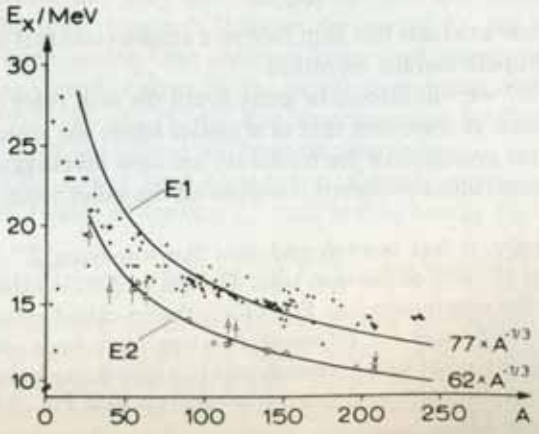

Figure 1.8. The energy of the giant dipole and the isoscalar giant quadrupole resonance as a function of mass number [Wa 73].

In spite of these deficiencies, the boson model presented so far has been extensively used over the years and has proved quite successful in explaining many features of the nuclear spectra [EG 70]. The reason for this is that many low-lying nuclear excitations have a rather collective character and can be represented to a good approximation as bosons. The parameters B_λ and C_λ may not be given very well in the liquid drop model, but, as we will shown in Chapters 8 and 9, there are microscopic theories for fermions which allow more reliable calculations of B_λ and C_λ; therefore, we should consider B_λ and C_λ more as open adjustable parameters than as determined by the LDM.

The microscopic theories also will show that the harmonic approximations (1.17) have only a very rough validity in the limit of very small vibrations. For collective motions with larger amplitudes, one has to take into account anharmonic terms such as

$$\alpha^4, \alpha^2 \cdot \dot{\alpha}^2, \dot{\alpha}^4, \ldots.$$

Again the corresponding parameters can be adjusted to experiment or calculated from a microscopic many-body theory (see Chap. 9).

1.5 Rotations and Vibrations for Deformed Shapes

1.5.1 The Bohr Hamiltonian

The pure liquid drop model has a stable equilibrium only for spherical surfaces. As we shall see later (Sec. 2.8) it can happen as a consequence of quantum mechanics—i.e., shell effects—that the potential $V(\alpha)$ in the collective Hamiltonian has minima at finite non-vanishing values of $\alpha = \alpha_0$. In such cases the nucleus can have a stable ground state deformation.

In this case, the nucleus can exhibit *rotations* which can be described by time-dependent surface parameters $\alpha_{\lambda\mu}$ in the laboratory frame. We shall call these rotations collective ones: This kind of rotation will not be possible around an axis of symmetry, because we cannot distinguish the rotated system from the original one in our variables $\alpha_{\lambda\mu}$.

In a quantum mechanical description, a system with an axis of symmetry (for example, the z-axis) is given by a wave function which is an eigenfunction of the angular momentum operator J_z, and any rotation about this axis produces only a phase. The rotating system has, therefore, the same wave function as the ground state, and the same energy.

This does not mean that there are no other degrees of freedom in the system that can be excited (for instance, single-particle degrees of freedom) and carry angular momentum parallel to the symmetry axis. Such a "rotation," however, we do not call collective rotation.

Since in almost all nuclei the quadrupole degree of freedom plays a fundamental role, we will restrict the following considerations to the case $\lambda = 2$.

Assuming that the nucleus has a stable ground state deformation, it is preferable to transform to the body-fixed system, defined by the principal axes of the mass distribution (as discussed in Sec. 1.3).

After this transformation, we have five dynamical variables Ω, β, γ* instead of the variables $\alpha_{2\mu}$ ($\mu=-2,-1,0,+1,+2$). We start again from the Hamiltonian (1.17). Only the potential in (1.17) is changed. It now has the form:

$$V(\beta,\gamma)=\tfrac{1}{2}C_{20}\big(a_{20}(\beta,\gamma)-a_{20}^0\big)^2+C_{22}\big(a_{22}(\beta,\gamma)-a_{22}^0\big)^2. \qquad (1.46)$$

This corresponds to a quadratic approximation in the vicinity of a deformed minimum β_0, γ_0. The idea is that the nucleus has this deformation in its ground state, and the excitations are rotations and small oscillations around this equilibrium deformation.

Microscopic calculations of potential landscapes show, for certain nuclei, well pronounced minima of V for finite values $\beta_0\simeq 0.2-0.3$ and $\gamma_0=0$. These axially symmetric shapes are, therefore, the most important ones, and we will restrict a large part of our discussion to them.

The next step is the transformation of the kinetic energy in Eq. (1.17) to the body-fixed system. Applying Eq. (1.11), we have to differentiate the variables a_{20}, a_{22}, and Ω with respect to the time. Since the derivation is quite lengthy, and the intention in this chapter is not to be complete, we simply give the result (for the derivation, see, for example, [EG 70 Vol. I, Chap. 5]) for the so-called Bohr Hamiltonian [Bo 52]:

$$T=T_{\rm rot}+\tfrac{1}{2}B_2(\dot\beta^2+\beta^2\dot\gamma^2) \qquad (1.47)$$

with

$$T_{\rm rot}=\tfrac{1}{2}\sum_{\kappa=1}^{3}\vartheta_\kappa\omega_\kappa^2,$$

where ω_κ is the angular velocity around the body-fixed κ-axis and ϑ_κ are functions of β and γ given by

$$\vartheta_\kappa=4B_2\beta^2\sin^2\Big(\gamma-\frac{2\pi}{3}\kappa\Big), \qquad \kappa=1,2,3. \qquad (1.48)$$

In case we have fixed deformations β,γ, $T_{\rm rot}$ is the kinetic energy of a rotor with the moment of inertia ϑ_κ. As soon as we allow for changes of β and γ, the rotational and vibrational degrees of freedom are coupled by the deformation dependence of the moments of inertia. In this case, we no longer have a pure rotor. In fact, we see that in the case of $\beta_0=0$ the system can be transformed back to a harmonic vibrator (1.17) which has a harmonic spectrum.

However, even in the well deformed case with large stiffness parameters C and finite β_0 (where a constant $\beta=\beta_0$ is a rather good approximation),

*Unfortunately, the set of Euler angles $\Omega=(\alpha,\beta,\gamma)$ also contains the letters β and γ. However, we do not want to change this nomenclature [Ed 57] and we, as far as possible, use the abbreviation Ω.

ϑ_κ are not the moments of inertia of a rigid rotor. Using (1.30), we get from Eq. (1.48) the so-called irrotational moment of inertia:

$$\vartheta_\kappa^{\rm irr}=\frac{3}{2\pi}mAR_0^2\beta^2\sin^2\Big(\gamma-\frac{2\pi}{3}\kappa\Big), \qquad \kappa=1,2,3.$$

It differs from the moment of inertia of a rigid body with the same deformation

$$\vartheta_\kappa^{\rm rig}=\frac{2}{5}mAR_0^2\Big(1-\sqrt{\frac{5}{4\pi}}\ \beta\cos\Big(\gamma-\frac{2\pi}{3}\kappa\Big)\Big) \qquad (1.49)$$

in the following ways.

(i) In the γ-dependence (Fig. 1.9), $\vartheta^{\rm irr}$ vanishes about the symmetry axes.

(ii) $\vartheta^{\rm irr}$ shows a strong dependence on the deformation ($\sim\beta^2$), whereas $\vartheta^{\rm rig}$ changes much less with β (its main part is the moment of inertia of a rigid sphere).

(iii) The experimental moment of inertia $\vartheta^{\rm exp}$ can be found from the energy of the first 2^+ state of a rotational band [see Eq. (1.64)] $\vartheta^{\rm exp}=3/E_{2^+}$ [MeV^{-1}]. Applying the empirical rule (1.40) and the formula (1.74) for the $BE2$ value, we get a connection between the deformation parameter β and the moment of inertia

$$\vartheta^{\rm exp}=\frac{27}{80\pi^2}r_0^4\frac{A^{4/3}\cdot\beta^2\cdot Z^2e^2}{E_{2^+}\cdot BE2}\approx\frac{27(1.2)^4\cdot\beta^2A^{7/3}}{80\pi^225}$$
$$\approx\frac{\beta^2A^{7/3}}{400}\ [\text{MeV}^{-1}]. \qquad (1.50)$$

In the case of well deformed nuclei ($\beta\sim 0.2-0.4$), $\vartheta^{\rm irr}$ is usually smaller by a factor of 2–3 than the experimental values. On the other side, the values of $\vartheta^{\rm rig}$ are a factor of 2 too large:

$$\vartheta^{\rm irr}<\vartheta^{\rm exp}<\vartheta^{\rm rig}. \qquad (1.51)$$

This shows that the flow structure within the nuclei is certainly not irrotational. On the other hand, it is not a rigid rotor, either.

The next step is again a quantization of the classical Hamiltonian (1.47). It is well known that there is no unique prescription for the quantization of a classical Hamiltonian in the general case [Me 61]. The ambiguity comes from the freedom in ordering noncommutable operators.* Commonly one adopts the Pauli prescription [Pa 33], which calculates the Laplace operator in curvilinear coordinates. If the classical kinetic energy has the form

$$T=\tfrac{1}{2}\sum_{ij}^{f}g_{ij}(\xi)\dot\xi_i\dot\xi_j, \qquad (1.52)$$

*A discussion with a list of references on the quantization problem is found in [MD 73].

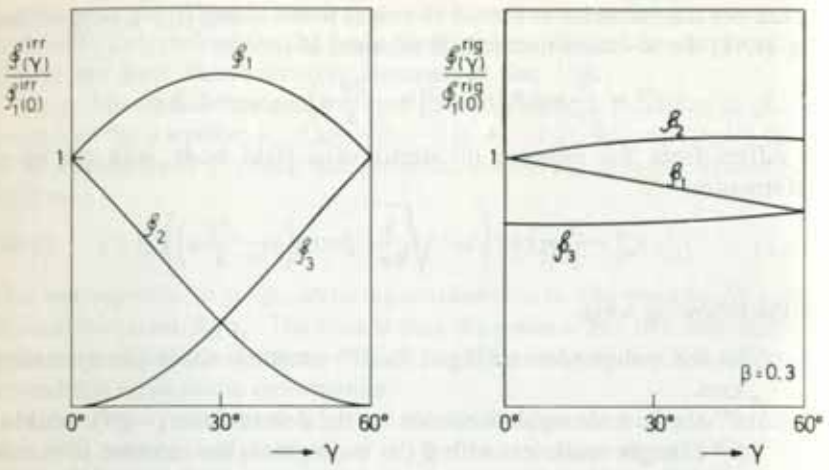

Figure 1.9. The γ-dependence of the irrotational (ϑ_k^{irr}) and the rigid (ϑ_k^{rig}) moments of inertia for fixed values of β.

then the corresponding quantized form is*

$$\hat{H}_{kin} = -\frac{\hbar^2}{2}\sum_{ij} g^{-1/2}\frac{\partial}{\partial\xi_i} g^{1/2}(g^{-1})_{ij}\frac{\partial}{\partial\xi_j}, \tag{1.53}$$

where g is the determinant and g^{-1} is the inverse of the matrix g_{ij}.

Applying this prescription to the Bohr Hamiltonians (1.46) and (1.47), we obtain:

$$\hat{H}_{coll} = \frac{-\hbar^2}{2B_2}\left[\beta^{-4}\frac{\partial}{\partial\beta}\left(\beta^4\frac{\partial}{\partial\beta}\right) + \frac{1}{\beta^2\sin 3\gamma}\frac{\partial}{\partial\gamma}\left(\sin 3\gamma\frac{\partial}{\partial\gamma}\right)\right] + \hat{T}_{rot} + V(\beta,\gamma), \tag{1.54}$$

where the rotational energy is found to be

$$\hat{T}_{rot} = \frac{\hat{I}_1^2}{2\vartheta_1} + \frac{\hat{I}_2^2}{2\vartheta_2} + \frac{\hat{I}_3^2}{2\vartheta_3}. \tag{1.55}$$

The operators $\hat{I}_k$ are the projections of the total angular momentum $\hat{\mathbf{I}}$ represented in the Euler angles onto the body-fixed axes (for details, see Appendix A). Figure (1.10) shows the total angular momentum and its components $\hat{I}_z = M$ and $\hat{I}_3 = K$. The eigenfunctions of $\hat{\mathbf{I}}^2, \hat{I}_z, \hat{I}_3$ are given by

$$|IMK\rangle = \sqrt{\frac{2I+1}{8\pi^2}}\, D^{I*}_{MK}(\Omega). \tag{1.56}$$

Since H_{coll}, $\hat{\mathbf{I}}^2$ and $\hat{I}_z$ commute, the eigenfunctions of the collective Hamil-

* To see that the Hamiltonian (1.53) is Hermitian, one has to take into account the volume element $\sqrt{g}\; d\xi_1 \ldots d\xi_f$.

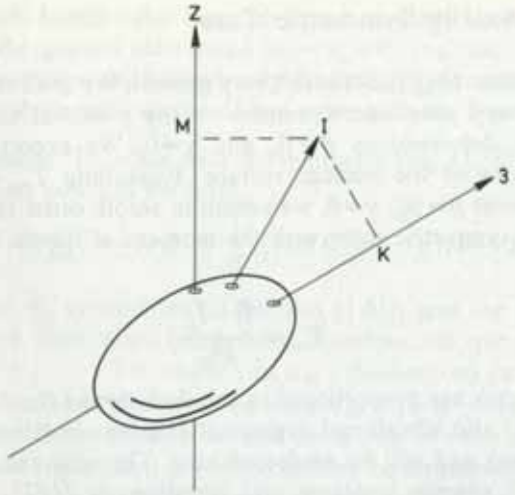

Figure 1.10. The relation between the total angular momentum **I** and its projection M onto the laboratory z axis and its projection K onto the body-fixed 3-axis.

tonian (1.54) have the general form

$$|\Psi^I_M\rangle = \sum_K g_K(\beta,\gamma)|IMK\rangle.$$

The triaxial rotor has certain discrete symmetries. $\hat{H}_{coll}$ is invariant under the point group D_2 [Bo 52]. Therefore, one classifies the eigenstates according to the irreducible representations of this group, and one can derive from this some properties of the spectra [Da 68].

One example is the rotation of 180° around the 1-axis,

$$\mathcal{R}_1 = e^{i\pi\hat{I}_1}, \tag{1.57}$$

which is equivalent to a reflection with respect to the 2, 3-plane together with a parity transformation. It commutes with $\hat{H}_{coll}$ and we require our eigenfunctions to have eigenvalue +1*:

$$\mathcal{R}_1|\Psi^I_M\rangle = |\Psi^I_M\rangle. \tag{1.58}$$

Using relation (A.24) of Appendix A, we find that this is only possible with

$$g_K(\beta,\gamma) = (-)^I g_{-K}(\beta,\gamma). \tag{1.59}$$

If we require, in the same way, symmetry with respect to

$$\mathcal{R}_2 = e^{i\pi\hat{I}_2}, \tag{1.60}$$

we get

$$g_K(\beta,\gamma) = (-)^{I+K} g_{-K}(\beta,\gamma). \tag{1.61}$$

* As we shall see in Eq. (11.123), the microscopic intrinsic wave function of the system is an eigenstate of this operation with eigenvalue +1 (see also [Bo 76 b]).

1.5.2 The Axially Symmetric Case

The Hamiltonian $\hat{H}_{\text{coll}}$ (1.54) is still very general. We shall restrict ourselves to cases of very pronounced minima in the potential surface at axially symmetric deformations $\beta=\beta_0$ and $\gamma=0$. We expect rotations and small vibrations of the nuclear surface. Expanding $T_{\text{rot}}-\hat{I}_3^2/2\vartheta_3$ (1.55) around the point $\beta=\beta_0$, $\gamma=0$, we obtain in zeroth order the Hamiltonian of an axially symmetric rotor with the moment of inertia $\vartheta_0=\vartheta_1(\beta_0,0)=\vartheta_2(\beta_0,0)$,

$$T'_{\text{rot}}=\frac{\hat{\mathbf{I}}^2-\hat{I}_3^2}{2\vartheta_0}. \tag{1.62}$$

First-order terms are proportional to the deviations $(\beta-\beta_0)$ and γ. They mix rotational and vibrational degrees of freedom (rotational–vibrational coupling terms) and will be neglected here. The only remaining term in H_{coll} that still couples rotations and vibrations is $\hat{I}_3^2/2\vartheta_3$. It cannot be expanded, since ϑ_3 vanishes for $\gamma=0$. However (as T'_{rot}), it commutes with $\hat{I}_3$ and K is therefore a good quantum number.

We now have to distinguish

(i) K = 0 bands ($I_3=0$). In this case, the rotational and vibrational motions decouple. The wave function is of the type

$$|\Psi^I_{M0}\rangle=g_0(\beta,\gamma)|IM0\rangle. \tag{1.63}$$

They are eigenfunctions of the rotational part of the Hamiltonian (1.54). $\mathfrak{R}_1$-symmetry (1.59) requires the spin sequence $I=0,2,4,\ldots$. A detailed investigation of the vibrational part of H_{coll} [EG 70, Vol. I, Chap. 6] shows that it is easier to handle in the variables a_{20} and a_{22} (1.13). In the first step one neglects terms in the potential $V(a_{20},a_{22})$, which couple these two degrees of freedom. In this case, the motion in the coordinate a_{20} (usually called β-vibration) decouples from the motion in the coordinate a_{22} (usually called γ-vibration). Axial symmetry with respect to the 3-axis is preserved by the β-vibration (quantum number n_β), but violated by the γ-vibration (quantum number n_γ). Both types of motion are shown qualitatively in Fig. 1.11.

Superimposed on each vibrational state (n_β,n_γ) is a rotational band. The spectrum is given by (see [EG 70, Vol. I, Chap. 6])

$$E_{n_\beta n_\gamma}(I)=E_{n_\beta n_\gamma}(0)+\frac{\hbar^2}{2\vartheta_0}I\cdot(I+1) \tag{1.64}$$

with the band head

$$E_{n_\beta n_\gamma}(0)=\hbar\omega_\beta(n_\beta+1/2)+\hbar\omega_\gamma(2n_\gamma+1),$$
$$n_\beta=0,1,2,\ldots,\qquad n_\gamma=0,1,2,\ldots, \tag{1.65}$$

where ω_β and ω_γ are the frequencies of β- and γ-vibrations.

$$\omega_\beta=(C_{20}/B_2)^{1/2}\qquad \omega_\gamma=(C_{22}/B_2)^{1/2}$$

In fact, such bands have been observed in many even–even nuclei, in particular the ground state band ($n_\beta=n_\gamma=0$) and the "β-band" ($n_\beta=1$, $n_\gamma=0$). However, as we have already discussed, the constants ϑ_0 and $\omega_\beta,\omega_\gamma$ of the hydrodynamical model do not agree with the experimental data.

(ii) K ≠ 0 bands. Together with $\mathfrak{R}_1$-symmetry [Eq. (1.58)], we see that the wave function now has the form

$$|\Psi^I_{MK}\rangle=g_K(\beta,\gamma)\frac{1}{\sqrt{2}}\{|IMK\rangle+(-)^I|IM-K\rangle\}. \tag{1.66}$$

The $\mathfrak{R}_1$ and $\mathfrak{R}_2$ symmetries ((1.59) and (1.61)) give the selection rule: K must be even. Such $K\neq0$ bands have, therefore, the spin sequence $I=|K|$, $|K|+1$, $|K|+2,\ldots$. The motion in a_{20} (β-vibration) can again be separated from the rest. However, the term $\hat{I}_3/2\vartheta_3=K^2/16B_2a_{22}^2$ couples the γ-vibration with the rotation around the 3-axis. We can easily understand this fact if we realize that a γ-vibration can be represented as a superposition of two rotations of a triaxial nucleus around the 3-axis, but with opposite K-values [BM 75, p. 656].

The following spectrum is obtained [EG 70, Vol. I, Chap. 6]

$$E_{K,n_\beta,n_\gamma}(I)=E_{K,n_\beta,n_\gamma}(0)+\frac{\hbar^2}{2\vartheta_0}\big(I(I+1)-K^2\big) \tag{1.67}$$

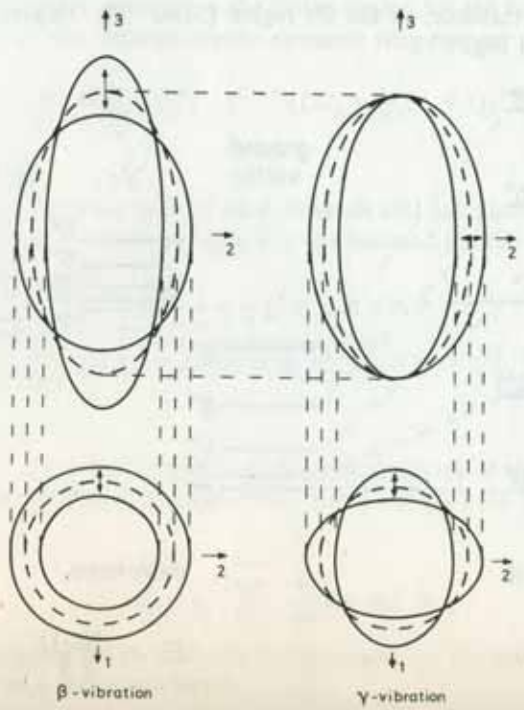

Figure 1.11. Schematical representation of β- and γ-vibrations by a cut along the (1, 3) and (1, 2) planes.

with the bandheads

$$E_{K,n_\beta,n_\gamma}(0)=\hbar\omega_\beta\left(n_\beta+\frac{1}{2}\right)+\hbar\omega_\gamma\left(2n_\gamma+1+\frac{|K|}{2}\right). \tag{1.68}$$

In fact, such bands have also been observed, especially the so-called "γ-band" in many deformed nuclei, which has the quantum numbers $K=2$, $n_\beta=0$, $n_\gamma=0$. This γ-band has the vibrational quantum number $n_\gamma=0$, however, one is not allowed to apply the classical picture of no vibration in this case. It would correspond to $\gamma=0$ and imply $\vartheta_3=0$, which would forbid a rotation with $K\neq 0$. Only the quantum mechanical zero point vibration in the γ-direction makes this possible.

Figure 1.12 shows the qualitative structure of the collective ($\lambda=2$) excitation in deformed and spherical nuclei.

The spherical nuclei have a harmonic spectrum. In the deformed nuclei we observe several rotational bands built on the ground state, on the β-vibrational state $K=0$, $n_\beta=1$, $n_\gamma=0$, and on the γ-vibrational state $K=2$, $n_\beta=n_\gamma=0$. However, these pure cases are not exactly realized in nature. In fact, we already observe in spherical nulcei a splitting of the two-boson triplet $(0^+,2^+,4^+)$ and in the deformed nuclei deviations from the $I(I+1)$ law. There is also a wide range of transitional nuclei in between these two limits. Going from isotope to isotope, one can sometimes observe a gradual transition from a vibrational to a rotational spectrum (for instance, in the Os region [SDG 76]). This is indicated by dashed lines in Fig. 1.12.

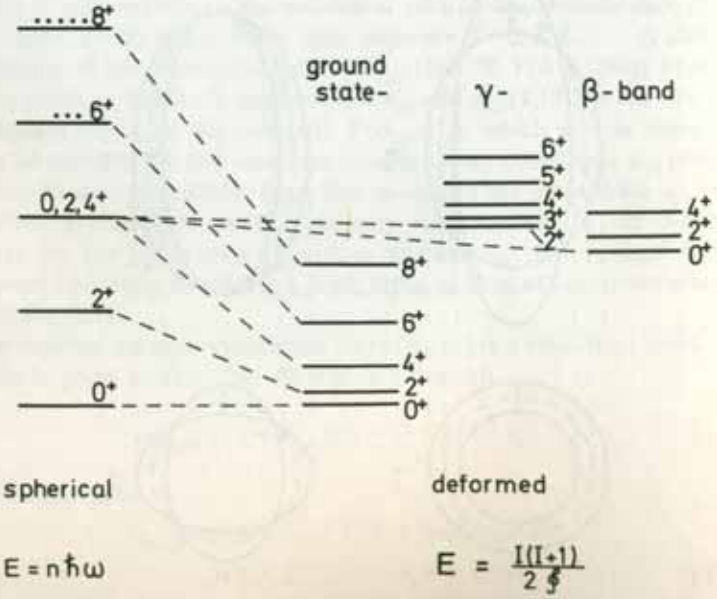

Figure 1.12. Schematic level schemes of spherical and deformed nuclei. (From [SDG 76].)

For a theoretical description of deviations from the $I\cdot(I+1)$ law, one has taken into account the rotational-vibrational coupling terms in $\hat{H}_{\text{coll}}$ which one gets by expanding ϑ_κ in powers of the deviations $(\beta-\beta_0)$ and γ[FG 62, FG 64, FGS 65, 66, ABP 68]. This rotation–vibration interaction causes changes in the moment of inertia of a band and corresponds to a change of the nuclear shape under the influence of the rotation (stretching effect). However, there also exist quite different excitations of nuclei in this energy region, for instance, two quasi-particle states and pairing vibrations (see Chap. 8), which have a much stronger influence on the rotational bands, and which are not taken into account in this simple model of a liquid drop with surface oscillations.

Before we leave this section, we want to discuss very briefly how to calculate electromagnetic moments and transition probabilities. In Eqs. (1.35) and (1.36) we defined the electric multipole and the magnetic moment operator in the coordinates $\alpha_{\lambda\mu}$. They are obviously written down in the laboratory system. In a deformed nucleus it is usually very easy to calculate the moments in the intrinsic system. To get the moments in the laboratory frame—the experimental values—one has to apply the transformation (1.11) of spherical tensors:

$$\hat{Q}^{\text{intr}}_{\lambda\mu}=\sum_{\mu'}D^{\lambda}_{\mu'\mu}\hat{Q}^{\text{lab}}_{\lambda\mu'}. \tag{1.69}$$

Since Q^{intr} does not depend on the Euler angles, we get from [Ed 57, Eqs. 4.6.2 and 5.4.1] the reduced matrix elements with respect to $|IMK\rangle$:

$$\langle I_1K_1\|\hat{Q}^{\text{lab}}_{\lambda}\|I_2K_2\rangle=\sum_{\mu'}Q^{\text{intr}}_{\lambda\mu'}(-)^{I_1-K_1}((2I_1+1)(2I_2+1))^{1/2}\begin{pmatrix} I_1 & \lambda & I_2\\ -K_1 & \mu' & K_2\end{pmatrix}. \tag{1.70}$$

We restrict ourselves now to pure K-bands and calculate only intraband $E2$-transitions ($n_{\gamma_1}=n_{\gamma_2}$, $n_{\beta_1}=n_{\beta_2}$). For the reduced matrix element we find

$$\langle n_\beta n_\gamma I_1K\|\hat{Q}^{\text{lab}}_2\|n_\beta n_\gamma I_2K\rangle$$
$$=\sqrt{\frac{5}{16\pi}}\;Q_0(n_\beta,n_\gamma)\sqrt{(2I_1+1)(2I_2+1)}\;(-)^{I_1-K}\begin{pmatrix} I_1 & 2 & I_2\\ -K & 0 & K\end{pmatrix}, \tag{1.71}$$

where $Q_0(n_\beta,n_\gamma)$ is the intrinsic quadrupole moment of this band. In the ground state band with fixed β-value, and $\gamma=0$ we have [Eqs. (1.13) and (1.35)]

$$Q_0=\sqrt{\frac{16\pi}{5}}\;\frac{3}{4\pi}Ze\cdot R_0^2\cdot\beta. \tag{1.72}$$

From (B.73) and (1.71) we obtain, for example, for the so-called stretched $BE2$-values in a rotational band,

$$B(E2,I+2\to I)=Q_0^2\frac{5}{16\pi}|C^{I+2\;2\;I}_{K\;0\;K}|^2, \tag{1.73}$$

which, for $K=0$ bands, gives

$$B(E2, I+2\to I)=Q_0^2\frac{5}{16\pi}\frac{3}{2}\frac{(I+1)(I+2)}{(2I+3)(2I+5)}. \tag{1.74}$$

For the spectroscopic quadrupole moments $Q=\sqrt{16\pi/5}\,\langle IIK|\hat{Q}_{20}^{\text{lab}}|\,IIK\rangle$ [Eq. (B.32)], we get

$$Q=Q_0\frac{3K^2-I\cdot(I+1)}{(2I+3)(I+1)}. \tag{1.75}$$

The quotient of $Q:Q_0$ is the expectation value of $D_{00}^2=P_2(\cos\beta)$ in the state $M=I$. This means that one cannot measure the internal quadrupole moment Q_0, but only the value averaged over the rotational motion. In fact, Q_0 is not a physical observable. Its definition depends on the introduction of a body-fixed system which moves with the nucleus and has a model character. For the band head we usually have $I=K$. That means the spectroscopic quadrupole moment Q of ground states with $I=0$ vanishes and we can get information about Q_0 only for the excited states (for instance, by the reorientation effect in Coulomb excitation [BE 68], which gives the sign and the absolute value of Q_0). Another way to determine the absolute value of Q_0 is the measurement of the $B(E2)$-values (1.73) in the transitions within a band. Recent measurements up to high spin states [WCL 76, HJE 78] have shown that in many deformed nuclei the value of Q_0 stays fairly constant within these bands, even in cases where the spectrum shows deviations from the $I(I+1)$ character. This is a hint that these deviations are not caused by the change of deformation (stretching effect).

1.5.3 The Asymmetric Rotor

The rotational–vibrational interaction model discussed so far has been on the basis of a symmetric rotor. Further attempts to explain the deviations from the $I(I+1)$ law and the low-lying second 2^+ states in many nuclei have been undertaken by Davydov et al. using the picture of a pure triaxial rotor [DF 58, DR 59, Da 59, Da 65b]. As a first step they do not consider the vibrational excitations and diagonalize only the rotational energy (1.55). With the moments of inertia (1.48), this operator is proportional to β^{-2} and one can diagonalize it for all values of γ. The constant factor can afterwards be adjusted so as to reproduce the first 2^+ state. Using the symmetries $\mathfrak{R}_1$ and $\mathfrak{R}_2$ (1.59 and 1.61), the wave functions have the form

$$|\Psi_M^I\rangle=\sum_{K=0,2,\ldots}g_K\{|IMK\rangle+(-)^I|IM-K\rangle\}. \tag{1.76}$$

Figure (1.13) shows the corresponding energy eigenvalues. For $\gamma=0°$ and $\gamma=60°$ one gets the $I(I+1)$ spectrum. Even for strong triaxial deformations one gets only slight deviations of this form. However, additional $2^+, 3^+, 4^+$ levels come down in energy. It is a characteristic of this structure to have a low-lying second 2^+ state. Although one can, with such a model, reproduce quite reasonably the experimental

data in some regions of the periodic table (for instance, for the Os-isotopes), strong objections can be raised to it:

(i) It is impossible to describe β-vibrations. In this case, one has to include additional vibrational degrees of freedom [DC 60]
(ii) Well pronounced minima in the energy surface that could justify a stable γ-deformation have not been found. Microscopic calculations for such transitional nuclei usually show only very shallow valleys in the γ direction [KB 68, ASS 69, GPA 72, GG 78].*

In recent years, stable γ-deformations have found new interest, because:

(i) Experimental data in odd–even transitional nuclei can be very well reproduced by a model of a particle coupled to an asymmetric rotor (see Chap. 5 and [MSD 74, Me 75, TF 75]).
(ii) Theoretical calculations for very high spin states (see Sec. 1.7 and [ALL 76]) show that nuclei can become triaxial in certain spin regions.

One can get a rough estimate of the level structure of triaxial nuclei by assuming a maximal triaxiality ($\gamma=30°$). In this case, $\vartheta_2=\vartheta_3=\frac{1}{4}\vartheta_1=\frac{1}{3}\vartheta_0$ (ϑ_0 is the moment of inertia at $\gamma=0$), and we have symmetry about the 1-axis (in the kinetic energy). The projection α of I on to this axis is a good quantum number and one finds

$$E_\alpha(I)=\frac{3\hbar^2}{8\vartheta_0}(4I\cdot(I+1)-3\alpha^2). \tag{1.77}$$

* Wilets and Jean [WJ 56] proposed a model which is completely γ-soft, i.e., $C_{22}=0$ in Eq. (1.46).

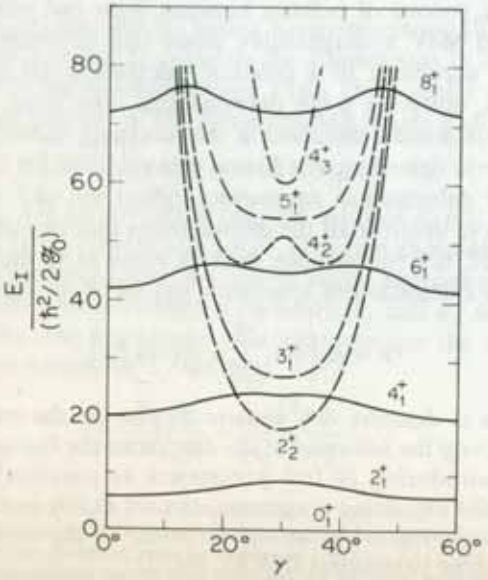

Figure 1.13. The energy eigenvalues of a deformed, asymmetric rotor with the hydrodynamic moments of inertia. (From [Me 75].)

$\mathfrak{R}_1$ and $\mathfrak{R}_2$ symmetry requires I and α to be even. For each I the level with the lowest energy (the so-called "yrast" level) has $\alpha = I$. Next in energy comes the band with $\alpha = I-2$, then $\alpha = I-4$, and so on. Therefore, we have a sequence of bands characterized by the "wobbling" quantum number $n = I-\alpha$ [BM 75]. One can calculate that the states with the same n are connected by large $E2$-transition probabilities. We get their spectrum from (1.77):

$$E_n(I) = \frac{3\hbar^2}{8\vartheta_0}(I(I+4)+3n(2I-n)). \tag{1.78}$$

However, one has to keep in mind that the structure of the spectrum (Fig. 1.13) depends drastically on the γ-dependence of the moments of inertia. There the hydrodynamical values have been used. For the rigid body values the spectrum would certainly look quite different.

1.6 Nuclear Fission

Up to now we have studied only small vibrations around the equilibrium shape in the liquid drop model. Shortly after the discovery of nuclear fission, attempts were made to understand this phenomenon using the concept of the nuclear drop [MF 39, Fr 39, BW 39].

In fact, a uniformly charged classical drop is only stable against fission (and spherical) if the Coulomb energy does not exceed a certain critical value. The Coulomb repulsion wants to deform the drop, the particles then being, on the average, further apart. The surface energy, on the contrary, being proportional to the surface of the drop, wants to keep it spherical. It is thus a subtle process of balance between these two effects (each being several hundred MeV in magnitude), which tells us whether there will be fission or not, according to a classical calculation. Of course, for such fission process, involving large deformations, one must go beyond the harmonic approximation discussed in the foregoing sections [BW 39].

The first step in describing the fission process [HW 53] is the choice of a suitable set of deformation parameters, which we call α. It has to be general enough to describe all the deformations that can occur. Cohen and Swiatecki [CS 62, 63], for instance, took as many as 18 multipolarities into account for the calculation of symmetric shapes of the form

$$R = R_0\left(1+\sum_{l=1}^{18}\alpha_l P_l(\cos\theta)\right). \tag{1.79}$$

This allows one to describe very general shapes. On the other hand, if one knows qualitatively the behavior of the droplet in the fission process, one is interested in introducing as few parameters as possible. Since one also wants to describe separated fragments, the set (1.79) is certainly not the most suitable one. For a realistic description of the fission process one needs at least three parameters [NS 65, Ni 72]:

(i) a parameter c, which describes in some way the length of the major semi-axis at the beginning of the fission process, and goes over into the distance between the separated fragments (*elongation coordinate*);

(ii) a parameter h which characterizes the thickness of the neck between the fragments in formation (*neck coordinate*);

(iii) an asymmetry parameter α_s which measures the deviation from symmetry in the mass distribution of the separating fragments (in the case of asymmetric fission) (*fragmentation coordinate*).

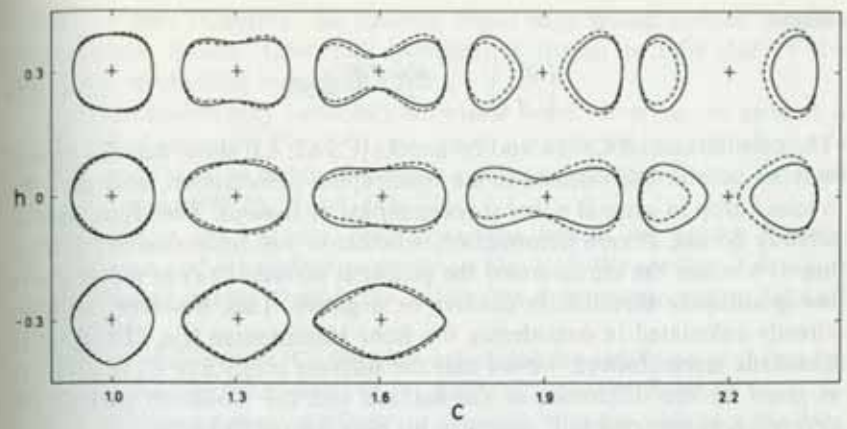

Figure 1.14. Some shapes in a suitable parameterization $\{c, h\}$. Solid lines show symmetric shapes. Dotted lines have a non-vanishing asymmetry parameter α_s. (Taken from [BDJ 72].)

Figure 1.14 shows an example for such a parameterization [BDJ 72].

In the next step, one has to calculate the *Hamiltonian* in the parameters α. The first part is the *potential energy* $V(\alpha)$. One usually measures it in units of the surface energy* of the corresponding sphere and gets

$$V(\alpha) = (B_S(\alpha)-1)+2x\cdot(B_C(\alpha)-1), \tag{1.80}$$

where B_S and B_C are the surface energy [in units of $E_S(0)$] and Coulomb energy [in units of $E_C(0) = \frac{3}{5}(eZ)^2/R_0$]. They are calculated as in Eqs. (1.32) and (1.33). However, now one can no longer suppose small deformations and must carry out the integrals explicitly. B_S and B_C depend only on the geometry. The only parameter that characterizes the nucleus is the so-called fissibility parameter x. We find

$$x = \frac{E_C(0)}{2E_S(0)} = \frac{Z^2/A}{(Z^2/A)_{\text{crit}}}, \tag{1.81}$$

*As we have discussed earlier, the potential energy can have a volume dependence corresponding to the intrinsic kinetic energy. For the large deformations implied in the fission process the dynamics can, however, have an important effect on $V(\alpha)$: Usually one assumes that the process of spontaneous fission is so slow that the nucleons have time to adjust their momentum distribution in such a way that it gives minimal total energy at each deformation. This momentum distribution is, of course, the spherical one. (For a more detailed discussion of this point, see Chap. 13.)

where

$$\left(\frac{Z^2}{A}\right)_{\text{crit}} = \frac{40\pi}{3}\frac{r_0^3\sigma}{e^2} \approx 50. \tag{1.82}$$

The calculations of Cohen and Swiatecki [CS 62, 63] show that the easiest way to deform the nucleus is the quadrupole deformation, and that the nuclear drop in general either stays spherical or fissions. Therefore, we can already decide, at zero deformation, whether or not fission occurs according to whether the curvature of the potential surface $V(\alpha)$ at the origin in the quadrupole direction is positive or negative. This, however, we have already calculated in considering the Bohr Hamiltonian [Eq. (1.17)] up to quadratic terms. Indeed, we see that the stiffness coefficient C_2 [Eq. (1.34)] is given by the difference of the surface and the Coulomb part of the deformation energy and C_2 starts to go negative for [Wi 64]

$$\frac{Z^2}{A} = \left(\frac{Z^2}{A}\right)_{\text{crit}} \quad \text{or} \quad x = 1. \tag{1.83}$$

This means that the classical droplet stays stable and spherical for $Z^2/A \lesssim 50$ or $x < 1$. For $x > 1$, it fissions immediately. This can be verified experimentally in giving increasing charge on a mercury drop.

For ^{238}U the mass formula (1.4) gives a Coulomb energy $E_C(0) = 830$ MeV and a surface energy $E_S(0) = 520$ MeV; for the fissibility parameter, we therefore obtain $x \simeq 0.8$, which is a typical value for the mass region

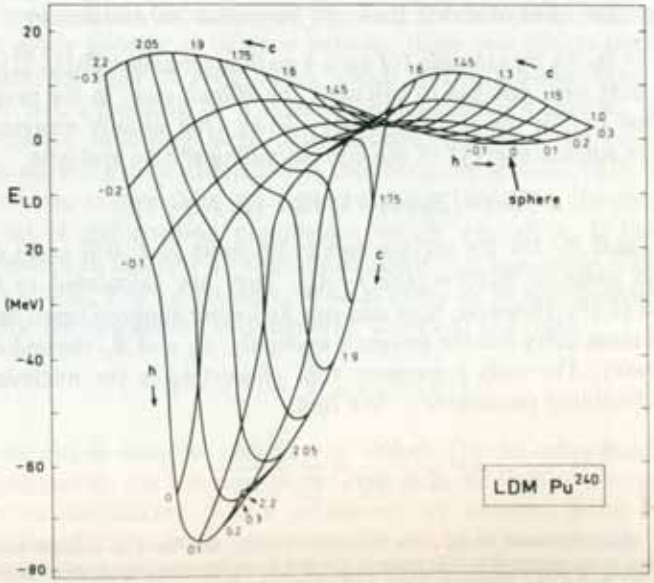

Figure 1.15. Perspective plot of the liquid drop model energy surface of ^{240}Pu. h describes the elongation and c the necking degree of freedom. (From [BDJ 72].)

$230 < A < 240$. Therefore, the classical liquid drop model cannot describe spontaneous fission. Observed spontaneous fission is thus due to the quantum mechanical tunnelling effect.

The potential energy surface (1.80) of the liquid drop has, in general, a complicated structure. For $x < 1$, we expect a minimum corresponding to a sphere, and for large distances outgoing valleys corresponding to different fragmentations [NS 65, Ni 69, MN 76].

Considering, for instance, only symmetric fission, we get for the two parameters c and h a surface as shown in Fig. 1.15. We see that it develops a well-defined saddle. Outside the saddle, the deformation energy falls off very steeply.

Cohen and Swiatecki [CS 63] have calculated the saddle-point shapes for many x-values with the ansatz (1.79). Some of them are shown in Fig. 1.16.

The meaning of these saddle-point shapes is that for a given x the drop would inevitably undergo fission if one, roughly speaking, elongates it a little bit more; conversely, it would fall back into its spherical shape if it was shortened a little bit. Going over the saddle along a line of steepest descent, the "bottom" of the fission valley defines a one-dimensional path. The length along this path is usually called the fission coordinate s. Figure 1.17 shows schematically the potential energy along this coordinate.

The fission barrier E_B is typically only a few, say, 5–7 MeV high. (This should be compared to several thousand MeV of total binding energy). Far out, the slope of the curve is due purely to Coulomb repulsion of the two droplets and thus falls off quite steeply for large Z.

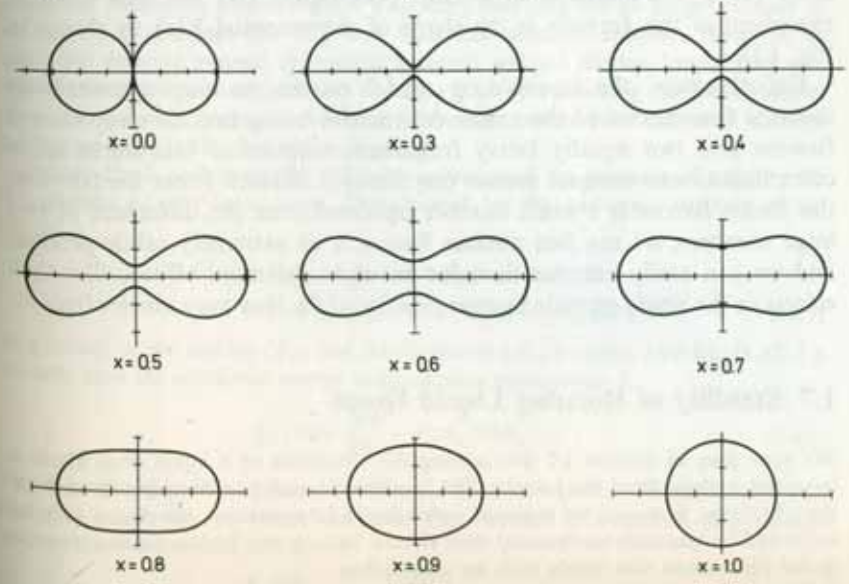

Figure 1.16. Saddle-point shapes for various values of the fissibility parameter x. (From [CS 63].)

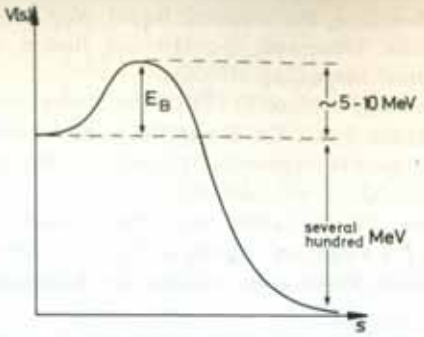

Figure 1.17. Schematic representation of the liquid drop fission barrier.

The next step in a dynamical description of fission would be the calculation of the *kinetic energy* (i.e., of mass parameters, which certainly depend on the deformation [HD 71, Gr 71]. Since the hydrodynamic model has not given good mass parameters for small oscillations, we cannot expect that it would work here either. We shall see in Section 12.3.7 how one usually calculates such quantities.

The final step would be a proper *quantization* and *solution* of the resulting Schrödinger equation. It goes far beyond the scope of this chapter to discuss such problems in detail. We only wish to mention that one usually calculates the lifetime for spontaneous fission from a WKB formula for a one-dimensional barrier penetration [Wi 64]. An essential ingredient of this formula is the shape of the potential $V(s)$, as shown in Fig. 1.17.

Unfortunately, the liquid drop model can in no way quantitatively describe fission, one of the major deficiencies being that the drop always fissions into two equally heavy fragments, whereas in fact nuclei quite often fission into unequal masses (asymmetric fission). From the fact that the fission barrier is a small number obtained from the difference of two huge numbers, we see that nuclear fission is an extremely subtle process, and we can easily imagine that, for example, quantum effects, like shell effects in the single particle motion (see Sec. 2.9), may very much affect it.

1.7 Stability of Rotating Liquid Drops

We have seen in Section 1.5 that among the vibrations of a liquid drop about a spherical surface there are rotation-like motions. In order to decouple them from the vibrations, however, we required stable finite deformations, which can only be explained by quantum mechanical shell effects. In fact, one finds rotational spectra in the experiment that justify such an assumption.

Heavy ion experiments allow the transfer of very large amounts of angular momentum (up to 80–100$\hbar$) to a nucleus. At such high excitations, one should expect that quantum effects no longer play any role, and one can then ask how a classical liquid drop having such angular velocities behaves.

In this section, we are therefore only interested in the purely classical problem of how a charged and incompressible liquid drop with a sharp surface and a certain surface energy behaves under rotation around a fixed axis in space. We are not interested in surface vibrations and therefore look for the stable shapes in this system.

Again we have to say something about the flow structure in this drop, and we shall assume rigid rotation; i.e., the moment of inertia is given by

$$\vartheta = \vartheta^{\text{rig}} = \int_V r_\perp^2 \rho_0 \, d^3r, \tag{1.84}$$

where $r_\perp$ is the distance of the volume d^3r from the rotational axis. As we shall see in Section 3.4, this assumption is very reasonable, because one expects the nuclear moment of inertia to approach the rigid value for high angular momenta.

The problem is very similar to the old astronomical problem of gravitating and incompressible homogeneous rotating masses. There the attractive force is the gravitation, which has the same structure (but the opposite sign) as the Coulomb force, and a surface force is neglected. Beginning with Newton, this problem has been studied by many famous mathematicians (for a historical review, see [Ch 69, Chap. 1]).

One of the results is that a gravitating droplet without surface tension has, for vanishing angular velocity ω, a spherical shape. With $\omega > 0$, it assumes first exact oblate spheroidal shapes where the rotational axis is an axis of symmetry (*Maclaurin shapes*). For increasing ω it flattens more and more, up to a certain angular velocity ω_I. For ω-values larger than ω_I, a new type of stable shape develops*—triaxial ellipsoids (*Jacobi shapes*)—and the drop rotates around the shortest principal axis. This point, ω_I, is called a bifurcation point, because for $\omega > \omega_I$ the Maclaurin shapes are still stationary, but they are no longer minima in all degrees of freedom [Ro 67]. One calls this *secularly unstable*. However, in uniformly rotating systems (gyrostatic systems) without friction forces, they can represent a stable motion (*ordinary stability*) [Ly 58]. Following the Jacobi shapes for higher ω-values, one reaches further bifurcation points. New shapes of stability develop and finally the droplet disintegrates.

Cohen, Plasil, and Swiatecki [CPS 74] investigated the problem of stability for the rotating nuclear liquid drop. They looked for the stationary surfaces of the energy

$$\begin{aligned} E(\alpha) &= E_S(\alpha) + E_C(\alpha) + E_R(\alpha) \\ &= E_S(0)(B_S(\alpha) + 2x \cdot B_C(\alpha) + yB_R(\alpha)). \end{aligned} \tag{1.85}$$

In addition to the surface (E_S) and the Coulomb (E_C) energies (see Eq. (1.32) f.), we now have the rotational energy at an angular momentum I:

$$E_R(\alpha) = \frac{\hbar^2 I^2}{2\vartheta(\alpha)} = yE_S(0)B_R(\alpha). \tag{1.86}$$

The moment of inertia is given by Eq. (1.84): $\vartheta(0) = \frac{2}{5}MR_0^2$. In addition to the fissibility parameter x, which measures the relation of Coulomb and surface energy, there is now the parameter

$$y = \frac{E_R(0)}{E_S(0)} = \frac{5}{16\pi} \frac{\hbar^2 I^2}{\sigma m r_0^4} \frac{1}{A^{7/3}} \approx 2I^2 A^{-7/3}, \tag{1.87}$$

*This corresponds to a second-order phase transition [BR 76].

which measures the relation of rotation and surface energy. The parameters x and y are determined by the properties of the nucleus and by the angular momentum one is interested in; again, the rest is pure geometry.

The result of these investigations [CPS 74] is that the nucleus behaves similarly to the gravitating droplet. At low angular momenta (low y-values), one gets flattened shapes with axial symmetry around the rotational axis. They are called *Hiskes shapes* and look similar to exact spheroids (Maclaurin shapes). They remain stable up to a critical value y_I, which corresponds to the *Jacobi point*. The value of y_I depends on x. For very heavy nuclei $x > 0.81$ the system fissions for $y > y_I$. For the rest of the nuclei a new kind of stable shape develops. These are called *Beringer–Knox shapes* [BK 61] and are similar to the Jacobi shapes. For very large angular momenta, these shapes get nearly axially symmetric around an axis perpendicular to the symmetry axis and finally become unstable against fission (y_{II}).

These calculations involve a large number of deformation parameters. One can describe the same features under the restriction of pure ellipsoidal shapes, whose half-axes a_1, a_2, a_3 are given by the two parameters β and γ*:

$$a_\kappa = R_0 \exp\left\{ \sqrt{\frac{5}{4\pi}}\ \beta \cos\left(\gamma - \frac{2\pi}{3}\kappa\right)\right\} \qquad (\kappa = 1, 2, 3). \tag{1.88}$$

This definition guarantees volume conservation.

* We have used the Hill–Wheeler coordinates β and γ already for the description of small quadrupole deformations [Eq. (1.13)] of the nuclear surface. Here we define the nuclear surface as an exact ellipsoid by its half axis. This was the original definition of Hill and Wheeler [HW 53]. It agrees with Eq. (1.7) only for small β-values.

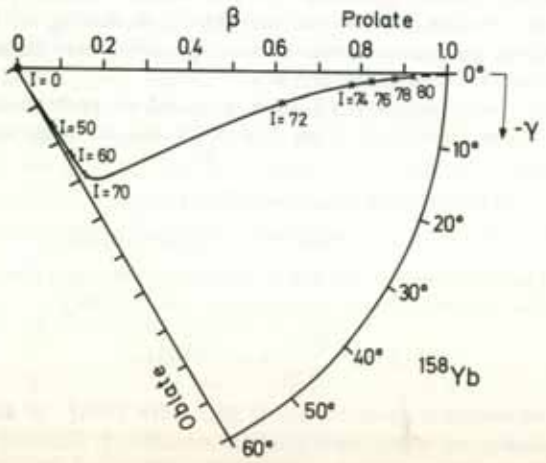

Figure 1.18. The equilibrium shapes (in terms of β and γ) of a rotating liquid drop as a function of angular momentum I. Since the 1-axis is the axis of rotation, we need negative γ-values, in contrast to the usual case where the three axes are equivalent. The nucleus ^{158}Yb has a value of $x = 0.618$. (From [ALL 76].)

It is relatively easy to calculate the rigid moment of inertia, and the surface and the Coulomb energies for these ellipsoids* as a function of β and γ and to look for the minimum of the energy surface for each value of I. Connecting these stable shapes, one gets a trajectory in the β–γ plane, as in Fig. 1.18.

For each I, we have an energy surface whose local minima are investigated. As in the case of $I = 0$ (Sec. 1.6), there also exists, besides the minimum, a fission valley with a saddle point. Because of the centrifugal force, the barrier height gets smaller for increasing angular momentum and a family of shapes becomes unstable against fission if the barrier disappears. As an example, we take the nucleus ^{127}La [CPS 74]. At angular momentum $I = 0$ its LDM fission barrier is 40.0 MeV high. Its Jacobi point (y_I) corresponds to $I = 67.8\hbar$. At this angular momentum it has an excitation energy of 44.31 MeV [$E_S(0) = 49.5$ MeV] and the barrier height is only 7.8 MeV.

From this consideration it becomes clear that no nucleus can support more than a limiting angular momentum, otherwise it becomes unstable against fission. Figure 1.19 shows the angular momenta I_{II} at which the fission barrier vanishes as a function of the mass number A in the valley of beta stability [approximated by $N = A/2 + 0.2 \cdot A^2/(200 + A)$]. Light nuclei cannot support many units of angular momentum, because of their small size. Heavy nuclei have a reduced stability caused by the Coulomb energy. Nuclei with $A \simeq 130$ can reach the highest angular momenta of $\sim 100\hbar$. Experiments with heavy ions [BES 76] seem to be consistent with these limiting values of the liquid drop model.

* See, for instance, [Ca 61, CM 63].

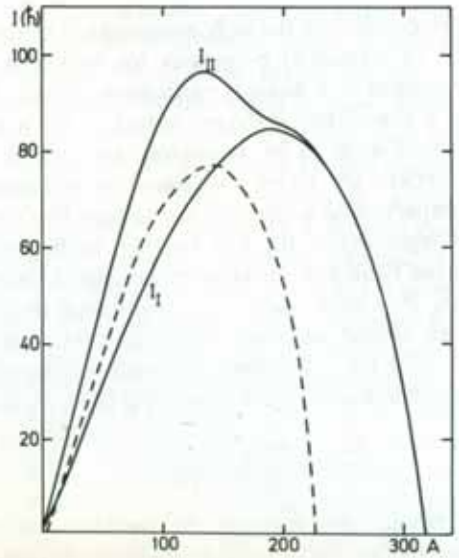

Figure 1.19. Maximal angular momentum I_{II} that a β-stable nucleus with mass number A can support, and the critical angular momentum I_I (Jacobi-bifurcation point). The dashed line corresponds to fission barrier heights of 8 MeV, which guarantees a reasonable lifetime against fission. (From [CPS 74].)

CHAPTER 2

The Shell Model

2.1 Introduction and General Considerations

In the last chapter we considered the bulk properties of the nucleus, that is, we discussed (static or dynamic) properties for which at least a good fraction of all the nucleons in a nucleus participate. In this chapter we are going to talk about a completely different aspect of the nucleus. Indeed, many nuclear properties seem to be describable in terms of the idea that the nucleons in a nucleus are to be considered as independent particles moving on almost unperturbed single particle orbits. The reasons for this, as we stated at the beginning of the first chapter, is the fact that, mostly due to the action of the Pauli and uncertainty principles, the nucleus is not a very dense system. It is now quite well established that the nucleon–nucleon force has an almost infinitely repulsive core (see [Vi 78]) at a radius c of about $c=0.4$ fm. Therefore, the ratio of the closest packed volume V_c to the actual volume V of a nucleus is [BM 69, Sec. 2.5]

$$\frac{V_c}{V}=\left(\frac{c}{2r_0}\right)^3\simeq\frac{1}{100}.$$

Thus the known "strong" character of the nucleon–nucleon forces is considerably reduced by the fact that the nucleons are, on the average, quite far apart, and therefore "feel" only the tail of the attractive part of the nuclear force. In other words, the violent interactions due to the singular force occur only quite seldom and the system can be described, at least in a first approximation, in terms of independent particle motion. The fact that despite these considerations the nucleus develops a very well-defined surface, contrary to a gas, is due to a very subtle interplay of the nuclear forces and the Pauli principle [BP 77a]. For a further, more elaborate discussion of these considerations, see also [BM 69, Sec. 2.5]. The mean free path of the nucleons in a nucleus, as can be estimated from scattering experiments, seems to be at least of the order of the dimension of the nucleus [BM 69, Sec. 2.1; KK 68] and is mentioned as the first piece of experimental evidence for the unperturbed particle motion in a nucleus.

The idea of independent particles accepted, it is quite natural to envisage that this single particle motion is governed by some average potential created by all the nucleons in the nucleus. Of course, the motion of the nucleons will be considerably different in the interior of the nucleus, where it is more or less force free, from the one at the surface where the Pauli principle ceases to act and the particles feel a force confining them to the interior of the nucleus.

In this chapter we will briefly describe further experimental evidence for, and the phenomenological description and consequences of, such an average potential.

2.2 Experimental Evidence for Shell Effects

If the validity of an average potential in which the nucleons can move independently can be assumed, this immediately has some obvious consequences similar to those with which we are familiar from atomic physics.

The occurrence of the so-called magic numbers 2, 8, 20, 28, 50, 82, and 126 has, from the experimental point of view, been one of the strongest motivations for the formulation of a nuclear shell model. At these proton or neutron numbers, effects analogous to shell closure of electron shells in atoms are observed. Here we will mention just a few of them.

The single-particle separation energy is defined as the energy required to remove the least bound particle from the nucleus. In Fig. 2.1 the observed separation energies for protons and neutrons are shown.

For most nuclei the separation energy is about 8 MeV, although there are quite prominent exceptions at the magic numbers. The separation energy is largest for doubly magic nuclei. Similar exceptions for the separation energy are found for the electrons in noble gases.

The magic numbers can be seen in Fig. 2.2, which shows that the magic and doubly magic nuclei are exceptionally strongly bound. Strong binding means that the nucleus is very stable against excitations, and in Fig. 1.7 we have already shown the variation of the first 2^+ state in nuclei as a function of nucleon number. We can see especially pronounced shell effects at the magic numbers, the excitation energy rising sharply in the neighborhood of shell closures. Other collective excitations show the same variation. These examples should be sufficient as a demonstration of the occurrence of magic numbers in nuclei and of the shells corresponding to

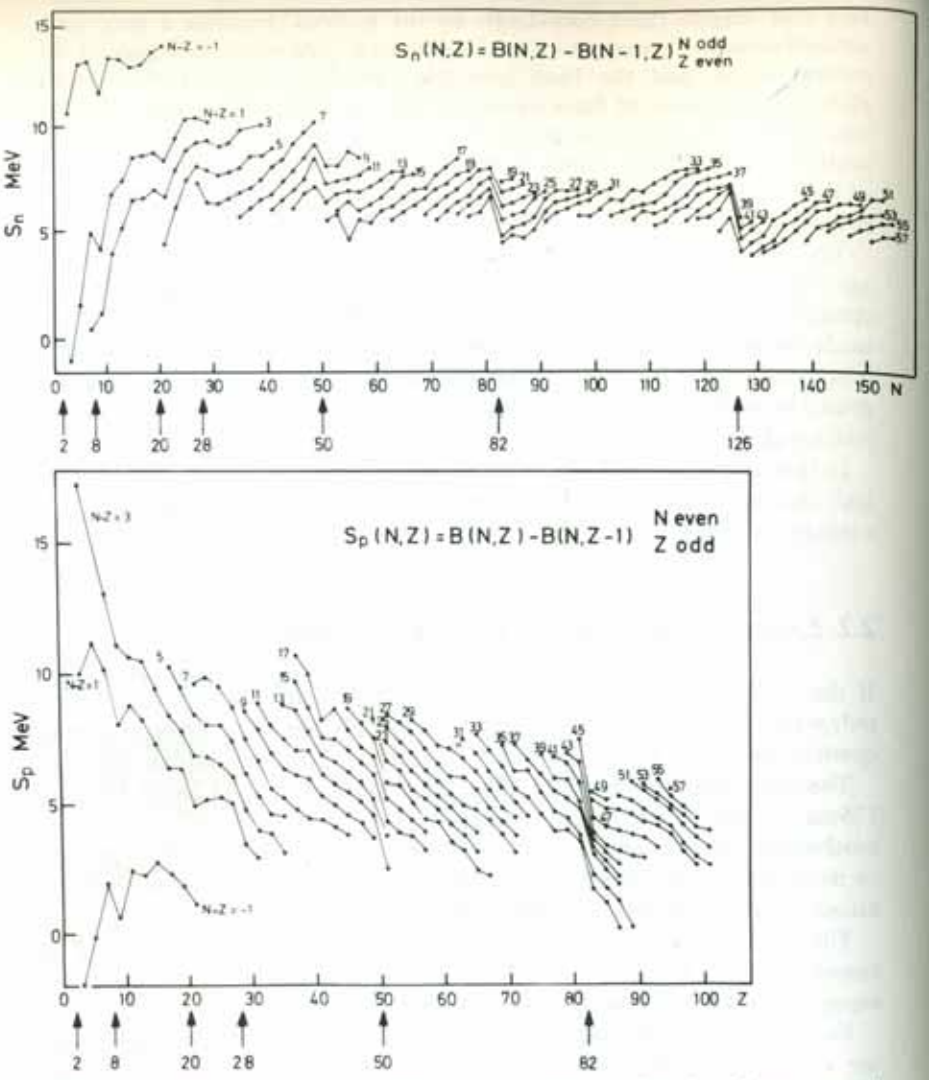

Figure 2.1. Neutron and proton separation energies as a function of neutron and proton number, respectively. (From [Ir 72].)

an average potential analogous to the ones observed in atoms. (More details may be found in [MJ 55].)

2.3 The Average Potential of the Nucleus

As mentioned above, the exceptional role of the magic numbers reveals a strong analogy to the situation of the electrons in an atom. There the strong central Coulomb potential of the nucleus imposes sphericity. As a consequence, there exist groups of degenerate levels with quite large energy differences in between the electron shells.

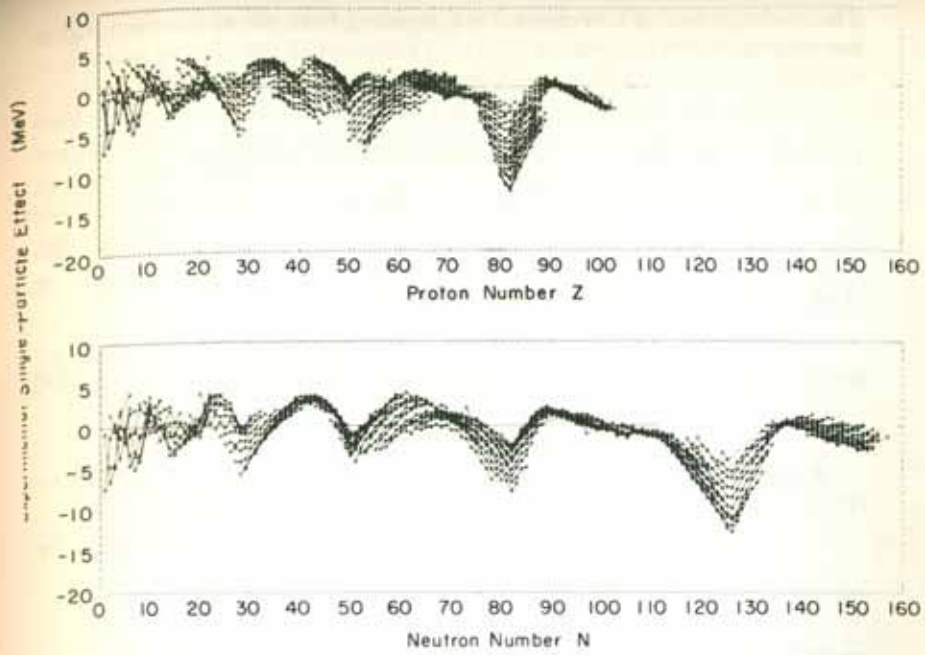

Figure 2.2. Deviations of nuclear masses from their mean values plotted as a function of neutron and proton number. (From [MS 66].)

For the nucleons of a nucleus, there exists a priori no such central field. As we have already discussed in the introduction, however, we can imagine such a potential as being built up by the action of all the nucleons. (Such an average potential also exists in the case of the electrons in an atom; there it makes an extra contribution and has to be added to the nuclear Coulomb potential. The whole is then well known as the Hartree or Hartree–Fock potential of the atom.) A model which describes the dynamics of the nucleons only with such an average potential treats the nucleons as completely independent of one another (the nucleon–nucleon interaction nevertheless comes into it in an indirect way, since it gives rise to the average potential in the first place). In the following, we will call such a model the shell model or independent particle model.

In Chapter 5 we will discuss, in great detail, how one can derive the form of this average field from a microscopic two-body force. In this chapter, we will assume that we have such a one-body potential which describes, to a good approximation, the effects of the mutual interaction between the nucleons, and investigate their consequences.

For further consideration, we have to discuss first the shape of the ad hoc introduced shell model potential. A nucleon close to the center of the nucleus will feel the nuclear forces uniformly, that is, there will be no net force

$$\left(\frac{\partial V(\mathbf{r})}{\partial r}\right)_{r=0} = 0. \tag{2.1}$$

The nuclear binding forces get stronger going from the surface ($r = R_0$) to the interior of the nucleus:

$$\left(\frac{\partial V}{\partial r}\right)_{r<R_0} > 0. \tag{2.2}$$

Because of the finite range of the nuclear forces, we have:

$$V(r) \simeq 0, \qquad r > R_0. \tag{2.3}$$

An analytic ansatz which represents these conditions quite well, and also yields quite reasonable density distributions, is the Fermi function or *Woods–Saxon potential* [WS 54] (Fig. 2.3):

$$V^{\mathrm{W.S.}}(r) = -V_0\left[1+\exp\left(\frac{r-R_0}{a}\right)\right]^{-1} \tag{2.4}$$

with

$$R_0 = r_0 A^{1/3}; \qquad V_0 \simeq 50\,[\mathrm{MeV}]; \qquad a \simeq 0.5\,[\mathrm{fm}]; \qquad r_0 \simeq 1.2\,[\mathrm{fm}].$$

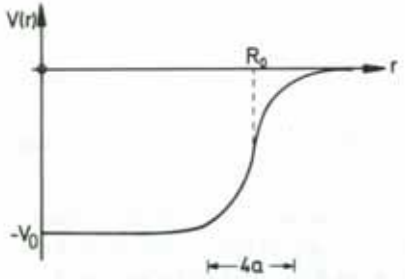

Figure 2.3. Shape of the Woods–Saxon potential.

(The Woods–Saxon potential actually has a finite but negligible slope at $r = 0$.) Since the eigenfunctions for this potential cannot be given in closed form, one often uses the following two approximations for qualitative considerations, and also for calculations:

(i) harmonic oscillator

$$V(r) = -V_0\left[1-\left(\frac{r}{R_0}\right)^2\right] = \frac{m}{2}\omega_0^2(r^2 - R_0^2) \tag{2.5}$$

(ii) square well

$$V(r) = \begin{cases} -V_0 & \text{for } r \leqslant R_0, \\ +\infty & \text{for } r > R_0. \end{cases} \tag{2.6}$$

Before we discuss the solutions of Eqs. (2.4), (2.5), and (2.6) in more detail, we should perhaps note that all three potentials are spherically symmetric. For the moment, we will restrict our considerations to this case; the discussion of deformed potentials will be taken up in Section 2.8. Furthermore, it should be pointed out that (2.5) and (2.6) represent somewhat unphysical potentials, since they are infinite. However as long as we are only interested in bound single-particle states, this is not too serious a drawback, as only the exponential tails of the wave functions are affected. If one considers excitations in these potentials, however, one easily gets into regions in which the states in the realistic potential (2.4) would be in the continuum. The use of infinite potentials in such cases is then to be considered with extreme care.

After these preliminary remarks, we want to discuss the energy levels obtained from the solution of the eigenvalue problem

$$\left\{-\frac{\hbar^2}{2m}\Delta + V(\mathbf{r})\right\}\phi_i(\mathbf{r}) = \epsilon_i\phi_i(\mathbf{r}) \tag{2.7}$$

for the case of the potentials (2.5) and (2.6).

As is well known, the harmonic oscillator gives equidistant energy levels

$$\epsilon_N = \hbar\omega_0\left(N+\frac{3}{2}\right) - V_0 \tag{2.8}$$

with

$$N = 2(n-1)+l, \qquad \text{where } n = 1, 2, \ldots, \text{ and } l = 0, 1, 2, \ldots. \tag{2.9}$$

These levels are $D(N)$-fold degenerate:

$$D(N) = \frac{1}{2}(N+1)(N+2), \tag{2.10}$$

where N is the number of quanta in the oscillator, n is the radial quantum number, l is the angular momentum, and ω_0 is the oscillator frequency. The oscillator constant ω_0 is usually determined from the mean square radius of a sphere

$$\langle R^2\rangle = \frac{1}{A}\sum_{i=1}^{A}\langle r^2\rangle_i \simeq \frac{3}{5}(1.2A^{1/3})^2\,[\mathrm{fm}^2]. \tag{2.11}$$

For oscillator states we can calculate $\langle r^2\rangle_i$ and get

$$\frac{m}{2}\omega_0^2\langle r^2\rangle_i = \frac{\hbar\omega_0}{2}\left(N_i+\frac{3}{2}\right).$$

Together with Eq. (2.10), we find [Mo 57, p. 469]

$$\hbar\omega_0 \simeq \frac{5}{4}\left(\frac{3}{2}\right)^{1/3}\frac{\hbar^2}{mr_0^2}A^{-1/3} = 41\cdot A^{-1/3}\,[\mathrm{MeV}] \tag{2.12}$$

and for the oscillator length

$$b = \sqrt{\frac{\hbar}{m\omega_0}} = 1.010\cdot A^{1/6}\,[\mathrm{fm}]. \tag{2.13}$$

The levels with a definite N we call an oscillator shell. Because of Eq. (2.9), the oscillator shells only contain either even or odd l-values, that is one oscillator shell contains only states with the same parity. It also follows from (2.9) that levels with the same N and with different n and l are degenerate. This accidental degeneracy of the harmonic oscillator is removed in the square-well potential (Fig. 2.4). The true energies lie between the two limits given by the potentials of Eqs. (2.5) and (2.6).

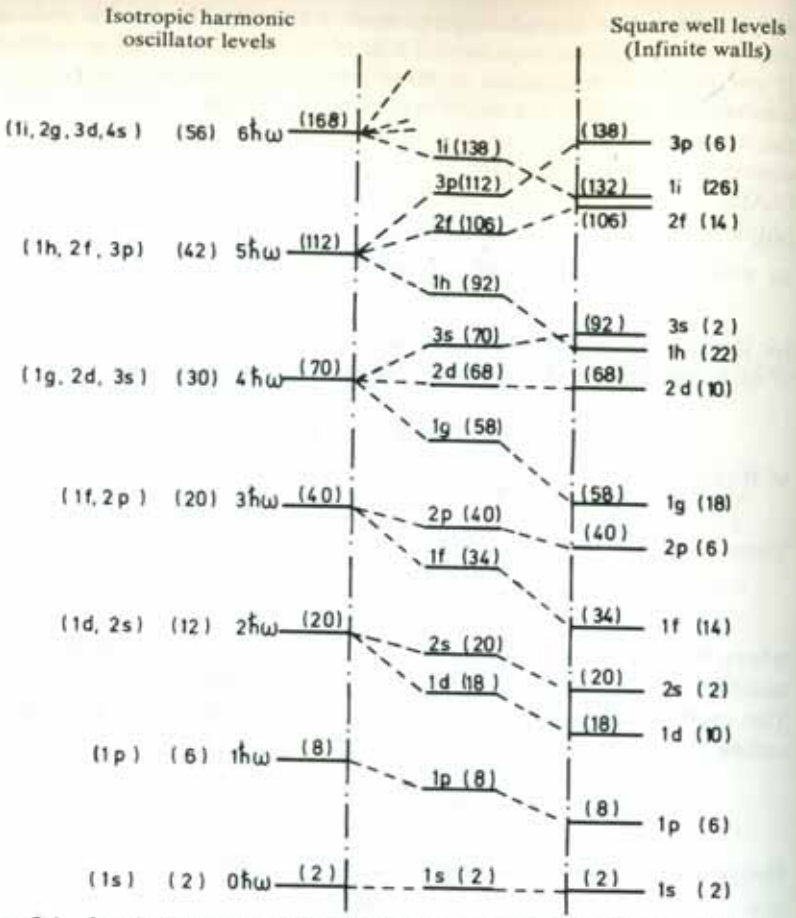

Figure 2.4. Level scheme of the isotropic harmonic oscillator (l.h.s.) and of the infinite square well (r.h.s.). (From[MJ 55]).

Filling up the level scheme with nucleons (by analogy with the periodic system of the atoms), we see that according to the Pauli principle, $D(N)$ protons and $D(N)$ neutrons can be put into each oscillator shell. This means that both potentials reproduce the magic numbers 2, 8, and 20. This model can therefore account for the unusual stability of ${}^{4}_{2}\mathrm{He}_2$, ${}^{16}_{8}\mathrm{O}_8$, and ${}^{40}_{20}\mathrm{Ca}_{20}$. On the other hand, Fig. 2.4 contains no indications for the higher magic numbers. We will see in the next section how this deficiency of this simple model can be removed. Later, we will also discuss how the Coulomb interaction of the protons influences the average potential (Sec. 2.5).

2.4 Spin Orbit Coupling

Up to now, we have not taken into account the spin of the nucleons (apart from a factor of 2 in determining the magic numbers), that is, we considered the nuclear forces as spin independent. Treating the electrons in atoms relativistically yields a spin dependent force in the form of a spin orbit coupling

$$f(r)\mathbf{ls}. \tag{2.14}$$

This gives a splitting of the otherwise degenerate levels with $j = l \pm \frac{1}{2}$. In the nucleus such a splitting has also been found experimentally. Scattering of protons or neutrons on α particles yields for the lowest resonance the (unbound) ground state of ${}^{5}\mathrm{Li}$ or ${}^{5}\mathrm{He}$. According to Fig. 2.4 these lowest resonances should have the quantum numbers $l=1$, $j=\frac{1}{2},\frac{3}{2}$, as the 1s-shell in ${}^{4}\mathrm{He}$ is closed. One observes resonances at 1.25 and 2.4 MeV for the scattering of neutrons and protons, respectively. At these energies the angular distributions show that the resonances are predominantly $j=\frac{3}{2}$, whereas the $j=\frac{1}{2}$ resonances lie a few MeV higher in energy.

It was a decisive idea (Haxel, Jensen, and Suess [HJS 49]; Goeppert–Mayer [Ma 49]) to incorporate a strong spin orbit term into the single-particle Hamilton operator of Eq. (2.7). It was only then that the success of the shell model was confirmed. Mathematically this yields a *jj*-coupling scheme, since $\mathbf{l}\cdot\mathbf{s}$ commutes with $\mathbf{s}^2, \mathbf{l}^2, \mathbf{j}^2, j_z$ but not with l_z and s_z. The levels are characterized in this coupling scheme by the quantum numbers n, l, j (e.g., $(2d\frac{5}{2}) \triangleq (n=2, l=2, j=2+\frac{1}{2})$), and a single particle wave function takes the following form*:

$$\phi(\mathbf{r})_{nsljm} = \langle \mathbf{r} | nsljm \rangle = \phi_{nl}(r) \sum_{m_l m_s} C^{\frac{1}{2}\ l\ j}_{m_s\ m_l\ m} Y_{lm}(\theta,\phi) | \tfrac{1}{2} m_s \rangle. \tag{2.15}$$

With the relations

$$\begin{aligned} 2\mathbf{ls}|sljm\rangle &= (\mathbf{j}^2 - \mathbf{l}^2 - \mathbf{s}^2)|sljm\rangle \\ &= \left[j(j+1) - l(l+1) - \tfrac{3}{4} \right] |sljm\rangle \end{aligned} \tag{2.16}$$

we are able to give the spin orbit splitting of the doubly degenerate levels $|slj = l \pm \frac{1}{2}\rangle$ for $f(r) = \text{const.}$:

$$\Delta E(l) \sim \left[l - (-l-1) \right] = 2l + 1. \tag{2.17}$$

An attractive spin orbit potential will assure the experimentally observed fact that the $l+\frac{1}{2}$ levels are energetically always below the $l-\frac{1}{2}$ levels. Equation (2.17) shows furthermore that the splitting increases with growing values of l.

Inclusion of the spin orbit interaction to the interpolated level scheme of Fig. 2.4 yields the modified level scheme of Fig. 2.5. The model now reproduces all magic numbers correctly. The sequence of the levels within the different shells depends on the choice of $f(r)$.

The value of $f(r)$ which one could derive by analogy with the theory of electrons in an atom using a Lorentz invariant treatment of the electromagnetic interactions of the nucleons (Thomas term: cf. [MJ 55, p. 60] and [EG 70, Chap. 8]) turns out to be about an order of magnitude too small.

* For calculations one has to pay particular attention to the coupling order of the angular momenta, since a different order introduces a phase which is the source of frequent errors.

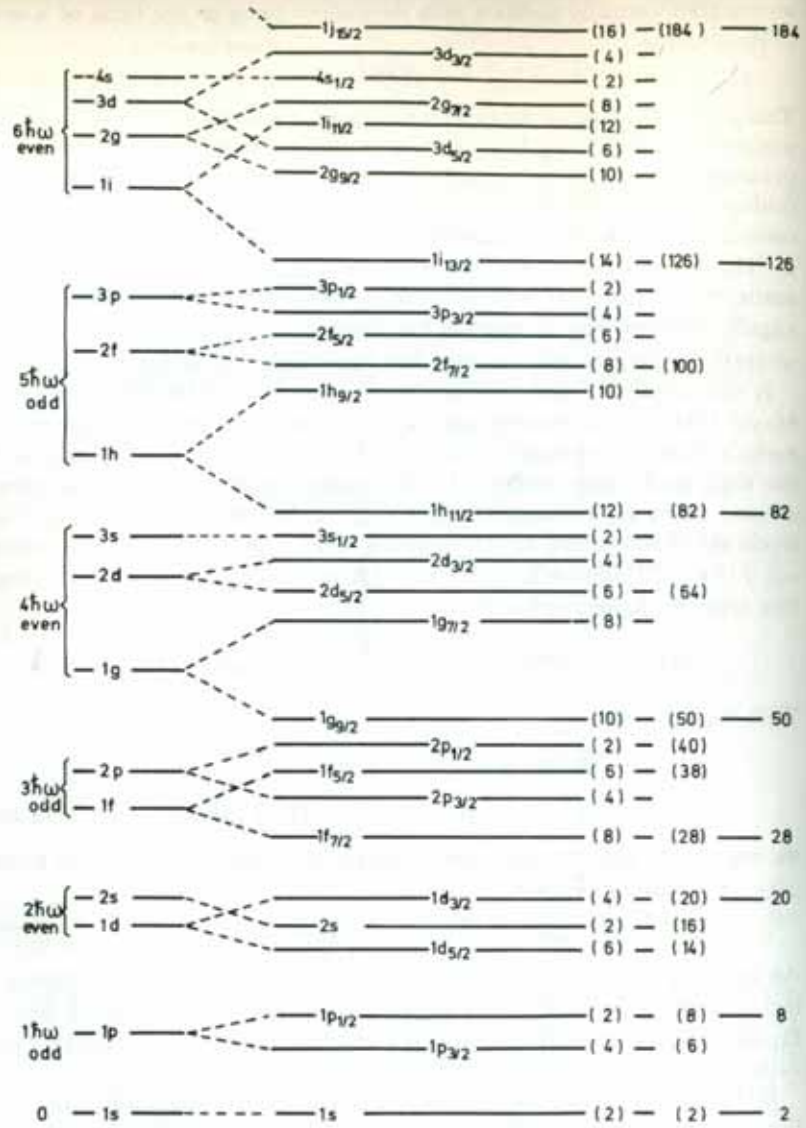

Figure 2.5. Schematic nuclear levels of the shell model with spin orbit term. (From [MJ 55].)

As we will discuss in Chapter 4, the nucleon–nucleon forces exhibit strong spin orbit parts, and it is thus not very surprising that the average single particle potential also has a spin orbit part with a strength compatible with the strong nuclear forces.*

* Recent investigations have shown that one obtains the proper spin orbit term in the single-particle potential by a relativistic Hartree–Fock treatment of one-boson-exchange-potentials [Br 78].

One can show [Ho 75] that $f(r)$ is peaked at the nuclear surface. By analogy with the electronic case, one quite often chooses $f(r)$ related to the spin independent part of the average potential in the following way—

$$f(r)=\lambda\frac{1}{r}\frac{dV}{dr}; \qquad \lambda\simeq -0.5\ [\mathrm{fm}^2] \tag{2.18}$$

—but also other surface-peaked radial dependences of $f(r)$ can be envisaged. It is interesting to note that the use of the Skyrme force (see Chap. 5) yields a spin orbit dependence for the average potential with $f(r)\sim(1/r)\cdot(d\rho/dr)$, where ρ is the single particle density. Since $V(r)$ roughly follows the form of ρ, this is consistent with Eq. (2.18).

2.5 The Shell Model Approach to the Many-Body Problem

The single-particle model takes into account the individual nucleons. It therefore provides a microscopic description of the nucleus. This is certainly only an approximation of the exact many-body problem. We will see, however, in the following, that the shell model can be used as a basis for more elaborate many-body theories, so before we talk about further details of the model, we want to discuss some general properites of the single particle model.

The microscopic theory of the nucleus is usually based on the following three properties.

(i) The nucleus is a quantum mechanical many-body system.
(ii) The velocities in the nucleus are small enough so that one can neglect relativistic effects $[(v/c)^2\sim 1/10]$.
(iii) The interaction between the nucleons has a two-body character.

A full microscopic theory of the nucleus would then be given by the solution of the many-body Schrödinger equation

$$H\Psi=\left\{\sum_{i=1}^{A}-\frac{\hbar^2}{2m}\Delta_i+\sum_{i<j}^{A}v(i,j)\right\}\Psi(1,\ldots,A)=E\Psi(1,\ldots,A), \tag{2.19}$$

where i represents all coordinates of the ith nucleon, for instance,

$$(i)=(\mathbf{r}_i,s_i,t_i), \tag{2.20}$$

where t_i will be $\frac{1}{2}$ for neutrons and $-\frac{1}{2}$ for protons. With the assumption of the nuclear shell model, the above equation reduces to the much simpler equation

$$H_0\Psi=\left\{\sum_{i=1}^{A}h_i\right\}\Psi=\sum_{i=1}^{A}\left\{-\frac{\hbar^2}{2m}\Delta_i+V(i)\right\}\Psi=E\Psi. \tag{2.21}$$

The solutions Ψ of Eq. (2.21) are anti-symmetrized products of single-particle functions, which are eigenfunctions to the single-particle Hamilto-

nian h_i:

$$h_i\phi_k(i)=\epsilon_k\phi_k(i). \tag{2.22}$$

The functions ϕ_k provide an orthogonal basis for an occupation number representation within the framework of second quantization (see Appendix C). To each level k corresponds a pair of creation and annihilation operators a_k^+, a_k which create or annihilate particles with wave function ϕ_k. Since nucleons are Fermions, each level can be occupied only once, and the operators a_k, a_k^+ obey Fermi commutation relations (C. 23).

The shell model Hamiltonian H_0 has the form

$$H_0=\sum\epsilon_k a_k^+ a_k.$$

Using the bare vacuum $|-\rangle$ its eigenfunctions can be represented as

$$|\Phi_{k_1\ldots k_A}\rangle=a_{k_1}^+\ldots a_{k_A}^+|-\rangle.$$

They are Slater determinants

$$\Phi_{k_1\ldots k_A}(1,\ldots,A)=\begin{vmatrix}\phi_{k_1}(1) & \cdots & \phi_{k_1}(A)\\ \vdots & & \vdots\\ \phi_{k_A}(1) & & \phi_{k_A}(A)\end{vmatrix} \tag{2.23}$$

with eigenvalues

$$E_{k_1\ldots k_A}=\epsilon_{k_1}+\cdots+\epsilon_{k_A}. \tag{2.24}$$

In the ground state the levels are filled successively according to their energy (see Fig. 2.6)

$$|\Phi_0\rangle=a_1^+\ldots a_A^+|-\rangle. \tag{2.25}$$

Thus we have for closed shells the following unique prescription for the construction of the A particle ground state as well as for the A particle excitation spectrum: Starting with the $(1s_{1/2})$ level, one has to occupy each level $|nsljm\rangle$ with just one particle until all A particles are used up. We thus obtain an A nucleon ground state where all different quantum states are occupied with just one particle up to the Fermi level (the highest occupied level); above the Fermi level all levels are unoccupied.

The independent particle picture of the nucleus is different from that in an atom in the sense that in a nucleus there are *two* different kinds of particles, the proton and the neutron, whereas in an atom there is only the

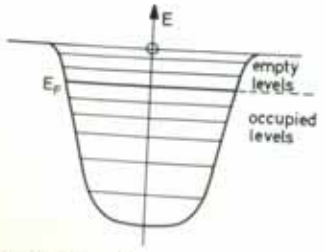

Figure 2.6. Shell model potential and Fermi level.

electron. Protons and neutrons feel different average potentials for two reasons:

(i) Protons also interact via the *Coulomb force*. One therefore usually adds the potential of a homogeneously charged sphere

$$V_C(\mathbf{r})=\begin{cases}\dfrac{Ze^2}{R}\dfrac{1}{2}\left(3-\left(\dfrac{r}{R}\right)^2\right) & r\leqslant R,\\[2ex] \dfrac{Ze^2}{r} & r>R.\end{cases} \tag{2.26}$$

Sometimes (see Sec. 2.8), this feature is approximated by using different potential parameters for protons and neutrons.

(ii) The *symmetry energy* [see Eq. (1.4)] favors a configuration with an equal number of protons and neutrons. Because of the Coulomb repulsion for heavier nuclei, one has a neutron excess: If, in the nucleus, we replace a neutron by a proton, we gain symmetry energy and lose Coulomb energy. Since the Coulomb energy is already taken into account by Eq. (2.26), there must be an additional difference between the single-particle potential for protons and neutrons, which is caused by the symmetry energy. The *nuclear* part of the proton potential is therefore deeper (see Fig. 2.7, dashed line).

These two effects go in opposite directions, but they do not cancel. In the end, the Fermi surfaces for protons and neutrons must be equal, otherwise protons would turn into neutrons by β-decay or vice versa, whichever is energetically favored.

In $N\neq Z$ nuclei, energy levels with the same quantum numbers for protons and neutrons are therefore shifted with respect to one another by an amount Δ_ϵ resulting from a positive contribution Δ_C from the Coulomb force and a negative contribution $-\Delta_S$ from the symmetry energy

$$\epsilon_{nlj}^{(p)}-\epsilon_{nlj}^{(n)}=\Delta_\epsilon=\Delta_C-\Delta_S. \tag{2.27}$$

In heavy nuclei, this difference is such that the protons and neutrons at the Fermi surface belong to different major shells.

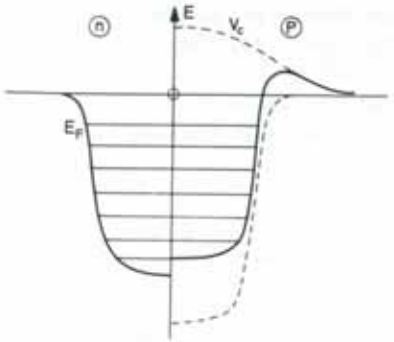

Figure 2.7. Comparison of the shell model potential for neutrons and protons in a nucleus with neutron excess.

Strong support of the independent particle idea comes from the experimental fact that magic numbers are the same for protons and neutrons (see Fig. 2.2; the magic number 126 exists only for neutrons, since for the heaviest nucleus known so far we only have $Z=103$). If correlations played a major role, then, for example, the neutron excess in heavier nuclei would eventually influence the proton magic numbers in these nuclei (the nuclear force is almost charge independent; see Chap. 4) to be different from the corresponding neutron numbers. However, as we have said, this is not the case. The subshells of a major shell have, in some cases, a different order.

In the shell model, the *excitations of the system* are given by analogy with the free Fermi gas by a transfer of nucleons from below the Fermi level to levels above it. In the case of only a single nucleon transfer, we talk of an $1p-1h$ state with excitation energy of $\sim\hbar\omega_0$. For $^{40}_{20}Ca_{20}$ such a state is, for example, given by

$$(2s\tfrac{1}{2})^{-1}(1f\tfrac{7}{2}).$$

The Fermi level coincides in this case with the $1d_{3/2}$ level (see Fig. 2.5).

If we use the indices i, j for the levels below the Fermi surface ($\epsilon_i \leqslant \epsilon_F$), and the indices m, n for the levels above the Fermi surface ($\epsilon_n > \epsilon_F$), the lowest excitations in the shell model are then *ph* excitations of the form

$$|\Phi_{mi}\rangle := a_m^+ a_i|\Phi_0\rangle = \pm a_m^+ a_1^+ \ldots a_{i-1}^+ a_{i+1}^+ \ldots a_A^+|-\rangle \tag{2.28}$$

with excitation energy $\epsilon_{mi} = \epsilon_m - \epsilon_i$.

In fact one has observed such states in magic nulcei. They are, however, not the lowest states. As we have already seen in Chapter 1, there are low-lying collective states which cannot be explained in the independent particle model.

The Slater determinants (2.23) form a *complete set* of states for the A nulceon system [Lö 55]. Each state of the system is characterized by the distribution of the nucleons among the levels of the single particle potential, that is, by the "occupation numbers" of the levels. It is usual to classify all excited states by taking the ground state as a reference state. The nucleons that are missing in the ground state are denoted by holes, those above the Fermi levels by particles. A typical multiparticle–multihole configuration is shown in Fig. 2.8

Starting from a magic nucleus with the mass number A, we can add a particle and obtain a nucleus with the mass number $A+1$. If we put the

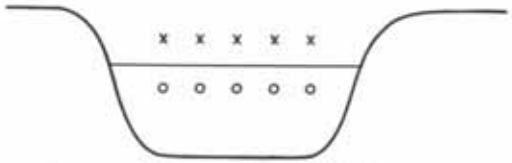

Figure 2.8. Schematic representation of a typical five-particle (crosses), five-hole (open circles) state.

particle into the level m, the wavefunction is

$$|\Phi_m\rangle = a_m^+|\Phi_0\rangle \tag{2.29}$$

and we get the energy difference

$$\epsilon_m = E_m(A+1) - E_0(A). \tag{2.30}$$

In this way one is able to measure the single-particle energies (see Sec. 2.7). These are the simplest states in $A+1$ nuclei. More complicated states have a $2p-1h$ structure, and so on. In complete analogy, there are $1h$, $1p-2h$, etc., states in $A-1$ nuclei.

It often turns out to be very convenient to define quasiparticles by the operators

$$\begin{aligned} \alpha_m^+ &= a_m^+, & \alpha_m &= a_m, & &\text{for } \epsilon_m > \epsilon_F; \\ \alpha_i^+ &= a_i, & \alpha_i &= a_i^+, & &\text{for } \epsilon_i \leqslant \epsilon_F. \end{aligned} \tag{2.31}$$

These quasiparticles are again fermions. They are particles for states above, and holes for states below, the Fermi surface, so that we have

$$\alpha_k|\Phi_0\rangle = 0, \tag{2.32}$$

that is, the ground state of the magic nucleus is a "vacuum" with respect to these quasi-particles; *ph* states are two-quasi-particle states, and so on. The multi-quasi-particle states

$$|\Phi_{k_1 \ldots k_N}\rangle = \alpha_{k_1}^+ \ldots \alpha_{k_N}^+|\Phi_0\rangle \tag{2.33}$$

form a complete orthogonal set in the many-body Hilbert space.

This basis is often used for further investigation of the many-body Hamiltonian H (2.19). In the shell model, one decomposes H,

$$H = T + \sum_{i<j} v(i,j) = H_0 + V_R, \tag{2.34}$$

with the residual interaction

$$V_R = \sum_{i<j} v(i,j) - \sum_i V(i) \tag{2.35}$$

in such a way that V_R is as small as possible and can be neglected. More elaborate theories investigate V_R in the basis in which H_0 is diagonal, the shell model basis (see Chap. 8).

The exact ground state wave function of a magic nucleus has the form

$$|\Psi_0\rangle = C_0|\Phi_0\rangle + \sum_{mi} C_{mi}\alpha_m^+\alpha_i^+|\Phi_0\rangle + \tfrac{1}{4}\sum_{\substack{mi \\ m'i'}} C_{mim'i'}\alpha_m^+\alpha_{m'}^+\alpha_i^+\alpha_{i'}^+|\Phi_0\rangle + \cdots. \tag{2.36}$$

If the shell model is a good approximation to the nucleus, the coefficients C_{mi}, $C_{mim'i'}$, etc. should be small (see Fig. 10.3).

At this point we would like to again stress the fact that we have always been talking about a *spherical shell model* potential. Since, as we shall see, spherical nuclei exist only in the neighborhood of magic nuclei, by the same token this means that we have restricted our discussion to such nuclei. As this spherical average potential is created by the nucleons themselves, it may depend (though not abruptly) on the nucleon number A in quite a subtle way, in contrast to the atomic case. It is such that we

cannot take a once-and-for-all fixed single-particle potential and hope to find the corresponding single-particle states realized very accurately, be it even over a very limited range of neighboring nuclei.

We should keep these precautions in mind when talking about the shell model. As we said, the filling of the shells is without ambiguity, if we have closed shells. When we start filling neutrons and protons in *unfilled shells* these states will be degenerate, because the j-shells have a $(2j+1)$-fold degeneracy. The configuration of the nucleus can then be characterized by two numbers, κ and λ, which stand for the proton and neutron numbers, respectively, in the partially filled j-shell. Let the partially filled neutron shell be characterized by the quantum numbers $(n\ l\ j)$, and the partially filled proton shell by $(n'\ l'\ j')$. One then denotes the configuration by

$$(\nu nlj)^{\kappa}(\pi n' l' j')^{\lambda}.$$

Because of the $2j+1$-fold degeneracy of each j-shell, all possible shell model states corresponding to this configuration are also degenerate. The number of antisymmetric, linearly independent products is given by the product of the binomial coefficients

$$\binom{2j+1}{\kappa}\binom{2j'+1}{\lambda}. \tag{2.37}$$

The degeneracy of all these states will, of course, be removed in reality due to the action of the residual interaction V_R (2.35), which is neglected in the shell model. Taking one of the phenomenological nucleon–nucleon forces, as discussed in Chapter 4, one can diagonalize V_R in the subspace (2.37). Usually one takes not only this subspace into account, but also the one which corresponds to the nearly degenerate levels of a whole major shell. The $s_{1/2}$, $d_{5/2}$, $d_{3/2}$ levels of the $s-d$ shell is such a case, covering nuclei from ^{16}O up to ^{40}Ca. One can easily be convinced that the dimension of the matrices to be diagonalized becomes exceedingly large for more than two particles in open shells. Special procedures have been developed to diagonalize such huge matrices [Wh 72, SZ 72, WWC 77].

To reduce the size of these matrices, symmetries such as isospin or angular momentum (see Sec. 2.6) can be of great help (see, for instance, [FHM 69, WMH 71, HMW 71, GED 71, VGB 72, Wi 76]).

2.6 Symmetry Properties

2.6.1 Translational Symmetry

For any solution of the eigenvalue problem (2.19) we must require that a series of symmetry or invariance properties are fulfilled. Among these are, for example, translational and rotational invariance.* In the shell model one of these invariances is always violated: the *translational invariance*. This comes from the fact that we have to fix the potential in space in contradiction to the homogeneity of space. The most serious consequence of this violation is the appearance of spurious states in the excitation spectrum of the system. This occurs because we have introduced redundant degrees of freedom. If we fix the nucleus in space, it has only $3A-3$ spatial degrees of freedom left. The shell model, however, contains $3A$ variables. These spurious states are therefore not true excitations of the system, but correspond to motions of the nucleus as a whole. Almost all approximation schemes in nuclear physics have inherent symmetry violations. In Chapter 11 we will, therefore, show in fair detail how such violations can be removed.

* Besides these exact symmetries, in some regions of the periodic table one often also has approximate symmetries, as, for instance, the isospin (see Sec. 2.6.3), which can be used for a classification of spectra (see [He 73a]).

2.6.2 Rotational Symmetry

The spherical shell model Hamiltonian H_0 (**ls** term included) conserves rotational symmetry. Therefore, it is possible to construct eigenstates of the total angular momentum

$$\mathbf{J} = \sum_{i=1}^{A} \mathbf{j}^{(i)} \qquad \text{and} \qquad J_z = \sum_{i=1}^{A} j_z^{(i)} \tag{2.38}$$

by a linear combination of the Slater determinants (2.23). The closed shell ground state is not degenerate; the only nondegenerate angular momentum eigenstate has $I=0$, which is therefore identified with the ground state. This consequence is experimentally confirmed with no exception. It is then clear that, having only one nucleon outside closed shells, the ground state angular momentum of such even–odd nuclei will correspond to the j-value of the odd nucleon. The same, of course, is true if there is one nucleon missing (a hole) in a filled shell. This rule is also experimentally confirmed with only very few exceptions.

If we fill (remove) more than one particle into (from) an unfilled (filled) j-level, the situation gets more complicated, because different I-values will be degenerate. Again, we can remove this degeneracy by diagonalizing the residual interaction. The matrices are now much smaller as we get one for each I value.

The construction of eigenfunctions of $\mathbf{J}^2$ will be shown explicitly for a very simple example (for more complicated situations, see [ST 63]). Suppose that in a j-shell there are only two protons, the configuration of which is then $(\pi j)^2$. Out of the degenerate two-particle states (which we want to denote by $|m_1 m_2\rangle$, m being the magnetic quantum number), we construct, according to the rules of angular momentum coupling, an eigenstate $|IM\rangle$ of $\mathbf{J}^2$ and J_z with

$$\mathbf{J}^2 = (\mathbf{j}_1 + \mathbf{j}_2)^2. \tag{2.39}$$

We obtain

$$|IM\rangle = \frac{1}{\sqrt{2}} \sum_{m_1 m_2} C^{j\ j\ I}_{m_1\ m_2\ M} |m_1 m_2\rangle. \tag{2.40}$$

CHAPTER 3

Rotation and Single-Particle Motion

3.1 Introduction

The experimental level schemes of nuclei show an enormous complexity. On the way to understanding at least the basic features of their structure, we have introduced in the first part of this book two rather contrasting models: On the one hand the liquid drop model describes collective phenomena, such as vibrations and rotations, where many nucleons are involved. On the other hand the shell model treats the individual nucleons as independent particles and provides an understanding of single-particle excitations. However, these two models are only limiting cases that are never realized exactly in nature. We always have some deviations and we usually find all kinds of transitions between these extreme models.

For a deeper understanding of the underlying structures, we have to solve, in principle, the nuclear many-body problem and investigate in which limits solutions are provided corresponding to the above simple phenomenological pictures, and in which cases new models must be introduced to obtain a simple description. In the following chapters of this book, we will treat such microscopic methods in much detail, and will reproduce many of the results of the phenomenological models. Although such theories are extremely useful for an understanding of principal questions, they usually involve a terrible amount of numerical effort and are not very useful for a fast and qualitative interpretation of experimental data.

Therefore, it seems to be worthwhile going further on the phenomenological path in this chapter and trying to describe more complicated spectra by a combination of the collective model and the single-particle model. In the last chapter, we saw that such a combination is very useful in describing bulk properities such as nuclear binding energies and deformations. In that case, we had to deal with fluctuations of the level density, and we did not have to take into account the individual degrees of freedom in detail. Now we want to describe individual spectra. For this we have to again try a combination of the single-particle and collective models. We can, for instance, couple one or a few particles to a collective rotor or vibrator. This so-called "*unified model*" was introduced by Bohr and Mottelson [Bo 52, BM 53], and has been described in great detail in many textbooks (see, for instance, [Da 68, EG 70, Ro 70, SF 74, or BM 75]). In the case of collective vibrations, we will deduce the corresponding Hamiltonian and discuss the model of a particle coupled to a vibrator in Chapter 9. In the case of rotations, such a derivation from first principles has been missing till now. Methods have been developed to describe rotations microscopically (see Chap. 11), but they turn out to be extremely complicated. Only in the limit of strong deformations is it possible to deduce a simple rotational model, the cranking model.

In the last few years considerable experimental effort has been made to investigate rotations, and a great variety of new phenomena has been observed. Since these phenomena can be understood to a large extent by the interplay between single-particle motion and collective rotational motion, we think it is necessary to introduce in this chapter two theoretical but phenomenological models which deal with these effects.

In Section 3.2 we give a general survey of the features one expects in rotating nuclei. In Section 3.3 we discuss the rotational part of the unified model, the so-called particle-plus-rotor model (PRM), and in Section 3.4 we present the microscopic cranking model.

We want to emphasize, however, that we do not give a complete description of nuclear rotation in this chapter. The residual interactions in the form of pairing correlations play an important role in this context. They will be treated in Chapter 7.

3.2 General Survey

3.2.1 Experimental Observation of High Spin States

New experimental techniques, namely, heavy ion fusion reactions [MG 63, SLD 65], Coulomb excitation with heavy projectiles [HZ 53, AW 66, 74, WCL 76], and pion capture reactions [EAD 75] have made it possible to excite nuclear states with angular momenta large enough to generate major modifications in the nuclear structure (for a review, see [JS 73, St 76, LR 78]).

The most important such reactions are of the (HI, xn) type, where one bombards the target with heavy ions (α, Ne, Ar, etc.) carrying a large amount of orbital angular momentum. After fusion, the combined system evaporates some neutrons and ends up in highly excited states with very large spin (depending on the projectile and the incoming energy up to $\sim 100\ \hbar$). This highly excited final nucleus then de-excites in a cascade of γ-radiation. The fastest transitions are *statistical E1-transitions*. They carry away much energy, but only a few units of angular momentum. In a plot of the energy versus the angular momentum (Fig. 3.1), these statistical cascades correspond to nearly vertical lines. They end up at the so-called *yrast line*,* the line which connects the levels of lowest energy to each angular momentum (or the levels with highest angular momentum at a given energy). The rest of the cascade has to follow this line. For deformed nuclei these are *collective E2-transitions* ($\Delta I = 2$), which finally go over into the well-known ground state rotational band (see Sec. 1.5).

Until now, only the last part of these cascades could be resolved into discrete lines (see Fig. 3.5). The highest angular momenta observed in this way lie between 30 and 40 $\hbar$. The rest of the cascade is measured as a γ-continuum, and one can draw only indirect conclusions from these data [GG 67, BSC 75, SBC 76, Di 76, HLM 78, ABH 78, WF 78b]. There are, however, indications that collective transitions along lines parallel to the yrast line (see Fig. 3.1) play an important role, and that there is a competition between collective and statistical effects in the region of a few MeV above the yrast line [SBD 77].

*The Swedish word *yrast* means "fastest rotating" [Gr 67]. One also uses the name *yrare* for the level with the second lowest energy at each I-value.

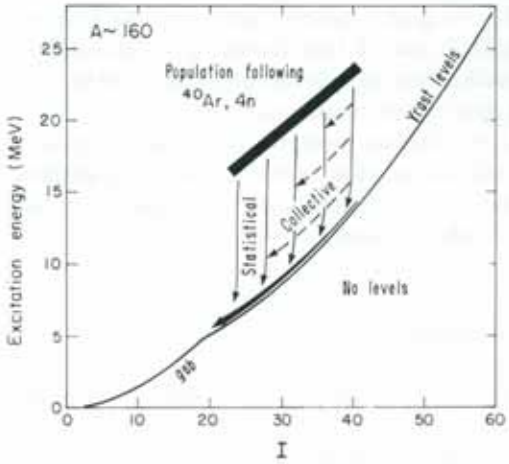

Figure 3.1. Excitation energy as a function of angular momentum I for the reaction (^{40}Ar, $4n$). After the evaporation of four neutrons, the nucleus decays by a γ-cascade of statistical $E1$- and collective $E2$-transitions down to the yrast line, and then to the ground state by a series of $E2$-transitions along this line. The yrast band shows an increasing intensity, because it collects all the statistical transitions ("side feeding"). (From [SBD 77].)

3.2.2 The Structure of the Yrast Line

In Section 1.7 we saw that a *classical liquid drop* [CPS 74] rotates at low angular frequencies around the symmetry axis of its oblate shape (Hiskes regime, Fig. 3.2a). Only for very high angular velocities does it undergo a phase transition to the Beringer–Knox regime, where it has a triaxial, but nearly prolate, shape and the rotational axis is perpendicular to the approximate symmetry axis (Fig 3.2b). For still higher frequencies it finally fissions (Fig. 3.2c).

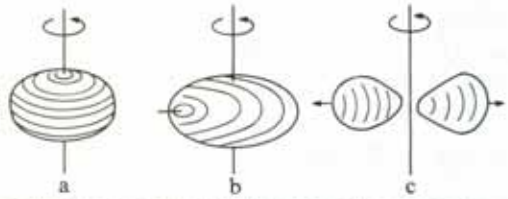

Figure 3.2. The behavior of a classical liquid drop for increasing angular velocity.

The *real nucleus*, however, is a quantum mechanical system. It shows shell effects (see Chap. 2.9), which cause stable deformations already in the ground state for some regions of the periodic table. The yrast line corresponds to the lowest energy for each angular momentum; all the excitation energy of several tens of MeV with respect to the ground state is rotational energy and used to generate angular momentum. Consequently, the level density along this line is low, much lower than the level density of the $I = 0$ states at the corresponding energy. It resembles that of the ground state, though we will see that there are characteristic deviations from it. Since the nucleus is cold in the yrast region, we can expect a high degree of order. Shell effects play an important role.

The prolate deformations caused by the shell effects are of the same order of magnitude as the oblate deformations of a classical drop at high angular velocities (see Sec. 1.7). We therefore expect a delicate interplay between macroscopic centrifugal effects and microscopic shell structure when we study the nuclear shapes as a function of the angular momentum.

Let us first study the case of well-deformed heavy nuclei (for instance, in the rare earth region). In the ground state they show a prolate axial symmetric quadrupole deformation caused by shell effects. The levels in the corresponding deformed potential are occupied pairwise by nucleons with the opposite single-particle angular momentum ($\pm\Omega$). We will see in Chapter 6 that the two nucleons in such a pair do not move independently, as was assumed in the last chapter, but are coupled by a pairing force to the so-called Cooper pairs with spin zero; that is, these deformed nuclei

show a *superfluid behavior* and their ground state energy is lowered by a few MeV.

With increasing angular momentum, we can distinguish several regimes where the yrast states show quite a different structure [BM 74]:

(a) For low angular momenta $I=0,2,4,\ldots$, the yrast line follows the *ground state rotational band*, as discussed in Section 1.5. The rotation is collective, that is, it has to be perpendicular to the symmetry axis (see Fig. 3.3a, where we have indicated the coupled pairs of nucleons oriented along the symmetry axis).

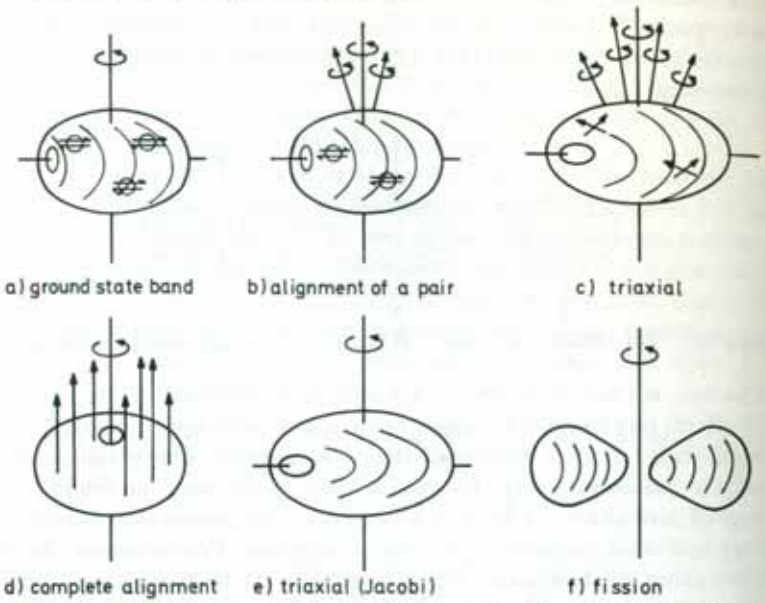

Figure 3.3. Possible structures along the yrast line of a deformed nucleus.

The nucleus feels a slowly rotating deformed potential (for a more detailed discussion, see Sec. 3.4). The Coriolis forces act on both spins of a pair with opposite angular momenta $\pm\Omega$ in opposite directions and try to align them parallel to the rotational axis, that is, they try to break the Cooper pairs [*Coriolis anti-pairing* (*CAP*) *effect*]. However, for low angular momenta the Coriolis forces are weak and unable to break pairs: The nucleus rotates more or less with the same structure as the ground state.

We have to emphasize, however, that in a microscopic picture the total angular momentum has to be generated by the angular momenta of single nucleons. In a collective rotation this is achieved by aligning all the particles a little bit in the direction of the rotational axis. For each pair this effect is very small; the spins of the pairs are still oriented nearly anti-parallel along the symmetry axis of the potential. By summing up all the small contributions we obtain the total angular momentum $I=2,4,\ldots,$.

(b) Going to higher and higher angular momenta, the Coriolis force, increases more and more and at a certain angular momentum it will be able to break pairs. Therefore, at some critical angular momentum I_c we expect that all pairs are broken. The pairing correlations break down completely and a *phase transition* from the superfluid phase to the normal phase is observed. This effect was predicted by Mottelson and Valatin in 1960 [MV 60]. More detailed investigations, however, have shown that the Coriolis force is proportional to the size of the single-particle angular momentum j of the nucleon under consideration. We have seen in Section 2.8 that the nucleons in the vicinity of the Fermi surface belong to subshells with rather different j-values, and we expect those nucleons with large j-values to align first along the rotational axis. These are usually the levels with high spin and opposite parity, shifted downwards by the spin orbit term, as for instance the $i_{13/2}$ shell for neutrons in the rare earth region (Stephens–Simon effect [SS 72a]).

In the second regime of the yrast line (Fig. 3.3b), we therefore expect *alignment processes* of one or the other broken pairs, whereas the rest of the nucleus stays more or less unchanged. The yrast band can then no longer be identified with the ground state band, but rather with a band of two aligning particles sitting on the rotating core. Two $i_{13/2}$ particles can contribute 12 units of angular momentum to the rotation. Such an alignment is therefore connected with a rapid increase of the angular momentum I as a function of the collective angular velocity and leads to a series of anomalies in the spectra [JRS 71, JRH 72], for example, the "back-bending phenomenon" (see below).

(c) Each alignment process is connected with a certain change in the collective properties by its influence on the mean field: Broken pairs no longer contribute to the pairing correlations; because of the blocking effect (see Sec. 6.3.4.) these correlations will disappear completely after a few alignments. Particles aligned to the rotational axis have an oblate density distribution, with the rotational axis as the symmetry axis. We therefore get triaxial admixtures to the prolate density distribution of the core.

In a third regime (Fig. 3.3c) which should correspond roughly to angular momenta $30\lesssim I\lesssim 50$, we expect the Coriolis and centrifugal forces to produce effects comparable in strength to the shell structure effects, namely, changes in the shapes to *triaxial deformations*. Such a system without a symmetry axis shows more collective states than the axial symmetric rotor (see Sec. 1.5.3): We expect a sequence of rotational states parallel to the yrast line corresponding to a *wobbling motion*.

(d) If an essential part of the nucleons are aligned parallel to the rotational axis, we finally expect an *axially symmetric oblate shape*.

The nuclear wave function is symmetric with respect to rotations around this axis. The rotation is no longer collective. Instead, the total angular momentum is made up by reoccupation of distinct particles in the deformed well.

This kind of motion is called "*single-particle*" *rotation*. The energy of the states along the yrast line in this region is determined by the single-particle energies in the rotating oblate well. The energy differences between adjacent states vary statistically. Only on the average do they follow an $I\cdot(I+1)$ law with the moment of inertia of a rigid rotor (see Sec. 3.4.6.). The transition from one state to the next corresponds to a reoccupation, and the matrix elements should adopt single-particle values, that is, the transition probability should be drastically reduced.

Because of the statistical nature of the levels in that region of the yrast line, one also expects long lived *high spin isomeric states*, so-called *yrast traps* [BM 74] which could eventually produce a delayed decay such that we could observe the whole yrast cascade of discrete lines without the background of all statistical transitions.

(e) For very large angular momenta we finally expect only the macroscopic properties to be essential, that is, the nucleus should again undergo a transition from oblate to triaxial and prolate shapes before it fissions (Fig. 3.3e, f).

So far, only discrete levels in the regimes (a) and (b) have been observed; the rest of these considerations is to a large extent speculation. We will see in Sec. 3.4.5 the kind of models one has used to obtain theoretical predictions. In fact, in the calculations one has found all the different regimes discussed above.

It seems to be possible, however, that many nuclei do not pass through all these stages. In particular, weakly deformed or spherical nuclei adopt from the beginning the regime (d), namely, a rotation of an oblate shape around the symmetry axis before going triaxial and fissioning. On the other hand, in many well-deformed nuclei the change in deformation produced by the alignment processes is not strong enough to compensate the shell effect of a prolate deformation. They only become triaxial (Fig. 3.3c, d), not oblate, before fissioning. Experimentally, one has observed longliving high spin isomers (yrast traps) only for weakly deformed nuclei (see Sec. 3.4.6). This seems to be in agreement with theoretical calculations.

Besides the yrast band, one has observed many other rotational bands in the low and *medium spin region*. They are based on more complex configurations, such as quasi-particle excitations or vibrational states.

Depending on the size of the j shell orbitals, which are involved in such configurations, one can imagine a large variety of alignment processes. For example, in an odd mass nucleus the alignment of the odd neutron in the $i_{13/2}$ shell, which leads to so-called *decoupled bands*. Another example is the rotational band in an odd-odd nucleus, where only the neutron in the $i_{13/2}$ shell aligns, whereas the proton stays oriented along the symmetry axis. Such a band has a *semidecoupled* structure [NVR 75].

The particle-plus-rotor model discussed in Section 3.3 provides a phenomenological method to describe such processes. In that section we will come back to some examples of this type in more detail.

3.2.3 Phenomenological Classification of the Yrast Band

Over the years some phenomenological models have been introduced to characterize the properties of rotational bands. In the low spin region (Fig. 3.3a), the spectra often follow exactly the $I\cdot(I+1)$ law, but for higher I-values there occur deviations to a greater or lesser extent*. In order to describe the deviations from the ideal rotational spectrum, one often applies the following parametrization:

$$E(I)=A\cdot I\cdot(I+1)+B\cdot(I(I+1))^2+C\cdot(I(I+1))^3+\cdots. \tag{3.1}$$

It turns out that in many cases the convergence of this expansion is rather poor and an expansion in the *angular frequency* ω is more appropriate.

In principle, ω is not a measurable quantity. We can define it, however, semiclassically as

$$\omega=\frac{dE}{dJ}, \qquad \text{with} \quad J=\sqrt{I(I+1)}\,. \tag{3.2}$$

Replacing the differential quotient by a quotient of finite differences,† we obtain a definition of an "experimental" value for the *angular velocity*‡

$$\omega_{exp}\simeq\left.\frac{\Delta E}{\Delta\sqrt{I(I+1)}}\right|_{I,I-2}\simeq\frac{E(I)-E(I-2)}{\sqrt{I(I+1)}-\sqrt{(I-2)(I-1)}}\,. \tag{3.3}$$

The *moment of inertia* is defined by

$$\mathcal{I}=\frac{J}{\omega}=\frac{1}{2}\left(\frac{dE}{dJ^2}\right)^{-1}\simeq\frac{2I-1}{\Delta E_{I,I-2}}\,. \tag{3.4}$$

With these definitions, we can calculate values of ω and $\mathcal{I}$ for each level of the yrast band.

Harris [Ha 65a] proposed the following parametrization of the spectrum:

$$E(I)=\alpha\omega^2+\beta\omega^4+\gamma\omega^6+\cdots. \tag{3.5}$$

Odd powers in ω do not occur, since E cannot change by reversing the angular velocity. For ω as a function of I we can either choose the experimental value (3.3) or avoid the ambiguity of its definition by using a similar expansion of J. From

$$\frac{dE}{d\omega}=\frac{dE}{dJ}\frac{dJ}{d\omega}=\omega\frac{dJ}{d\omega} \tag{3.6}$$

we obtain

$$J(I)=\sqrt{I(I+1)}=2\alpha\omega+\frac{4}{3}\beta\omega^3+\frac{6}{5}\gamma\omega^5+\cdots.$$

* For a compilation of such data, see [SHJ 73, SSM 75].

† This replacement is not unique, however, and some groups use different prescriptions (see [JS 73, So 73, LR 78]).

‡ Within this chapter we always use the units $\hbar=1$.

Of course, this expansion is valid only as long as J is not a multivalued function of ω, that is, it is of no use in the backbending region (see Sec. 3.2.4.).

Another model which is widely used for the classification of rotational and even transitional nuclei is the *variable moment of inertia* (VMI) model [MSB 69, SDG 76]. The moment of inertia ϑ is considered as a variable on which the intrinsic energy V depends:

$$E(I,\vartheta)=\frac{1}{2\vartheta}I(I+1)+V(\vartheta). \tag{3.7}$$

According to the variation principle (discussed in Sec. 5.2), the total energy E has to be minimized for a fixed value of I with respect to ϑ. This determines the functional dependence $\vartheta(I)$. Assuming we know $V(\vartheta)$, $\vartheta(I)$ is implicity given by

$$\left.\frac{dE}{d\vartheta}\right|_I=-\frac{1}{\vartheta}\frac{I(I+1)}{2\vartheta}+\frac{dV}{d\vartheta}=0.$$

Usually one expands on $V=\frac{1}{2}C(\vartheta-\vartheta_0)^2$, where ϑ_0 is the value of ϑ at $I=0$. The coefficients C and ϑ_0 are adjusted to the experimental spectrum $E(I)$. With the identification $J=\omega\cdot\vartheta$ this corresponds to the Harris model to order ω^4, but the ansatz (3.7) is certainly more general [DB 73, SDG 76].

3.2.4 The Backbending Phenomenon

In the region between 10 and 20 units of angular momentum, an anomaly is observed in the yrast band of many nuclei. It can be most easily demonstrated if one plots the moment of inertia ϑ as a function of ω^2. In lowest order in the VMI model ($\vartheta=\vartheta_0+b\omega^2+\cdots$) this should give a straight line. The deviation from a constant is then a measure of the validity of the $I\cdot(I+1)$ law. Figure 3.4 gives two examples for such curves, measured by the Jülich group [LR 78].

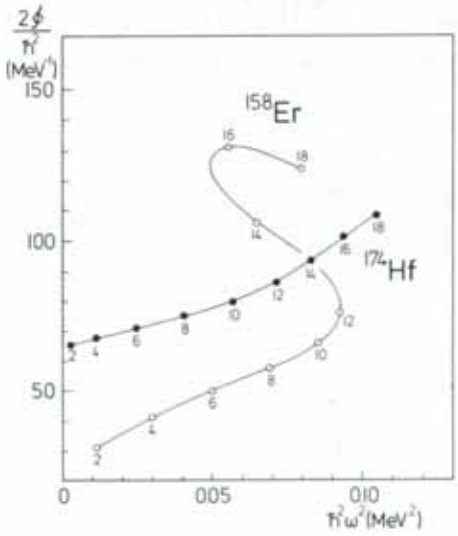

Figure 3.4. Moment of inertia ϑ as a function of the rotational frequency squared for ^{158}Er and ^{174}Hf.

For low spin values one indeed finds straight lines. In the nucleus ^{174}Hf the deviations are, in fact, smooth. In ^{158}Er, however, a very steep increase occurs for certain I values, the curve even bending backwards, ("backbending" phenomenon [JRH 72]). This means experimentally that the transition energy $\Delta E_{I,I-2}$, which should increase linearly with I for the constant rotor as

$$\Delta E_{I,I-2}=\frac{1}{2\vartheta}(4I-2), \tag{3.8}$$

does not increase, but decreases for certain I values. Figure 3.5 shows the experimental data that correspond to Figure 3.4.

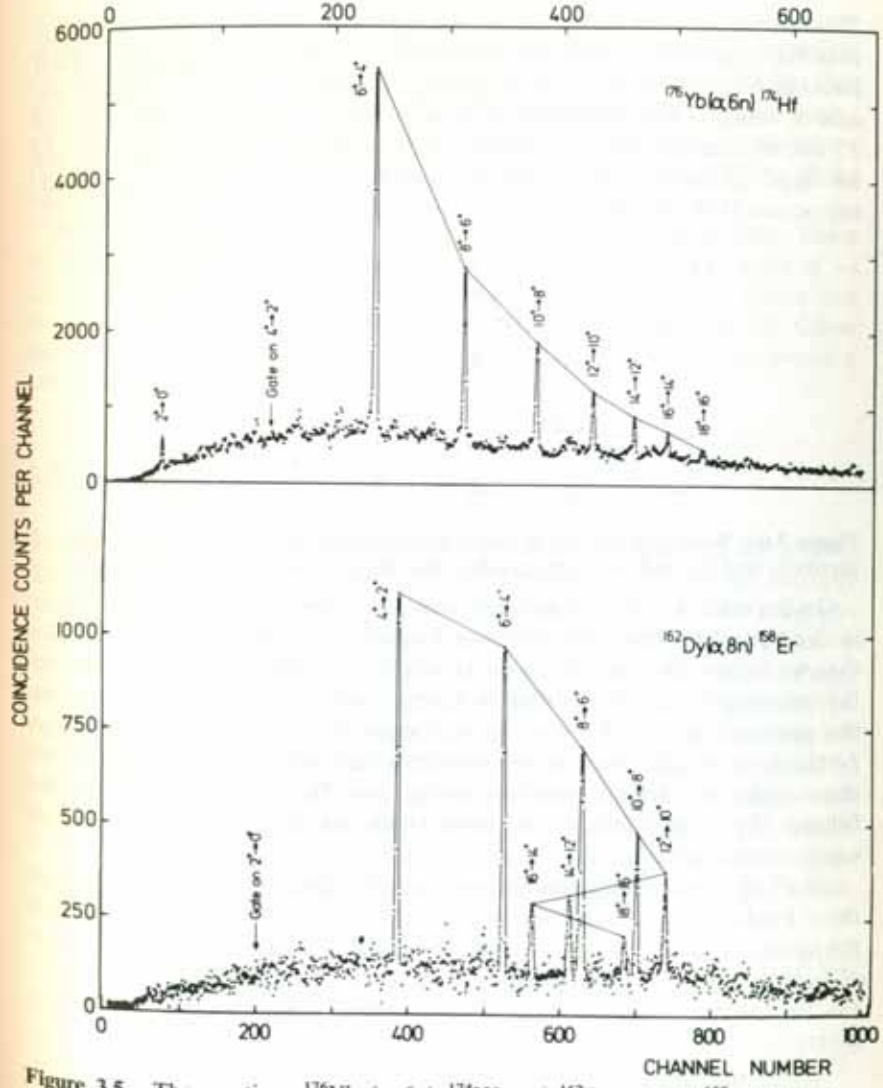

Figure 3.5. The reactions ^{176}Yb $(\alpha, 6n)$ ^{174}Hf and ^{162}Dy $(\alpha, 8n)$ ^{158}Er. The last reaction shows the anomaly called backbending in the I region 10^+-14^+. This is revealed in combining descendent peak heights by straight lines. (From [LR 78].)

Such a phenomenon can easily be reproduced as an effect due to the crossing of two bands (in some cases one has even observed the second band experimentally, see Fig. 7.6 and [KSM 78]). To see this, let us assume that the two bands have different moments of inertia (Fig. 3.6) corresponding to two parabolas in an E versus I plot. If $\mathcal{I}_2 > \mathcal{I}_1$ the bands cross in a certain region of I. Because of the residual interaction, such a crossing does not take place (the no-crossing rule; see Sec. 2.8.4), and we can get a region in which the second derivative is negative:

$$0 > \frac{d^2E}{dI^2} = \frac{d\omega}{dI}. \tag{3.9}$$

This means we have an increasing J with decreasing ω, while at the same time the properties of the bands are exchanged. In fact, it is easy to fit such backbending curves by a band mixing calculation with few parameters, one of which is the interaction V between the bands. For small values of V, one obtains a sudden transition which produces backbending, whereas for large values of V the transition region is very broad and no backbending occurs [MR 72, GG 74b].

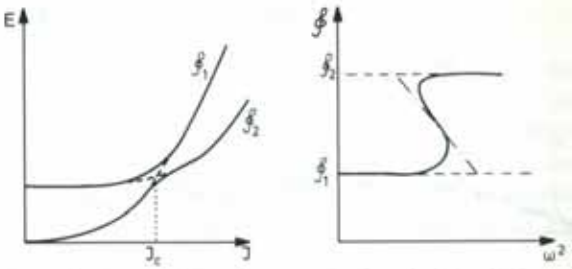

Figure 3.6. Schematic picture of two intersecting bands with different moments of inerita $\mathcal{I}_1$ and $\mathcal{I}_2$, and the corresponding backbending plot. (From [LR 78].)

On the other hand, it is also clear that the strange backbending behavior in the plot of the moment of inertia $\mathcal{I}$ against ω^2 has its origin in the fact that we follow the yrast line in the critical region, that is, we switch over to the crossing band with a different internal structure. If we would stay in the ground state band, which is no longer the yrast band for the large I-values, we would obtain a very smooth behavior for the ω-dependence of the moment of inertia (dashed-line in Fig. 3.6). The reason that one usually follows the yrast band is that these levels are experimentally the most easily accessible.

In all of these considerations, one should, however, keep in mind that these kinds of phenomenological descriptions only give a classification of the spectra and do not say anything about their physical origin. In the case of backbending there is, for instance, the question concerning the nature of the second band. Three types of theoretical interpretations have been given:

(i) In the second band the nucleus has a different deformation, for instance, a triaxial one. This means that backbending is caused by a sudden change of deformation [Th 73, SV 73].

(ii) The second band is not superfluid, as in the ground state band. This would interpret backbending as a phase transition from a superfluid to a normal-fluid state (Mottelson–Valatin effect [MV 60]).

(iii) The second band is a two quasi-particle band of particles which are rotationally aligned along the axis of rotation (see Sec. 3.3). Then backbending would correspond to a sudden alignment of a pair of nucleons (as proposed by Stephens and Simon [SS 72a]).

The general result of theoretical investigations, which include all these degrees of freedom (see Sec. 7.7), is that for the well deformed nuclei (the classical rotors) the reduction of the pairing correlations is only responsible for the slow change of the moment of inertia at low spin values, but that sudden effects such as backbending are due to alignment of a single high j pair of nucleons. There is also a large number of experimental indications [GSD 73, RSS 74, WBB 75, NLM 76, St 76] for this interpretation of the backbending phenomenon.

In the rare earth nuclei, the $i_{13/2}$ neutrons play an essential role. There is, however, experimental evidence for a second irregularity at spins of $\sim$ 26–30 h [LAD 77, BBB 79a] a so-called *second backbending*, which has been interpreted as the alignment of an $h_{11/2}$ proton pair [FP 78]. Other high j-orbitals may play similar roles in different regions of the periodic table.

3.3 The Particle-plus-Rotor Model

To describe the interplay between the motion of particles and the collective rotation, Bohr and Mottelson [BM 53] proposed to take into account only a few so-called valence particles, which move more or less independently in the deformed well of the core, and to couple them to a collective rotor which stands for the rest of the particles. The division into core and valence particles is not always unique. It is, however, reasonable to use the unpaired nucleon in an odd mass nucleus as a valence nucleon on an even–even core. One also can attribute the particle and the hole of a particle–hole excitation to the valence particles. More generally, one divides the Hamiltonian into two parts: an intrinsic part H_{intr}, which describes microscopically a valence particle or a whole subgroup of particles near the Fermi level; and a phenomenological part H_{coll} which describes the inert core:

$$H = H_{\text{intr}} + H_{\text{coll}}. \tag{3.10}$$

The *intrinsic part* has the form

$$H_{\text{intr}} = \sum_k \epsilon_k a_k^+ a_k + \frac{1}{4} \sum_{klmn} \bar{v}_{klmn} a_k^+ a_l^+ a_n a_m, \tag{3.11}$$

where ϵ_k are single-particle energies in the deformed potential (e.g., Nilsson energies) and $\bar{v}$ is the interaction between the valence particles which is, or can be, neglected in many cases.*

The *collective part* describes the rotations of the inert core:

$$H_{\text{coll}} = \frac{R_1^2}{2\vartheta_1} + \frac{R_2^2}{2\vartheta_2} + \frac{R_3^2}{2\vartheta_3}, \tag{3.12}$$

where the R_i are the body-fixed components of the collective angular momentum of the core. Together with the angular momentum of the valence particles $\mathbf{j}$ (which is the sum over the single-particle angular momenta) it forms the total angular momentum $\mathbf{I}$ (see Appendix A):

$$\mathbf{I} = \mathbf{R} + \mathbf{j}. \tag{3.13}$$

Eliminating $\mathbf{R}$, H_{coll} can be decomposed into three parts:

$$H_{\text{coll}} = H_{\text{rot}} + H_{\text{rec}} + H_{\text{cor}}, \tag{3.14}$$

where

$$H_{\text{rot}} = \frac{I_1^2}{2\vartheta_1} + \frac{I_2^2}{2\vartheta_2} + \frac{I_3^2}{2\vartheta_3} \tag{3.15}$$

is the pure rotational operator of the rotor [Eq. (1.55)], which acts only on the degrees of freedom of the rotor, that is, the Euler angles. The term

$$H_{\text{rec}} = \sum_{i=1}^{3} \frac{j_i^2}{2\vartheta_i} \tag{3.16}$$

is usually called the recoil term. It represents a recoil energy of the rotor. This operator acts in the coordinates of the valence particles only. For more than one valence particle, it contains a two-body interaction.

Finally, the coriolis interaction

$$H_{\text{cor}} = -\sum_{i=1}^{3} \frac{I_i j_i}{\vartheta_i} \tag{3.17}$$

couples the degrees of freedom of the valence particles to the degrees of freedom of the rotor. This purely kinematic coupling is the only coupling in the model.

It should be noticed that the total angular momentum operators in the laboratory system I_x, I_y, I_z commute with the Hamiltonian (3.10). Although the rotational symmetry is violated in the intrinsic frame (e.g., in the Nilsson Hamiltonian), the model conserves angular momentum for the total system, because the operators I_x, I_y and I_z act only on the Euler angles and commute with the intrinsic components I_1, I_2 and I_3 (see Appendix A). However, it must be emphasized that this rotational invariance is achieved only through the introduction of a phenomenological

*We will see in Chapter 6 that pairing correlations play an important role in deformed nuclei and we should therefore talk about quasi-particles rather than particles. This only yields simple occupation factors to the formulae shown below, which we give sometimes for the sake of completeness, however. For a deeper understanding, the reader is referred to Chapter 6.

core. If one wants to treat all particles microscopically (the limit of vanishing core), the Euler angles are redundant variables (see Sec. 11.3).

The wave function of the system may be written as

$$|\Psi_M^I\rangle = \sum_K \Phi_K |IMK\rangle, \tag{3.18}$$

where Φ_K depends on the coordinates of the valence particles and the $|IMK\rangle$ depend on the Euler angles and are defined in Eq. (A.21). In the simplest case, there is only one valence particle and an axially symmetric rotor. Using this model a large number of the experimental spectra of odd nuclei has been reproduced very accurately, and from this point of view it is certainly one of the most powerful models in nuclear physics. However, until now a clear-cut microscopic derivation has been missing. Such a derivation should start from a many-body Hamiltonian (2.19). The set of $3A$ particle coordinates should be transformed in a proper way into a set of $3A-3$ internal coordinates and 3 Euler angles which describe the collective motion. To this transformation should correspond a decomposition of the Hamiltonian into an internal and a collective part, as in Eq. (3.10). Finally, one could hope to describe the internal motion by a deformed shell model.

Many attempts have been made in this direction and we give a short discussion of them in Section 11.3, but up to the present time the problem has still not been completely solved. In the case of well deformed nuclei the model can be backed by the following arguments.

(i) Microscopic Hartree–Fock calculations show very pronounced minima in the energy surface at axial symmetric deformations, which justifies the notion of a rotating core.

(ii) The model is to some extent equivalent to the cranking model (see Sec. 3.4), which is microscopically founded at least in the limit of strong nearly axial symmetric deformations.

(iii) Villars and Cooper [VC 70] have shown that, in introducing redundant coordinates, a Hamiltonian of a form similar to that in Eq. (3.10) can be found with, however, additional coupling terms. In the limit of strong deformation and with further assumptions, they obtained the correct expression for the moment of inertia.

The particle-plus-rotor model has, however, also been applied with great success to nuclei in the region of small deformations and to transitional nuclei. It is not clear at the present time how this can be explained microscopically.

3.3.1 The Case of Axial Symmetry

Assuming that the rotor has the 3-axis as axis of symmetry, that is, $\vartheta_1 = \vartheta_2 = \vartheta$, there can be no collective rotation around this axis and the 3-component of $\mathbf{R}$ has to vanish (see Sec. 1.5). From Eq. (3.13) it follows

immediately that K, the 3-component of the total angular momentum $\mathbf{I}$, has to be equal to Ω, the 3-component of $\mathbf{j}$:

$$K = \Omega. \tag{3.19}$$

For the different terms of the Hamiltonian (3.10), (3.14), we obtain in this case

$$H_{\text{intr}} = \sum_{i,\Omega} \epsilon^i_\Omega a^+_{i\Omega} a_{i\Omega}, \tag{3.20}$$

$$H_{\text{rot}} = \frac{\mathbf{I}^2 - I_3^2}{2\vartheta}, \tag{3.21}$$

$$H_{\text{rec}} = \frac{1}{2\vartheta}(j_1^2 + j_2^2), \tag{3.22}$$

$$H_{\text{cor}} = -\frac{1}{\vartheta}(I_1 j_1 + I_2 j_2) = -\frac{1}{2\vartheta}(I_+ j_- + I_- j_+). \tag{3.23}$$

In (3.20) we have neglected the residual interaction. The single-particle levels in the axially symmetric well are labeled by $k = (i, \Omega)$ and the corresponding eigenfunctions will be denoted by Φ^i_Ω.

The recoil term acts only in the intrinsic coordinates. It is often neglected, because the intrinsic single-particle energies ϵ^i_Ω are adjusted to experimental data. We follow this argument in the following discussion and omit H_{rec} for the moment. Only in Section 3.3.2.1 will we take it up again. The Hamiltonian (3.20–3.23) has eigenfunctions of the type (3.18), which can be found by a numerical diagonalization of the Hamiltonian (3.10). However, the different terms in (3.20–3.23) are of different importance, depending on the physical situation. Therefore, it is useful to consider three limits in which one of the terms becomes predominant and which as a consequence can be solved analytically (for a review, see [St 75a]):

In the *strong coupling limit*, the odd particle adiabatically follows the rotations of the even mass core. It is realized if the coupling to the deformation is much stronger than the perturbation of the single particle motion by the Coriolis interaction.

In the *weak coupling limit*, which is realized for very small deformations, the odd particle essentially moves on spherical shell model levels only slightly disturbed by, for example, the quadrupole vibrations (see Sec. 9.3.3).

In the *decoupling limit*, the Coriolis force is so strong that the coupling to the deformation of the core may be neglected. The total angular momentum and the single-particle angular momentum are then parallel to one another.

3.3.1.1 The Strong Coupling Limit (Deformation Alignment). The strong coupling limit is realized when the Coriolis interaction matrix elements are small compared with the level splitting of the single-particle energies in the deformed shell model for different values of Ω. We should expect that this is the case

(i) for large deformations β, because the level splitting in the Nilsson Hamiltonian is $\propto \beta$, whereas the rotational constant $\hbar^2/2\vartheta$ is, according to a simple empirical rule (Eq. (1.50), $\propto \beta^{-2}$; and

(ii) for small Coriolis matrix-elements. As we shall see in Eq. (3.33), they are $\propto [(I(I+1) - K^2)(j(j+1) - \Omega^2)]^{1/2}$, that is, they are small either for low spins I or for nucleons in orbitals with small particle angular momenta j. For large j-values they can only be neglected for high Ω values.

It is called the *strong coupling* or *deformation aligned* limit because in this case K is a good quantum number. The angular momentum $\mathbf{j}$ of the valence particles is strongly coupled to the motion of the core. In a semiclassical picture, $\mathbf{j}$ precesses around the 3-axis, which is shown in the coupling scheme of Fig. 3.7a. Since H_{cor} is the only term in the Hamiltonian which couples the particle and rotor degrees of freedom, the eigenfunctions are in this limit products of the functions Φ^i_K (eigenfunctions of H_{intr}, e.g., the single-particle Nilsson functions) and the eigenfunctions of the symmetric rotor $|IMK\rangle$ (see Appendix A).

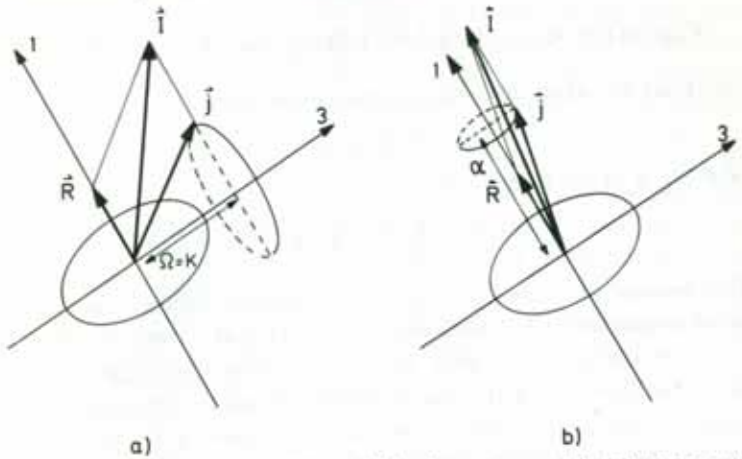

Figure 3.7. Coupling schemes in the particule-plus-rotor model: (a) strong coupling; (b) rotational alignment.

We have seen in Section 1.5.1 that the Hamiltonian (3.10) has an additional symmetry, $\mathcal{R}_1$, which describes a rotation of the core by 180° around the 1-axis of the body-fixed system

$$\mathcal{R}_1 = e^{i\pi R_1} = e^{i\pi I_1} e^{-i\pi j_1}. \tag{3.24}$$

We therefore have to symmetrize the wave function (3.18) and get together with Eq. (A.24) the following set of eigenfunctions [Ke 56]

$$|\Psi^I_{MK}\rangle \frac{1}{\sqrt{2(1+\delta_{K0})}} \{\Phi^i_K |IMK\rangle + (-)^I e^{-i\pi j_1} \Phi^i_K |IM-K\rangle\}. \tag{3.25}$$

If we know the decomposition of Φ^i_K into eigenstates of $\mathbf{j}^2$

$$|\Phi^i_{K=\Omega}\rangle = \sum_{nj} C^i_{nj}|nj\Omega\rangle, \tag{3.26}$$

we find

$$e^{-i\pi j_1}|\Phi^i_{K=\Omega}\rangle = \sum_{nj} C^i_{nj}(-)^{-j}|nj-\Omega\rangle. \tag{3.27}$$

The energy spectrum which corresponds to (3.25) is given by

$$E^i_K(I) = \epsilon^i_K + \frac{1}{2\vartheta}(I\cdot(I+1)-K^2) \tag{3.28}$$

[usually, instead of ϵ^i_K in (3.28), we have quasi-particle energies E^i_K as they are defined in Eq. (6.72)]. This is the spectrum of a rotational band. The lowest possible spin is $I_0 = K$. The bandhead $E^i_K(I_0)$ is not precisely ϵ^i_K, but shifted a little, especially if we take into account the recoil term and the residual interaction. The spectrum has a spacing $\Delta I = 1$ and its moment of inertia is that of the rotor.

In this strong coupling limit we have neglected the Coriolis interaction completely. Taking it into account at least in first order perturbation theory, we get a contribution only for $K = 1/2$ bands

$$E^i_{K=1/2}(I) = \epsilon^i_{K=1/2} + \frac{1}{2\vartheta}\left\{I(I+1) - \frac{1}{4} + a^i\left(I+\frac{1}{2}\right)(-)^{I+1/2}\right\}, \tag{3.29}$$

where the so-called *decoupling factor* is given by

$$a^i = i\langle\Phi^i_{1/2}|j_+ e^{-i\pi j_1}|\Phi^i_{1/2}\rangle \tag{3.30}$$

or if Φ^i_K is of the form (3.26),

$$a^i = -\sum_{nj}|C^i_{nj}|^2(-)^{j+1/2}(j+\tfrac{1}{2}). \tag{3.31}$$

This means, for example, that for a positive decoupling factor (major components with $j+\frac{1}{2}$ odd) the levels with odd values of $I+\frac{1}{2}$ ($I=\frac{1}{2}, \frac{5}{2}, \frac{7}{2}, \cdots$) are shifted downwards. This explains very nicely the rather distorted bands for $K=\frac{1}{2}$ in many nuclei [ABH 56] where there are, in fact, two bands having $\Delta I = 2$ each (even and odd values of $I+\frac{1}{2}$) shifted against one another. The reason for this decoupling comes from the symmetrization Eq. (3.25) with respect to $\mathfrak{R}_1$ mixing states with $K=\frac{1}{2}$ and $K=-\frac{1}{2}$ via the Coriolis matrix elements. The strength of the decoupling factor a^i depends on the j-components which contribute to the single-particle wave function $\Phi^i_{1/2}$. If levels with large single-particle angular momenta are involved, it is very strong. However, perturbation theory is no longer valid in such cases, and also other matrix elements of the Coriolis operator come into play. Therefore, the strong coupling limit is no longer realized and we have to consider a different limit.

3.3.1.2 The Weak Coupling Limit (No Alignment). As we have said, the strong coupling approximation breaks down if the Coriolis matrix elements are no longer negligible compared to the energy splitting of the single-particle levels belonging to different K values. Let us therefore study the Coriolis matrix elements in more detail.

$$\langle\Psi^I_{MK+1}|H_{\text{cor}}|\Psi^I_{MK}\rangle = -\frac{1}{\vartheta}\sqrt{I(I+1)-K(K+1)}\,\langle\Phi_{\Omega+1}|j_x|\Phi_\Omega\rangle. \tag{3.32}$$

If Φ_Ω is of the form shown in Eq. (3.26), we obtain

$$\langle\Psi^I_{MK+1}|H_{\text{cor}}|\Psi^I_{MK}\rangle = -\frac{1}{2\vartheta}\sum_{nj}|C_{nj}|^2\sqrt{I(I+1)-K(K+1)}\,\sqrt{j(j+1)-\Omega(\Omega+1)}\,. \tag{3.33}$$

We see that these matrix elements are large for large values of I/K and j/Ω. That is, if, for example, levels with large j and small Ω values are involved. Particles in such levels have high angular momentum and a density distribution close to the 3-axis. Therefore, it is clear that a rotation of the core perpendicular to this axis has a great influence on the motion of these particles.

A well known example is the neutron $1i_{13/2}$ level, which lies in the vincinity of the Fermi level for light rare earth nuclei such as Dy and Er. One can estimate the Coriolis matrix element for the $\Omega=\frac{1}{2}$ case to be $0.1\times I$ [MeV], which is in fact quite large compared with the level spacing of H_{intr}. Since such levels with high j-values are drastically shifted downwards by the spin orbit term of the shell model (see Sec. 2.4) into a shell with a different N-quantum number, these levels are rather pure configurations, that is, $C_{nj}\simeq 1$ (intruder state). It is therefore sufficient in the following to consider *only one such single j-shell*. The $1i_{13/2}$ shell is not the only such case. The energy of the largest j-value in each major shell is lowered drastically and has an important role in many rotational spectra.

Vogel [Vo 70] proposed a limit (usually called weak coupling or no alignment limit) in which the K-splitting of H_{intr} is totally neglected. (This, of course, can only be a valid approximation for small deformation.) Now $\mathbf{j}^2$ and $\mathbf{R}^2$ commute with H_{intr} and we can construct eigenfunctions of $\mathbf{R}^2$ and R_3 (the eigenvalue of the latter is, of course, zero). A proper angular momentum coupling gives*

$$|\Psi^{IR}_M\rangle = \sum_K (-)^{j-K} C^{I\ \ j\ \ R}_{K\ -K\ 0}\,\Phi_K|IMK\rangle. \tag{3.34}$$

These wave functions diagonalize $\mathbf{R}^2$, and the corresponding spectrum is of the form

$$E(I) = E_{\text{intr}} + \frac{1}{2\vartheta}R(R+1), \tag{3.35}$$

with

$$|j-R| \leqslant I \leqslant j+R;\ R=0,2,4,\cdots(\mathfrak{R}_1\text{ symmetry}). \tag{3.36}$$

This means that for each rotational quantum number R, $\mathbf{j}$ can have $2j+1$ orientations without changing the energy of the system (zero cou-

*Since we couple the angular momenta $\mathbf{I}$ and $-\mathbf{j}$ to $\mathbf{R}=\mathbf{I}-\mathbf{j}$, we have to apply a coupling rule as in the *ph*-case of Eq. (2.46).

pling). The splitting of the $2j+1$ levels can be taken into account in first-order perturbation theory (we will take a Nilsson term $\sim\beta r^2 Y_{20}$ as perturbation).

$$E(I)=E_0+\frac{1}{2\vartheta}R(R+1)-\beta\hbar\omega_0\langle\Psi_M^{IR}|r^2Y_{20}|\Psi_M^{IR}\rangle. \tag{3.37}$$

To each orientation of **j** there is a whole rotational band of the core with $\Delta R=2$. The levels with the highest I values $I=R+j$ for a given energy (i.e., for a given R) correspond to the yrast levels. These levels are connected by strong $E2$ transitions [Re 75a] and are experimentally the most easily accessible. They are called *favored states** [St 75a] and their energy is given by

$$E(I)=E_{\text{intr}}+\frac{1}{2\vartheta}(I-j)(I-j+1). \tag{3.38}$$

This means that these states lie on a parabola with a minimum at $I\simeq j$, which is experimentally widely confirmed, an example of which is shown in Fig. 3.8.

* Levels with a lesser degree of alignment (e.g. $I=j+R-1$) are called *unfavored states*.

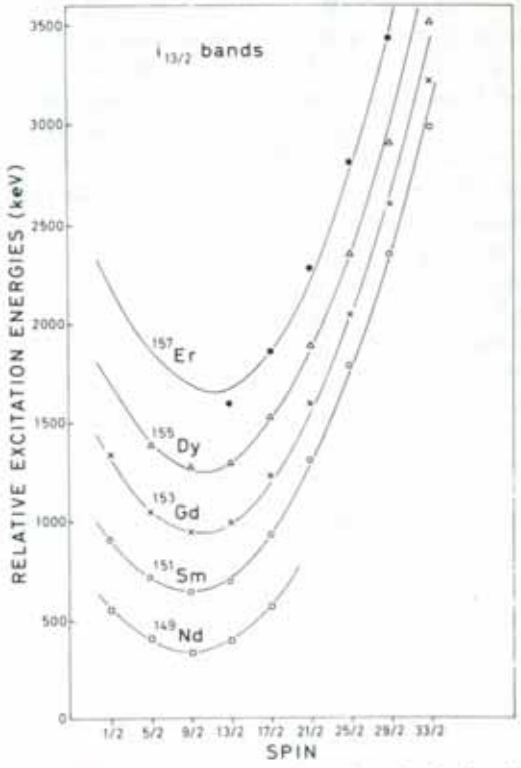

Figure 3.8. Relative excitation energies as a function of spin for the $i_{13/2}$ bands in some $N=89$ nuclei. (The experimentally observed band members are plotted such that the $13/2^+$ states are equally spaced (300 keV).) (From [LR 76].)

On the right branch of this parabola **j** and **R** are aligned (**j** $\parallel$ **R**),

$$I=j+R=j,j+2,j+4,\ldots,$$

and on the left branch **j** and **R** are anti-aligned (**j** $\parallel -$**R**); the core rotates in the opposite direction as **j***:

$$I=j-R=j-2,j-4,\ldots,\ \tfrac{3}{2}\ (\text{or}\ \tfrac{1}{2}).$$

As an empirical rule one can say that the weak coupling limit is strictly valid only for very small deformations $|\beta A^{2/3}|<4$. We shall see in the next section, however, that the states with **I** $\parallel$ **j** are energetically favoured even in the case of stronger deformations, where neglecting the Ω-dependence of H_{intr} is no longer justified. Therefore, the formula (3.38) is also valid for many levels in more deformed nuclei (see for instance Fig. 3.8) in the so-called rotation aligned coupling scheme.

3.3.1.3 The Decoupling Limit (Rotational Alignment). In the case of intermediate deformations, the energy splitting in the intrinsic part of the Hamiltonian can no longer be neglected. In this case, the orientation of the external large j-particle is no longer independent of the motion of the core. Stephens et al. [SDN 73] realized that the requirement of maximal overlap of the single-particle density distribution (which is concentrated mostly in a plane perpendicular to j) with the core can be fulfilled if the external particle is aligned along the rotational axis of a prolate nucleus (see also Sec. 2.8.4).

Mathematically, we can understand this in the model of a single j-shell ($C_{nj}\simeq 1$, like, for example, in the $i_{13/2}$ case). Neglecting $\mathbf{l}^2$ and **ls**-term, the Nilsson energies are simply given by the diagonal matrix element

$$\begin{aligned}\epsilon_\Omega&=\epsilon_0-\beta\cdot\hbar\omega_0\langle nlj\Omega|r^2Y_{20}|nlj\Omega\rangle\\&=\epsilon_0+\beta k\frac{3\Omega^2-j(j+1)}{4j(j+1)}=\epsilon_0-\frac{1}{4}\beta k+C\Omega^2,\end{aligned} \tag{3.39}$$

where k and C do not depend on Ω. Also, the recoil term (3.22) can be calculated as a diagonal matrix element and yields

$$H_{\text{rec}}=\frac{1}{2\vartheta}\{j(j+1)-\Omega^2\}. \tag{3.40}$$

Therefore, the Hamiltonian (3.10) in this approximation is:

$$H=\epsilon_0-\frac{1}{4}\beta k+\frac{1}{2\vartheta}(I(I+1)+j(j+1))+\left(C-\frac{1}{\vartheta}\right)\hat{I}_3^2+H_{\text{cor}}. \tag{3.41}$$

In a certain region of deformation, where $C\simeq 1/\vartheta$, there is thus a cancellation of the K dependence coming from the intrinsic and rotational parts of the Hamiltonian. This turns out to apply for a rather broad domain of intermediate deformations. Unfortunately, the eigenfunctions of H_{cor} which we needed to solve (3.41) cannot be given analytically in the general case. Thus, we wish to give a qualitative discussion. Writing the

* In principle, there are also anti-aligned states with $R>j$ [PO 78].

Coriolis term in the form*

$$H_{\text{cor}} = -\frac{1}{\vartheta}\mathbf{I}_{\perp}\mathbf{j}_{\perp}, \tag{3.42}$$

we see that it has its lowest expectation value for the wave functions with $\langle\mathbf{I}\rangle \parallel \langle\mathbf{j}\rangle$. Since $\mathbf{R}$ is perpendicular to the 3-axis, one gets the lowest eigenvalue for wave functions with a single-particle angular momentum aligned along a rotational axis perpendicular to the symmetry axis. For this purpose, we choose the 1-axis and accordingly construct eigenfunctions $|\tilde{\Phi}_\alpha\rangle$ of j_1 with eigenvalues α by rotating the eigenfunctions $|\Phi^j_K\rangle$ of j_3 through 90° about the 2-axis:

$$|\tilde{\Phi}_\alpha\rangle = \sum_K d^j_{K\alpha}\left(-\frac{\pi}{2}\right)|\Phi^j_K\rangle, \tag{3.43}$$

where $d^j_{K\alpha}$ is the Wigner function of this rotation [Ed 57].

For the total wave function it is, however, not so easy to make such a construction in which α is a good quantum number. The ansatz

$$|\Psi^I_{M\,j\,\alpha}\rangle = \sum_K d^j_{K\alpha}\left(-\frac{\pi}{2}\right)\Phi^j_K|IMK\rangle \tag{3.44}$$

is an eigenfunction of H_{cor} at least for $I \gg K$. With

$$I_-|IMK\rangle = \sqrt{I(I+1)-K(K+1)}\;|IMK+1\rangle \simeq I|IMK+1\rangle \tag{3.45}$$

we then easily get

$$H_{\text{cor}}|\Psi^I_{M\,j\,\alpha}\rangle = -\frac{1}{\vartheta}I\cdot\alpha|\Psi^I_{M\,j\,\alpha}\rangle \qquad (I \gg K), \tag{3.46}$$

which shows that α is the projection of $\mathbf{j}$ onto $\mathbf{I}$.

From Eq. (A24) and [Ed 57, Eq. (4.2.4)] we obtain

$$\mathcal{R}_1|\Psi^I_{M\,j\,\alpha}\rangle = (-)^{I-\alpha}|\Psi^I_{M\,j\,\alpha}\rangle, \tag{3.47}$$

which means that $I-\alpha$ has to be even in order to fulfill the symmetry condition $\mathcal{R}_1 = 1$.

In the case of $C \simeq 1/\vartheta$, we find for the spectrum of the Hamiltonian (3.41):

$$E(I,\alpha) = \text{const.} + \frac{1}{2\vartheta}(I(I+1)+j(j+1)-2I\alpha)$$

$$= \text{const.} + \frac{1}{2\vartheta}(I-\alpha)(I-\alpha+1) \tag{3.48}$$

$$= \text{const.} + \frac{1}{2\vartheta}R(R+1) \tag{3.49}$$

where $R = I-\alpha = 0, 2, 4, \ldots$ has to be even because of the symmetry condition (3.47).

The lowest lying states are therefore the ones which are maximally aligned ($\alpha = j$, *favored states*). This corresponds exactly to the picture of a valence particle whose spin is oriented perpendicular to the 3-axis while the core is completely decoupled and rotates with $R = I-\alpha$, giving rise to a spectrum $\Delta I = 2$, but which is otherwise equivalent to that of the neighboring even nucleus. Such bands have been seen, for example, in weakly deformed nuclei (see Figs. 3.8 and 3.9).

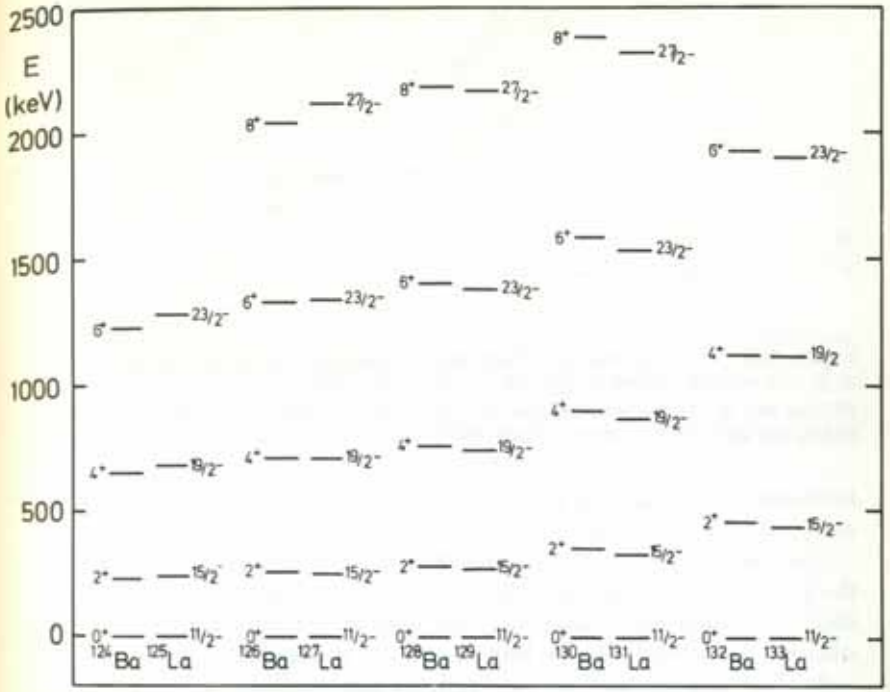

Figure 3.9. Comparison of ground band levels in some Ba isotopes with negative parity bands in the neighboring La nuclei. In most cases the La 11/2 level is not the ground state, and its energy has been subtracted from all levels shown for that isotope. (From [SDL 72].)

Lesser aligned states (*unfavored states*) have $\alpha = j-1$. They often lie at higher energies and are then not populated in (HI, xn) reactions.

Figure 3.10 shows the exact solution of the axially symmetric particle-plus-rotor model for one valence nucleon in a $1h_{11/2}$ shell as a function of the deformation β. For very small β-values, one has the weak coupling scheme of several nearly degenerate multiplets. On the oblate side ($\beta < 0$) the strong coupling is realized. In this case, the lowest level in the Nilsson scheme (see Fig. 2.21.) is the $\Omega = 11/2$ level. Its Coriolis matrix element is very small and a strongly coupled band with $\Delta I = 1$ is observed. On the prolate side the opposite is true: The lowest level has $\Omega = \frac{1}{2}$ and a very large Coriolis matrix element. The yrast band (the levels with the highest I-values) is now formed by a decoupled band $I = 11/2, 15/2, 19/2, \ldots$ with $\Delta I = 2$ and a level spacing, which is more or less that of the rotor (as seen at $\beta = 0$). We see also that for these completely aligned yrast levels the rotation aligned coupling scheme is very well realized over a wide range of

*$\mathbf{I}_\perp$ and $\mathbf{j}_\perp$ are the components of $\mathbf{I}$ and $\mathbf{j}$ perpendicular to the symmetry axis.

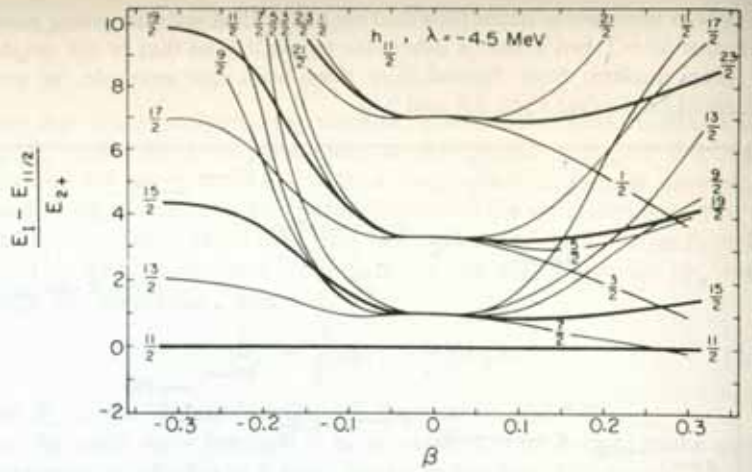

Figure 3.10. The eigenvalues of an axially symmetric particle-plus-rotor model, with one particle sitting in the $1h_{11/2}$ shell, as a function of the deformation β. Plotted are the excitation energies over the $I=11/2$ level. The Fermi surface λ is below the entire $h_{11/2}$ orbital. (From [St 75a].)

intermediate β-values: $0.13 \sim \beta < 0.23$. Only at very large deformations does one find deviations.

The structure of the bands also depends, of course, on the position of the Fermi level. We had here the simplest case of only one particle in the shell. The complete analogue is one hole in the high j-shell. There the situation is reversed: On the prolate side are the levels with large Ω-values —that is, one observes a strongly coupled scheme—and on the oblate side are the levels with small Ω-values and a decoupled scheme.

These considerations show that the structure of the rotational bands built on such high j levels provides an excellent tool to distinguish experimentally between prolate and oblate deformations in the transition region.

Summarizing the results of this section, we can say that

(i) In many cases, the Coriolis interaction can be neglected. Then the valence nucleons rotate around the symmetry axis of the core and change their orientation with it (strong coupling $\Delta I=1$).

(ii) In cases of small deformation and strong Coriolis interaction, the valence nucleons orient their angular momentum more or less independently of the orientation of the core. The core rotates with $\Delta I=2$ (weak coupling).

(iii) For intermediate deformations it can happen by a cancellation effect that a rotational alignment takes place. The valence particles orient their angular momentum parallel to the collective angular momentum (perpendicular to the symmetry axis of the core) and again we have $\Delta I=2$.

3.3.2 Some Applications of the Particle-plus-Rotor Model

The model of a few valence particles coupled to a symmetric rotor has been used in a very large number of cases to fit the experimental rotational bands. In general, it has been very successful. We do not want here to go into the many different versions which have been used but wish to discuss a few characteristic examples.

3.3.2.1 Strongly Mixed Bands in Well-Deformed Odd Mass Nuclei. The spectra of odd mass nuclei in the deformed region show many rotational bands which reveal very nicely the strong coupling picture. Only in cases where the particle sits in a single-particle shell with a high j-value (e.g., the $1i_{13/2}$ shell in the Er region), one also observes very distorted bands.* For small I values they start out like strongly coupled bands with $\Delta I=1$, but soon we observe staggering: The levels with $I+1/2$ even are shifted more and more against the levels with $I+1/2$ odd, so that in the end we have two separate bands with $\Delta I=2$ (see the positive parity band in Fig. 3.11 and [BDL 75]).

* For a comparison of these distorted bands with the backbending behavior in neighboring even nuclei, see [SKS 74].

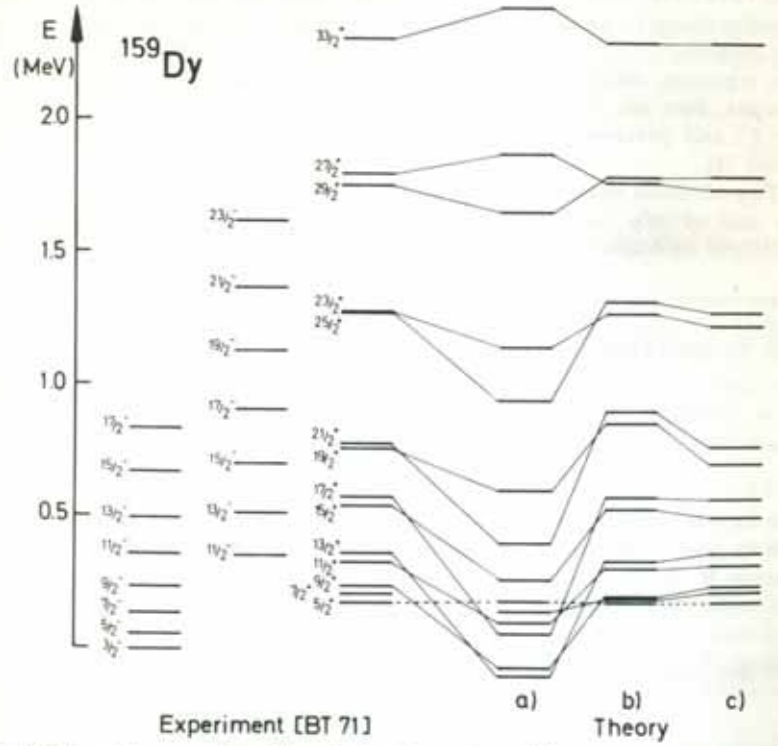

Figure 3.11. Three rotational bands in the nucleus ^{159}Dy. The $3/2^-$ and the $11/2^-$ bands are strongly coupled ($\Delta I=1$). The positive parity band with the band head $I=5/2$ is strongly perturbed, as discussed in the text. It is compared with three calculations: (a) a particle-plus-rotor fit without attenuation ρ, (b) a particle-plus-rotor fit with attenuation $\rho=0.5$, and (c) a self-consistently determined attenuation according to Eq. (3.56). (From [Ri 77].)

To describe these bands one usually diagonalizes the Hamiltonian (3.10) in the strong coupling basis (3.25). The single (quasi-) particle energies are taken from a Nilsson model and the parameters like the deformation β (and the gap Δ, see Chap. 6) are used to fit the spectrum. It thereby turns out that one can only reproduce the experimental spectrum if one introduces an additional parameter ρ—the *attenuation factor*—which weakens the Coriolis interactions, that is, if we use $\rho \cdot H_{cor}$ instead of H_{cor} [HRH 70, LRB 72, HK 77]. The original Coriolis force turns out to be much too strong and it has to be reduced by a factor $\rho \sim 0.4-0.8$. With this ad hoc attenuation and the other parameters of the model reasonably chosen, we are able to reproduce the distorted bands and find that for low I-values, that is, for small Coriolis interaction, one is in the strong coupling limit with $\Delta I = 1$. For higher I-values, however, the Coriolis force gets stronger and aligns the odd particle with the large j-value parallel to the rotational axis. For I-values $I \gtrsim j$, we have a rotational aligned motion, that is, large K-mixing and a splitting of the band in favored states with maximal alignment $\alpha = j$ for $(I-j)$ even, and unfavored states with lesser alignment $\alpha = j-1$ for $(I-j)$ odd. For the same value of angular momentum R of the core, which is given by $R = I-\alpha$, these two bands are almost degenerate (see Fig. 3.11).

Several attempts have been made to explain the *attenuation factors* as a kind of effective charge in the linear response approach [BPC 72, HK 75]. It turns out that this problem is closely connected with a proper treatment of the recoil term (3.22). The argument, that it is already taken into account in the fit of the band head energies, does not apply because in the one-particle case it is proportional to j^2-K^2 and therefore has a strong K-dependence which shifts the band heads [ORG 75].

To understand qualitatively the effect of the recoil term we restrict ourselves to the case of only one particle and rewrite the particle-plus-rotor Hamiltonian (3.20ff) in the following way [Kr 79].

$$H = H_{intr} + \frac{1}{2\vartheta}(I(I+1) - \mathbf{j}^2) + H'_{cor} \tag{3.50}$$

with the new Coriolis term

$$H'_{cor} = -\frac{1}{\vartheta}(\mathbf{I}-\mathbf{j})\mathbf{j}_\perp = -\frac{1}{\vartheta}\mathbf{R}\mathbf{j} = -\omega \mathbf{j}, \tag{3.51}$$

where the collective angular velocity is given by

$$\omega = -\mathbf{R}/\vartheta. \tag{3.52}$$

The Coriolis term H'_{cor} in Eq. (3.51) is attenuated compared to H_{cor} (3.23). To see this we go into the limit, where the odd particle is nearly aligned to the collective rotation $\mathbf{R}$. We then have

$$\mathbf{R} \simeq \mathbf{I}_\perp\left(1-\frac{\alpha}{I}\right) \tag{3.53}$$

and find that H'_{cor} is in this case proportional to H_{cor}:

$$H'_{cor} = \left(1-\frac{\alpha}{I}\right)H_{cor} = \rho \cdot H_{cor} \tag{3.54}$$

with an I-dependent attenuation factor

$$\rho = 1-\frac{\alpha}{I}. \tag{3.55}$$

Only for very high I-values does the attenuation disappear.

So far, the discussion of the influence of the recoil term has been restricted to the pure single-particle part of this operator. In fact, it also contains a two-body term $\mathbf{j}_{ik} \cdot \mathbf{j}_{lm} a_i^+ a_j^+ a_m a_k$, which produces an interaction with the particles of the core. We can treat it in the mean field approximation [Ri 77] and end up with a self-consistent attenuation factor

$$\rho = 1 - \frac{\langle j_1 \rangle}{\sqrt{I(I+1) - \langle j_3^2 \rangle}}. \tag{3.56}$$

At the limit of alignment it goes over into the form (3.55). We can also show that this approximation is equivalent to the cranking model (see Sec. 3.4). In a microscopic treatment of rotational bands in odd mass nuclei within the self-consistent cranking model (see Sec. 7.7), the attenuation of the Coriolis interaction is automatically incorporated [RMB 74, RM 74].

3.3.2.2 Backbending in Even Nuclei. The backbending phenomenon (see Sec. 3.2.4.) has been explained by Stephens and Simon [SS 72a] as an alignment of two neutrons in the $1i_{13/2}$ shell. If these two neutrons, instead of rotating around the 3-axis, align along the rotation axis of the nucleus, this adds an additional $13/2 + 11/2 = 12$ units of angular momentum. Therefore, the nucleus can decrease its collective rotation while increasing its total angular momentum through the addition of single-particle angular momentum.

To describe this idea mathematically, Stephens and Simon diagonalized the Hamiltonian (3.10) (with attenuation of the Coriolis term) taking as the basis the Slater determinant of the unperturbed core

$$|\Phi_0\rangle = |IMK=0\rangle$$

and two quasi-particle excitations (see Chap. 7)

$$|\Phi_K\rangle = \beta_{K_1}^+ \beta_{K_2}^+ |IMK = K_1 + K_2\rangle, \tag{3.57}$$

where β_K^+ is a creation operator for a quasi-particle in the state $\Omega = K$ of the $1i_{13/2}$ shell.

For low I values, the yrast states are given mainly in the zero quasi-particle state $|\Phi_0\rangle$ of the pure rotor. The excited bands are two quasi-particle bands. For higher I-values, the particles align their angular momenta along the axis of rotation, one of them to $\alpha = j = 13/2$, the second to $\alpha = j-1 = 11/2$. Thus, we find a mixing of the states Φ_0 and Φ_K $(K=0, 1, \ldots)$ and arrive, at the limit of full alignment, at a two-quasi-particle state of the form [see Eq. (3.44)]:

$$|\Phi\rangle_{al} = \sum_{K_1 K_2} d^j_{K_1 j}\left(-\frac{\pi}{2}\right) d^j_{K_2 j-1}\left(-\frac{\pi}{2}\right) \beta_{K_1}^+ \beta_{K_2}^+ |IMK_1 + K_2\rangle. \tag{3.58}$$

It can be written schematically as $\tilde{\beta}_j^+ \cdot \tilde{\beta}_{j-1}^+ |\Phi_0\rangle$, where the $\tilde{\beta}_a^+$ are the quasi-particle operators quantized along the 1-axis.

Stephens and Simon [SS 72a] were able to reproduce the experimental backbending spectra reasonably well with this method. Since they did not take into account, however, the gradual change in the pairing correlations caused by the Coriolis–anti-pairing effect, they could not obtain the deviations from the $I \cdot (I+1)$ law at low spin values.

In spite of the fact that this model describes the important effect of two aligning particles properly, it does not allow us to decide whether there is any other mechanism which could be the origin of the observed backbending phenomenon. To decide whether it is caused by a change in shape, by a phase transition to a normal fluid state, or by an alignment process, one has to carry out a microscopic calculation which allows for all these degrees of freedom. Such investigations have been done (see Sec. 7.7). They show that the rotational alignment of two particles is

the most important effect. These processes are found in all nuclei in which a high j-shell exists in the vicinity of the Fermi surface. However, it is another question as to whether they produce backbending. This depends finally on the strength of the interaction between the two crossing bands: Only for rather small coupling matrix elements do we observe a sudden transition, that is backbending.*

3.3.3 The Triaxial Particle-plus-Rotor Model

We have already seen in Section 1.5.3 that Davydov et. al. [DF 58] used a triaxial rotor to explain the low lying 2^+ states in some transitional nuclei. The model can also be extended to odd mass nuclei by the coupling of an external particle to a triaxial rotor [Pa 61, HS 62, PR 62, PS 65, MSD 74, Me 75, FT 75, TF 75, Le 76, DF 77, LLR 78]. It has been applied to cases where the external particle sits in a high j-shell, and has turned out to be very powerful as a description of energy levels and decay schemes of many transitional nuclei.† However, at present the microscopic foundation is missing. Using microscopic theories, the calculations of static energy surfaces in these mass regions show no pronounced minima at triaxial deformations, which would justify this simple picture. In fact, there exist other models based on a *vibrational picture* [AP 76, PVD 77, YNN 76] that are also able to reproduce such spectra. It is not clear at present whether there is any connection between these two pictures of transitional nuclei.

We restrict ourselves in the following discussion to one external particle in a high j-shell (e.g., $h\,11/2$) and couple it to a triaxial rotor. In this case, the Hamiltonian has the form [MSD 74]:

$$h=\sum_{i=1}^{3}\frac{R_i^2}{2\mathcal{I}_i}+h_0+kr^2\beta\left\{\cos\gamma Y_{20}+\sin\gamma\frac{1}{\sqrt{2}}(Y_{22}+Y_{2-2})\right\}. \qquad (3.59)$$

The β,γ-dependence of the moment of inertia $\mathcal{I}_i$ is that for irrotational flow [eq. (1.48)] and only the overall constant is adjusted. The constant k is given by the splitting of the j-shell in the Nilsson scheme. h_0 is the spherical harmonic oscillator. Usually a single-particle pairing field with constant gap Δ is also taken into account.

Figure 3.12 shows the spectrum of the Hamiltonian (3.59) as a function of γ at a typical deformation $\beta=5A^{-2/3}$. On the prolate side ($\gamma=0$) and on the oblate side ($\gamma=60°$) we see again the same spectra as in Fig. 3.10. However, these two limits are now connected through a circle in the β,γ plane (Fig. 1.4) with constant deformation β. We no longer pass through the weak coupling limit at $\beta=0$. On both sides the spectra do not depend very drastically on the triaxiality γ. The essential transition from the strongly coupled to the decoupled scheme takes place in a relatively small γ region around $\gamma=30°$. There are many spectra in weakly deformed transitional nuclei that can be nicely reproduced with γ-values between 20° and 40°. This agreement can be improved even more by incorporating the change of the moment of inertia in a VMI-model type calculation [FT 75].

* Recently, Bengtsson et al. [BHM 78] have found an oscillating behavior of this interaction as a function of the chemical potential λ. For an interpretation of this fact see [FPS 80] and the references given there.

† For extension of the triaxial rotor model to multiparticle configurations, see [TNV 77, YTF 77, TYF 77, YTF 78].

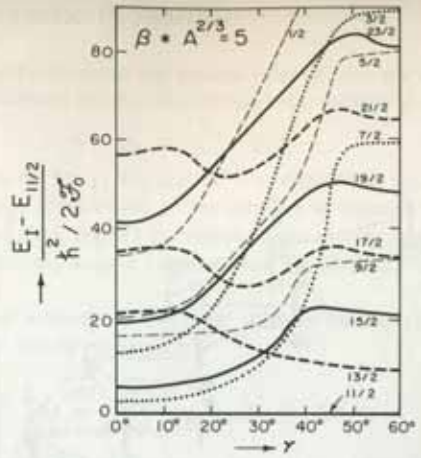

Figure 3.12. Spectrum of a $j=11/2$ particle coupled to an asymmetric rotor with all yrast levels $I<23/2$ as function of γ. (From [MSD 74].)

The *dynamical behavior* of a system of an odd high-j particle coupled to a rotating trixial core is determined by three physical effects (see [Me 75]):

(i) The core prefers to rotate around the axis with the maximal moment of inertia in order to minimize the rotational energy.
(ii) The particle moving in the deformed well prefers maximal mass overlap with the core, because in this case its potential energy is minimal.
(iii) The Coriolis interaction tries to align the angular momenta of the particle **j** and the core **R**.

For high j-values the alignment dominates as long as we have only one particle in the j-shell. Since the density distribution of an aligned particle is oblate with j as symmetry axis, condition (ii) is optimally satisfied if the core is oblate ($\gamma=60°$), which corresponds to the 2-axis as the symmetry axis. However, in this case $\mathcal{I}_2=0$ and condition (i) is violated. Therefore, **R** will be perpendicular to the 2-axis and we no longer have alignment. In the triaxial case, $\mathcal{I}_2$ no longer vanishes and conditions (i), (ii), and (iii) can all be satisfied together. There is an alignment of **j** and **I** along the 2-axis. In fact, the calculations show that the odd particle tends to align along the 2-axis of the core. This axis serves as an approximate symmetry axis in the sense that the approximate quantum numbers $\bar{K}$ and $\bar{\Omega}$ (representing the projections of **I** and **j** onto the 2-axis) are meaningful for a classification. The result is a new level scheme characteristic for a triaxial rotor.

The yrast levels are given by $\bar{\Omega}=j$ and $\bar{K}=j, j\pm2, j\pm4$, as in the rotation aligned coupling scheme of Stephens. For these levels, **I**, **j**, **R**, and the 2-axis are parallel. They lie on the usual parabola with $\Delta I=2$ (see Fig. 3.13). Contrary to the axial symmetric case, where the direction of the alignment was arbitrary in the 1, 2 plane (usually one chooses the 1-axis), we have the asymmetric case with no such symmetry. Alignment favors the 2-axis. This has the consequence that on each yrast level there exists a rotational band with the spin order $\Delta I=1$. In fact, such levels have been experimentally observed [ABR 75].

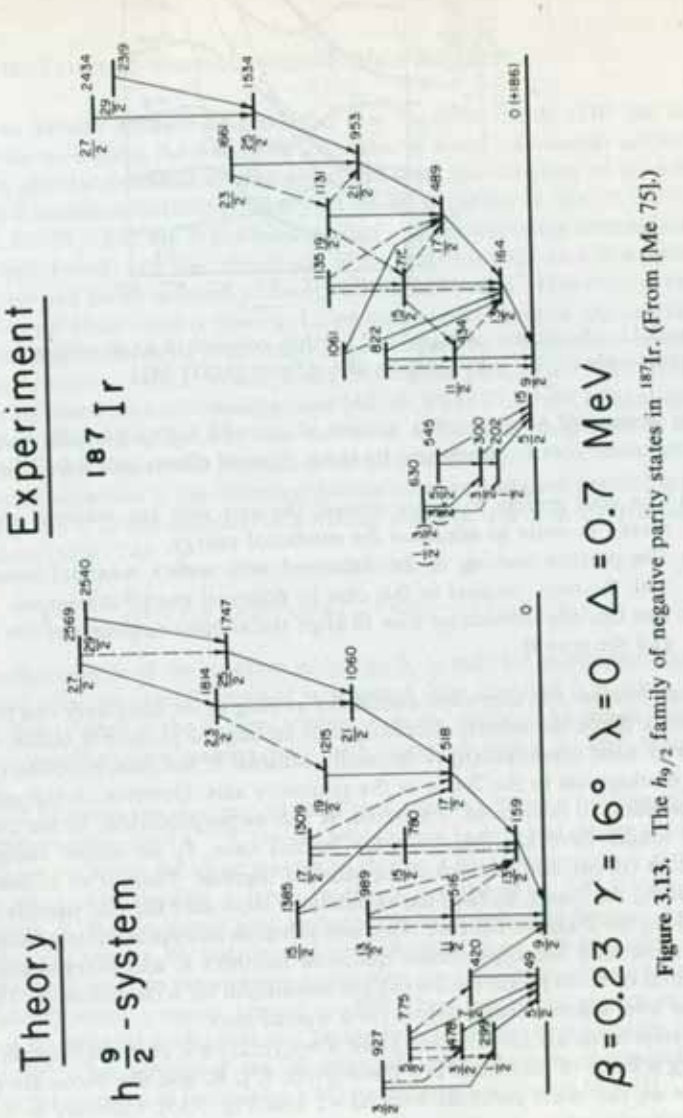

Figure 3.13. The $h_{9/2}$ family of negative parity states in ^{187}Ir. (From [Me 75].)

3.3.4 Electromagnetic Properties

According to the separation of the system into valence particles and a core, we also have two contributions for the electromagnetic multipole operators:

$$Q_{\lambda\mu} = Q^{(c)}_{\lambda\mu} + Q^{(p)}_{\lambda\mu}. \tag{3.60}$$

The core part is given by Eq. (1.35) and $Q^{(p)}$ is defined in Eqs. (B.23, B.24) where the sum over i however is restricted to the number of valence particles.

In the following we shall restrict ourselves to the axially symmetric case without pairing. It is then relatively simple to generalize the formulae to more complicated cases.

The *magnetic dipole moment* of the rotor is given by Eq. (1.36) as $\boldsymbol{\mu} = \mu_N \cdot g_R \mathbf{R}$. We therefore gain for the $M1$ operator:

$$\mathbf{M}_1 = \sqrt{\frac{3}{4\pi}}\ \mu_N \cdot g_R(\mathbf{I}-\mathbf{j}) + \mathbf{M}^{(p)}_1. \tag{3.61}$$

The magnetic dipole moment is defined in Eq. (B.31). With the wave function of Eq. (3.25) we obtain for $K \neq 1/2$, using the projection theorem (2.66),

$$\mu = \sqrt{\frac{4\pi}{3}}\ \langle \Psi^I_{IK} | M_{1z} | \Psi^I_{IK} \rangle = \mu_N \left\{ g_R \frac{I(I+1)-K^2}{I+1} + g_K \frac{K^2}{I+1} \right\} \tag{3.62}$$

where we have introduced the gryomagnetic ratio g_K in the following way.

$$\begin{aligned} g_K \cdot K &= \frac{1}{\mu_N} \sqrt{\frac{4\pi}{3}}\ \langle \Phi_K | M^{(p)}_{13} | \Phi_K \rangle \\ &= \langle \Phi_K | g_s \cdot s_3 + g_l l_3 | \Phi_K \rangle \\ &= g_l K \cdot + (g_s - g_l) \cdot \langle \Phi_K | s_3 | \Phi_K \rangle. \end{aligned} \tag{3.63}$$

The matrix element $\langle \Phi_K | s_3 | \Phi_K \rangle$ can be calculated with a Nilsson wave function. For $K = 1/2$ one gets an additional contribution to the magnetic moment which contains the decoupling factor a of Eq. (3.30).

The magnetic moments obtained from Eq. (3.62) have been calculated for a large range of nuclei [MN 59, NN 65 p. 653] and one has found that agreement with experimental data is usually better for protons than for neutrons. A detailed investgation shows, however, that one again needs polarization charges for g_s: $g_s^{\text{eff}} \simeq 0.7 g_s^{\text{free}}$ (see [BM 75 p. 302ff]).

Similarly, we can calculate the reduced matrix elements for $M1$-*transitions*. The operator I does not cause any transitions. For the rest we use Eq. (1.70) and get for $K \neq 1/2$ and $I_i \neq I_f$:

$$B(M1, I_i \to I_f) = \frac{1}{2I_i+1} \left| \langle \Psi^{I_f}_K \| M_1 \| \Psi^{I_i}_K \rangle \right|^2 = \frac{3}{4\pi} \mu_N^2 (g_K - g_R)^2 K^2 \left| C^{I_i\ 1\ I_f}_{K\ 0\ K} \right|^2. \tag{3.64}$$

These $M1$-transitions are only possible for rotational bands in odd nuclei. Also, reasonable agreement with experiment has been found [SBP 67].

Again using Eq. (1.70) we can also derive the $B(E2)$ values for *electric quadrupole transitions*. For transitions between states with the same K value the core contribution is much larger than the particle contribution because of the large Q_0 values. Therefore, the latter can be neglected, and we obtain

$$B(E2, I_i \to I_f) = Q_0^2 \frac{5}{16\pi} \left| C^{I_i\ 2\ I_f}_{K\ 0\ K} \right|^2. \tag{3.65}$$

This equation is used to determine the experimental values for the deformations appearing in Q_0. In Sec. 2.8.6 we saw that they agree with the theoretically determined deformations. Therefore, the particle-plus-rotor model gives the proper $E2$ transition probabilities for transitions with the same K-value.

For transitions with different K-values, the collective part vanishes. Such transitions are, in fact, very weak (*K-forbidden*) because the single-particle part contains only the single-particle matrix element of r^2Y_{20} in the intrinsic frame. We have already seen in Section 2.7.2 that they are small compared to the collective values. On the other hand, a pure single-particle model cannot explain the effective charges in spherical nuclei (see Sec. 2.7.2). The same difficulties occur here again. For a detailed discussion, see the paper of Löbner and Malinskog [LM 66], which contains much experimental data together with possible ways to improve the simple Nilsson estimate.

Finally, we have to mention that the above considerations apply only to pure K-bands. For transition probabilities and electromagnetic moments in K-mixed bands, like rotational aligned bands or bands in an asymmetric rotor, we have to take into account the mixing coefficients.

3.4 The Cranking Model*

We have seen in the last section how the motion of particles in a deformed well can be connected with the idea of a rigid rotor. This model is very successful in the description of the level structure of rotational and even transitional nuclei. However there exists no straightforward microscopic derivation; in particular, one cannot calculate the inertial parameters in this model.

On the other hand, nearly all fully microscopic theories of nuclear rotation are based on or related in some way to the cranking model, which was introduced by Inglis [In 54, 56] in a semiclassical way, but as we shall see in Section 11.4, it can be derived fully quantum mechanically, at least in the limit of large deformations, and not too strong K-admixtures ($K \ll I$).

The cranking model has the following advantages.

(i) In principle, it provides a fully microscopic description of the rotating nucleus. There is no introduction of redundant variables, therefore, we are able to calculate the rotational inertial parameters microscopically within this model and get a deeper insight into the *dynamics* of rotational motion.

(ii) It describes the collective angular momentum as a sum of single-particle angular momenta. Therefore, collective rotation as well as single-particle rotation, and all transitions in between such as decoupling processes, are handled on the same footing.

(iii) It is correct for very large angular momenta, where classical arguments apply (even if the quantum mechanical derivation does not work in this limit [BMR 70]).

* In this chapter, we treat only cranking theory for rotations. We can, however, also apply a similar theory for general collective motions, as discussed in Section 12.3.7.

The shortcomings of the model are:

(i) As we shall see, it is basically a nonlinear theory. Only in the limit of small angular momenta can one linearize it using perturbation theory (cranking formula for the moment of inertia). In general, the calculations are therefore complicated, especially in cases where one has several solutions.

(ii) The resulting wave functions are not eigenstates of the angular momentum operators. It is therefore not clear a priori how one has to calculate, for example, electromagnetic transition probabilities. In fact, we shall see in Section 11.4 that cranking model wave functions are in a sense only *internal wave functions* and that one has to use projection techniques to get the wave functions in the laboratory system.

In the following we shall give the usual semiclassical derivation (see, for instance, [Vi 57b, So 73]) and discuss the cranking model in connection with a pure single-particle Hamiltonian. Many of the arguments in the next sections can, however, also be applied to a general two-body Hamiltonian (see Sec. 7.7).

3.4.1 Semiclassical Derivation of the Cranking Model

The basic idea of the cranking model is the following classical assumption: If one introduces a coordinate system which rotates with constant angular velocity ω around a fixed axis in space, the motion of the nucleons in the rotating frame is rather simple if the angular frequency is properly chosen; in particular, the nucleons can be thought of as independent particles moving in an average potential well which is rotating with the coordinate frame.

In Section 11.4, we will see how the consequences of this picture can also be derived from quantum mechanics using projection techniques. For the moment, however, we want to stay with the classical description because of its intuitive character. Also, we do not want to take into account any residual interaction. Therefore, we assume a single-particle potential V of fixed shape, which rotates in space, and accordingly we must consider the time-dependent single-particle Hamiltonian

$$h(t) = \frac{\mathbf{p}^2}{2m} + V(\mathbf{r}, t) \tag{3.66}$$

and the corresponding Schrödinger equation

$$h(t)\psi(t) = i\hbar \frac{\partial}{\partial t}\psi(t). \tag{3.67}$$

Introducing spherical coordinates r, θ, φ with respect to the axis ω, we can represent the time-dependence of $V(t)$ in the following way. If $V(\mathbf{r}, 0)$ is the

potential at time $t=0$, then we have at time t:

$$V(\mathbf{r},t)=V(r,\theta,\varphi-\omega t,0). \tag{3.68}$$

Again we realize that V is only time dependent if it depends on φ. In other words, V should not have axial symmetry around the rotational axis, because then there can be no collective rotation possible around an axis of symmetry for a quantum mechanical system (see Sec. 1.5.1). Because of the very simple time dependence of $V(t)$ in Eq. (3.68), a unitary transformation exists which eliminates this time dependence. It is

$$U=e^{i\omega t} \tag{3.69}$$

with $\boldsymbol{\omega}\cdot\mathbf{l}=(\hbar/i)\omega\cdot\partial/\partial\varphi$. U produces a rotation of an angle ωt around the rotational axis $\boldsymbol{\omega}$.

We find the time-dependent operator

$$Uh(t)U^{-1}=h(0) \tag{3.70}$$

and define

$$\tilde{\psi}=U\psi, \tag{3.71}$$

with

$$i\hbar\dot{\tilde{\psi}}=i\hbar U\dot{\psi}+i\hbar\dot{U}\Psi=(h(0)-\omega\mathbf{l})\tilde{\psi}. \tag{3.72}$$

Equation (3.72) is a time-dependent Schrödinger equation with an explicitly time-independent effective Hamiltonian h_ω. It thus can be solved as an eigenvalue problem in the standard way:

$$h_\omega\tilde{\psi}=(h(0)-\omega\mathbf{l})\tilde{\psi}=\epsilon'_\omega\tilde{\psi}, \tag{3.73}$$

where ϵ'_ω are eigenvalues of the effective Hamiltonian. To get the energies of the original Hamiltonian, we have to calculate

$$\epsilon_\omega=\langle\psi|h(t)|\psi\rangle=\langle\tilde{\psi}|h(0)|\tilde{\psi}\rangle=\epsilon'_\omega+\omega\langle\tilde{\psi}|\mathbf{l}|\tilde{\psi}\rangle. \tag{3.74}$$

The term $\boldsymbol{\omega}\mathbf{l}$ is usually called the Coriolis term.

We have now solved the time-dependent Schrödinger equation in a rotating potential and found that we must diagonalize an effective time-independent Hamiltonian. We want to emphasize that we have not derived a priori the Hamiltonian as it is seen from the rotating coordinate system, since we transformed only the coordinates and not the momenta. In fact, in the case of pure translational motion, we would get a similar result [$h_v=h(0)-\mathbf{v}\cdot\mathbf{p}$], but from Galilean invariance we require that the Hamiltonian seen from the moving coordinate system is the same as in the rest frame. Nevertheless, it turns out that in the special case of rotations, h_ω in Eq. (3.73) is identical with the Hamiltonian as seen from the rotating system [Va 56; Br 64, p. 69]. From the term $\boldsymbol{\omega}\mathbf{l}$, we can derive the Coriolis force as well as the centrifugal force.

For systems with spin the operator which generates rotations is $\mathbf{j}=\mathbf{l}+\mathbf{s}$. The orientation of the rotational axis is usually chosen as parallel to the x-axis because it is understood to be perpendicular to the axis of symmetry, which for $\omega=0$ is the z-axis. For higher angular momenta, one also investigates nonsymmetric single-particle potentials. Nevertheless, we require that $\boldsymbol{\omega}$ is parallel to a principal axis of the potential. Therefore, the many-body Hamiltonian of the cranking model is given by ($J_x=\sum_{i=1}^{A}j_x^{(i)}$):

$$H_\omega=H-\omega J_x=\sum_{i=1}^{A}h_\omega^{(i)}, \tag{3.75}$$

where H is a sum of deformed single-particle Hamiltonians.

Within the cranking model we must now diagonalize H_ω, and the resulting ground state wave function Φ_ω is a Slater determinant. As in the normal shell model (with $\omega=0$) the question arises how the levels in the single-particle potential should be filled to obtain the lowest energy state for any given angular momentum (the yrast level). The answer to this question (given in Sec. 11.4) is that we have to minimize the energy $E'=\langle\Phi|H-\omega J_x|\Phi\rangle$, that is, we have to fill up the potential in the usual way *in the rotating frame*.

For the energy in the laboratory system, from Eq. (3.74) we get

$$E(\omega)=\langle\Phi_\omega|H|\Phi_\omega\rangle=\langle\Phi_\omega|H_\omega|\Phi_\omega\rangle+\omega\langle\Phi_\omega|J_x|\Phi_\omega\rangle. \tag{3.76}$$

Since $E(\omega)$ cannot depend on the sign of ω, one finds

$$E(\omega)=E(0)+\frac{1}{2}\mathcal{I}_1\omega^2+\cdots \tag{3.77}$$

and, since for $\omega=0$ $\langle\Phi_0|J_x|\Phi_0\rangle=0$,

$$J(\omega)=\langle\Phi_\omega|J_x|\Phi_\omega\rangle=\mathcal{I}_2\omega+\cdots. \tag{3.78}$$

We can show that the constants $\mathcal{I}_1$ and $\mathcal{I}_2$ are equal [Sch 61],

$$\mathcal{I}_1=\mathcal{I}_2, \tag{3.79}$$

using the fact that $E(\omega)$ is the lowest eigenvalue of H_ω. According to the variation principle of Ritz, we get Φ_ω as a solution of the equation

$$\delta\langle\Phi|H-\omega J_x|\Phi\rangle=0, \tag{3.80}$$

where $|\Phi\rangle$ is any one from the family of all possible Slater determinants. The condition is also fulfilled if we take $|\Phi\rangle$ to be taken out of the set $\{\Phi_{\omega'}\}$, where $\Phi_{\omega'}$ is an eigenfunction of $H-\omega' J_x$, and ω' runs through all real numbers. Then we find from Eq. (3.80):

$$\frac{d}{d\omega'}\langle\Phi_{\omega'}|H|\Phi_{\omega'}\rangle-\omega\frac{d}{d\omega'}\langle\Phi_{\omega'}|J_x|\Phi_{\omega'}\rangle=0 \tag{3.81}$$

or

$$\mathcal{I}_1=\frac{1}{\omega}\frac{d}{d\omega}E(\omega)\bigg|_{\omega=0}=\frac{d}{d\omega}J(\omega)\bigg|_{\omega=0}=\mathcal{I}_2.$$

We also derive from Eq. (3.80);

$$\omega=\frac{dE}{dJ}. \tag{3.82}$$

To have a comparison with experiment, we have to determine the value of

the angular velocity. Inglis [In 54] proposed to include the zero-point oscillations at least semiclassically by requiring

$$J = \langle \Phi_\omega | J_x | \Phi_\omega \rangle = \sqrt{I(I+1)} \ . \tag{3.83}$$

In first order we get

$$\omega = \frac{\sqrt{I(I+1)}}{\vartheta_1} \tag{3.84}$$

and, from (3.77),

$$E(I) = E(0) + \frac{1}{2\vartheta_1} I \cdot (I+1). \tag{3.85}$$

For higher ω-values there are deviations from this $I(I+1)$ law. In general, the moment of inertia is defined as

$$\vartheta = \frac{J}{\omega} \ . \tag{3.86}$$

Up to now we have investigated only completely independent particle motion, by which we mean that we have even neglected the influence of the rotation on the average field. In Section 7.7 we will show how this can be taken into account.

3.4.2 The Cranking Formula

In the case of a pure $I(I+1)$ spectrum, we need calculate only one constant, the *moment of inertia*. It is already determined by the 2^+ state and therefore it seems meaningful to apply perturbation theory for such small I-values.

We start with the unperturbed system of a deformed potential, which is filled up to the Fermi level. Levels below will be called holes (indices $i, i', \ldots$); levels above will be called particles (indices $m, m', \ldots$). The shell model basis consists of the ground state $|\Phi_0\rangle$, *ph*-states $|mi\rangle = a_m^+ a_i |\Phi_0\rangle$, $2p$-$2h$ states, and so on. The perturbation $\omega \cdot J_x$ is a one-particle operator and can therefore excite only one *ph* pair at a time. Therefore, we get for the perturbed wave function up to first order

$$|\Phi\rangle = |\Phi_0\rangle + \omega \sum_{im} \frac{\langle mi | J_x | \Phi_0 \rangle}{\epsilon_m - \epsilon_i} a_m^+ a_i |\Phi_0\rangle, \tag{3.87}$$

where ϵ_i and ϵ_m are the single-particle energies of the Hamiltonian H. The expectation value of J_x up to first order in ω is then

$$J = \langle \Phi | J_x | \Phi \rangle = 2\omega \sum_{mi} \frac{|\langle mi | J_x | \Phi_0 \rangle|^2}{\epsilon_m - \epsilon_i} \ , \tag{3.88}$$

which, together with (3.78) gives for the moment of inertia*

$$\vartheta_{\text{Inglis}} = 2 \cdot \sum_{mi} \frac{|\langle m | J_x | i \rangle|^2}{\epsilon_m - \epsilon_i} \ . \tag{3.89}$$

* In molecular physics a similar formula has been derived by Wick [Wi 48].

This is the well known *Inglis formula* for the moment of inertia [In 54, BM 55].

The moments of inertia that result from this formula are usually very close to the rigid body value of the moment of inertia [Eq. (1.49)]. In fact, we shall see in Section 3.4.3 that, in the case of a pure anisotropic oscillator, this will be an exact result. Lüders [Lü 60] showed that this is the result for any independent particle model in the limit of large particle numbers (see also [AB 59, Ro 59, SB 64, Da 75, KG 78]).

We can understand this result qualitatively, if we realize that the velocity distribution of the ground state in a deformed static potential is nearly isotropic (see Sec. 13.3), and that this fact is not changed in the rotating system by Coriolis or centrifugal forces (see [BJ 76b]). Then there is no net flow in the intrinsic system and from the laboratory frame we observe a rigid-rotation velocity distribution.

As we have seen in Section 1.5.1, the experimental moments of inertia are a factor of 2 to 3 smaller than their rigid body values. Bohr and Mottelson [BM 55, Mo 56] already indicated that residual two-body interactions would lower these values. The most important influences in this respect are the correlations of the pairing type. Since they can be included very easily within the BCS-formalism (see Chap. 6) in a single-particle description, we give here the derivation of the so-called Belyaev formula [Be 59, 61], which is the extension of the Inglis formula (3.89) that includes pairing correlations. (Readers not familiar with this formalism are referred to Chapter 6.)

In this case, $|\text{BCS}\rangle$ represents the BCS-ground state (6.31) and excitations are given by the two-quasi-particle states $\alpha_k^+ \alpha_{k'}^+ |\text{BCS}\rangle$, four-quasi-particle states, etc. By analogy with Eq. (3.87), we obtain the perturbed wave function

$$|\Phi\rangle = |\text{BCS}\rangle + \omega \sum_{k<k'} \frac{\langle \text{BCS} | \alpha_{k'} \alpha_k J_x | \text{BCS} \rangle}{E_k + E_{k'}} \alpha_k^+ \alpha_{k'}^+ |\text{BCS}\rangle, \tag{3.90}$$

where $E_k + E_{k'}$ is the excitation energy of the quasi-particle pair k, k'. The quasi-particle energies are given by

$$E_k = \sqrt{(\epsilon_k - \lambda)^2 + \Delta_k^2} \ . \tag{3.91}$$

Proceeding as in Eqs. (3.88) and (3.89), we find for the moment of inertia

$$\vartheta_{\text{Belyaev}} = 2 \sum_{k<k'} \frac{|J_{x_{kk'}}^{20}|^2}{E_k + E_{k'}} \ . \tag{3.92}$$

From Eq. (E.16), we find J_x^{20} and get

$$\vartheta_{\text{Belyaev}} = 2 \sum_{k,k'>0} \frac{|\langle k | J_x | k' \rangle|^2}{E_k + E_{k'}} (u_k v_{k'} - u_{k'} v_k)^2. \tag{3.93}$$

This formula for the moment of inertia indeed yields lower values as compared to expression (3.89). Two effects are responsible for this:

(i) The energy denominator is much larger than the particle-hole energies in Eq. (3.89). The parameter Δ [Eq. (3.91)] produces a gap of at least $2\Delta \simeq 2$ MeV for the important levels in the neighborhood of the Fermi surface

(ii) The factor $(u_k v_{k'} - u_{k'} v_k)^2$ is usually somewhat smaller than unity.

The lowering of the moment of inertia in the BCS-theory, as compared to the rigid body value, corresponds to a superfluid slippage of some nucleons as the nucleus rotates [Mi 59, 60].

Extended numerical calculations [GR 60, NP 61, MT 75] for realistic nuclei show a remarkable agreement with the experimental values. As we shall see in the next section, it is very important to apply the Inglis or the Belyaev formula to self-consistent wave functions, that is, those calculated at deformations that correspond to the energy minimum. In most of these calculations, this is achieved by using Nilsson wave functions and energies at the experimentally observed deformations as well as the experimentally determined values of the gap Δ (see also [MN 59]).

The success of these calculations, which produce roughly correct moments of inertia lying between the (too small) irrotational values and the (too large) rigid body value gives us great confidence that the picture of rotational nuclei as a deformed superfluid many-body system is correct.

Of course, we can investigate the influence of the *residual interaction* on the moment of inertia. This can be done within the framework of linear response theory (see Sec. 8.5.3 and [MSV 72]). In this kind of theory, the external field represented by the Coriolis operator J_x can excite virtual vibrations of the core which, in turn, have an influence on the moment of inertia. There are two types of such vibrations: surface oscillations (*ph* vibrations), which correspond to the stretching effect, and oscillations in the pairing correlations (*pp*-vibrations; see Sec. 8.3.5). The net result of such calculations is that both effects more or less cancel, and we get roughly the same values for the moments of inertia (Fig. 3.14) as given by the BCS theory.

We have now discussed the application of perturbation theory to the calculation of the expectation value of J_x, that is, the moment of inertia. In a similar fashion, we can calculate other properties of the rotating nucleus, for example, the *gyromagnetic ratio* g_R or the magnetic moment of the first 2^+ state. Since the magnetic moment μ is defined as the expectation value of μ_z in the state $|I, M=I\rangle$ [Eq. (B.31)] and the cranking model wave functions are not eigenfunctions of angular momentum, it is not clear at this point how to calculate μ. In Sec. 11.4, we will see that a projection technique has to be applied. In lowest order, we get a very simple result, which can be understood easily within the semiclassical picture of the cranking model:

$$\mu = \langle \Phi_\omega | \mu_x | \Phi_\omega \rangle. \tag{3.94}$$

We can therefore define the gyromagnetic ratio (1.37) by

$$\mu = g_R \cdot J = g_R \cdot \langle \Phi_\omega | J_x | \Phi_\omega \rangle. \tag{3.95}$$

From (3.90), in first order perturbation theory, we get

$$g_R = \frac{1}{\hbar} \sum_{k,k'>0} \frac{(\langle k|J_x|k'\rangle\langle k'|\mu_x|k\rangle + \text{c.c.})}{E_k + E_{k'}} (u_k v_{k'} - u_{k'} v_k)^2. \tag{3.96}$$

The values calculated with these formulae are smaller than the liquid drop value $g_R = Z/A$ [Eq. (1.37)] and agree quite well with the experimental data [MSV 72].

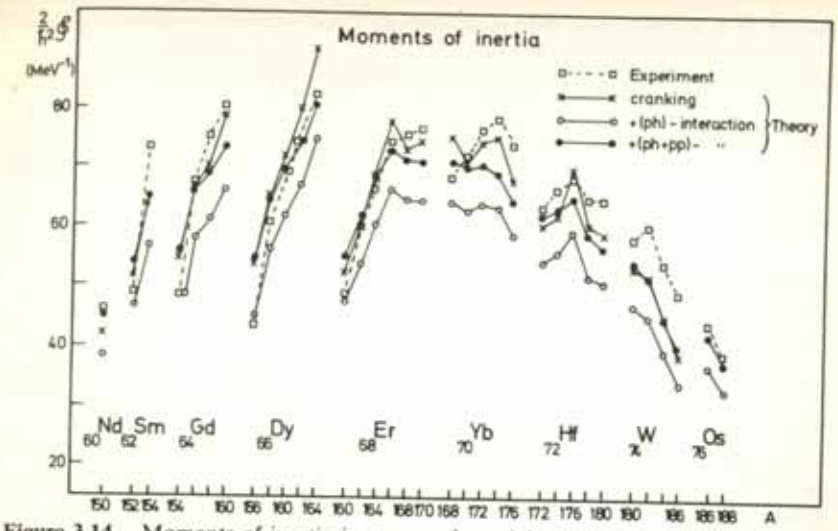

Figure 3.14. Moments of inertia in rare earth nuclei. The squares indicate experimental values [NP 61]; the crosses are obtained from the Belyaev formula (3.93). The open circles take into account only the stretching effect (*ph* interaction); in addition to that, the closed circles also take into account the antipairing effect (*pp*-interaction). (From [MSV 72].)

As we have seen in Section 3.2, deviations from the $I(I+1)$ law occur as we go to higher angular momenta. To calculate the *B and C coefficients* [Eq. (3.1)] connected with these deviations, one has used perturbation theory in higher order, including the effects of a residual interaction [Ma 65, Ma 67a, MR 70], so that the most important effect is the so-called Coriolis-antipairing effect, which we will discuss in Section 7.7. As we shall see, it is only at the very high spin states with $I > 30$ or 40 that one can expect the pairing correlations to vanish.

3.4.3 The Rotating Anisotropic Harmonic Oscillator

We have seen in Section 2.8.3 that the anisotropic harmonic oscillator can be solved analytically and that it provides at least a qualitative model for a deformed nucleus. It turns out that it can also be solved analytically in the rotating frame (see [Va 56, Ze 75, RBK 75, GMZ 78]), because $l_x = yp_z - zp_y$ is a quadractic form in the coordinates x, y, z and momenta p_x, p_y, p_z.

We can forget about the spin, since the potential does not depend on it (the term $-\omega s_x$ in the Coriolis operator can be diagonalized separately in the spin space and gives only a diagonal contribution). The Hamiltonian then has the form

$$h_\omega = -\frac{\hbar^2}{2m}\Delta + \frac{1}{2}m(\omega_x^2 x^2 + \omega_y^2 y^2 + \omega_z^2 z^2) - \omega(yp_z - zp_y). \tag{3.97}$$

We introduce the creation and annihilation operators for the harmonic oscillator

bosons in x, y, and z directions a_x, a_y, and a_z:

$$x=\left(\frac{\hbar}{2m\omega_x}\right)^{\frac{1}{2}}(a_x+a_x^+) \qquad p_x=\frac{\hbar}{i}\left(\frac{m\omega_x}{2\hbar}\right)^{\frac{1}{2}}(a_x-a_x^+),$$

$$y=i\left(\frac{\hbar}{2m\omega_y}\right)^{\frac{1}{2}}(a_y-a_y^+) \qquad p_y=\hbar\left(\frac{m\omega_y}{2\hbar}\right)^{\frac{1}{2}}(a_y+a_y^+), \tag{3.98}$$

$$z=\left(\frac{\hbar}{2m\omega_z}\right)^{\frac{1}{2}}(a_z+a_z^+) \qquad p_z=\frac{\hbar}{i}\left(\frac{m\omega_z}{2\hbar}\right)^{\frac{1}{2}}(a_z-a_z^+).$$

In these operators, h_ω is of the form

$$h_\omega=\hbar\omega_x\left(a_x^+a_x+\frac{1}{2}\right)+\hbar\omega_y\left(a_y^+a_y+\frac{1}{2}\right)+\hbar\omega_z\left(a_z^+a_z+\frac{1}{2}\right)$$
$$+\frac{\hbar\omega}{2\sqrt{\omega_y\omega_z}}\{(\omega_y-\omega_z)(a_y^+a_z^++a_ya_z)+(\omega_y+\omega_z)(a_y^+a_z+a_z^+a_y)\}. \tag{3.99}$$

The Coriolis operator in (3.99) has two contributions. The first one creates or annihilates two oscillator quanta. Therefore, it couples shells with major quantum numbers N and $N\mp2$.* The second part conserves the total number of quanta, but shifts quanta from the y-direction into the z-direction and vice versa.

3.4.3.1 The Inglis Formula. First we want to treat the Coriolis term in perturbation theory. In the Inglis formula (3.89), the $\Delta N=\pm2$ part has the energy denominator $\pm\hbar(\omega_y+\omega_z)$ and the $\Delta N=0$ part has the denominator $\pm\hbar(\omega_y-\omega_z)$. The matrix elements of a, a^+ are given in Eq. (C. 12f),

$$\langle n-1|a|n\rangle=\sqrt{n}\ , \qquad \langle n+1|a^+|n\rangle=\sqrt{n+1}\ ,$$

and we get, from (3.89)

$$\mathcal{I}_{\text{Inglis}}=\frac{\hbar}{2\omega_y\omega_z}\left\{\frac{(\omega_y-\omega_z)^2}{\omega_y+\omega_z}(N_y+N_z)+\frac{(\omega_y+\omega_z)^2}{\omega_y-\omega_z}(N_z-N_y)\right\}, \tag{3.100}$$

where the

$$N_{x,\,y,\,z}=\sum_{i=1}^{A}\left(n_{x,\,y,\,z}+\frac{1}{2}\right)_i \tag{3.101}$$

satisfy the relations

$$\bar{x}^2=\frac{1}{A}\sum_{i=1}^{A}\langle x^2\rangle_i=\frac{1}{A}\frac{\hbar}{m\omega_x}\sum_{i=1}^{A}\left(n_x+\frac{1}{2}\right)_i=\frac{\hbar}{Am\omega_x}\cdot N_x. \tag{3.102}$$

Very important for the following discussion is the *self-consistency condition*, [BM 75], namely, that the potential (given by $\omega_x, \omega_y, \omega_z$) has the same shape as the density distribution (given by $\bar{x}^2$, $\bar{y}^2$ and $\bar{z}^2$):

$$\sqrt{\bar{x}^2}\ :\sqrt{\bar{y}^2}\ :\sqrt{\bar{z}^2}=\frac{1}{\omega_x}:\frac{1}{\omega_y}:\frac{1}{\omega_z}\ . \tag{3.103}$$

Together with Eq. (3.102), we find

$$\omega_xN_x=\omega_yN_y=\omega_zN_z=C. \tag{3.104}$$

* It vanishes for small deformations ($\omega_y\simeq\omega_z$) and is therefore often neglected [ALL 76].

With this condition we can rewrite Eq. (3.100):

$$\mathcal{I}_{\text{Inglis}}=\hbar\left\{\frac{N_y}{\omega_y}+\frac{N_z}{\omega_z}\right\}. \tag{3.105}$$

The value of the moment of inertia so obtained is identical to the rigid body value. From Eq. (3.102) we get

$$\mathcal{I}^{\text{rig}}=m\sum_{i=1}^{A}(\langle y^2\rangle_i+\langle z^2\rangle_i)=\hbar\left(\frac{N_y}{\omega_y}+\frac{N_z}{\omega_z}\right). \tag{3.106}$$

Once again, we would like to stress the point that the self-consistency condition (3.104) is crucial for this result. If we occupied the y- and z-direction with the same number of oscillator quanta ($N_y=N_z$), we would get from Eqs. (3.100) and (3.102) a value

$$\mathcal{I}=\hbar\frac{(N_y/\omega_y-N_z/\omega_z)^2}{(N_y/\omega_y+N_z/\omega_z)}=Am\frac{(\bar{y}^2-\bar{z}^2)^2}{\bar{y}^2+\bar{z}^2}\ , \tag{3.107}$$

which is proportional to the irrotational flow value [BM 75].

3.4.3.2 Exact Solution. In the next step, we go beyond perturbation theory and diagonalize the single-particle Hamiltonian (3.99) exactly.* It is a quadratic form in the boson operators a, a^+ and can therefore be diagonalized [RBK 75] in the same way as one diagonalizes quadratic forms of the RPA-type (see Chap. 8).

To diagonalize the single-particle Hamiltonian, we introduce a canonical transformation among the momenta p_y, p_z and the coordinates y, z [Va 56]:

$$\begin{aligned}
Q_2&=\alpha_2(y+\beta p_z),\\
Q_3&=\alpha_3(z+\beta p_y),\\
P_2&=\alpha_2^{-1}(1-\delta\beta)^{-1}(p_y+\delta z),\\
P_3&=\alpha_3^{-1}(1-\delta\beta)^{-1}(p_z+\delta y),
\end{aligned} \tag{3.108}$$

which guarantees that the Q_i, P_i fulfill the commutation relations of momenta and coordinates. The constants β and δ are determined by the requirement that the Hamiltonian (3.97) contains no mixed terms P_2Q_3 or P_3Q_2 in the new representation. The constants α_2 and α_3 normalize the new coordinates in such a way that the mass parameter is again m. In the new variables, the Hamiltonian has the form [Va 56]

$$h_\omega=\left(-\frac{p_x^2}{2m}+\frac{1}{2}m\omega_x^2x^2\right)+\left(-\frac{P_2^2}{2m}+\frac{1}{2}m\Omega_2^2Q_2^2\right)+\left(-\frac{P_3^2}{2m}+\frac{1}{2}m\Omega_3^2Q_3^2\right). \tag{3.109}$$

The coordinates x, Q_2, Q_3 are the normal coordinates of the problem, and the frequencies Ω_i are given by

$$\Omega_{2,\,3}^2=\omega^2+\omega_+^2\pm\sqrt{\omega_-^4+4\omega^2\omega_+^2}\ , \tag{3.110}$$

with

$$\omega_\pm^2=\frac{1}{2}(\omega_y^2\pm\omega_z^2). \tag{3.111}$$

* For the calculation of matrix elements in this rotating oscillator basis, see [LR 77].

We can now define rotating bosons B_2^+, B_3^+ in analogy to Eq. (3.98):

$$B_2^+ = (2\hbar m\Omega_2)^{-\frac{1}{2}}(P_2 + im\Omega_2 Q_2), \tag{3.112}$$

$$B_3^+ = -i(2\hbar m\Omega_3)^{-\frac{1}{2}}(P_3 + im\Omega_3 Q_3),$$

and obtain for the Hamiltonian

$$h_\omega = \hbar\omega_x\left(a_x^+ a_x + \frac{1}{2}\right) + \hbar\Omega_2\left(B_2^+ B_2 + \frac{1}{2}\right) + \hbar\Omega_3\left(B_3^+ B_3 + \frac{1}{2}\right). \tag{3.113}$$

The corresponding eigenstates

$$|n_x, n_2, n_3\rangle \propto (a_x^+)^{n_x}(B_2^+)^{n_2}(B_3^+)^{n_3}|-\rangle \tag{3.114}$$

are characterized by the numbers of rotating bosons.

Their single-particle energies are

$$\epsilon'_{n_x n_2 n_3} = \hbar\omega_x\left(n_x + \frac{1}{2}\right) + \hbar\Omega_2\left(n_2 + \frac{1}{2}\right) + \hbar\Omega_3\left(n_3 + \frac{1}{2}\right). \tag{3.115}$$

Assuming again a fixed occupation in a Slater determinant $|\ \rangle$, that is, a fixed set of numbers N_x, N_2, N_3 defined in analogy to Eq. (3.101) for rotating bosons, we find for the total energy in the rotating frame,

$$E'(\omega) = \langle H_\omega\rangle = N_x\hbar\omega_x + N_2\hbar\Omega_2 + N_3\hbar\Omega_3. \tag{3.116}$$

Remembering that $\langle H_\omega\rangle$ is stationary with respect to variations of the eigenfunctions, we can calculate the expectation value of the angular momentum [RBK 75].

$$\langle L_x\rangle = -\left\langle\frac{\partial H_\omega}{\partial\omega}\right\rangle = -\frac{\partial}{\partial\omega}E' = \omega\left\{\frac{4\omega_+^2}{\Omega_2^2-\Omega_3^2}\left(\frac{N_3}{\Omega_3}-\frac{N_2}{\Omega_2}\right) - \left(\frac{N_2}{\Omega_2}+\frac{N_3}{\Omega_3}\right)\right\} \tag{3.117}$$

and the shape parameters $\bar{x}^2, \bar{y}^2, \bar{z}^2$,

$$\bar{x}^2 = \langle x^2\rangle = \frac{1}{m\omega_x}\left\langle\frac{\partial H_\omega}{\partial\omega_x}\right\rangle = \frac{1}{m\omega_x}\frac{\partial E'}{\partial\omega_x}, \qquad \bar{y}^2 = \cdots, \tag{3.118}$$

and so on. The moment of inertia is given by

$$\mathcal{I} = \frac{\langle L_x\rangle}{\omega} = m\langle y^2+z^2\rangle + \frac{4\hbar}{\Omega_2^2-\Omega_3^2}(N_3\Omega_3 - N_2\Omega_2). \tag{3.119}$$

For the final construction of the many-body Slater determinant, however, we have to fix the occupation numbers N_x, N_2, N_3.

In the nonrotating case, the numbers N_x, N_y, N_z were determined by the self-consistency condition (3.104). It can be motivated by different arguments, which all give the same results at $\omega = 0$. For $\omega \neq 0$ this is no longer the case. Several methods have been proposed:

(i) *Minimizing the expectation value* $E'(\omega)$ in Eq. (3.116) for fixed occupation as a function of the deformation parameters ω_x, ω_y and ω_z, and the frequency ω under the constraint of constant volume ($\bar{x}^2\cdot\bar{y}^2\cdot\bar{z}^2 =$ const.) and fixed angular momentum $\langle L_x\rangle$ [St 78, TA 79].

(ii) Requiring an *isotropic velocity distribution* in the rotating frame [RBK 75]. This is reasonable for heavy nuclei, where there are many level crossings and one has always filled up the lowest levels in the potential (see Sec. 13.3). We then get the modified self-consistency condition

$$N_x\omega_x = N_2\Omega_2 = N_3\Omega_3. \tag{3.120}$$

It can be shown that under this condition the shape of the mass distribution (given by $\bar{x}^2, \bar{y}^2, \bar{z}^2$) is proportional to the shape of the potential if one includes the centrifugal potential $\frac{1}{2}m\ (\boldsymbol{\omega}\times\mathbf{r})^2$.

From Eq. (3.119) we see that the self-consistency condition (3.120) yields the rigid-body value for the moment of inertia* at the actual deformation, which may change for large I-values.

3.4.4 The Rotating Nilsson Scheme

For realistic heavy nuclei, the pure harmonic oscillator is only of a limited importance, because it does not contain the drastic energy shift of high j shell orbitals due to the $\mathbf{l}\cdot\mathbf{s}$ term. As we have seen in Section 3.3, they play a crucial role in the interpretation of rotational spectra in all heavy nuclei.

One therefore has extended the Nilsson model and added a Coriolis term $-\omega j_x$ to the single-particle Hamiltonian (2.89) [ALL 76, RNS 78]:

$$h'(\omega) = h - \omega j_x \tag{3.121}$$

Figure 3.15 shows the qualitative behavior of some of the single-particle levels thus obtained as a function of ω. It shows the following features.

(i) At $\omega = 0$ are the usual Nilsson levels. They are twofold degenerate with respect to time reversal symmetry ($\pm\Omega$). For $\omega \neq 0$, this symmetry is broken by the Coriolis term, and a split into two single levels is observed.

(ii) The cranked Nilsson Hamiltonian is still invariant under a rotation of 180° around the x-axis, that is, the two levels belong to eigenstates of the operator

$$\mathcal{R}_x = e^{i\pi j_x} \tag{3.122}$$

with the eigenvalues $r_x = \pm i$ ("*signature*" [Bo 76a, b]).

(iii) Some levels show an extremely strong level splitting with increasing ω. They belong to orbits with large j- and small Ω-values (e.g., $1i_{13/2}$, $660\frac{1}{2}$, $651\frac{3}{2}$, $642\frac{5}{2}$). They show strong Ω-mixing and alignment along the x-axis (decoupled bands).

(iv) For even nuclei at moderate angular velocities, however, pairing correlations, as discussed in Section 3.2.2. and 7.7, should be taken into account. They counteract the rotational alignment and try to keep the particles in pairwise occupied orbits. In a full microscopic description of the backbending effect, the pair correlations must be taken into account self-consistently (see Sec. 7.7).

(v) For large frequencies, the alignment effect brings levels from higher major shells down into the neighborhood of the Fermi surface.

*It has recently been shown [FR 76b] that electrons confined by a harmonic potential and submitted to a constant magnetic field are rotating uniformly around the axis formed by the field; this is the analogous effect to the rigid body value of the moment of inertia discussed here.

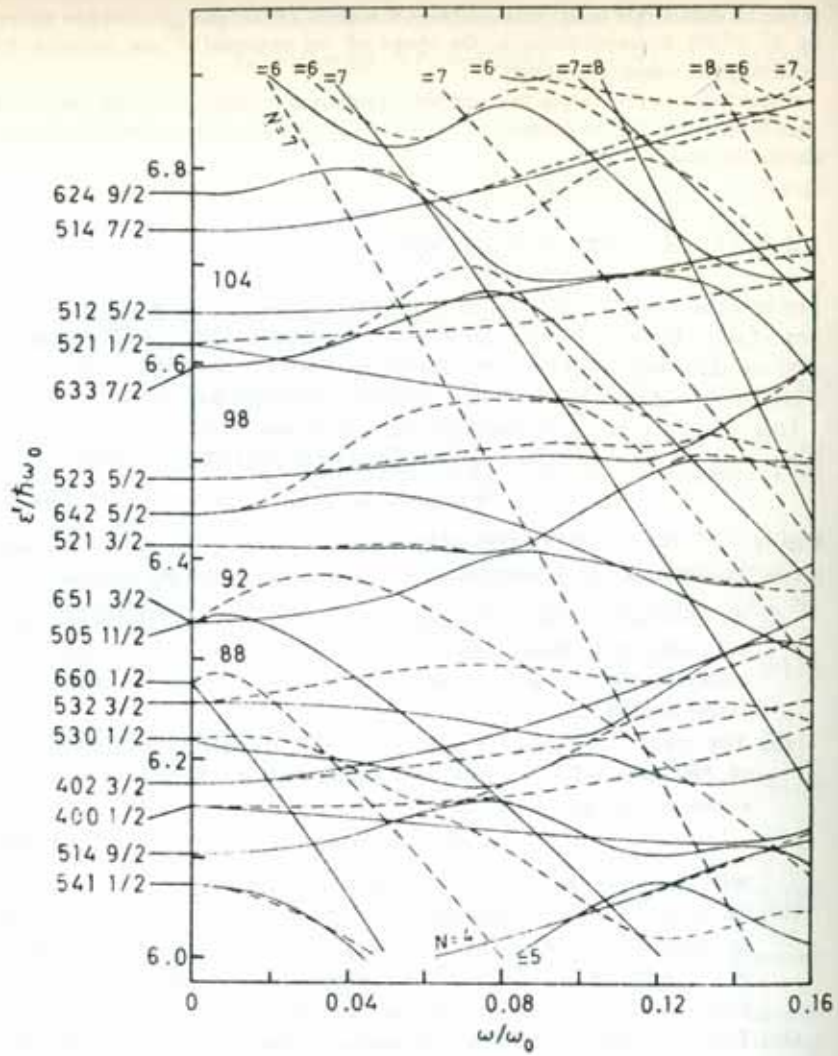

Figure 3.15. Qualitative behavior of the single-particle levels in a cranked Nilsson model at a prolate deformation ($\delta = 0.25$) as a function of the cranking frequency ω in units of $\hbar\omega_0$. Dashed lines correspond to levels with different r_x-quantum numbers. (We are grateful to Dr. R. Bengtsson for the preparation of this figure.)

(vi) Eventually, new shell closures with new magic numbers develop at high angular momenta, which can influence the energy surface for the fission process (see Sec. 3.4.5).

3.4.5 The Deformation Energy Surface at High Angular Momenta

As we already discussed in Section 2.9, the pure Nilsson model cannot be used for the calculation of total energies nor for the calculation of the shape of the energy surfaces at large deformations, because the average part of the energy is not reproduced in a proper way within this model. Therefore, we calculate only the oscillating part of the deformation energy within this model and replace the smooth part by the liquid drop energy at the same deformation.

In the same way, we can calculate energy surfaces at a fixed angular momentum I as a function of the deformation. For an ellipsoidal shape [characterized by the parameters β and γ (Eq. 1.88)], the total energy is then given by

$$E(\beta, \gamma, I) = E_{\mathrm{LDM}}(\beta, \gamma, I) + E_{\mathrm{sh}}(\beta, \gamma, I) - \tilde{E}_{\mathrm{sh}}(\beta, \gamma, I). \quad (3.123)$$

Here E_{LDM} is the deformation energy at a rotating ellipsoid with the rigid-body moment of inertia $\vartheta_{\mathrm{rig}}(\beta, \gamma)$, because one assumes that at high angular momenta pairing correlations can be neglected.* E_{sh} is the shell model energy and is obtained by summing up the single-particle energies. $\tilde{E}_{\mathrm{sh}}$ is the averaged part of it, and is calculated by an appropriate smoothing procedure (see Sec. 2.9).

There are two ways to derive these quantities from the diagonalization of a deformed single-particle potential in the rotating frame: Work either at constant frequency ω [NPF 76] or at constant angular momentum I [ALL 76]. Both methods agree, if one uses a deformed Wood–Saxon potential, where the averaged moment of inertia is very close to the rigid-body value† [BJ 76b, NTP 77].

Several groups have carried out investigations along this line [BLL 75, NP 75, NPF 76, ALL 76, FDG 76, NTP 77] in many regions of the periodic table. Qualitatively they have found similar results:

(i) For spherical or *weakly deformed nuclei* at the beginning of the rare earth region, the nuclei behave similarly to the classical liquid drop (Fig. 1.18): Up to angular momentum $I = 50$–$70\hbar$ they are oblate and rotate around the symmetry axis. In this region, the rotation is

*In fact, multiplicity measurement of the γ-cascade indicates the nucleus reaches the rigid-body moment of inertia at high spin values [SBC 76].

†The I^2 term in the Nilsson potential (2.89) is non-local and gives contribution to the effective mass. It produces an averaged moment of inertia which is ~30–40% larger than the rigid body value [Ty 70, 71, BR 71b, Je 73]. One has used scaling procedures to compensate for this effect [NTP 77].

not collective and one expects yrast traps (see Sec. 3.4.7). For higher I-values they rapidly change the shape to triaxial and prolate deformations (Jacobi-shapes; see Sec. 1.7). This transition corresponds to a drastic increase of the angular momentum ("*giant backbending*") as shown in Fig. 3.16. Finally, the nucleus fissions.

(ii) Nuclei in the *middle of the rare earth region* start at low I-values at prolate shapes and rotate around an axis perpendicular to the symmetry axis. With increasing rotation the Coriolis force aligns more and more particles parallel to this axis, and at $I \sim 40$–50 we find a transition to triaxial and sometimes even oblate shapes,* as in Fig. 3.17. At very high angular momenta the nucleus again becomes triaxial and finally fission takes place.

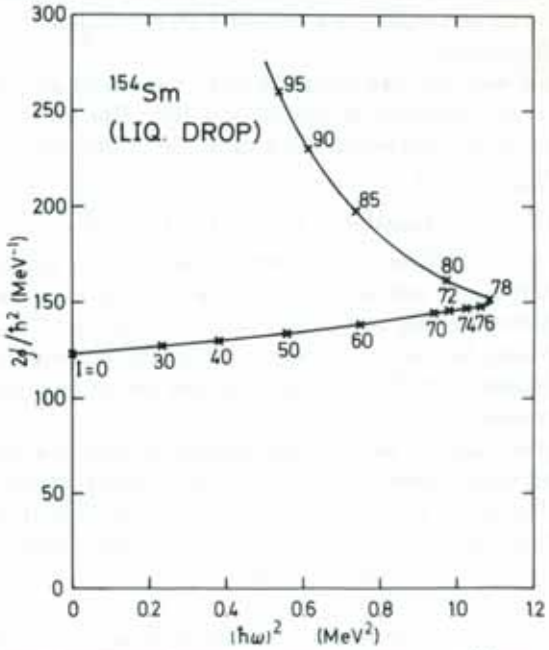

Figure 3.16. Backbending plot for the yrast spectrum of ^{154}Sm in terms of the rotating liquid drop model. (From [ALL 76].)

We want to conclude this section with the remark that such calculations can only give a qualitative impression of the behavior of the nuclear many-body system at such high angular momenta. Only for very low excitations and for energy surfaces with deep minima can we expect the nucleus to have a fixed deformation. In general, it will carry out quantum mechanical zeropoint fluctuations around these minima which ought to be described by a dynamical theory (see, for instance, Chap. 10).

*In calculations based on a Wood–Saxon potential [NTP 77], the nucleus does not reach such drastic γ-deformatione, and fissions without having obtained an oblate shape.

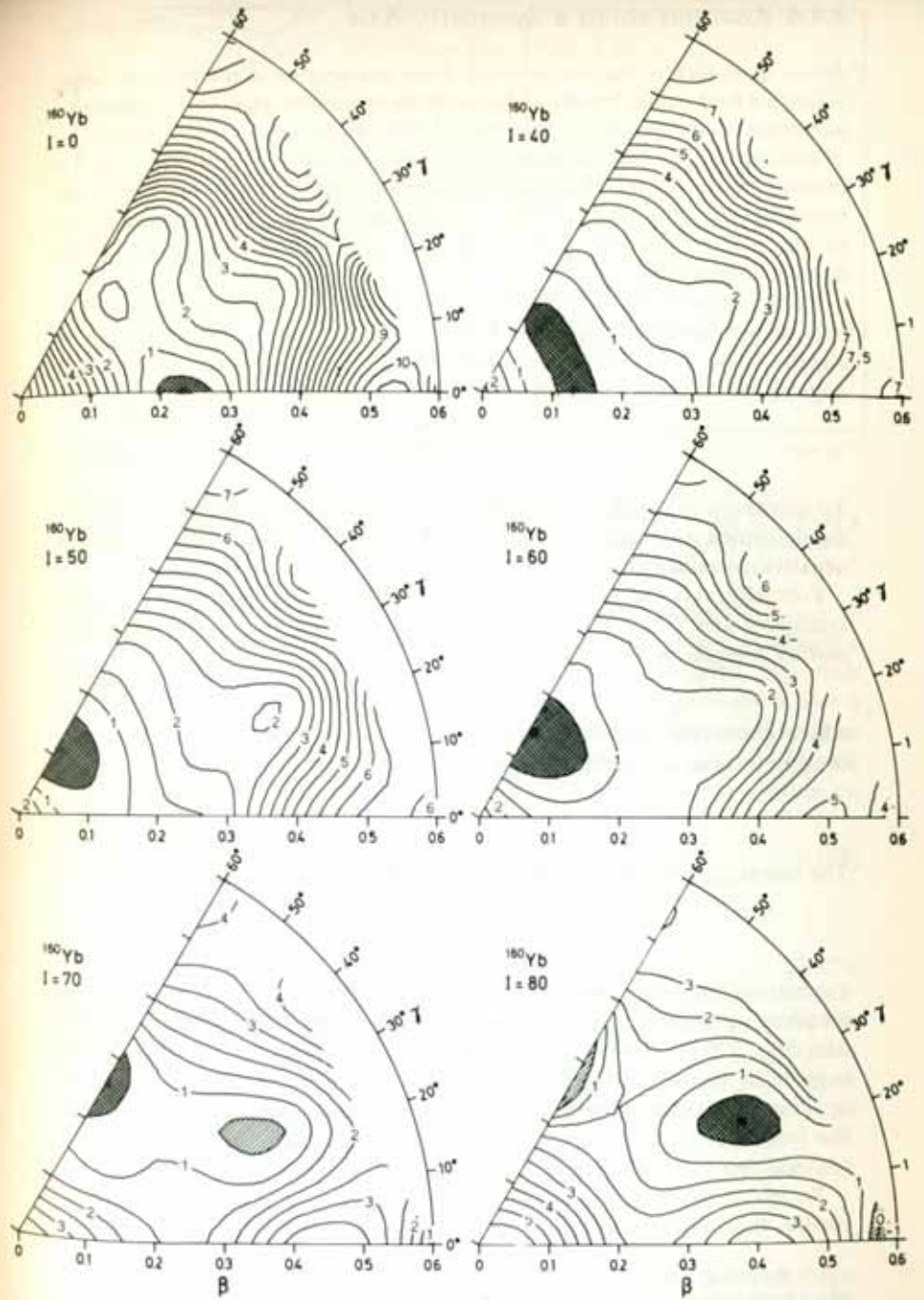

Figure 3.17. Potential energy surfaces in the (β, γ) plane with inclusion of shell corrections for ^{160}Yb as a function of angular momentum. (From [All 76]. Notice that these authors replace the Hill–Wheeler coordinate γ by $-\gamma$.)

3.4.6 Rotation about a Symmetry Axis

As we have seen in the last sections, there are regions in the periodic table where we find nuclei "rotating" around the symmetry axis. This happens in particular at the beginning and end of each major shell. At the beginning of each shell are a few particles sitting on a more or less spherical core. To create a large amount of angular momentum they all must align along the rotational axis (the x-axis), that is, classically speaking these particles have to run in the equatorial plane around the nucleus and produce an oblate density distribution.*

Such a configuration is certainly not collective rotation, since there are only a few particles involved. Each single particle wavefunction is an eigenfunction of j_x with the eigenvalue α_i. The component of the total angular momentum in the direction of the symmetry axis is given by

$$\langle J_x \rangle = \sum_{i=1}^{A} \alpha_i \tag{3.124}$$

To increase the angular momentum we have to change the occupation in the deformed well and to put particles from levels with lower (for instance negative) α-values into those with higher (positive) α-values.

Formally, this can be done again by a cranking procedure around the symmetry axis. Since the operator j_x commutes with h, we get the *single-particle energies in the "rotating frame."*

$$\epsilon_i' = \epsilon_i - \omega\alpha_i, \tag{3.125}$$

where ϵ_i are the eigenvalues of h in the nonrotating frame. These are straight lines as a function of ω (Fig. 3.18a) whose slope is given by

$$\frac{d\epsilon_i'}{d\omega} = -\alpha_i. \tag{3.126}$$

The condition to minimize the energy in the rotating frame

$$E' = \sum_{i=1}^{A} (\epsilon_i - \omega\alpha_i) \tag{3.127}$$

guarantees that one always occupies the lowest levels ϵ_i'. With increasing frequency ω we thus obtain a stepwise increasing of the angular momentum (Fig. 3.18b). The distance between two steps and the size of the steps is given by the distances of the levels ϵ_i and the angular momentum values α_i. Therefore there is a statistical increase of the angular momentum with the frequency ω. The *moment of inertia* $\Im$ is defined only on the average (dashed line in Fig. 3.18b).

To get an estimate for the size of this moment of inertia [Bo 76b], we realize that each line in Fig. 3.18a has the slope $-\alpha_i$ (increasing or

* At the end of a major shell similar arguments can be applied for holes. We then end up with a rotation about the symmetry axis of a prolate density distribution. In the middle of a shell there are many valence particles forming a prolate deformed shape. It is easy to generate large angular momentum from a few alignment processes, without too drastic changes in deformation.

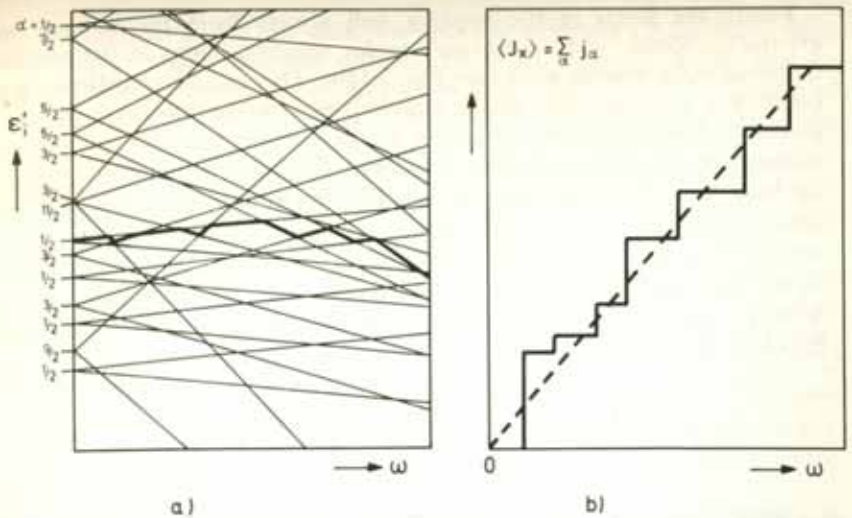

Figure 3.18. (a) Schematic representation of the eigenvalues ϵ_i' in Eq. (3.125) as a function of the cranking frequency. (b) The angular momentum $\langle J_x \rangle$ obtained by increasing values of ω and by always occupying the lowest levels in (a).

decreasing, depending on the sign of α). For $\omega = 0$ the levels $\pm\alpha_i$ are all occupied pairwise. The resultant angular momentum vanishes. For finite ω some of these levels with negative α are no longer occupied, but other downward-coming levels with positive α-values are occupied anew. For a fixed value of α (for instance $\alpha = \frac{1}{2}$) the number of newly occupied levels is on the average $\omega\alpha g(\alpha)$, where $g(\alpha)$ is the density of levels with the quantum number α. Therefore, we obtain for the angular momentum on the average

$$\langle J_x \rangle_{\text{av}} = \sum_{i < \epsilon_F} \alpha_i = \sum_{\alpha} \alpha \cdot \omega \cdot \alpha \cdot g(\alpha) = \omega \sum_{\alpha} \alpha^2 \cdot g(\alpha), \tag{3.128}$$

and for the average moment of inertia

$$\Im_{\text{av}} = \sum_{\alpha} \alpha^2 g(\alpha). \tag{3.129}$$

An evaluation of this quantity within the Thomas–Fermi approximation gives exactly the rigid-body value for the moment of inertia [Bo 76b]. On the average, "single-particle" rotation around the symmetry axis therefore shows quite a similar behavior to collective rotation, although the internal structure is completely different.

3.4.7 Yrast Traps

Since the level spacing in the case of a rotation around the symmetry axis has a statistical character, one expects *yrast traps* (high spin isomeric states). They are defined as yrast states which cannot undergo a rapid γ-transition and have been predicted by Bohr and Mottelson [BM 74].

Filling the levels in the rotating well always from the bottom, we eventually obtain, with increasing angular velocity, jumps in the angular momentum by several units (see Fig. 3.18b). This can be visualized most easily in a representation of the eigenvalues ϵ_i in the nonrotating oblate deformed Nilsson well as a function of the components α of the angular momentum along the symmetry axis (Fig. 3.19). For small deformations we have rather pure j-configurations. The eigenvalues ϵ_i for levels in the same j-shell lie on approximate parabolas [see Eq. (3.39); we have only to replace Ω by α]. At oblate deformations ($\beta<0$) the highest α-values, that is, the most aligned states, have the deepest energy, because their oblate density distribution in the equatorial plane has the maximal overlap with the oblate density of the core.

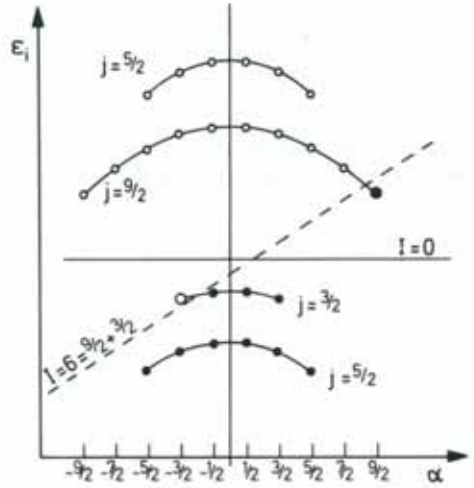

Figure 3.19. Schematic representation of the single-particle energies ϵ_i in an oblate deformed Nilsson well as a function of α (the eigenvalue of j_x) with the Fermi surface at $I=0$ (full line) and at $I=6$ (dashed line).

At $\omega=0$, the Fermi surface is a horizontal line and all levels below it are occupied. At finite ω-values, according to Eq. (3.125), the Fermi level in the rotational frame has a slope ω. As the value of ω increases, levels with negative α-values are vacated and those with positive α-values are newly occupied. In Fig. 3.19 we show a situation where a jump of 6 units of angular momentum occurs. The remaining I-values on the yrast line can be obtained by constructing *ph*-configurations with respect to the rotated energy surface. This is usually connected with an increase in energy.

Therefore, it may happen that the yrast line is no longer a monotonically increasing function of I, and a certain level with $I=I_0$ can have a deeper energy than the neighboring levels with $I=I_0-1, I_0-2, \ldots$. A fast γ transition of $E1$-, $E2$-, $M1$- or $M2$-character (i.e., with low multipolarity; see Appendix B) is then not allowed (so-called *energy spin traps*).

Even if this is not the case, the internal structure of the states with I_0-1, I_0-2 might be rather different from the structure of the state I_0. Then the transition matrix elements can be very small and the lifetime of the state I_0 is very large (*structure spin traps*). Examples are cases where the states with I_0-1 or I_0-2 can only be reached from the state I_0 by a $2p$-$2h$ excitation, or cases where the γ-transition matrix element is hindered by the intrinsic selection rules of the single-particle wave functions (for instance, l-forbidden $M1$-transitions; see Sec. 2.7.2.).

Several groups have investigated the theoretical possibility of yrast traps by searching for cases of rotation around the symmetry axis in the energy surfaces at high angular momenta and by investigating the detailed single-particle structure in these cases [ALL 76, CDS 77, AK 77, DNM 77, PFL 78, PTF 78, AHL 78, Ab 78, MDN 78]. Some regions in the periodic table have been found in which they should be expected. These are mostly weakly deformed nuclei such as Te, Ba, Ce, Sm, neutron deficient rare earth isotopes, and nuclei in the Pb-region.

On the *experimental side* we have known for a long time about states with large angular momenta and very long lifetimes for spherical nuclei. These are states with rather pure high j-shell configurations, which have no allowed γ-transition matrix elements of low multipolarity to other states at deeper energy. The most famous example [PAG 62] is the 18^+ isomer in ^{212}Po with a lifetime of 45 sec, which consists of an aligned $(\pi h_{9/2})^2(\nu i_{11/2})^2$ configuration.

Another group of high spin isomers, usually called *K-isomers*, were observed in well deformed nuclei, such as the $4s$ and the $31y$ isomers in ^{178}Hf, which can be interpreted as a $K^\pi=8^-$ and a $K^\pi=16^+$ band head, whose γ-decay is K-forbidden [HR 68, KL 77].

Finally, in recent years an island of about 20 adjacent nuclei in the light rare earth region with long lived isomers has been found [PBB 77]. They are probably associated with oblate deformation and "single-particle" rotation [AHL 78].

The properties of nuclei in the vicinity of ^{208}Pb have usually been studied in terms of the spherical shell model with residual interaction and a proper angular momentum coupling. Since these configurations are rather pure, some calculations of this type could explain measured excitation energies with extraordinary accuracy [BBH 77].

The physical reason for the aligned high spin configurations having such a long lifetime is the same in this picture as we have explained in the model of rotations around a symmetry axis: Two nucleons with aligned spins gain energy because their residual interaction is largest for wave functions with a large spacial overlap* (see Sec. 4.4.8.). Therefore, these high spin levels are lower in energy than the neighboring states with smaller I-values, and fast γ-transitions are forbidden. In the description of

*This effect has been called the MONA-effect (Maximal Overlap of the Nuclear wave function by Alignment [FPD 76]).

these nuclei by the mean field approach in a rotation about a symmetry axis, the same effect shows up in the fact that (as discussed in Fig. 3.18) aligned levels with maximal α-values and oblate density distribution are shifted downwards in energy because of their large overlap with the oblate core.

Both methods—shell model calculations in a spherical basis based on angular momentum coupling techniques and cranking calculations in a slightly deformed well—are certainly hard to compare. The spherical shell model is certainly much better (though it takes more effort) as long as one can assume the spherical core to be inert, otherwise one has to take into account multiparticle–multihole configurations. It is therefore limited to the very close vicinity of magic nuclei. On the other side, the cranking model treats the residual interaction by a deformed well and is therefore much easier to handle over a wide range of nuclei. It allows, however, only very qualitative predictions, since it violates conservation of angular momentum and is microscopically derived only in the regions of well deformed nuclei with rotations perpendicular to the symmetry axis (see Sec. 11.4).

CHAPTER 4

Nuclear Forces

4.1 Introduction

Up to now we have only taken into account the forces acting between nucleons in a very qualitative way. We have used some of their properties —such as their short range and saturation character—to explain the volume and surface terms in the liquid drop model. We have also assumed that they give rise to an average single-particle potential. By adjusting a few parameters, we are able to reproduce a large quantity of experimental data. The success of these phenomenological models gives us the confidence to go a step further and investigate the nuclear many-body problem from a more microscopic point of view. In particular, we wish to apply the techniques of modern many-body theory.

The starting point for all these considerations is obviously the two-body interaction between nucleons. There are three basic assumptions in this concept:

(i) Dynamical mesonic degrees of freedom can be neglected and the nucleus can be described as a system of A nucleons whose interaction can be represented by a potential.
(ii) Relativistic effects are negligible.
(iii) Only two-body forces are important.

Even with these rather drastic assumptions, we immediately run into two difficulties when we try to proceed in the way we have discussed:

(i). There exists no derivation of the *nucleon–nucleon force* from first principles. Though this should be possible in principle with the modern theory of gauge fields for quarks and gluons, attempts in this direction are only in their infancy [De 78]. On the other hand, theories that start out from an effective Lagrangian for interacting mesons and nucleons have recently proved quite successful (see, for example, [CLL 73, LLR 75, DSB 77, Vi 78, Ho 80]). The basic ingredient is the pion–nucleon coupling constant, which is known from experiment. The nucleon–nucleon force is obtained without a free parameter for particle distances greater than 0.8 fm. The part from 0 to 0.8 fm is represented by a phenomenological potential containing six parameters in each isospin channel. Excellent fits to the measured nucleon–nucleon phase shifts are achieved.

The potentials used until now have been almost entirely phenomenological (besides the Yukawa part resulting from the one-pion exchange; see below) and contain up to about 50 parameters. The experimental phase shifts are also very well reproduced with these potentials. On the basis of these forces, which we shall discuss very briefly in Section 4.2.2, we should be able to apply the method of many-body theory and to derive the phenomenological properties discussed in the preceding chapters in a quantitative way.

(ii). There is, however, a second difficulty in nuclear theory. These bare nuclear forces are, from a numerical point of view, very ill behaved. They show strong repulsion at short distances (hard core) and cannot be treated straightforwardly by the usual many-body techniques. For instance, they are too strong to be treated by perturbation theory and the hard core makes a direct self-consistent field approach (see Chap. 5), for example, impossible. In fact, the nucleons within a nucleus do not feel the bare nucleon–nucleon interaction. Taking into account that they interact with one another in the presence of many other nucleons permits one to introduce an *effective nucleon–nucleon interaction*, which is rather well behaved and allows application of the usual many-body methods, such as Hartree–Fock theory (Chap. 5). Much work has been done to derive this effective interaction from the bare nucleon–nucleon force. We will in Sec. 4.3 discuss the basic ideas that have been used to achieve this goal. As a result, a great deal has been learned about the properties and the structure of these effective forces. However, in order to reproduce experimental data quantitatively one still needs phenomenological renormalization parameters, and from this point of view the theory is not yet very satisfying.

In most of the so-called microscopic descriptions of the nucleus one uses *phenomenological effective forces*, which are constructed on the basis of these considerations, but depend on some parameters that are adjusted to fit experimental data.

In this chapter we do not want to go into such attempts to derive the bare nucleon–nucleon force [BJ 76a]. In the second section we will discuss some invariance principles that should be obeyed by the bare forces and which already allow one to draw some conclusions about their analytical structure. In the third section, we briefly present the microscopic description of effective interactions and discuss their properties and their field of application. The fourth section presents a number of phenomenological potentials that have been used to represent the residual interaction between the nucleons moving in a given average potential.

We wish to emphasize that in this chapter we are only dealing with the nuclear interaction. The *Coulomb interaction* has to be treated separately. When a comparison with experimental data is required one has always to subtract Coulomb effects first.

4.2 The Bare Nucleon–Nucleon Force

4.2.1 General Properties of a Two-Body Force

The most general quantum mechanical two-body potential V is completely specified by its matrix elements between two-body states (in a coordinate representation $|\mathbf{r}_1, s_1, t_1; \mathbf{r}_2, s_2, t_2\rangle$; where $s_i = \pm\frac{1}{2}$ and $t_i = \pm\frac{1}{2}$ are spin and isospin coordinates) as:

$$\langle \mathbf{r}_1' s_1' t_1' \mathbf{r}_2' s_2' t_2' | V | \mathbf{r}_1 s_1 t_1 \mathbf{r}_2 s_2 t_2 \rangle. \tag{4.1}$$

The space of two-particle states $|\mathbf{r}_1, s_1, t_1; \mathbf{r}_2, s_2, t_2\rangle$ is a product space of the coordinate wave functions $|\mathbf{r}_1\rangle$ and $|\mathbf{r}_2\rangle$ and the spin and isospin vectors $|s_1\rangle$, $|s_2\rangle$ and $|t_1\rangle$, $|t_2\rangle$. Since any operator in the spin space of one particle can be represented as a linear combination of the spin matrices $\sigma_1, \sigma_2, \sigma_3$ and the unity matrix $\sigma_0 = 1$, the most general form of the operator V is

$$V = \sum_{i,k=0}^{3} V_{ik} \sigma_i^{(1)} \sigma_k^{(2)}. \tag{4.2}$$

The function V_{ik} also depends analogously on the isospin operators $\boldsymbol{\tau}^{(1)}$ and $\boldsymbol{\tau}^{(2)}$. In addition to this isospin dependence, the V_{ik} are, in general, integral operators in coordinate space

$$V|\mathbf{r}_1\mathbf{r}_2\rangle = \int V(\mathbf{r}_1', \mathbf{r}_2', \mathbf{r}_1, \mathbf{r}_2) |\mathbf{r}_1'\mathbf{r}_2'\rangle \, d^3r_1' \, d^3r_2'. \tag{4.3}$$

In the special case in which $V(\mathbf{r}_1', \mathbf{r}_2', \mathbf{r}_1, \mathbf{r}_2)$ has the form

$$V(\mathbf{r}_1, \mathbf{r}_2, \mathbf{r}_1', \mathbf{r}_2') = \delta(\mathbf{r}_1 - \mathbf{r}_1') \delta(\mathbf{r}_2 - \mathbf{r}_2') V(\mathbf{r}_1, \mathbf{r}_2) \tag{4.4}$$

V is called a *local potential*, and we have

$$V|\mathbf{r}_1\mathbf{r}_2\rangle = V(\mathbf{r}_1, \mathbf{r}_2)|\mathbf{r}_1\mathbf{r}_2\rangle. \tag{4.5}$$

In this case the interaction between the two particles depends only on the points $\mathbf{r}_1$ and $\mathbf{r}_2$ (and eventually on the spin and isospin). It does not, for instance, depend on the velocity of the particles.

We shall show that, in general, nonlocal potentials correspond to a velocity dependence. We therefore expand*

$$|\mathbf{r}_1', \mathbf{r}_2'\rangle = |\mathbf{r}_1\mathbf{r}_2\rangle + (\mathbf{r}_1' - \mathbf{r}_1)\frac{\partial}{\partial \mathbf{r}_1}|\mathbf{r}_1\mathbf{r}_2\rangle + (\mathbf{r}_2' - \mathbf{r}_2)\frac{\partial}{\partial \mathbf{r}_2}|\mathbf{r}_1\mathbf{r}_2\rangle + \cdots$$

$$=: \exp\left\{(\mathbf{r}_1' - \mathbf{r}_1)\frac{\partial}{\partial \mathbf{r}_1} + (\mathbf{r}_2' - \mathbf{r}_2)\frac{\partial}{\partial \mathbf{r}_2}\right\} : |\mathbf{r}_1\mathbf{r}_2\rangle \tag{4.6}$$

and get, from (4.3),

$$V|\mathbf{r}_1\mathbf{r}_2\rangle = \int V(\mathbf{r}_1', \mathbf{r}_2', \mathbf{r}_1, \mathbf{r}_2)\exp\left\{\frac{i}{\hbar}(\mathbf{r}_1' - \mathbf{r}_1)\mathbf{p}_1 + \frac{i}{\hbar}(\mathbf{r}_2' - \mathbf{r}_2)\mathbf{p}_2\right\}|\mathbf{r}_1\mathbf{r}_2\rangle\, d^3r_1'\, d^3r_2'$$

$$= \tilde{V}(\mathbf{r}_1, \mathbf{p}_1, \mathbf{r}_2, \mathbf{p}_2)|\mathbf{r}_1\mathbf{r}_2\rangle. \tag{4.7}$$

This means that the most general potential can be represented by Eq. (4.2) where the V_{ik} are operators in coordinate space of the form (4.7) (for reasons of simplicity we neglected the isospin dependence).

In the following we investigate the symmetry properties of such potentials $V(1,2) = V(\mathbf{r}_1, \mathbf{p}_1, \boldsymbol{\sigma}^{(1)}, \boldsymbol{\tau}^{(1)}, \mathbf{r}_2, \mathbf{p}_2, \boldsymbol{\sigma}^{(2)}, \boldsymbol{\tau}^{(2)})$. The form of this general function can, however, be restricted by requiring the imposition of a number of symmetries.

In particular, we require the following eight symmetries:

(i) Hermeticity

(ii) Invariance under an exchange of the coordinates

$$V(1,2) = V(2,1). \tag{4.8}$$

This property is strongly connected with the symmetry of the two-particle wave function $|12\rangle$. Since nucleons are fermions, they have to be totally antisymmetric. For example, if we take a product wave function built out of ordinary space, a spin and an isospin part

$$\langle \mathbf{r}_1 s_1 t_1, \mathbf{r}_2 s_2 t_2 \,|\, 12\rangle = \varphi(\mathbf{r}_1, \mathbf{r}_2)\chi(s_1, s_2)\zeta(t_1, t_2) \tag{4.9}$$

we have four combinations compatible with the Pauli principle, which are characterized by the symmetry of the coordinate space and spin part (Table 4.1). The isospin component is determined in each case by requiring the antisymmetry of the total wave function (4.9).

*: : means *normal ordering*, i.e., the derivatives $\partial/\partial \mathbf{r}_i$ should not act on the coordinates $\mathbf{r}_i$ in the expansion of the exponent.

Table 4.1 Characterization of the symmetries of the two-particle state (4.9)

φ	χ	abbreviation	ζ
even	singlet	es	+
even	triplet	et	−
odd	singlet	os	−
odd	triplet	ot	+

(iii) Translational invariance. The potential depends on the relative coordinate $\mathbf{r} = \mathbf{r}_1 - \mathbf{r}_2$ only

$$V(1,2) = V(\mathbf{r}, \mathbf{p}_1, \boldsymbol{\sigma}^{(1)}, \boldsymbol{\tau}^{(1)}, \mathbf{p}_2, \boldsymbol{\sigma}^{(2)}, \boldsymbol{\tau}^{(2)}). \tag{4.10}$$

(iv) Galilean invariance. The potential is not changed by a transformation to a system which moves with constant velocity, that is, it depends only on the relative momentum $\mathbf{p} = \frac{1}{2}(\mathbf{p}_1 - \mathbf{p}_2)$:

$$V(1,2) = V(\mathbf{r}, \mathbf{p}, \boldsymbol{\sigma}^{(1)}, \boldsymbol{\tau}^{(1)}, \boldsymbol{\sigma}^{(2)}, \boldsymbol{\tau}^{(2)}). \tag{4.11}$$

(v) Invariance under space reflection. Contrary to the weak interaction, there is no parity violation for strong interactions:

$$V(\mathbf{r}, \mathbf{p}, \boldsymbol{\sigma}^{(1)}, \boldsymbol{\tau}^{(1)}, \boldsymbol{\sigma}^{(2)}, \boldsymbol{\tau}^{(2)}) = V(-\mathbf{r}, -\mathbf{p}, \boldsymbol{\sigma}^{(1)}, \boldsymbol{\tau}^{(1)}, \boldsymbol{\sigma}^{(2)}, \boldsymbol{\tau}^{(2)}). \tag{4.12}$$

(vi) Time reversal invariance guarantees that the equations of motion do not depend on the direction in which the time evolves (for details, see [Me 61])

$$V(\mathbf{r}, \mathbf{p}, \boldsymbol{\sigma}^{(1)}, \boldsymbol{\tau}^{(1)}, \boldsymbol{\sigma}^{(2)}, \boldsymbol{\tau}^{(2)}) = V(\mathbf{r}, -\mathbf{p}, -\boldsymbol{\sigma}^{(1)}, \boldsymbol{\tau}^{(1)}, -\boldsymbol{\sigma}^{(2)}, \boldsymbol{\tau}^{(2)}). \tag{4.13}$$

(vii) Rotational invariance in coordinate space. Rotations in three-dimensional coordinate space act not only on the vectors $\mathbf{r}$ and $\mathbf{p}$ but also on the spin matrices $\boldsymbol{\sigma} = 2\cdot\mathbf{s}$. With respect to spin, the operator V has the form (4.2). It has to be a scalar under a rotation in coordinate space, which means in particular that V_{00} has to be a scalar. There exist three independent scalars which we can construct from the two vectors $\mathbf{r}$ and $\mathbf{p}$, namely $\mathbf{r}^2, \mathbf{p}^2$ and $\mathbf{r}\cdot\mathbf{p} + \mathbf{p}\cdot\mathbf{r}$. However, the latter expression can only appear quadratically because of time reversal invariance (vi). It is more convenient to express $(\mathbf{rp} + \mathbf{pr})^2$ through $\mathbf{r}^2, \mathbf{p}^2$ and $\mathbf{L}^2 = (\mathbf{r}\times\mathbf{p})^2$. V_{00} can then be written as a function of $\mathbf{r}^2, \mathbf{p}^2$ and $\mathbf{L}^2$. Because of invariance (ii) and (v) we find

$$V(\mathbf{r}, \mathbf{p}, \boldsymbol{\sigma}^{(1)}, \boldsymbol{\sigma}^{(2)}) = V(\mathbf{r}, \mathbf{p}, \boldsymbol{\sigma}^{(2)}, \boldsymbol{\sigma}^{(1)}). \tag{4.14}$$

The terms in (4.2) that are linear in $\boldsymbol{\sigma}^{(i)}$ therefore depend only on

$$\mathbf{S} = \tfrac{1}{2}(\boldsymbol{\sigma}^{(1)} + \boldsymbol{\sigma}^{(2)}). \tag{4.15}$$

To form a scalar, $\mathbf{S}$ has to be multiplied by a vector, which is invariant under space reflection. Only $\mathbf{L}$ fulfils this requirement

$$\mathbf{L}\cdot\mathbf{S} = \tfrac{1}{2}\mathbf{L}(\boldsymbol{\sigma}^{(1)} + \boldsymbol{\sigma}^{(2)}) \tag{4.16}$$

The quadratic terms in $\boldsymbol{\sigma}$ in Eq. (4.2) form a tensor. It can be decomposed into a scalar $\boldsymbol{\sigma}^{(1)}\cdot\boldsymbol{\sigma}^{(2)}$, a vector $\boldsymbol{\sigma}^{(1)}\times\boldsymbol{\sigma}^{(2)}$, and a symmetric tensor with vanishing trace $(\sigma_i^{(1)}\sigma_k^{(2)} + \sigma_k^{(1)}\sigma_i^{(2)})(1 - \frac{1}{3}\delta_{ik})$. Because of (4.14), $\boldsymbol{\sigma}^{(1)}\times\boldsymbol{\sigma}^{(2)}$ cannot appear. As shown by Okubo and Marshak [OM 58], the only possible independent combinations are

$$\boldsymbol{\sigma}^{(1)}\boldsymbol{\sigma}^{(2)},\ (\mathbf{r}\boldsymbol{\sigma}^{(1)})(\mathbf{r}\boldsymbol{\sigma}^{(2)}),\ (\mathbf{p}\boldsymbol{\sigma}^{(1)})(\mathbf{p}\boldsymbol{\sigma}^{(2)}),$$
$$(\mathbf{L}\boldsymbol{\sigma}^{(1)})(\mathbf{L}\boldsymbol{\sigma}^{(2)}) + (\mathbf{L}\boldsymbol{\sigma}^{(2)})(\mathbf{L}\boldsymbol{\sigma}^{(1)}). \tag{4.17}$$

Each of these terms can be multiplied by an arbitrary function of $\mathbf{r}^2, \mathbf{p}^2$ and $\mathbf{L}^2$.

(viii) Rotational invariance in isospin space. Within the isospin formalism, protons and neutrons are considered as quantum states of one elementary particle that

form a doublet (see Sec. 2.6.3) with isospin $\frac{1}{2}$. The two-dimensional representation of the rotational group reproduces all their transformation properties. Rotations within the isospin space (as long as they are not around the 3-axis) produce mixtures of protons and neutrons. Rotational invariance of the nuclear force therefore means the same as charge independence, that is, the proton–proton interaction has the same strength as the neutron–neutron interaction. This has been confirmed by nucleon–nucleon scattering experiments as well as by the symmetry properties of mirror nuclei (e.g., He^3 and H^3). Mathematically speaking, this means that the nucleon–nucleon interaction $V(1,2)$ commutes with the operators of the total isospin

$$\mathbf{T}=\mathbf{t}_1+\mathbf{t}_2. \tag{4.18}$$

Eigenstates can then be constructed of $\mathbf{T}^2, T_3$ with eigenvalues $T=0$, $T_3=0$ and $T=1$, $T_3=-1,0,+1$ (isospin singlet and isospin triplet). Charge invariance means that $\mathbf{T}^2$ commutes with the operator of the nuclear force. Therefore, the interactions in $T=1$ states have to be the same (*pp*, *nn*, or symmetric *pn* states). However, they may be different in the $T=0$ state (antisymmetric *pn* system).

The formalism of isospin matrices $\boldsymbol{\tau}=(\tau_1,\tau_2,\tau_3)$ is identical to that of regular spin. Since there is no other vector in isospin space, the only isospin invariant combination of the isospin matrices corresponding to particle 1 and 2 is

$$V_0+V_\tau\boldsymbol{\tau}^{(1)}\boldsymbol{\tau}^{(2)}. \tag{4.19}$$

The functions V_0 and V_τ depend on the remaining coordinates such as $\mathbf{r}, \mathbf{p}, \boldsymbol{\sigma}_1, \boldsymbol{\sigma}_2$, as we have already discussed.

Not all of the combinations possible from the symmetric point of view have been used to describe the nuclear force. We will mention here only the most important terms:

(i). Among the local forces, which do not depend on the velocity, the *central force* is the most important. It depends only on the distance r between the nucleons:

$$V_C(1,2)=V_0(r)+V_\sigma(r)\boldsymbol{\sigma}^{(1)}\boldsymbol{\sigma}^{(2)}+V_\tau(r)\boldsymbol{\tau}^{(1)}\boldsymbol{\tau}^{(2)}+V_{\sigma\tau}(r)\boldsymbol{\sigma}^{(1)}\boldsymbol{\sigma}^{(2)}\boldsymbol{\tau}^{(1)}\boldsymbol{\tau}^{(2)}. \tag{4.20}$$

(ii). The only remaining local part is the *Tensor force*

$$V_T(1,2)=\left[V_{T_0}(r)+V_{T_\tau}(r)\boldsymbol{\tau}^{(1)}\boldsymbol{\tau}^{(2)}\right]\cdot S_{12} \tag{4.21}$$

with

$$S_{12}=\frac{3}{r^2}(\boldsymbol{\sigma}^{(1)}\mathbf{r})(\boldsymbol{\sigma}^{(2)}\mathbf{r})-\boldsymbol{\sigma}^{(1)}\boldsymbol{\sigma}^{(2)}.$$

The term $-\boldsymbol{\sigma}^{(1)}\boldsymbol{\sigma}^{(2)}$ is added to make sure that an average of $V_T(1,2)$ taken over all directions of $\mathbf{r}$ vanishes:

$$\int V_T(1,2)\,d\Omega=0 \quad \text{where} \quad \mathbf{r}=(r,\Omega). \tag{4.22}$$

An experimental hint of the existence of a tensor component in the

nucleon–nucleon potential is given by the quadrupole moment of the deuteron, which cannot be explained by pure central forces.

(iii). The most important nonlocal term is the *two-body spin orbit interaction*

$$V_{LS}=V_{LS}(r)\mathbf{L}\cdot\mathbf{S}. \tag{4.23}$$

As we shall see in Chap. 5, such a two-body spin orbit potential causes the one-body spin orbit term in the average single-particle nuclear potential, used to explain the magic numbers in nuclei.

(iv). One sometimes also uses a *second-order spin orbit interaction*:

$$V_{LL}=V_{LL}(r)\left\{(\boldsymbol{\sigma}^{(1)}\boldsymbol{\sigma}^{(2)})\mathbf{L}^2-\frac{1}{2}\left[(\boldsymbol{\sigma}^{(1)}\mathbf{L})(\boldsymbol{\sigma}^{(2)}\mathbf{L})+(\boldsymbol{\sigma}^{(2)}\mathbf{L})(\boldsymbol{\sigma}^{(1)}\mathbf{L})\right]\right\}. \tag{4.24}$$

4.2.2 The Structure of the Nucleon–Nucleon Interaction

The central force (4.20) is the most important part of the nucleon–nucleon interaction. It can also be represented in terms of exchange or projection operators.

The operators

$$P^\sigma=\frac{1}{2}(1+\boldsymbol{\sigma}^{(1)}\boldsymbol{\sigma}^{(2)}), \qquad P^\tau=\frac{1}{2}(1+\boldsymbol{\tau}^{(1)}\boldsymbol{\tau}^{(2)}) \tag{4.25}$$

exchange the spin and isospin coordinates, respectively, in a wave function. For instance, we can apply P^σ to the wave function (4.9) and obtain

$$P^\sigma\varphi(\mathbf{r}_1\mathbf{r}_2)\chi(s_1,s_2)\zeta(t_1,t_2)=\varphi(\mathbf{r}_1,\mathbf{r}_2)\chi(s_2,s_1)\zeta(t_1,t_2). \tag{4.26}$$

This is easy to understand by using the operator of the total spin $\mathbf{S}$ (4.15). The eigenstates of $\mathbf{S}^2$ are singlet and triplet states and we find:

$$P^\sigma=\frac{1}{2}\left(1+2(\mathbf{S}^2-\mathbf{s}^{(1)^2}-\mathbf{s}^{(2)^2})\right)=S(S+1)-1=\begin{cases}1 & \text{for triplet}\\ -1 & \text{for singlet.}\end{cases} \tag{4.27}$$

We can also define an operator P^r which exchanges the spacial coordinates $\mathbf{r}_1$ and $\mathbf{r}_2$ of the particles.* Since the wave function has to be antisymmetric under the exchange of all coordinates of the particles 1 and 2, the Pauli principle may be written in the form

$$P^rP^\sigma P^\tau=-1. \tag{4.28}$$

We can therefore express the operator $P^\tau=-P^rP^\sigma$ and eliminate the products $\boldsymbol{\sigma}^{(1)}\boldsymbol{\sigma}^{(2)}$ and $\boldsymbol{\tau}^{(1)}\boldsymbol{\tau}^{(2)}$ in Eq. (4.20).

*The operator P^r can be represented by a nonlocal operator in coordinate space, viz:

$$V(\mathbf{r})P^r\psi(\mathbf{r}_1,\mathbf{r}_2)=\int V(\mathbf{r}_1-\mathbf{r}_2)\delta(\mathbf{r}_1'-\mathbf{r}_2)\delta(\mathbf{r}_2'-\mathbf{r}_1)\psi(\mathbf{r}_1',\mathbf{r}_2')\,d^3r_1'\,d^3r_2'.$$

In this sense only Wigner forces (4.30) are local.

Finally, we obtain

$$V_C = V_W(r) + V_M(r)P^r + V_B(r)P^\sigma + V_H(r)P^rP^\sigma \tag{4.29}$$

with the following relations

$$\begin{aligned} V_W &= V_0 - V_\sigma - V_\tau + V_{\sigma\tau} && \text{(Wigner force)} \\ V_M &= -4V_{\sigma\tau} && \text{(Majorana force)} \\ V_B &= 2V_\sigma - 2V_{\sigma\tau} && \text{(Bartlett force)} \\ V_H &= -2V_\tau + 2V_{\sigma\tau} && \text{(Heisenberg force).} \end{aligned} \tag{4.30}$$

The names of these different components of the nuclear force go back to the years following 1930, when the first models of the nucleus were introduced and the saturation property of nuclear forces was explained by exchange terms without introducing a hard core (for a historical review of this work see [Br 65a]).

A third way of representing the central force uses projection operators

$$\begin{aligned} \Pi_s^\sigma &= \frac{1}{2}(1 - P^\sigma), \quad \Pi_t^\sigma = \frac{1}{2}(1 + P^\sigma), \\ \Pi_s^\tau &= \frac{1}{2}(1 - P^\tau), \quad \Pi_t^\tau = \frac{1}{2}(1 + P^\tau), \\ \Pi_o^r &= \frac{1}{2}(1 - P^r), \quad \Pi_e^r = \frac{1}{2}(1 + P^r). \end{aligned} \tag{4.31}$$

These are projection operators ($P^2 = P, P^+ = P$), which project onto the singlet (s) and triplet (t), and onto the even (e) and odd (o) part of the nuclear two-body wave function (4.9) in the sense of Table 4.1. We can express the exchange operators P^σ, P^r by these projection operators and obtain

$$V(1,2) = V_{et}(r)\Pi_e^r\Pi_t^\sigma + V_{es}(r)\Pi_e^r\Pi_s^\sigma + V_{ot}(r)\Pi_o^r\Pi_t^\sigma + V_{os}(r)\Pi_o^r\Pi_s^\sigma. \tag{4.32}$$

This representation is especially useful in practical applications; for instance, in p–p scattering experiments we have only isospin triplet states, (i.e., only es and ot are important). Table 4.2 shows those functions obtained if one operates with the different representations on wave functions with different symmetry.

Table 4.2 Connections between the different representations of a central force

$\sigma^{(1)}\sigma^{(2)}$	$\tau^{(1)}\tau^{(2)}$	$V(\sigma^{(1)}\sigma^{(2)}, \tau^{(1)}\tau^{(2)})$	$V(P^r, P^\sigma)$	$V(\Pi^r, \Pi^\sigma)$	$\lvert 12\rangle$
1	−3	$V_{00} + V_{0\sigma} - 3V_{0\tau} - 3V_{0\sigma\tau}$	$V_W + V_M + V_B + V_H$	V_{et}	$\lvert et\rangle$
−3	1	$V_{00} - 3V_{0\sigma} + V_{0\tau} - 3V_{0\sigma\tau}$	$V_W + V_M - V_B - V_H$	V_{es}	$\lvert es\rangle$
1	1	$V_{00} + V_{0\sigma} + V_{0\tau} + V_{0\sigma\tau}$	$V_W - V_M + V_B - V_H$	V_{ot}	$\lvert ot\rangle$
−3	−3	$V_{00} - 3V_{0\sigma} - 3V_{0\tau} + 9V_{0\sigma\tau}$	$V_W - V_M - V_B + V_H$	V_{os}	$\lvert os\rangle$

The *radial dependence* of the functions V cannot be deduced from invariance principles. In 1937, Yukawa proposed an explanation of the nuclear force using a meson field theory. The nucleons influence each other by the exchange of one or several mesons. The simplest form is the one-pion exchange potential (OPEP). It has the radial dependence of the

Yukawa potential [Yu 35]

$$V_Y(r) = \frac{e^{-\mu r}}{\mu r}, \tag{4.33}$$

where $1/\mu = \hbar/m_\pi c$ is the Compton wavelength of the pion. The asymptotic form of this potential is uniquely determined by the properties of the pion and its coupling strength to the nucleonic field $g^2/\hbar c \simeq 0.081$:

$$V^{\text{OPEP}} = \frac{g^2}{3\hbar c} m_\pi c^2 \frac{e^{-\mu r}}{\mu r} (\tau^{(1)}\tau^{(2)}) \left\{ \sigma^{(1)}\sigma^{(2)} + \left(1 + 3\frac{1}{\mu r} + 3\left(\frac{1}{\mu r}\right)^2\right) S_{12} \right\}. \tag{4.34}$$

A phase shift analysis of the nucleon–nucleon scattering data shows that the OPEP-potential (4.34) is well able to reproduce the phase shifts for large orbital angular momenta $L \geqslant 6$ [Br 67b]. Since these high partial waves only feel the tail of the nuclear force at large distances ($r \geqslant 2$ fm), we can assume that the OPEP potential describes the nuclear force properly at such large distances. For smaller distances we must, in addition, also introduce the two-pion exchange and the ρ- and ω-meson exchange in order to obtain the medium-range part of the force. This has been achieved very successfully [BJ 76a, CLL 73, LLR 75, DSB 77, Vi 78, Ho 80], so that only the short-range part of the force still has to be fitted by a phenomenological ansatz. Only six parameters are needed for each isospin state. As we mentioned in the introduction, this potential is not used very much as yet, therefore phenomenological counterparts have been employed until now. These phenomenological parametrizations consist of combinations of central, tensor, spin orbit, and higher terms, and more or less arbitrary radial functions containing up to 50 parameters, which are fitted to the experimental scattering phase shifts and to the deuteron data. There are attractive and repulsive components. At large distances they go over into the OPEP-potential, whereas at short distances they have an extremely repulsive core. Several authors have therefore used a *hard core* [$V(r) = \infty$ for $r < r_c \simeq 0.4$ fm]. Others use a very repulsive core which goes to infinity only for $r \to 0$. Such potentials are called *soft core* potentials.

Examples of such realistic nucleon–nucleon potentials using a hard core are the Hamada Johnston potential [HJ 62] and the Yale potential [LHR 62]. The Tabakin potential [Ta 64] is a nonlocal potential, separable in momentum space.

The Reid soft core potential [Re 68] is also widely used. It has the structure

$$V = V_C(\mu r) + V_T(\mu r)S_{12} + V_{LS}(\mu r)\mathbf{LS}. \tag{4.35}$$

$V_C(x)$ and $V_{LS}(x)$ have the simple form

$$V_C(x) = \sum_{n=1}^{\infty} a_n \frac{e^{-nx}}{x}, \qquad V_{LS} = \sum_{n=1}^{\infty} c_n \frac{e^{-nx}}{x}, \tag{4.36}$$

and $V_T(x)$ is given by

$$V_T(x) = \frac{b_1}{x}\left\{\left(\frac{1}{3} + \frac{1}{x} + \frac{1}{x^2}\right)e^{-x} - \left(\frac{k}{x} + \frac{1}{x^2}\right)e^{-kx}\right\} + \sum_{n=2}^{\infty} b_n \frac{e^{-nx}}{x}. \tag{4.37}$$

The constants are different for all values of T, S and $I < 2$. Only a_1, b_1, and c_1 are fixed in such a way that we obtain the OPEP-potential for large distances. For $I > 2$, Reid uses the OPEP-potential.

4.3 Microscopic Effective Interactions

The bare nucleon–nucleon force has—as we have already seen in the preceding section—certain features that are rather difficult to handle in practice.

There is, for instance, the hard core (or at least the very repulsive core), which would make some of the usual concepts of nuclear many-body physics extremely complicated if not inapplicable (as in the Hartree–Fock case; see Chap. 5).* This comes from the infiniteness of the matrix elements of a force with a hard core. In these theories, a way out of this situation is to use, in place of the bare interaction, a so-called effective interaction, which is itself an infinite sum of scattering processes of two nucleons in the nuclear medium. The bare interaction is then simply the Born term of this series. The object of this procedure is twofold: First, in re-summing the series one gets rid of the hard core problem, since the new interaction is well-behaved at short distances. Second, we can show that in replacing the bare interaction by its effective counterpart we have at the same time consistently summed up more of the many-body effects than if one had taken just the bare interaction.

The main fields of application are: (i) the ground state properties of nuclei, where the scattering of two nucleons within the nuclear medium has to be considered; (ii) the forces between the so-called valence nucleons; and (iii) effective forces between "particles" and "holes." There are also effective three-body forces which we will ignore in this section.

4.3.1 Brückner's G-Matrix and Bethe Goldstone Equation†

One of the most important effective interactions in nuclear physics is the so-called Brückner G-matrix [Br 55, Da 67, and references therein]. It is, for two nucleons in the nuclear medium—in a sense yet to be specified—the analogue of the scattering matrix for two nucleons in free space.

We therefore start our considerations with the Lippmann–Schwinger equation for the scattering matrix (T-matrix; see Fig. 4.1) of two particles (Messiah [Me 61] Chap. XIX, Sec. 14):

$$T^E_{\mathbf{k}_1\mathbf{k}_2,\,\mathbf{k}'_1\mathbf{k}'_2} = \bar{v}_{\mathbf{k}_1\mathbf{k}_2,\,\mathbf{k}'_1\mathbf{k}'_2} + \frac{1}{2}\sum_{\mathbf{p}_1\mathbf{p}_2} \bar{v}_{\mathbf{k}_1\mathbf{k}_2,\,\mathbf{p}_1\mathbf{p}_2} \frac{1}{E - (\mathbf{p}_1^2/2m) - (\mathbf{p}_2^2/2m) + i\eta} T^E_{\mathbf{p}_1\mathbf{p}_2,\,\mathbf{k}'_1\mathbf{k}'_2}, \tag{4.38}$$

where $\mathbf{k}_1, \mathbf{k}_2$ and $\mathbf{k}'_1, \mathbf{k}'_2$ are the momenta of the incoming and outgoing particles, respectively, and E is the total scattering energy.

If we consider the scattering of two nucleons within a nuclear medium we can show (this is derived in Sec. F.4) that it makes sense to define a scattering matrix G^E analogous to that for free particles. The changes to be made for nucleons in a nucleus are almost obvious: the plane wave indices have to be changed to shell model indices, the kinetic single-particle energies figuring in the denominator of the r.h.s. of Eq. (4.38) have to be replaced by the corresponding shell model energies, and the sum over the intermediate states has to be restricted so that it does not include states below the Fermi surface. This latter feature comes from the fact that two nucleons below the Fermi surface can only scatter into states above the Fermi surface, because all other levels are occupied and are thus excluded by the Pauli principle. Therefore, we get the following equation for the G-matrix, which is usually known under the name Bethe–Goldstone equation [BG 57] (for its mathematical derivation, see Sec. F.4).

$$G^E_{ab,\,cd} = \bar{v}_{ab,\,cd} + \frac{1}{2}\sum_{\substack{m,\,n \\ >\epsilon_F}} \bar{v}_{ab,\,mn} \frac{1}{E - \epsilon_m - \epsilon_n + i\eta} G^E_{mn,\,cd}, \tag{4.39}$$

where $ab, \ldots, mn$ are shell-model indices and ϵ_F is the Fermi energy. This equation is usually represented graphically in an obvious way, as shown in Fig. 4.2. Two lines connecting two interactions represent the "propagator" $1/(E - \epsilon_n - \epsilon_m)$. (More will be explained about graphs in Chap. 8 and Appendix F.) For $E < \epsilon_F$, we can ignore the $i\eta$ in the denominator of (4.39), and in this case the G-matrix is obviously Hermitian as can be checked immediately by iterating Eq. (4.39). Equation (4.39) is also often

Figure 4.1. Graphical representation of the T-matrix.

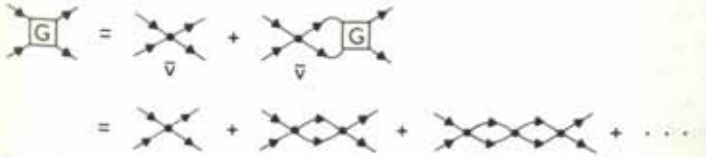

Figure 4.2. Graphical representation of the Bethe–Goldstone equation.

*In this section, we must quite often anticipate theories and methods which are only treated later in this book. This is contrary to our usual strategy, which is to avoid this situation as much as possible. As the reader will notice, however, the microscopic theory of effective interactions is not in a very satisfactory state, so we prefer to give a short survey here together with the description of phenomenological forces, rather than devote an extra chapter to it later. (See also Appendix F.)

†The discussion in this section is partially based on Gomes, Walecka, and Weisskopf [GWW 58] and the textbook of Fetter and Walecka [FW 71].

written in the operator form:

$$G = \bar{v} + \bar{v}\frac{Q_F}{E - H_0}G, \tag{4.40}$$

where H_0 is the shell model Hamiltonian and

$$Q_F = \sum_{\substack{m<n \\ >\epsilon_F}} |mn\rangle\langle mn| \tag{4.41}$$

is a projection operator excluding all occupied states.

In a very qualitative way, we can see from Eq. (4.40) how it can happen that G stays finite for points where $\bar{v}$ is infinite. Solving Eq. (4.40) formally yields

$$G = \frac{\bar{v}}{1 - \bar{v}Q_F/(E - H_0)}. \tag{4.42}$$

If $\bar{v}$ tends to infinity, G may stay finite. This is, of course, only a very crude argument and we shall in a definite example show in detail how this occurs. Before this, we have to discuss, however, some general features of Eq. (4.39). Despite the fact that Eq. (4.39) is formally very similar to Eq. (4.38), there are certain essential differences concerning, for instance, the boundary condition in the case of $E < \epsilon_F$ of the wave function defined in analogy to the scattered wave of two free particles by [Me 61, Chap. XIX 10]:

$$|\psi_{ab}\rangle \equiv \bar{v}^{-1}G|ab\rangle = \left(1 + \frac{Q_F}{E - H_0}G\right)|ab\rangle$$

$$= |ab\rangle + \frac{Q_F}{E - H_0}\bar{v}|\psi_{ab}\rangle, \tag{4.43}$$

with

$$\langle \mathbf{r}_1\mathbf{r}_2 \,|\, ab\rangle = \frac{1}{\sqrt{2}}(\varphi_a(\mathbf{r}_1)\varphi_b(\mathbf{r}_2) - \varphi_a(\mathbf{r}_2)\varphi_b(\mathbf{r}_1)) \tag{4.44}$$

and

$$H_0|ab\rangle = (\epsilon_a + \epsilon_b)|ab\rangle. \tag{4.45}$$

The wave equation (4.43) formally resembles an equation for a scattered wave. However, contrary to the real scattering case, where the second term on the r.h.s. of (4.43) gives the outgoing scattered part of the wave function and thus does not vanish as the relative distance of the two particles $|\mathbf{r}_1 - \mathbf{r}_2|$ goes to infinity, in the present case of $E < \epsilon_F$, this term vanishes as $|\mathbf{r}_1 - \mathbf{r}_2|$ goes to infinity. This comes from the fact that for a real scattering process the T matrix of Eq. (4.38) enters Eq. (4.43) "on the energy shell," that is, the absolute value of the relative momenta of the two particles before and after the scattering process have to be the same; also, E must correspond to this value of the relative momentum. As a consequence, the corresponding energy denominator of Eq. (4.43) for a real scattering

process can be zero and introduce a singularity. In the present case this can never happen, since we suppose $E < \epsilon_F$ and therefore the second expression on the r.h.s. of Eq. (4.39) is never "on the energy shell," which is why it vanishes for large values of $|\mathbf{r}_1 - \mathbf{r}_2|$. A derivation is presented in a review article by Day [Da 67] which, however, would be too much of a digression to be repeated here. We have thus:

$$|\psi_{ab}^E\rangle \xrightarrow{|\mathbf{r}_1 - \mathbf{r}_2| \to \infty} |ab\rangle. \tag{4.46}$$

From Eqs. (4.43) and (4.41) we also immediately get the normalization condition for $a, b < \epsilon_F$:

$$\langle ij \,|\, \psi_{ij}\rangle = 1, \qquad i, j < \epsilon_F. \tag{4.47}$$

It is also instructive to expand the correlated pair function $|\psi_{ij}\rangle$ in an uncorrelated basis. From (4.43) we have:

$$|\psi_{ij}\rangle = |ij\rangle + \frac{1}{2}\sum_{mn} C_{mn}^{ij}|mn\rangle, \tag{4.48}$$

that is, the correlated function contains, in addition to $|ij\rangle$, components above the Fermi level. It turns out that in the most important applications of the G-matrix E lies below the Fermi level. For instance, in the Brückner Hartree–Fock theory (see Chap. 5) we must calculate $G_{ab,ij}^{E=\epsilon_i+\epsilon_j}$ with $i, j < \epsilon_F$. We will therefore treat the hard core for this case in a very simplified but explicitly solvable model which, however, shows the essential features.

Let us consider a large nucleus, the interior of which will be presumed to be not very much different from the situation where we consider an infinitely large nucleus, usually termed nuclear matter. In addition, we will make a further crude assumption, namely, that the interaction consists of a hard core only:

$$V(r) = 0 \text{ for } r > c \qquad \text{and} \qquad V(r) = \infty \text{ for } r < c.$$

Furthermore, we assume that we have two distinguishable particles, for example, a proton and a neutron, which will be sufficient as a demonstration of the principle. Let us now write Eq. (4.43) in the form:

$$(E - H_0)|\psi_{ab}\rangle = (E - H_0 + Q_F G)|ab\rangle, \tag{4.49}$$

which in our case ($E = \epsilon_i + \epsilon_j$) specializes to

$$(\epsilon_i + \epsilon_j - H_0)|\psi_{ij}\rangle = Q_F G|ij\rangle = Q_F\bar{v}|\psi_{ij}\rangle, \tag{4.50}$$

where for the last equality use has been made of (4.43). The general solution of (4.50) is much harder than the solution of an ordinary Schrödinger equation because of the operator Q_F, which is a nonlocal integral operator. This is best seen in the $\mathbf{r}$-representation

$$\langle \mathbf{r}_1\mathbf{r}_2|Q_F|\mathbf{r}_1'\mathbf{r}_2'\rangle = \sum_{\substack{m<n \\ >\epsilon_F}} \langle \mathbf{r}_1\mathbf{r}_2 \,|\, mn\rangle\langle mn \,|\, \mathbf{r}_1'\mathbf{r}_2'\rangle. \tag{4.51}$$

In nuclear matter it is clear that the single-particle wave functions that appear in (4.50) are plane waves. For simplicity we will also assume that the single-particle energies are purely kinetic energies (in a surrounding medium this will not gener-

ally be the case). Because of translational invariance, for nuclear matter the center of mass motion is trivial, and we have:

$$\langle \mathbf{r}_1\mathbf{r}_2 \,|\, \psi_{ij}\rangle \to \psi_{\mathbf{p}_1\mathbf{p}_2}(\mathbf{r}_1\mathbf{r}_2) = \frac{1}{(2\pi)^{3/2}} e^{i\mathbf{P}\mathbf{R}} \psi_{\mathbf{P}\mathbf{k}}(\mathbf{r}). \tag{4.52}$$

Here the following transformations to relative and center of mass coordinates have been made:

$$\begin{aligned} &\mathbf{P} = \mathbf{p}_1 + \mathbf{p}_2, \qquad \mathbf{k} = \frac{1}{2}(\mathbf{p}_1 - \mathbf{p}_2), \\ &\mathbf{R} = \frac{1}{2}(\mathbf{r}_1 + \mathbf{r}_2), \quad \mathbf{r} = \mathbf{r}_1 - \mathbf{r}_2. \end{aligned} \tag{4.53}$$

With all these assumptions, Eq. (4.50) acquires the form

$$\begin{aligned} &\frac{\hbar^2}{2m}\{p_1^2 + p_2^2 + \Delta_1 + \Delta_2\}\psi_{\mathbf{p}_1\mathbf{p}_2}(\mathbf{r}_1\mathbf{r}_2) \\ &\quad = \frac{1}{(2\pi)^6}\int_{p,\,p' > k_F} d^3p\, d^3p' \int d^3r_1'\, d^3r_2' e^{i(\mathbf{p}\mathbf{r}_1 + \mathbf{p}'\mathbf{r}_2 - \mathbf{p}'\mathbf{r}_1' - \mathbf{p}'\mathbf{r}_2')} v(|\mathbf{r}_1' - \mathbf{r}_2'|)\psi_{\mathbf{p}_1\mathbf{p}_2}(\mathbf{r}_1'\mathbf{r}_2'). \end{aligned} \tag{4.54}$$

Transforming this equation to relative and center of mass coordinates according to (4.53) we obtain

$$\begin{aligned} &\frac{\hbar^2}{m}\{k^2 + \Delta_r\} e^{i\mathbf{P}\mathbf{R}}\psi_{\mathbf{P}\mathbf{k}}(\mathbf{r}) \\ &\quad = \frac{1}{(2\pi)^6}\int\int_{\left|\frac{\mathcal{P}}{2} \pm \mathbf{p}\right| > k_F} d^3\mathcal{P}\, d^3p \int\int d^3R'\, d^3r'\, e^{i[\mathcal{P}\mathbf{R} + \mathbf{p}(\mathbf{r} - \mathbf{r}')]} e^{-i\mathcal{P}\mathbf{R}'} v(r') e^{i\mathbf{P}\mathbf{R}'} \psi_{\mathbf{P}\mathbf{k}}(\mathbf{r}'). \end{aligned} \tag{4.55}$$

Since $\mathcal{P}^2 = p^2 + 2pp'\cos\theta + p'^2$, we see that even under the restriction $p,\, p' > k_F$, $\mathcal{P}$ can take on all values from 0 to ∞. The integration over $\mathbf{R}'$ gives $\delta(\mathbf{P} - \mathcal{P})$ and we can therefore also perform the $\mathcal{P}$ integral. We are thus left with the following equation.

$$\frac{\hbar^2}{m}\{k^2 + \Delta_r\}\psi_{\mathbf{P}\mathbf{k}}(\mathbf{r}) = \frac{1}{(2\pi)^3}\int_{\left|\frac{\mathbf{P}}{2} \pm \mathbf{p}\right| > k_F} d^3p\, e^{i\mathbf{p}\mathbf{r}'} \int d^3r' e^{-i\mathbf{P}\mathbf{r}'} v(r')\psi_{\mathbf{P}\mathbf{k}}(\mathbf{r}'). \tag{4.56}$$

This equation is not only more complicated than a usual two-particle equation because of its integrodifferential structure, but also because the wave function has a nontrivial dependence on the center of mass momentum $\mathbf{P}$. For our purpose, it will be sufficient to evaluate it at $\mathbf{P} = 0$. Furthermore, we can decompose Eq. (4.56) into partial waves [Me 61 Chap. X, Sec. 8]:

$$\psi_{\mathbf{k}}(\mathbf{r}) = \sum_{lm} \psi_{kl}(r)\, Y_{lm}(\theta, \varphi). \tag{4.57}$$

Considering the equation for the s-wave and splitting the integral in (4.56) into two parts, $\int_{k_F}^{\infty} = \int_0^{\infty} - \int_0^{k_F}$, we obtain:

$$\begin{aligned} &\frac{\hbar^2}{m}\left(k^2 + \frac{\partial^2}{\partial r^2} + \frac{2}{r}\frac{\partial}{\partial r}\right)\psi_{\mathbf{k}}(r) \\ &\quad = v(r)\psi_{\mathbf{k}}(r) - (4\pi)^2 \int_0^{k_F} \frac{dp\, p^2}{(2\pi)^3} j_0(pr) \int_0^{\infty} dr' r'^2 j_0(pr') v(r')\psi_{\mathbf{k}}(r'), \end{aligned} \tag{4.58}$$

where j_0 is the lowest-order spherical Bessel function. With $\psi_{\mathbf{k}}(r) = (1/r)u_k(r)$, we finally get:

$$\frac{\hbar^2}{m}\left(k^2 + \frac{\partial^2}{\partial r^2}\right)u_k(r) = v(r)u_k(r) - k_F \int_0^{\infty} dr' \chi(r', r) v(r') u_k(r'), \tag{4.59}$$

with

$$\chi(r, r') = \frac{2rr'}{\pi k_F}\int_0^{k_F} dp\, p^2 j_0(pr) j_0(pr') = \frac{1}{\pi \cdot k_F}\left\{\frac{\sin k_F(r - r')}{r - r'} - \frac{\sin k_F(r + r')}{r + r'}\right\}. \tag{4.60}$$

It is now convenient to introduce the following dimensionless quantities:

$$x = k_F \cdot r; \qquad x' = k_F \cdot r'; \qquad K = \frac{k}{k_F}; \qquad \frac{mv}{k_F^2\hbar^2} = w. \tag{4.61}$$

This leads to

$$\left(\frac{d^2}{dx^2} + K^2\right)u_K(x) = w(x)u_K(x) - \int_0^{\infty} dx'\, \chi(x, x')w(x')u_K(x'). \tag{4.62}$$

For a square well barrier of finite height, the wave function and its first derivative are continuous at the edge of the barrier. We can be easily convinced that the first derivative of the wave function becomes discontinuous at the edge as the barrier height goes to infinity, that is:

$$u_K'(c + \epsilon) = A, \tag{4.63}$$

where A is a constant, $r = c$ is the radius of the hard core, and ϵ is an infinitesimally small positive quantity. In order to produce such a discontinuity for u of Eq. (4.62), the product $w \cdot u$ must be proportional to a δ function for $r = c$. Since for $r > c$ the potential w is zero and u finite, the product $w \cdot u$ vanishes outside the hard core radius. The wave function u cannot penetrate inside the infinite hard core ($u = 0$); since there $w = \infty$, the product $w \cdot u$ may be finite and we can write, with $c' = ck_F$:

$$w(x)u_K(x) = A\delta(x - c') + l(x)\theta(c' - x). \tag{4.64}$$

The function $l(x)$ can be determined from the requirement that for $x < c'$ the left hand side of Eq. (4.62) must be zero, since $u \equiv 0$ for $x < c'$. We therefore have from Eq. (4.62) with Eq. (4.64)

$$l(x) = A\chi(x, c') + \int_0^{c'} dx'\, \chi(x, x')l(x') \qquad \text{for} \quad x < c'. \tag{4.65}$$

Since the hard core is usually rather small ($c' = 0.57$ at the nuclear matter density for $c = 0.4$ fm), we can develop the kernel in Eq. (4.65) and obtain from Eq. (4.60)

$$\chi(x, x') \to \frac{2xx'}{3\pi} \qquad x < c'; \quad x' < c'. \tag{4.66}$$

With Eqs. (4.66) and (4.65), we see that $l(x)$ is of order c'^2, whereas any integral over $l(x)$ will be of order c'^3. In (4.62) we can therefore neglect the second term in (4.64) to obtain a result which is correct to first order in c'. We obtain

$$\begin{aligned} \left(\frac{d^2}{dx^2} + K^2\right)u_K(x) &\simeq A[\delta(x - c') - \chi(x, c')] + A\chi(x, c')\theta(c' - x) \\ &= A\frac{2xc'}{\pi}\int_1^{\infty} dp\, p^2 j_0(px) j_0(pc') + A\chi(x, c')\theta(c' - x) \\ &= F(x), \end{aligned} \tag{4.67}$$

where we have made use of the identity

$$\int_0^\infty dp\, p^2 j_l(pr) j_l(pr') = \frac{\pi}{2r^2}\delta(r-r'). \tag{4.68}$$

We remark that since the r.h.s. of Eq. (4.67) is only correct to first order in c', it is somewhat arbitrary whether to include the second term of the r.h.s. of Eq. (4.67), which is of second order. The general solution of Eq. (4.67),

$$u_K(x) = \frac{\sin Kx}{K}\int_{c'}^{x} dy\, F(y)\cos Ky - \frac{\cos Kx}{K}\int_{c'}^{x} dy\, F(y)\sin Ky, \tag{4.69}$$

is obviously zero for $x = c'$. Equation (4.69) is the solution to Eq. (4.67), as can be easily verified by direct insertion.

The only unknown in the solution (4.67, 4.69) is the constant A, which we are going to determine by the requirement (4.46) that u_K has to approach asymptotically the unperturbed value. To this end we will first show that the second integral on the r.h.s. of Eq. (4.69) is zero in the limit $x \to \infty$. Since we considered our solution in the limit of very small c', we can take the integral from 0 to ∞ instead of from c' to ∞, and thus have

$$\begin{aligned}\frac{1}{K}\int_0^\infty dy\, F(y)\sin Ky &= \frac{2Ac'}{\pi}\int_1^\infty dp\; p^2 j_0(pc')\int_0^\infty dy\; y^2 j_0(Ky) j_0(py)\\ &= \frac{2Ac'}{\pi}\int_1^\infty dp\; p^2 j_0(pc')\frac{\pi}{2Kp}\delta(K-p)\\ &= 0.\end{aligned} \tag{4.70}$$

The last integral vanishes because p is outside the Fermi sphere, whereas K is inside. For $r \to \infty$ we therefore find the result that the wave function approaches the unperturbed result ($\psi \to j_0$) [see Eq. (4.46)] only if

$$\int_0^\infty dy\, F(y)\cos Ky = 1, \tag{4.71}$$

and we therefore get, using Eq. (4.67):

$$A = \left\{\cos Kc' - \int_0^\infty dy \cos(Ky)\chi(y, c')\right\}^{-1}, \tag{4.72}$$

which completes the determination of the wave function $u_K(x)$ of Eqs. (4.67) and (4.69) for a hard sphere potential.

In Fig. 4.3 we show the solution $\psi_k(r)$ for $\mathbf{k}=0$, which reveals several interesting features. The wave function vanishes inside the hard core. With (4.69) and (4.72) it can easily be seen that it approaches rapidly (by

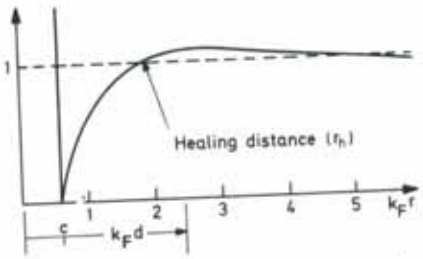

Figure 4.3. *S*-wave solution of the Bethe–Goldstone equation for a pure hard core potential in nuclear matter. For details of the figure, see text. (From [FW 71].)

damped oscillations) the value of the wave function for the noninteracting pair (which is itself equal to 1 for $k=0$ and all values of r). The r value at which the wave function first attains the unperturbed value is called the *healing distance* r_h, because it is only for distances smaller than this value that the hard core wave function differs appreciably from the unperturbed wave function. For the values chosen in our example, the healing distance is:

$$k_F r_h \simeq 1.9. \tag{4.73}$$

(This value is more or less independent of $\mathbf{P}$ and k, as a more general study of Eq. (4.59) shows [WG 67a]). It is important to note that this value is appreciably smaller than the average interparticle distance d in nuclear matter defined by the expression $1/d^3 \equiv N/V = (4\int_{p\le\hbar k_F} d\mathbf{p}\int d\mathbf{r})/V(2\pi\hbar)^3 = 2k_F^3/3\pi^2$, which would yield for the interparticle distance:

$$k_F d = \left(\frac{3\pi^2}{2}\right)^{1/3} = 2.46. \tag{4.74}$$

On the average, therefore, the nucleons return after a collision to their independent particle wave function *before* the next collision takes place. A great portion of the nuclear wave function therefore consists of a determinant built out of independent particle wave functions. This can be considered as a justification of the independent particle model—the Pauli principle suppressing the low momentum components of the scattering process, that is, suppressing the long range correlations. The nucleons thus move through the nucleus most of the time as independent particles because of the exclusion principle. That this can happen in a strongly interacting but dilute Fermi gas was first pointed out by Weisskopf [We 50].

We have seen that the solution of the Bethe–Goldstone Equation (4.39) is far from trivial, and one can easily imagine that the task can become tremendously difficult for finite nuclei, where the wave functions are no longer plane waves and translational invariance is also lost. Several approximation schemes have therefore been currently applied. As we have seen in our example, it is the projection operator Q_F which makes things so difficult. It has been proposed, that the Pauli principle should be treated only perturbatively in the *separation method* of Moszkowski and Scott [MS 60] and in the *reference spectrum method* of Bethe, Brandow, and Petschek [BBP 63]. We do not wish to go into details of these approximation methods and refer the reader to the text books of Brown [Br 64], de Shalit and Feshbach [SF 74], and the review article by Bethe [Be 71], in which these and further methods, like the use of the oscillator basis for the solution of the Bethe–Goldstone equation in finite nuclei, are explained in detail. Here we want to mention only one other approximation scheme which has recently become very successful in connection with the Brückner–Hartree–Fock theory (see Chap. 5). This is the *local density approximation* by Negele [Ne 70, 75], originally introduced by Brückner, Gammel, and Weitzner [BGW 58] and Brückner, Lockett, and Rotenberg [BLR 61]. The assumption is that the G-matrix at any place in a finite nucleus is the same as that for nuclear matter at the same density, so that locally one can

calculate the G-matrix as in a nuclear matter calculation [Be 71, Ne 75]. We shall come back to this approximation in Chapter 5.

4.3.2 Effective Interactions between Valence Nucleons

Another field to which the Brückner G-matrix has important applications is the effective forces between the so-called valence nucleons (for a review, see [Ku 74b] and references therein). As a definite example, let us take ^{18}O or ^{18}F, where we have two nucleons (the "valence nucleons") on top of a doubly magic nucleus ^{16}O. In the pure shell model approximation the two nucleons will be in the $1d5/2$ level. We may hope to get a good description of the low-lying states of ^{18}O by making a configuration mixing calculation using the states $1d5/2$, $2s1/2$, $1d3/2$ which just form the first shell above the ^{16}O core. Such shell model calculations have been described to some extent in Chapter 2 and will be treated in greater detail in Chapter 8, where we will show, for instance, that such two-valence nucleons may be well described by the particle–particle Tamm–Dancoff secular equation [see Chap. 8, Eq. (8.10)]:

$$\left(E_\rho^{TD}-\epsilon_m-\epsilon_n\right)R^\rho_{mn}=\frac{1}{2}\sum_{m'n'}\bar{v}_{mn,\,m'n'}R^\rho_{m'n'}. \tag{4.75}$$

Here the ϵ_m's are the single-particle energies of the phenomenological or self-consistent (see Chap. 5) single-particle Hamiltonian H_0 and all the indices in Eq. (4.75) are in the *model space* above the Fermi level of the core (e.g., the $d5/2$, $2s1/2$, and $d3/2$ states in our example). For the two-particle interaction in Eq. (4.75), we cannot take the bare interaction, since this force has to simulate and correct at least approximately the omission of (a) the rest of the two-particle configuration above the Fermi level, and (b) contributions from higher configurations of the shell model basis like $3p$–$1h$, $4p$–$2h$, etc.

In the following we will derive an exact equation, formally almost identical to Eq. (4.75), with, however, $\bar{v}$ replaced by an effective (energy dependent) interaction, calculable at least in principle, from the bare interaction (such as, e.g., the Hamada–Johnston potential). We start out with the observation of Chapter 2 that the shell model provides a complete set of states; therefore, any exact wave function can be expanded in this basis. A convenient way to do this is given by the formalism of second quantization, in which the expansion of, for example, an $A+2$ nucleon state can be written in the following way (see also Chap. 8). (In the following, the indices m, n, r, p, and i, j shall be states above and below the Fermi level, respectively.)

$$|A+2,\tau\rangle=\sum_{m<n}R^\tau_{mn}a_m^+a_n^+|HF\rangle+\sum_{m<n<r,\,i}R^\tau_{mnr,\,i}a_m^+a_n^+a_r^+a_i|HF\rangle$$
$$+\sum_{\substack{m<n<r<p\\ i<j}}R^\tau_{mnrp,\,ij}a_m^+a_n^+a_r^+a_p^+a_ia_j|HF\rangle. \tag{4.76}$$

Here we assume that the ground state $|HF\rangle$ of the A nucleus in the shell model is ideally given by a Hartree–Fock calculation (see Chap. 5), but our considerations hold equally for any phenomenological shell model. The indices m, n, r, p and i, j in Eq. (4.76), of course, correspond to the shell model potential in question. The expansion consists of multiparticle–multihole components ranging from $2p$–$0h$ up to, in principle, $(A+2)p$–Ah components. We now introduce two projectors P and Q. The projector P projects on those $2p$–$0h$ states which lie within the given model space and Q projects onto the rest, that is, on those $2p$–$0h$ components which do not lie in the model space and on *all* $3p$–$1h$, $4p$–$2h$, etc. components. Therefore, $1=P+Q$ and

$$P=\sum_{m<n}{}'a_m^+a_n^+|HF\rangle\langle HF|a_na_m, \tag{4.77}$$

where the prime on the sum indicates that it goes over the model space only. We also have the usual relations for projectors, viz:

$$Q^2=Q;\qquad P^2=P;\qquad P^+=P;\qquad Q^+=Q;\qquad PQ=QP=0. \tag{4.78}$$

With the aid of these projectors we can write for Eq. (4.76):

$$|\tau\rangle=P|\tau\rangle+Q|\tau\rangle=PR|HF\rangle+QS|HF\rangle, \tag{4.79}$$

where $R=\sum'_{m<n}R^\tau_{mn}a_m^+a_n^+$, the prime having the same meaning as in Eq. (4.77); the operator S is then defined in an obvious way by Eqs. (4.76) and (4.79). The Schrödinger equation $(H_0+V)|\tau\rangle=E_\tau|\tau\rangle$, where H_0 is the shell model Hamiltonian and V the residual interaction (see Chaps. 2 and 8) can now be written in the following form [Fe 62].

$$(-E_\tau+H_0+PVP)P|\tau\rangle=-PVQ|\tau\rangle, \tag{4.80}$$
$$(-E_\tau+H_0+QVQ)Q|\tau\rangle=-QVP|\tau\rangle. \tag{4.81}$$

Here we have multiplied the Schrödinger equation from the left once with P and once with Q and observed that P and Q commute with H_0. Solving Eq. (4.81) for $Q|\tau\rangle$ and substituting into Eq. (4.80) yields

$$\left(H_0+PV^{E_\tau}_{\text{eff}}P\right)P|\tau\rangle=E_\tau P|\tau\rangle \tag{4.82}$$

with

$$V^{E_\tau}_{\text{eff}}=V+VQ\frac{1}{E_\tau-H_0-QVQ}QV. \tag{4.83}$$

Multiplying Eq. (4.82) from the left with $\langle HF|a_na_m$, where n, m are in the model space, we can write:

$$\left\{\langle HF|\left[a_na_m,H_0\right]+\langle HF|a_na_mPV_{\text{eff}}P\right\}\sum_{m'<n'}{}'a_{m'}^+a_{n'}^+|HF\rangle R^\tau_{m'n'}$$
$$=\left(E_\tau-E_0^{HF}\right)R^\tau_{mn} \tag{4.84}$$

with

$$H_0|HF\rangle=E_0^{HF}|HF\rangle.$$

The commutator in Eq. (4.84) is easily evaluated, and we finally obtain an

equation which is formally very similar to the two-particle Tamm–Dancoff Eq. (4.75) but is, in fact, rigorously exact:

$$\left[(E_\tau - E_0^{HF}) - \epsilon_m - \epsilon_n\right] R^\tau_{mn} = \sum_{m'<n'}{}' \langle mn|V^{E_\tau}_{\text{eff}}|m'n'\rangle R^\tau_{m'n'}. \tag{4.85}$$

We see that the difference between Eqs. (4.85) and (4.75) is simply that the matrix elements of the phenomenological two-body interaction have been replaced by those of an effective energy dependent interaction which (at least in principle) can be calculated from the bare interaction.* The expression (4.83) can be rewritten as an integral equation for V_{eff}:

$$V_{\text{eff}} = V + VQ\frac{1}{E - H_0}QV_{\text{eff}}. \tag{4.86}$$

This can be verified either by expanding both (4.86) and (4.83) in powers of V, or by direct substitution of (4.83) in (4.86) and using decomposition into partial fractions. In order to investigate the simplest contributions to V_{eff}, we have to look at the structure of the projection operator Q. We can distinguish three different contributions: (i) $2p$–$0h$ excited states, where only one particle is outside the model space; (ii) two-particle excited states, where both particles of the $2p$–$0h$ components are outside the model space; (iii) those components which involve holes ($3p$–$1h$, etc.) The excited states of type (i) probably do not contribute very much, since it has been shown that their contribution vanishes exactly in nuclear matter [Ma 69], and are thus expected to be small in finite (but heavy) nuclei. Their contribution is thus omitted in practical calculations. The two-particle excited states give the most important contribution, as practical calculations have shown, therefore we want to study how they can be treated and what their relation to the Brückner G-matrix will be.

We shall call that part of Q which corresponds to the two-particle excited states (ii) Q_{2p}. Retaining in (4.86) only the Q_{2p} part and expanding in powers of V, we obtain up to second order

$$\langle mn|V_{\text{eff}}|m'n'\rangle = \bar{v}_{mn,\,m'n'} + \sum_{\substack{p<q \\ >\epsilon_{\max}}} \frac{\bar{v}_{mn,\,pq}}{\Omega_\tau - \epsilon_p - \epsilon_q}\bar{v}_{pq,\,m'n'} + \cdots, \tag{4.87}$$

where $\epsilon_{\max}$ is the upper limit of the model space and $\Omega_\tau = E_\tau^{A+2} - E_0^A$ in accordance with the footnote on this page (no problems with linked or unlinked terms appear at this level). This shows that this part of the

*The effective interaction defined by Eqs. (4.83) and (4.85) contains so-called unlinked contributions [Ma 69]. By reordering these terms in Eq. (4.85) we can show that one obtains an equation structurally equal to Eq. (4.85), where, however, E_0^{HF} is replaced by the exact ground state energy E_0^A of the core. The argument $E_\tau^{A+2} - H_0$ in the denominator of Eq. (4.83) is changed to $E_\tau^{A+2} - E_0^A - (H_0 - E_0^{HF})$ and only the linked contributions of Eq. (4.83) have to be taken into account. However, no integral equation for this quantity is known [compare Eq. (4.86)]. More details of this procedure can be found in the review articles by MacFarlane [Ma 69] and Barrett and Kirson [BK 73]. Brandow [Br 67a] has shown that we can also get rid of the energy dependence of the effective interaction by introducing the so-called "folded diagram" (see also [JB 71, EO 77]). The discussion of these rather involved techniques would go beyond the scope of this book, thus we refer the interested reader to the original literature.

effective interaction is equal to the Brückner G-matrix (4.39) with ϵ_F replaced by $\epsilon_{\max}$, that is,

$$\left(V^{(2p)}_{\text{eff}}\right)_{mn,\,m'n'} = G^{E_\tau^{A+2} - E_0^A}_{mn,\,m'n'}(\epsilon_F \to \epsilon_{\max}). \tag{4.88}$$

The whole intention and philosophy of rewriting the exact Schrödinger equation in the form (4.85) is based on the hope that V_{eff} is an operator which for the physical problem of two valence nucleons can be calculated to a good approximation in some perturbative way. One must therefore assume that V_{eff} is well behaved in the sense that it has, for instance, no strong energy dependence. The energy dependence of G in Eq. (4.88) is thus usually neglected and replaced by

$$\Omega_\tau \simeq \frac{1}{2}(\epsilon_m + \epsilon_n + \epsilon_{m'} + \epsilon_{n'}). \tag{4.89}$$

Also, all the other approximations commonly applied to solve the Bethe–Goldstone equation should not influence the result too much (see, for example, [Ma 69] and [SF 74]). Kuo and Brown [KB 66] have solved the Bethe–Goldstone equation in the harmonic oscillator approximation [SF 74] for ^{18}O and ^{18}F using as bare interaction the Hamada–Johnston force. This force was subsequently used in Eq. (4.85) for a diagonalization in the model space where the experimental values found in ^{17}O have been used for the single particle energies. In Fig. 4.4 we show a comparison of the

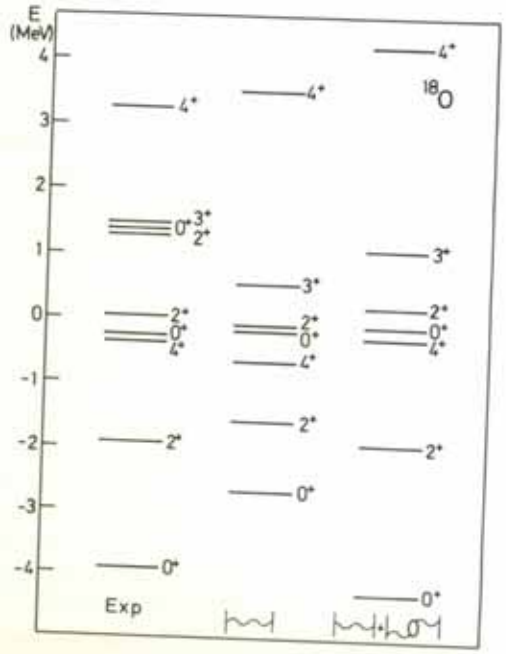

Figure 4.4. The spectrum of ^{18}O. The first column shows the experimental values. The second one was calculated with the pure G-matrix. The third also includes the polarization term (4.90). (From [HK 72].)

low-lying spectrum of ^{18}O as calculated by these authors, with the spectrum of the experiment; in Fig. 4.5 we show the same for the case of ^{210}Pb. The latter calculations were performed by Herling and Kuo [HK 72] using in principle the same method as Kuo and Brown. Their model space consisted of the following single-particle states:

neutrons: $2g9/2$ $1i11/2$ $1j15/2$ $3d5/2$ $4s1/2$ $2g7/2$ $3d3/2$
protons: $1h9/2$ $2f7/2$ $1i13/2$ $2f5/2$ $3p3/2$ $3p1/2$

As can be seen from Fig. 4.4 and Fig. 4.5, the comparison of these two calculations with experiment is not very satisfying and the agreement can be considered as qualitative only. The disagreement is probably not due to the various approximations which entered the solution of the Bethe–Goldstone equation, but rather to the omission of other configurations like $3p$–$1h$, etc. In both of the calculations mentioned it has been shown that at least perturbative inclusion of $3p$–$1h$ configurations improves agreement with experiment very much. The procedure was to calculate the contribution to V_{eff} from Q_{3p-1h} in Eqs. (4.83) and (4.85) in second order perturbation theory (omitting the unlinked terms, see footnote on page 166). This is

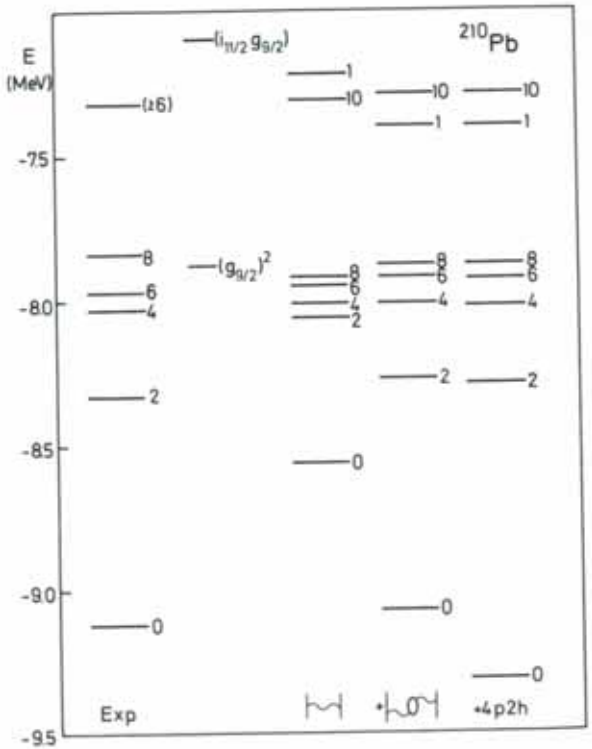

Figure 4.5. The spectrum of ^{210}Pb. The first three spectra have the same meaning as those of Fig. 4.4. In the fourth spectrum also, $4p$–$2h$ polarization terms were taken into account. Also indicated is the free two-particle energy. (From [HK 72].)

not too hard to carry out using our definition [(4.83) and (4.85)] and the result is:

$$\left(V_{\text{eff}}^{3p-1h}\right)_{mn,\,m'n'} = \left\{ \sum_{pi} \frac{\bar{v}_{mi,\,m'p}\,\bar{v}_{pn,\,in'}}{\Omega_\nu - \epsilon_{m'} - \epsilon_n - \epsilon_p + \epsilon_i} - (n' \leftrightarrow m') \right\} - \{m \leftrightarrow n\}. \tag{4.90}$$

In this expression we neglected all terms which give a renormalization of the single-particle energies, that is, terms of the structure $(V_{\text{eff}})_{mn,\,m'n'} = A_{mm'}B_{nn'} - (m' \leftrightarrow n')$, because it is believed that these terms are already included in the experimental single-particle energies used in the specific calculations. Usually one represents the term (4.90) graphically, as displayed in Fig. 4.6 (more about graphs is explained in Chap. 8 and Appendix F). The second order part however cannot be used as it stands because of the hard core potential. It can be shown [BK 67a] that it is a consistent re-summation of higher order terms to replace the bare interactions by their corresponding G-matrices in the second order contribution of the $3p$–$1h$ states to V_{eff} (e.g., (4.90)). We do not wish to go into the details of such arguments here because they would lead us outside the scope of this book. In Figs. 4.4 and 4.5 are also shown results with the inclusion of these "renormalized" second order $3p$–$1h$ contributions (the "core polarization") and, as can be seen, the agreement with experiment proves in both cases almost perfect. If this were the whole story, the results would be very satisfying, since we would have explained the low-lying part of the spectrum of these nuclei using essentially no free parameter. Unfortunately, things are far from being settled, since further studies have shown that inclusion of higher order terms will again worsen the results. This effect is shown in Fig. 4.5, where not only $3p$–$1h$ but also $4p$–$2h$ terms are included. More systematic but complicated studies in this direction have been performed by Barrett and Kirson [BK 73] and Kirson and Zamick [KZ 70], which show that great fluctuations of the results as a function of different higher order terms are observed and, therefore, no definite conclusions can be drawn; in particular, it remains unexplained why the second order $3p$–$1h$ inclusion gives such good agreement with experiment. One may, therefore, draw the conclusion that the microscopic theory of effective interactions is still not at a very satisfying stage.

Nevertheless, we want to come back to two formal points in the theory. The first concerns the energy dependence of the effective interaction V_{eff}^E. In all calculations this energy dependence has been more or less neglected. As we have already stated, this is, of course, only true as long as the energy

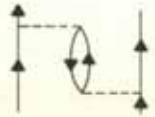

Figure 4.6. Graphical representation of a core polarization term.

dependence is really weak. However, it can happen that V_{eff}^{E} has poles, as a function of E, which lie close or even in the region of the low-lying states of interest; for example, this is the case for ^{18}O, where a collective $4p$–$2h$ pole comes very low in energy [Sch 75]. In this case, such a pole has to be treated separately, since it gives rise to a strong energy dependence in the region of interest. The states also cause difficulties in the case of the folded diagram formalism (see footnote on page 166), where they have been called *intruder states* [SW 72, 73]. There, it turns out that the perturbation series of the corresponding effective interaction in powers of the G-matrix very likely diverge in such cases. Special techniques have been developed to handle this problem [SW 72, 73, HLR 74].

Up to now we have considered only two-particle systems, however, the same considerations can be made for the case of more than two valence nucleons [Ma 69], although we do not want to go into these details.

4.3.3 Effective Interactions between Particles and Holes

The problem of effective interactions between particles and holes arises mainly in the study of vibrational states of closed shell nuclei (see Chap. 8). However, from a microscopic point of view this case has been much less investigated than the interaction between valence nucleons (see, for example, [BK 69, KBB 70]). One can argue that it would be desirable to express also the effective *ph* force by a microscopic G-matrix with perhaps some higher order corrections, like the polarization diagrams for the valence nucleons. This can, in fact, be achieved. The discussion is complicated by the fact that, for the most part, the random phase approximation, (see Chap. 8) is considered the appropriate theory and not the Tamm–Dancoff approximation, for the *ph* case. However, in order not to complicate things too much we shall restrict ourselves to the Tamm–Dancoff case.

The Tamm–Dancoff equation (see Chap. 8) has the following form.

$$\left(E_{\mu}^{\text{TDA}} - \epsilon_m + \epsilon_i\right) C_{mi}^{\mu} = \sum_{nj} \bar{v}_{mj,\,in} C_{nj}^{\mu}. \tag{4.91}$$

This equation, where m, n (i, j) are indices above (below) the Fermi level, is usually solved in a model space with, say, one shell below and one above the Fermi level. In analogy to the case of two valence nucleons, the phenomenological interaction entering Eq. (4.91) has to simulate the effect of the $1p$–$1h$ states not included in the model space, and also $2p$–$2h$, $3p$–$3h$, etc. effects.

In general, for a closed shell nucleus we can make the following expansion of such a vibrational state (see Chap. 8):

$$|\mu\rangle = \sum_{mi} C_{mi}^{\mu} a_m^{+} a_i |\text{HF}\rangle + \sum_{\substack{m<n \\ i<j}} C_{mn,\,ij}^{\mu} a_m^{+} a_n^{+} a_i a_j |\text{HF}\rangle + \cdots. \tag{4.92}$$

However, the procedure for arriving at an effective interaction starting from Eq. (4.92) has to be somewhat different from the valence nucleon case. First we introduce the projector P which projects onto the *whole* $1p$–$1h$ subspace, that is:

$$\begin{aligned} P &= \sum_{mi} a_m^{+} a_i |\text{HF}\rangle\langle\text{HF}| a_i^{+} a_m, \\ Q &= 1 - P, \end{aligned} \tag{4.93}$$

with no restriction on the sum. Using the same formalism as for arriving at Eq. (4.85), we obtain in the *ph* case

$$\left[E_{\mu} - E_0^{\text{HF}} - \epsilon_m + \epsilon_i\right] C_{mi}^{\mu} = \sum_{nj} \langle mi | V_{\text{eff}}^{E_{\mu}} | nj \rangle C_{nj}^{\mu}, \tag{4.94}$$

where V_{eff} is formally given by the same expression as in Eq. (4.83) with, however, the projection operators P and Q given by Eq. (4.93). The first contribution to Q comes from the $2p$–$2h$ components, that is, from Q_{2p-2h}. Calculating the contribution of this term to second order perturbation theory in V, we obtain:

$$\begin{aligned} \left(V_{\text{eff}}^{(2p-2h)}\right)_{mj,\,in} = & \sum_{m'<n'} \bar{v}_{mj,\,m'n'} \frac{1}{\Omega_{\mu} + \epsilon_i + \epsilon_j - \epsilon_{n'} - \epsilon_{m'}} \bar{v}_{n'm',\,in} \\ & - \sum_{i'<j'} \bar{v}_{j'i',\,ni} \frac{1}{\Omega_{\mu} - \epsilon_m - \epsilon_n + \epsilon_{i'} + \epsilon_{j'}} \bar{v}_{jm,\,i'j'} \\ & - \sum_{n'j'} \bar{v}_{mj',\,nn'} \frac{1}{\Omega_{\mu} - \epsilon_n + \epsilon_i - \epsilon_{n'} + \epsilon_{j'}} \bar{v}_{jn',\,ij'} \\ & - \sum_{m'i'} \bar{v}_{j'i',\,m'i} \frac{1}{\Omega_{\mu} - \epsilon_m + \epsilon_j - \epsilon_{m'} + \epsilon_{j'}} \bar{v}_{mm',\,i'n}, \end{aligned} \tag{4.95}$$

where $\Omega_{\mu} = E_{\mu}^{A} - E_0^{\text{HF}}$ and terms which renormalize single-particle energies are not included. The first term on the r.h.s. of Eq. (4.95) together with the first order term of V_{eff} just gives the first two terms of the G-matrix:

$$G_{mj,\,in}^{\Omega_{\mu} + \epsilon_i + \epsilon_j}. \tag{4.96}$$

Indeed, we can verify that to each order in V there exists in V_{eff} a term which corresponds to the corresponding order in Eq. (4.96). Therefore, V_{eff} consists of a first term which is the G-matrix (4.96). The second term on the r.h.s. of Eq. (4.95) represents hole–hole correlations which numerically are found to be small and therefore may be neglected. The third and fourth term are analogous to the polarization diagram (Fig. 4.6) for the case of two valence nucleons. Again, these terms cannot be used as they stand, but we can show that it is a consistent re-summation of higher order terms to replace the bare matrix elements by their corresponding G-matrix elements. The polarization diagram in the *ph* case is displayed in Fig. 4.7. The fact that we already have a G-matrix in the full *ph* space to lowest order is the essential difference between the *ph* and *pp* cases. In recognizing this, we may now convert Eq. (4.94) to one in a model *ph* space. For this purpose we split the projector P into a part P_M which projects onto the model *ph* space and into a part P_R which projects onto the rest of the *ph* space:

$$P = P_M + P_R.$$

Eliminating the components in Eq. (4.94) that are outside the model space with the aid of the Feshbach projection operator formalism [Fe 62], which we have already used [see, for example, Eqs. (4.80) and (4.81)], leads to a TDA equation in the model space. The effective interaction appearing there can be expanded up to

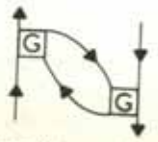

Figure 4.7. Polarization diagram in the particle-hole case.

second order in the G-matrix. The term which comes from Eq. (4.96) is shown in Fig. 4.8, where it should be appreciated that the summation over the intermediate lines goes only over states that are *not* in the modelspace. Realistic calculations [BK 69, KBB 70] show that the inclusion of the polarization diagram Fig. 4.7 has an important effect: Whereas RPA calculations (see Chap. 8) without it give imaginary solutions, the polarization contribution stabilizes the solutions. The reason for this—as discussed in more detail in Chap. 8—is that the RPA overestimates ground state correlations and polarization or screening terms have to be introduced to reduce them.

Figure 4.8. Second order contribution to V_{eff} in the model *ph* space. The broken intermediate lines shall indicate that one has to sum only over states not contained in the model space.

With these remarks we wish to finish our consideration of the microscopic effective interaction and, in the next section, turn to their phenomenological counterparts.

4.4 Phenomenological Effective Interactions

4.4.1 General Remarks

In Section 4.3 we saw how effective forces can be defined microscopically and how difficult it is in practice to calculate them and get quantitative agreement with experiment. Consequently, from the early days of nuclear physics the use of phenomenological forces, which contain a certain number of *fit parameters* adjusted to reproduce the experimental data has been adopted. In many cases this procedure has turned out to be extremely successful and, using only a few parameters chosen once and for all, much experimental data covering quite a large range of nuclear masses can be explained. Therefore, it is all the more disconcerting that a really satisfying microscopic theory able to explain the success of these phenomenological forces is somehow still missing.

There exists, of course, an enormous number of different phenomenological interactions that have been applied to problems in nuclear physics. Each of them has been used for a specific problem and their range of

validity and success varies very much. It lies outside the scope of this book to give a complete picture, and we will restrict our discussion to certain essential properties and the presentation of only the most successful examples. Most of them are only constructed for a special purpose, as, for example, for Hartree–Fock calculations (see Chap. 5), which calculate the nuclear self-consistent field, and bulk properties of nuclei such as binding energies and saturation densities. Others serve as effective forces between valence nucleons or between particles and holes (see Sec. 4.3). Therefore, we must be very careful in comparing these different types of interaction, even if, as we shall see, they look very similar in mathematical structure.

As we discussed in the last section, the effective interactions are used in a certain shell model configuration space: *the model space*. We therefore have to expect a certain dependence of the effective interaction on the space, that is, different interactions have to be taken for different sizes of the model space. As we have seen, the microscopically defined effective interaction is always energy dependent, while most of the time there is no explicit energy dependence in the phenomenological forces. It is usually sufficient to put all these dependences in a varying strength parameter.

It is evident that we prefer to choose the analytical form of the effective interaction to be as simple as possible. For example, it is often assumed that the effective interaction obeys the same *invariance principles* as the bare nucleon–nucleon interaction (see Sec. 4.2). This is certainly not always true. For instance, we should expect the renormalization procedure which describes the transition from the bare nucleon–nucleon interaction to the effective one to depend on the actual density of the system, that is, we get a different force in the interior of the system than in the surface and outer regions. For a shell model calculation in a fixed well, we should therefore not expect a translationally invariant residual interaction.

We know that the *range of the nuclear force* is rather short. We have seen in Section 4.3 that this is true even for the range of the effective G-matrix. The simplest ansatz therefore consists in using a *zero range* force whose radial dependence is described by a δ-function. In fact, such forces turn out to be rather useful because they are simple to handle and they describe many nuclear properties quite well. More realistic forces, however, need to have a finite non-vanishing range (see [AS 71, Sch 72b]). A *finite range* can be simulated by a *momentum dependence*. To show this we transform a function $V(\mathbf{r})$ of the relative distance $\mathbf{r}=\mathbf{r}_1-\mathbf{r}_2$ into momentum space

$$\langle \mathbf{p}|V|\mathbf{p}'\rangle = \frac{1}{(2\pi\hbar)^3}\int e^{-\frac{i}{\hbar}(\mathbf{p}-\mathbf{p}')\mathbf{r}}V(\mathbf{r})d^3r. \tag{4.97}$$

We see that a δ-force is a constant and that any range represents a p-dependence in momentum space. The simplest rotationally invariant one is of the form

$$(2\pi\hbar)^3\langle \mathbf{p}|V|\mathbf{p}'\rangle = V_0 + V_1\mathbf{p}'^2 + V_1\mathbf{p}^2 + V_2\mathbf{p}\mathbf{p}', \tag{4.98}$$

which in coordinate space corresponds to the momentum dependent operator

$$V(\mathbf{r}) = V_0\delta(\mathbf{r}) + V_1\left(\hat{\mathbf{p}}^2\delta(\mathbf{r}) + \delta(\mathbf{r})\hat{\mathbf{p}}^2\right) + V_2\hat{\mathbf{p}}\delta(\mathbf{r})\hat{\mathbf{p}}. \tag{4.99}$$

Effective forces usually depend on the density $\rho(\mathbf{r})$. Such *density dependence* is easy to understand if, for example, we consider expression (4.39) for the G-matrix: The range of the summation depends on the Fermi energy, which is itself a function of the density. It is also quite easy to see that the different projection operators Q entering the definition of the effective interactions [see Eqs. (4.40) and (4.77)] can be expressed as a nonlocal density which is therefore another source of density dependence.

Other simple forms that work surprisingly well are separable two-body forces, that is, forces which can be represented as products (or as a sum of products), in which each factor acts on only one of the two particles.

4.4.2 Simple Central Forces

There exists a large number of forces which use only the central part (4.20), but differ in their radial dependence $V(r)$. Some simple potentials that have been used are, for example, the Yukawa potential (4.33) or

$$V(r) = -V_0 e^{-r^2/r_0^2} \qquad \text{(Gauss potential)}, \tag{4.100}$$

$$V(r) = -V_0 \frac{e^{-r/r_0}}{1-e^{-r/r_0}} \qquad \text{(Hulthen potential)}, \tag{4.101}$$

$$V(r) = -V_0\delta\left(\frac{\mathbf{r}}{r_0}\right) \qquad \text{(contact potential)}. \tag{4.102}$$

The potential depth V_0 and the range r_0 are adjusted to fit experimental data. One finds $V_0 \simeq 50$ MeV and $r_0 \simeq 1-2$ fm (the Compton wavelength of the pion is 1.4 fm).

For the r-dependent coefficients $V(r)$ in Eq. (4.20) the same radial dependence is usually assumed; only their strength and sign are adjusted to fit empirical data. Here we do not wish to discuss which one of the different exchange mixtures is to be preferred; we wish only to give some of the most commonly used values of the coefficients (Table 4.3).

Table 4.3 Coefficients for the exchange mixtures

Mixture	a_{et}	a_{es}	a_{ot}	a_{os}
Wigner	1	1	1	1
Kurath [Ku 56, SW 66]	1	0.6	−0.6	−1
Serber [HS 57]	1	1	0	0
Rosenfeld [EF 57]	1	0.6	−0.34	−1.78
Ferrel–Visscher [VF 57]	1	0.634	−0.366	0
Soper [So 57]	1	0.46	0.14	−0.4
Gillet [GGS 66] I	1	0.6	−0.6	0.6
II	1	0.4	−0.2	0.2

$$V(1,2) = V_0 f\left(\frac{r}{r_0}\right)\left(a_{et}\Pi_e^r\Pi_t^\sigma + a_{es}\Pi_e^r\Pi_s^\sigma + a_{ot}\Pi_o^r\Pi_t^\sigma + a_{os}\Pi_o^r\Pi_s^\sigma\right). \tag{4.103}$$

Other forces of a similar type have been used by Kallio and Koltveit [KK 64] and by Elliott and Clark [CE 65]. The latter authors also include a tensor term and a two-body spin orbit force.

4.4.3 The Skyrme Interaction

In 1956 Skyrme [Sk 56, 59] proposed an effective interaction with a three-body term viz:

$$V = \sum_{i<j} V(i,j) + \sum_{i<j<k} V(i,j,k). \tag{4.104}$$

To simplify the calculations, he used a short-range expansion in the form of Eq. (4.99) for the two-body part:

$$\begin{aligned} V(1,2) = {} & t_0(1+x_0P^\sigma)\delta(\mathbf{r}_1-\mathbf{r}_2) \\ & + \tfrac{1}{2}t_1\left[\delta(\mathbf{r}_1-\mathbf{r}_2)\mathbf{k}^2 + \mathbf{k}^2\delta(\mathbf{r}_1-\mathbf{r}_2)\right] + t_2\mathbf{k}\delta(\mathbf{r}_1-\mathbf{r}_2)\mathbf{k} \\ & + iW_0(\boldsymbol{\sigma}^{(1)}+\boldsymbol{\sigma}^{(2)})\mathbf{k}\times\delta(\mathbf{r}_1-\mathbf{r}_2)\mathbf{k}, \end{aligned} \tag{4.105}$$

where $\mathbf{k} = (1/\hbar)\mathbf{p}$ is the operator of the relative momentum

$$\mathbf{k} = \frac{1}{2i}(\nabla_1 - \nabla_2). \tag{4.106}$$

For the three-body force Skyrme also assumed a zero range force of the form

$$V(1,2,3) = t_3\delta(\mathbf{r}_1-\mathbf{r}_2)\delta(\mathbf{r}_2-\mathbf{r}_3). \tag{4.107}$$

The five constants—t_0, t_1, t_2, t_3, x_0—and W_0 were adjusted to the experimental binding energies and radii. There are several sets of parameters called Skyrme I, II, etc. (see Sec. 5.6) resulting from different fits. We present here Skyrme III [BFG 75]:

$$\begin{aligned} t_0 &= -1128.75 \text{ MeV fm}^3; & t_1 &= 395.0 \text{ MeV fm}^5; \\ t_2 &= -95.0 \text{ MeV fm}^5; & t_3 &= 14000.0 \text{ MeV fm}^6; \\ W_0 &= 120 \text{ MeV fm}^5; & x_0 &= 0.45. \end{aligned} \tag{4.108}$$

The parameter t_0 describes a pure δ-force with a spin-exchange; t_1 and t_2 simulate an effective range, as in Eq. (4.99). The fourth term in Eq. (4.105) represents a two-body spin orbit interaction. It can be obtained [BS 56] from a normal spin orbit term [see Eq. (4.23)] in the short range limit.

In Chapter 5, we shall see that this force has been used extensively in

Hartree–Fock calculations. For spin saturated even–even nuclei, the three-body term (4.104) turns out to be equivalent to a density dependent two-body interaction*:

$$V_\rho(1,2)=\frac{1}{6}t_3(1+P^\sigma)\delta(\mathbf{r}_1-\mathbf{r}_2)\rho(\tfrac{1}{2}(\mathbf{r}_1+\mathbf{r}_2)). \tag{4.109}$$

Such a density dependent term can also be regarded as the phenomenological representation of the ρ-dependence of the microscopic effective interaction. This interpretation is preferrable to the view that the Skyrme force contains a three-body interaction, since we know that three-body interactions are rather weak in nuclei.

There are essentially three reasons why this force has gained so much importance over the last ten years:

(i) Vautherin and Brink [VB 72] (see Chap. 5) were able to reproduce the nuclear binding energies over the whole periodic table with a reasonable set of parameters and, at the same time, the nuclear radii. This had not been possible with the usual non-density dependent forces.

(ii) Negele and Vautherin [NV 72] gave the connection between this force and the more fundamental G-matrix discussed in the last sections.

(iii) The mathematical form of the force is extremely simple. The δ-functions simplify all types of calculations enormously.

There are similar types of interactions originally proposed by Moszkowski [Mo 70], the so-called *modified δ-interactions* (MDI). They differ from the Skyrme interaction by the absence of the t_2-term and the spin orbit force and also by a different ρ-dependence ($\sim\rho^\sigma$ with $\sigma<1$).†

4.4.4 The Gogny Interaction

Despite the great success of the Skyrme interaction, it has been argued that zero range forces might not be able to simulate the long range or even the intermediate range parts of the realistic effective interaction. In particular, the present versions of the Skyrme force are not able to properly describe pairing correlations in nuclei (see Chap. 6), therefore Gogny [Go 75b] replaced the t_0, t_1 and t_2 parts of the Skyrme force by a sum of two

*This is no longer true for systems without spin saturation. In such cases, the three-body term (4.107) in the Skyrme force, which is purely local and repulsive, favors parallel spin alignment, that is, nuclear ferromagnetism. This contradicts the observed spin saturation and the pairing properties in nuclei. This difficulty can be avoided by using either a density dependent two-body interaction [BJS 75] of the form (4.109) or a nonlocality in the three-body term [ON 78].

†There is a strong correlation between the nuclear compressibility and the exponent σ in the density dependence [CS 72].

Gaussians* with spin–isospin exchange mixtures (a force which was originally used by Brink and Booker [BB 67]) and got

$$\begin{aligned}V(1,2)=&\sum_{i=1}^{2}e^{-(\mathbf{r}_1-\mathbf{r}_2)^2/\mu_i^2}(W_i+B_iP^\sigma-H_iP^\tau-M_iP^\sigma P^\tau)\\&+iW_0(\boldsymbol{\sigma}_1+\boldsymbol{\sigma}_2)\mathbf{k}\times\delta(\mathbf{r}_1-\mathbf{r}_2)\mathbf{k}\\&+t_3(1+P^\sigma)\delta(\mathbf{r}_1-\mathbf{r}_2)\rho^{1/3}(\tfrac{1}{2}(\mathbf{r}_1+\mathbf{r}_2)).\end{aligned} \tag{4.110}$$

The parameters were adjusted to the properties of finite nuclei, and for nuclear matter (Table 4.4).

Table 4.4 Force parameters of the Gogny force (D1)

i	μ_i [fm]	W_i	B_i	H_i	M_i [MeV]	$W_0=+115$ [MeV fm^5]
1	0.7	−402.4	−100.	−496.2	−23.56	$t_3=1350$ [MeV fm^4]
2	1.2	−21.30	−11.77	37.27	−68.81	

4.4.5 The Migdal Force

This force was proposed by Migdal [Mi 67] in his theory of finite Fermi systems. Based on the interacting quasi-particle concept of Landau's theory of a Fermi liquid [La 59], Migdal introduces this force to describe the collective excitations in nuclei.†

Starting from the ground state of an even–even system, the quasi-particles are defined as the low-lying excitations in the neighboring odd mass nuclei. The ground state of the even system contains no quasi-particles, and excited states are characterized by the quasi-particle occupation numbers n_λ. A change of these occupation numbers by the amount δn_λ causes a change in the total energy E_0 of the system by the amount

$$\delta E_0=\sum_\lambda\epsilon_\lambda^0\delta n_\lambda+\frac{1}{2}\sum_{\lambda\lambda'}F_{\lambda\lambda'}\delta n_\lambda\delta n_{\lambda'},$$

where ϵ_λ^0 are the energies of a quasi-particle λ in the absence of any other quasiparticle and $F_{\lambda\lambda'}$ is the so-called quasi-particle interaction. Migdal introduces an effective particle–hole interaction F^ω and an effective particle–particle (or hole–hole) interaction F^ξ.

In an infinite system with translational invariance, the quasi-particles are characterized by the momentum $\mathbf{k}$, and Landau could show that the ph-interaction $F(\mathbf{k},\mathbf{k}')$ is given by the second derivative of the total energy

*Similar density dependent effective interactions have been used in [Kr 70, ZR 71, RPS 72, LMV 73, RBP 77].

†It would be beyond the scope of this book to go into the details of this theory. The reader may, however, find some basic ingredients in Section F.7.

E_0 with respect to the quasi-particle densities $n(\mathbf{k})$:

$$F^{ph}(\mathbf{k},\mathbf{k}') = \frac{\delta^2 E_0}{\delta n(\mathbf{k})\delta n(\mathbf{k}')} . \tag{4.111}$$

At the Fermi surface this is an exact relation.

In a finite system the quasi-particle density $\bar{\rho}_{\lambda\lambda'}$ is no longer completely determined by its diagonal elements (the occupation numbers n_λ), but it also contains information about the form of the single-particle wave functions φ_λ. The effective interaction then depends on four indices, and it has been proposed to derive this quantity, in analogy to Eq. (4.111), from the exact ground state energy [Br 71]

$$F^{ph}_{psqr} = \frac{\delta E_0}{\delta \bar{\rho}_{qp}\delta \bar{\rho}_{rs}} . \tag{4.112}$$

So far it has not been shown that this is an exact relation. However, a very similar expression is obtained in a quite different (*approximate*) theory: the time dependent Hartree–Fock theory in the limit of a motion with small amplitudes (see Sec. 8.5). Starting from the assumption that the wave function is a Slater determinant (i.e., $\rho^2=\rho$; see Sec. 5.3.3) and that the total energy can be expressed by a functional $E_0[\rho]$, we obtain in this case the effective *ph*-interaction as the second derivative of $E_0[\rho]$ with respect to ρ [Eq. (8.124)], just as in Eq. (4.112).

It is clear from the above that, for instance, the Skyrme force (Sec. 4.4.3) cannot be compared with the Migdal force directly, even though, as we shall see, it looks very similar. Within the approximation $\rho^2 \simeq \rho$, however, an indirect relation may be established by differentiating the ground state energy calculated with the Skyrme interaction twice with respect to the density.

Like the Skyrme force, the Migdal force is an expansion in momentum space. However, contrary to potentials suitable for Hartree–Fock calculations (such as the Skyrme force), the p^2-terms do not play an essential role, as the Migdal forces do not have to guarantee saturation (they are constructed to describe different physical situations anyway). In most calculations it is therefore sufficient to take into account only the constant in momentum space which gives a pure δ-force in coordinate space. On the other hand, spin and isospin exchange mixtures are now very important. They are different for the particle–particle and particle–hole forces:

$$V(1,2) = V_0\delta(\mathbf{r}_1-\mathbf{r}_2)(f+f'\boldsymbol{\tau}^{(1)}\boldsymbol{\tau}^{(2)}+g\boldsymbol{\sigma}^{(1)}\boldsymbol{\sigma}^{(2)}+g'\boldsymbol{\sigma}^{(1)}\boldsymbol{\sigma}^{(2)}\boldsymbol{\tau}^{(1)}\boldsymbol{\tau}^{(2)}). \tag{4.113}$$

V_0 is a strength parameter which has to be adjusted to the configuration space (e.g., in the ^{208}Pb region $V_0=380$ MeV fm^3). Guman and Birbrair [GB 65] proposed to take into account the different interaction strengths inside and outside the nucleus and the diffuseness of the nuclear surface by a linear density dependence of the constants f, f',

$$f = f^{ex} + (f^{in}-f^{ex})\rho(r), \tag{4.114}$$

where $\rho(r)$ has the form of a Fermi distribution

$$\rho(r) = \frac{1}{1+\exp[(r-R)/a]} . \tag{4.115}$$

The additional parameters R and a represent the radius and the diffuseness, respectively, of the nucleus. Contrary to a Hartree–Fock calculation with a density dependent interaction (see Chap. 5), the density (4.114) is not adjusted self-consistently. Therefore, the Migdal force violates translational invariance. Of course, this is no drawback, since the renormalization procedure is closely connected with the underlying single-particle potential, which also violates translational invariance. In fact, a proper choice of the effective residual interaction should restore this invariance (see Mikeska and Brenig [MB 69]). From this condition one can deduce additional relations among the parameters f, f', g, g' [NW 72, 74].

The Migdal force has been widely used to calculate low-lying collective vibrations in nuclei within the framework of the random phase approximation (see Chap. 8). The effective charges caused by such vibrations (see Chap. 9) provide an enormous amount of experimental data with which to adjust the six parameters f^{in}, f^{ex}, f'^{in}, f'^{ex}, and g, g' for the particle–hole and particle–particle forces (for details, see [RBS 73, BSK 73, BER 75]). For the particle–hole force Ring and Speth [RS 74a] found:

$$\begin{aligned} &f^{in}=0.0685; \quad f'^{in}=0.3315; \quad f^{ex}=-2.165;\\ &f'^{ex}=0.465; \quad g=0.575; \quad g'=0.725. \end{aligned} \tag{4.116}$$

It is important to note that this is an effective *ph*-force which does not have to be antisymmetrized [KMS 76]. It shows strong attraction outside the nucleus and is close to zero inside the nucleus.

4.4.6 The Surface-Delta Interaction (SDI)

Like the Migdal interaction, this force is thought of as an effective residual interaction among the particles near the Fermi surface. The main physical idea is that the nucleons move almost independently in the nuclear interior. In fact, the residual interaction of Migdal is rather weak inside the nucleus. Most of the collisions occur at the nuclear surface where the Pauli principle loses its importance and the nucleons feel the strong attractive interaction [GM 65]. The behavior of the force outside the surface is again not very important because there the wave functions have exponentially decaying tails, that is, the probability of finding a nucleon there goes rapidly to zero. Therefore, it is a meaningful approximation to restrict the whole interaction to the nuclear surface and to define the so-called surface delta interaction:

$$V(1,2) = -V_0\delta(\mathbf{r}_1-\mathbf{r}_2)\delta(|\mathbf{r}_1|-R_0). \tag{4.117}$$

V_0 can still depend on the spin and isospin coordinates in the usual way

(4.20). This force has very simple geometrical properties. Using the expansion of the δ-function in Legendre polynomials—

$$\delta(\mathbf{r}_1-\mathbf{r}_2)=\frac{\delta(r_1-r_2)}{r_1 r_2}\sum_l \frac{2l+1}{4\pi}P_l(\cos\theta_{12}), \tag{4.118}$$

where θ_{12} is the angle between the vectors $\mathbf{r}_1$ and $\mathbf{r}_2$—and the addition theorem of the spherical harmonics [Ed 57, Eq. 4.6.6], we get:

$$V(1,2)=-V_0\sum_{lm}\frac{\delta(r_1-R_0)}{r_1}Y^*_{lm}(\theta_1\varphi_1)\frac{\delta(r_2-R_0)}{r_2}Y_{lm}(\theta_2\varphi_2). \tag{4.119}$$

This is an infinite sum over separable terms. In a spherical basis, the matrix elements coupled to a good angular momentum become extremely simple because only one term of the sum in (4.119) survives. This model force has been applied [KS 63, PAM 66, FP 67, Fä 68, VPK 69] in many calculations. It has been used—like the Migdal force—as an effective force among the valence particles. It is, however, not meaningful to extend the underlying configuration space over more than two major shells, because in that case we have levels with the same angular momentum quantum numbers. Since the radial integrals are approximated by the value of the wave function at $r=R_0$, there is no cancellation for wave functions with different numbers of radial nodes. Consequently, the particles in such levels feel an unphysical strong interaction.

4.4.7 Separable Forces and Multipole Expansions

In the last section we saw that the surface-delta interaction is extremely simple to handle because of its separability in a shell model basis.

We call a force *separable in particle hole direction* if it can be written in second quantization in the form [: : means normal ordering in the sense of Eq. (C.50)]

$$V=:Q^+\cdot Q:, \tag{4.120}$$

where

$$Q=\sum_{k_1k_2}q_{k_1k_2}a^+_{k_1}a_{k_2} \tag{4.121}$$

is a one-particle operator. Acting on a Slater determinant, it creates a superposition of *ph*-pairs. A force is called *separable in pp-direction* if it has the form

$$V=P^+\cdot P, \tag{4.122}$$

where

$$P^+=\frac{1}{2}\sum_{k_1k_2}p_{k_1k_2}a^+_{k_1}a^+_{k_2} \tag{4.123}$$

is a pair creation operator. Acting on a Slater determinant, it creates a

superposition of *pp*-pairs. It seems very unlikely that a realistic force can be represented by so simple an ansatz as Eqs. (4.120) and (4.122), however, it has been shown that the matrix elements of these schematic forces with a suitably chosen strength are of the same magnitude as those calculated from a microscopic G-matrix with polarization terms (see Sec. 4.3 and F.5) [BK 67b].

We wish here to study the question of *separability* somewhat further and investigate a general *phenomenological effective force* without spin and isospin dependence. The force shall depend only on the relative distance between the nucleons, therefore we can expand in the following way [La 64].

$$V(|\mathbf{r}_1-\mathbf{r}_2|)=\sum_l V_l(r_1,r_2)\sum_m Y^*_{lm}(\theta_1\varphi_1)Y_{lm}(\theta_2\varphi_2), \tag{4.124}$$

with

$$V_l(r_1,r_2)=2\pi\int_{-1}^{1}V(|\mathbf{r}_1-\mathbf{r}_2|)P_l(\cos\theta_{12})\,d\cos\theta_{12}. \tag{4.125}$$

For a δ-force, $V=-V_0\delta(\mathbf{r})$, we find that V_l does not depend on l:

$$V_l(r_1,r_2)=-V_0\frac{\delta(r_1-r_2)}{r_1r_2}. \tag{4.126}$$

In Eq. (4.124) we have written a general force as an infinite sum of terms, each of which are separable in the angular coordinates. As we see from the δ-force, we cannot expect this expansion to converge rapidly for a short range force. In fact, we obtain an estimate for the effective range of each component in the expansion (4.124) if we restrict ourselves to a small region in space where $r_1\simeq r_2\simeq r$. The function $P_l(\cos\theta_{12})$ has its major contributions only in the region $0\leqslant\theta_{12}\lesssim 1/l$ (Fig. 4.9), that is, V_l (4.125) is small, if the range of the potential $V(r_{12})$ is large compared to r/l, that is,

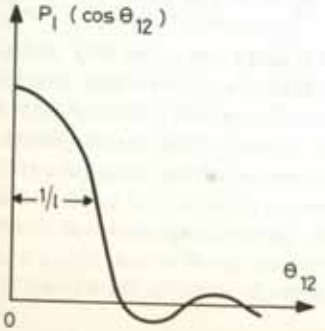

Figure 4.9. Legendre polynomial of degree l as a function of the angle θ_{12} between $\mathbf{r}_1$ and $\mathbf{r}_2$.

the larger the strength of the high l-components V_l, the shorter the range of the force. In a force with zero range (δ-force), all l-components have the same relative weight.

We now come back to the question of separability. The general force (4.124) and the δ-force (4.126) are not separable because of the radial dependence in $V_l(r_1, r_2)$. On the other hand, if one assumes that the interaction is surface peaked as the SDI-interaction (4.117), it then becomes a sum of separable terms because of the additional factor $\delta(r - R_0)$.

$$V_l^{\mathrm{SDI}}(r_1 r_2) = \frac{-V_0}{r_1}\delta(r_1 - R_0)\frac{1}{r_2}\delta(r_2 - R_0). \tag{4.127}$$

A more general separable ansatz of this kind is

$$V_l(r_1 r_2) = f_l(r_1)\cdot f_l(r_2). \tag{4.128}$$

One often chooses $f_l \sim r^l$ and obtains the multipole–multipole forces

$$V = -\frac{1}{2}\sum_{lm}\chi_l : Q_{lm}^{+} Q_{lm} : = -\frac{1}{2}\sum_{l}\chi_l : Q_l^{+}\cdot Q_l :, \tag{4.129}$$

where χ_l are constants and Q_{lm} is the multipole operator

$$Q_{lm} = \sum_{k_1 k_2}\langle k_1 | r^l Y_{lm}(\theta, \varphi) | k_2\rangle a_{k_1}^{+} a_{k_2}. \tag{4.130}$$

If we take into account only the components with small l-values, we obtain long range forces. The most well known is the quadruple–quadruple force [El 58, KS 63]. We shall see in Chapter 7 that it can be used to describe the quadrupole deformations of nuclei self-consistently.

Again we must emphasize that these multipole forces are only to be considered as an effective force between valence particles within a restricted configuration space. If there are many such valence particles we can apply a Hartree–Fock approximation for them* (see Chap. 5). However, such HF-calculations with multipole forces for valence nucleons should not be mixed up with the basic HF-calculations for the binding energies.

The expansion (4.124) turns out to be very useful for the *long range part* of the effective interaction, because in this case the functions V_l become small for higher l-values. To obtain a similar description of the *short range part* one uses a different kind of expansion. We shall restrict outselves to interactions between nucleons of the same type (for the treatment of short range correlations between protons and neutrons, see Sec. 7.5).

We now consider the general expression (4.3) of a not necessarily local force $V(\mathbf{r}_1, \mathbf{r}_2, \mathbf{r}_1', \mathbf{r}_2')$. In the case of a local force, we have $\mathbf{r}_1 = \mathbf{r}_1'$ and $\mathbf{r}_2 = \mathbf{r}_2'$, and the expansion (4.124) is made in the variables $\mathbf{r}_1, \mathbf{r}_2$. Now we require

*In such calculations, the exchange term (5.43) to the HF potential is usually neglected because it is small [BK 68, Ma 74].

instead $\mathbf{r}_1 = \mathbf{r}_2$ and $\mathbf{r}_1' = \mathbf{r}_2'$. We expand in $\mathbf{r}_1, \mathbf{r}_1'$ and obtain expressions similar to (4.124) and (4.125).

$$\begin{aligned}&\delta(\mathbf{r}_1 - \mathbf{r}_2)\delta(\mathbf{r}_1' - \mathbf{r}_2')V(\mathbf{r}_1, \mathbf{r}_1')\\ &\quad = \delta(\mathbf{r}_1 - \mathbf{r}_2)\delta(\mathbf{r}_1' - \mathbf{r}_2')\sum_{lm} V_l(r_1, r_1')\, Y_{lm}(\theta_1 \varphi_1) Y_{lm}^{*}(\theta_1' \varphi_1').\end{aligned} \tag{4.131}$$

The requirements $\mathbf{r}_1 = \mathbf{r}_2$ and $\mathbf{r}_1' = \mathbf{r}_2'$ already restrict us to a short range because it is only true if the two nucleons are at the same place. (This does not necessarily mean a δ-force, because we are allowing for nonlocal forces). At a first glance, the expansion (4.131) seems to be as poor as Eq. (4.124) for a short range force. However, we have to calculate matrix elements between two-particle wave functions. As we shall demonstrate in a moment, the lth term in (4.131) gives a contribution only to the matrix element when the two particles are coupled to spin $I = l$. For two particles in a single j-shell, for instance, we find that their wave functions have maximal spatial overlap for $I = 0$. In this case, the angular part of their wave function takes the form:

$$\langle \Omega_1 \Omega_2 \,|\, jjI = 0, M = 0\rangle \propto \sum_{m=-l}^{l} (-)^m Y_{lm}(\Omega_1) Y_{l-m}(\Omega_2) \propto P_l(\cos\theta_{12}). \tag{4.132}$$

(Because of the short range force, we assume only the spin singlet to be important.) Therefore, we find maximal interaction for $I = 0$, where the angular momenta $\mathbf{j}_1$ and $\mathbf{j}_2$ are antiparallel, and we can thus understand that the expansion (4.131) is meaningful for short range interactions.

Again, if we replace the non-separable radial term in (4.131) by a separable ansatz as in (4.129), we obtain

$$V_l(r_1, r_1') = -G_l r_1^l \cdot r_1'^l, \tag{4.133}$$

$$V = -\sum_{lm} G_l P_{lm}^{+} P_{lm} = -\sum G_l P_l^{+}\cdot P_l, \tag{4.134}$$

with

$$P_{lm}^{+} = \tfrac{1}{2}\sum_{k_1 k_2}\langle k_1 | r^l Y_{lm} | k_2\rangle a_{k_1}^{+} a_{\bar{k}_2}^{+}, \tag{4.135}$$

where $|\bar{k}\rangle$ is the time-reversed state to $|k\rangle$. In deriving Eq. (4.134) from (4.131) we must take care in handling the spin coordinate s, because the operator (4.133) is not separable in spin space a priori. Because of the δ-force character, however, we always have $s_1 = -s_2$, $s_1' = -s_2'$, which makes it possible to derive (4.134).

We are now able to calculate the matrix elements of a δ-force in a single j-shell, where the single-particle wave functions are given by $\langle \mathbf{r} | nljm\rangle = R_{nl}(r)\langle \Omega | ljm\rangle$. We construct pair operators A_{IM}^{+} with angular momentum I, M:

$$A_{IM}^{+} = \frac{1}{\sqrt{2}}\sum_{m_1 m_2} C_{m_1 m_2 M}^{j\, j\, I} a_{jm_1}^{+} a_{jm_2}^{+} \tag{4.136}$$

and use Eqs. (4.124) and (4.126) to obtain

$$V_\delta = -\sum_{I=0,2,\ldots} V_\delta(I) \sum_M A^+_{IM} A_{IM},$$

with*

$$V_\delta(I) = V_0 \cdot R_4 \frac{1}{2} \frac{1}{2I+1} |\langle j \| Y_I \| j \rangle|^2 = \frac{V_0}{8\pi} R_4 \frac{(2j+1)^2}{2I+1} |C^{I}_{1/2\ -1/2\ 0}|^2. \tag{4.137}$$

where R_4 is the radial integral

$$R_4 = \int_0^\infty dr\, r^2 R^4_{nl}(r).$$

From (4.137) we see that only the Ith term in the expansion (4.131) goes into the matrix element coupled to spin $I = I$. In the case of a δ-force, $V_\delta(I)$ is maximal for $I = 0$ and drops off rapidly with increasing I (Table 4.5).* The most important part of the force (4.134) is therefore the $I = I = 0$ part.

Table 4.5 The relative magnitude of the matrix elements $V_\delta(I)$ (4.137) in a single j-shell

$V_\delta(I)/V_\delta(0)$	$I=0$	2	4	6	8	10	12
$j=7/2$	1	0.238	0.117	0.058	—	—	—
9/2	1	0.242	0.126	0.075	0.040	—	—
11/2	1	0.245	0.131	0.082	0.053	0.025	—
13/2	1	0.246	0.133	0.087	0.060	0.038	0.019

To avoid complicated formulas, one usually introduces a slight modification of the Condon–Shortley phases (see [Ed 57]), the so-called BCS phases, and defines for $m > 0$:

$$|nljm\rangle_{\mathrm{BCS}} = |nljm\rangle_{\mathrm{CS}},$$
$$|nlj-m\rangle_{\mathrm{BCS}} = (-)^{l+j-m} |nlj-m\rangle_{\mathrm{CS}}. \tag{4.138}$$

The time reversal operator T [Eq. (2.45)] has a very simple form in this case. For $m > 0$, we find

$$|\overline{nljm}\rangle = T|nljm\rangle = |nlj-m\rangle; \qquad T|nlj-m\rangle = -|nljm\rangle. \tag{4.139}$$

The $I = 0$ part of Eq. (4.134), the so-called *pure pairing force*, has the form

$$V^P = -G \frac{1}{4} \sum_{\substack{kk' \\ \gtrless 0}} a^+_k a^+_{\bar{k}} a_{\bar{k}'} a_{k'}, \tag{4.140}$$

where $\bar{k}$ is again the time reversed state to k and the sum runs over all

* In the limit of large I- and j-values we find, by a semiclassical expansion [MJB 75],

$$|C^{I}_{1/2\ -1/2\ 0}|^2 \simeq \frac{2}{\pi \cdot j} \sqrt{1-\left(\frac{I}{2j}\right)^2}.$$

values of k, k'. This force has been widely used to describe short range correlations in nuclei within the BCS-formalism (see Chap. 6). It is again important to notice that it should only be applied in a restricted configuration space. The value of the force constant is connected with the size of this space. It is easy to generalize this simple model force and to take into account higher I-values in the expansion (4.131). They are called *multipole pairing forces*. They are separable in particle–particle direction and play an important role in the description of pairing vibrations (see Chap. 8 and [BB 71, BBN 74b]).

A very simple model force for heavy nuclei has been obtained by combining a quadrupole–quadrupole force and a pure pairing force to the pairing-plus-quadrupole force [KS 63, BK 68]:

$$V^{QP} = -\tfrac{1}{2}\chi : Q^+_2 \cdot Q_2 : -GP^+_0 \cdot P_0, \tag{4.141}$$

which takes into account the most important long-range correlations and the most important short-range correlations, and is very easy to handle (see Sec. 7.4). It contains basically three constants: χ and two different constants G_p and G_n for protons and neutrons. It should only be applied in a configuration not larger than one major shell. For actual values of χ and G, see [KS 60] or [BK 68].

4.4.8 Experimentally Determined Effective Interactions

Since the derivation of the effective interaction from a bare nucleon–nucleon force is rather complicated, some authors have tried to determine the matrix elements of the nucleon–nucleon force in a certain basis directly from the experimental data (for a review, see [ST 76] and [BPO 76]).

Elliott et al. [EJM 68] used the experimental phase shifts of nucleon–nucleon scattering to derive the matrix elements of an effective interaction directly in an oscillator basis (*Sussex force*). In this way, the problem of the hard core is avoided completely.

Less ambitious are attempts to derive special matrix elements from the spectra of "simple" nuclei. These are nuclei in which one has good reason to believe that their structure is determined only by a few matrix elements whose number does not exceed the number of the observed levels [Ta 62]. We may take, for example, the $1f7/2$ shell nuclei, where the $f7/2$ shell is well separated in the simple particle spectrum. One assumes in this case that there exist many pure $f7/2$ configurations in nuclei close to the double magic core ^{40}Ca with $N > 20$ and $Z > 20$. These levels are completely determined by the eight matrix elements $\langle (f7/2)^2 IT | V | (f7/2)^2 IT \rangle$ for $I = 0, 1, \ldots, 7$ ($T = 1$ for I even, $T = 0$ for I odd).

McCullen et al. [MBZ 64] have determined these matrix elements from the spectrum of the nucleus ^{42}Sc. It contains one neutron and one proton outside the ^{40}Ca core. Coupling to angular momentum I gives the interaction energy

$$V(I) = \langle j_1 j_2 I | V | j_1 j_2 I \rangle$$
$$= B(I, {}^{42}\mathrm{Sc}) - B(I, {}^{41}\mathrm{Sc}) - B(I, {}^{41}\mathrm{Ca}) + B(I, {}^{40}\mathrm{Ca}), \tag{4.142}$$

where B are the experimental binding energies of the level with spin I in ^{42}Sc and of the ground state of the other nuclei. Using these matrix elements, many energy levels and electromagnetic properties of the other $f7/2$ nuclei with more valence nucleons can be reproduced quite well. However, levels with a more complicated structure (e.g., holes in the ^{40}Ca core) are also encountered and it is not known how much they mix with the pure $f7/2$ configurations.

Schiffer [Sch 71b, 72b] and Molinari et al. [MJB 75] have made a more general investigation of many such simple nuclei with pure configurations where one nucleon is in a shell j_1 and the other in a shell j_2. The coupling of angular momentum yields multiplets with $|j_1-j_2| \leq I \leq j_1+j_2$. The interaction produces a splitting of the multiplets. It is convenient to plot not $V(I)$ (Eq. 4.137) versus I but rather the dimensionless ratio $V(I)/\bar{V}$ as a function of the "overlap angle" θ_{12} where $\bar{V}$ is the average two-body interaction energy

$$\bar{V} = \sum_I (2I+1)V(I) / \sum_I (2I+1). \tag{4.143}$$

This angle is the angle between the classical orbits of the two valence nucleons

$$\cos\theta_{12} = \frac{\mathbf{j}_1 \cdot \mathbf{j}_2}{|j_1|\,|j_2|} = \frac{I(I+1)-j_1(j_1+1)-j_2(j_2+1)}{2[j_1(j_1+1)]^{1/2}\cdot[j_2(j_2+1)]^{1/2}} \tag{4.144}$$

and it measures the spacial overlap of the two wave functions. In this plot (Fig. 4.10), the points for many different nuclei lie nearly on the same curves. As an example we show the plots for nuclei where the two valence nucleons are in the same orbit (Fig. 4.10) and compare them with the corresponding values for a pure δ-force. For identical particles ($T=1$) we again find that the absolute interaction

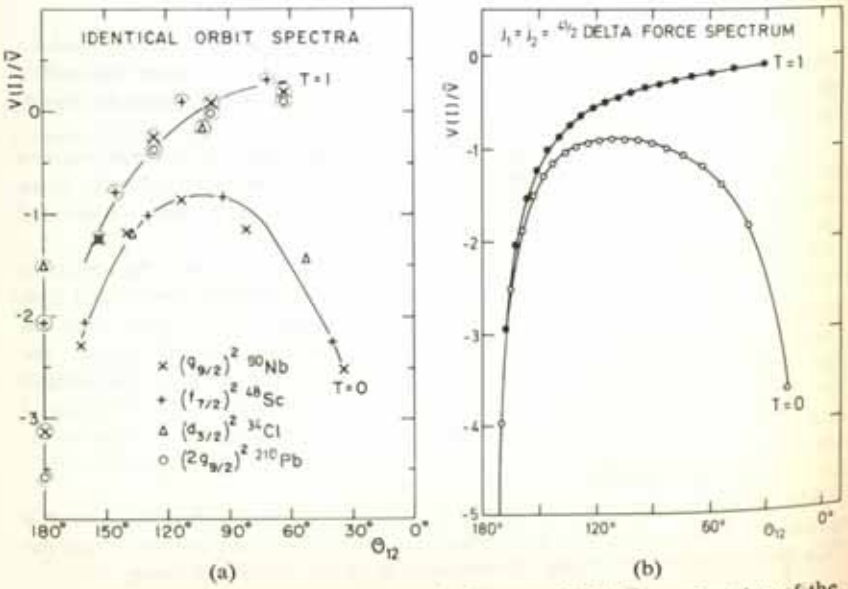

Figure 4.10. The relative interaction matrix elements $V(I)/\bar{V}$ as a function of the overlap angle θ_{12}. Experimental values for (a) four nuclei, (b) a pure δ-force spectrum and $j=41/2$. (From [AS 71].)

matrix elements are strongest for $\theta_{12}=180°$, that is, for antiparallel spins ($I=0$) and they drop off rapidly. For nonidentical particles in the case $T=0$ they also raise for $\theta_{12}=0$, that is, for parallel spins. For identical particles this configuration is prevented by the Pauli principle. This expresses the fact that a short-range force requires a large spacial overlap of the wave functions and it seems that an effective interaction of the δ-type can reproduce qualitatively the "experimentally" determined matrix elements. However, a quantitative comparison [Sch 72b, GSZ 74, AEE 78] shows that a long-range part is also needed to reproduce properties of odd–odd nuclei. The origin of this long-range part is as yet not completely understood. For a discussion of this point see [Mo 76c].

4.5 Concluding Remarks

In the second section of this chapter we discussed the bare forces acting between nucleons. We first restricted their analytical form, observing that they have to obey a certain number of invariance principles. It is well known that the long-range part of the nucleon–nucleon interaction is given by the one-pion exchange; at shorter distances, exchanges of two pions and heavier mesons become important. We have not presented recent results of such investigations because the bare nucleon–nucleon forces within nuclear physics represent a discipline all its own involving intermediate and high energy physics [BJ 76a]. We have discussed some of the more conventional phenomenological ansätze (which usually involve between 40 and 50 fit parameters), but which achieve perfect reproduction of the nucleon–nucleon scattering data. However, this fit gives us information only about the on-shell behavior of the nuclear force, the off-shell part which enters into many-nucleon systems remaining indeterminate (see, for instance, [SS 76]). Three-body calculations show, however, that the currently used two-body interactions like the Hamada–Johnston potential or the Reid soft core potential in their off-shell behavior should not be very different from one another. We thus have phenomenological bare nucleon–nucleon potentials which are, in fact, quite reliable.

These potentials have, however, the inconvenient feature of being very repulsive at short distances and they can thus not be directly applied in nuclear structure calculations. Many-body theory teaches us to use effective forces instead of bare ones, the former being already an infinite sum of the latter. This procedure not only sums up higher order many-body effects in a consistent manner, but at the same time gets rid of the hard core problem, since it turns out that the effective forces are well-behaved. We shall see in the next chapter that the application of the concept of effective forces is quite successful for the calculation of ground state properties of nuclei, although the most advanced purely microscopic calculations in this field (consistently taking three-body correlations into account [KLZ 78]) are still not able to get quantitative agreement with experimental binding energies. In all other calculations, some phenomenol-

ogy enters at a certain step. Nevertheless, we can say that for the ground state properties the theory gives very good results.

Far less satisfying is the situation for the case of effective forces between valence nucleons. For example, shell model calculations within a two-particle model space and with a phenomenological two-body force are able to reproduce the low-lying spectrum of, for example, ^{18}O very well, and we may suppose that this success can be microscopically justified by calculating the effective force between the two valence nucleons. Unfortunately, these attempts have met with only partial success and show that at a certain stage in the perturbative expansion of the interaction, good agreement with experiment is achieved; but going further with the expansion worsens the results again. Until now, the reasons for this agreement at an intermediate step have not been explained.

After these numerically very involved theories of effective interactions with their moderate success, in Section 4.4 we passed to the treatment of the phenomenological effective forces. There the situation is quite satisfying. A number of phenomenological ansätze exist which have been very successful in explaining much more nuclear data than there are fit parameters. One of these forces is the Skyrme force, whose success for the ground state properties of nuclei will be discussed in more detail in the next chaper. For nuclear structure calculations we have to mention the very simple but highly successful pairing-plus-quadrupole force. In the lead region the quasi-particle concept seems to work well, as shown by the quite impressive success of calculations using the Migdal force. But other very simple forces, like the surface-delta force, also do surprisingly well. In view of their successes, it appears to be a difficult but challenging task to give an explanation from a microscopic point of view.

CHAPTER 5

The Hartree–Fock Method

5.1 Introduction

The success of the phenomenologically introduced shell model justifies the assumption that nucleons move independently in an average potential produced by all of the nucleons. The question now is how to extract such a single-particle potential out of the sum of two-body interactions

$$V(1\ldots A)=\sum_{i<j=1}^{A} V(i,j)\simeq\sum_{i=1}^{A} V(i), \tag{5.1}$$

and how well this single-particle potential will agree with those used up to now, for example, the harmonic oscillator, the square well, or the Woods–Saxon potential. It will be shown that we can derive a single-particle potential from the two-body interaction by a variational principle using Slater determinants as trial wave functions.

In Section 5.2 we will discuss in general the variational method, which will be important in many of the following chapters. In Section 5.3, we describe the Hartree–Fock method in detail and in Section 5.4 we give an application to a very simple model. In Section 5.5 we treat symmetries in connection with the Hartree–Fock method, and in Section 5.6 we present the Hartree–Fock theory with density dependent forces.

5.2 The General Variational Principle

We first want to show that the exact Schrödinger equation

$$H|\Psi\rangle = E|\Psi\rangle \tag{5.2}$$

is equivalent to the variational equation

$$\delta E[\Psi] = 0, \tag{5.3}$$

with

$$E[\Psi] = \frac{\langle\Psi|H|\Psi\rangle}{\langle\Psi|\Psi\rangle}. \tag{5.4}$$

The variation (5.3) can be obtained from (5.4):

$$\langle\delta\Psi|H-E|\Psi\rangle + \langle\Psi|H-E|\delta\Psi\rangle = 0. \tag{5.5}$$

Since $|\Psi\rangle$ is, in general, a complex function, we can carry out the variation over the real and imaginary part independently, which is equivalent to carrying out the variation over $|\delta\Psi\rangle$ and $\langle\delta\Psi|$ independently. To see this we use the fact that Eq. (5.5) is valid for arbitrary infinitesimal $|\delta\Psi\rangle$. We can replace $|\delta\Psi\rangle$ by $i|\delta\Psi\rangle$ and get

$$-i\langle\delta\Psi|H-E|\Psi\rangle + i\langle\Psi|H-E|\delta\Psi\rangle. \tag{5.6}$$

Together with Eq. (5.5), we find

$$\langle\delta\Psi|H-E|\Psi\rangle = 0 \tag{5.7}$$

and the complex conjugate equation. Since $|\delta\Psi\rangle$ is arbitrary, Eq. (5.7) is equivalent to the eigenvalue problem (5.2).

The approximation of such variational methods consists of the fact that $|\Psi\rangle$ is usually restricted to a set of mathematically simple trial wave functions. As soon as the true function is not in this set, the minimal solution is no longer the exact eigenfunction, but only an approximation. The variational method is especially well suited for determining the ground state, since for any trial wave function $|\Psi\rangle$ we can show that

$$E[\Psi] > E_0, \tag{5.8}$$

and thus E_0 will always be the lower bound of a variational calculation. To prove this, we develop the trial wave function in terms of the exact eigenfunctions of the Hamiltonian:

$$|\Psi\rangle = \sum_{n=0}^{\infty} a_n|\Psi_n\rangle \tag{5.9}$$

with

$$H|\Psi_n\rangle = E_n|\Psi_n\rangle. \tag{5.10}$$

This yields

$$E[\Psi] = \frac{\sum_{nn'} a_n^* a_n E_n \delta_{nn'}}{\sum_n |a_n|^2} > \frac{\sum_n |a_n|^2 E_0}{\sum_n |a_n|^2} = E_0, \tag{5.11}$$

which is precisely Eq. (5.8). In cases where the ground state energy is not degenerate, the equality sign in (5.11) is valid, if and only if all the coefficients a_n with $n \neq 0$ vanish, that is, $|\Psi\rangle$ is proportional to $|\Psi_0\rangle$. If we are interested in the first excited state, we then have to carry out the variation within the subspace entirely orthogonal to $|\Psi_0\rangle$, that is, over all the wave functions $|\Psi\rangle$ with $a_0 = 0$. Within this subspace $|\Psi_1\rangle$ has the minimal expectation value of H. To find $|\Psi_1\rangle$, we must carry out the variation with the subsidiary condition $\langle\Psi_1|\Psi_0\rangle = 0$. In principle we can continue and calculate the whole spectrum using this method.

In practice, however, we do not know $|\Psi_0\rangle$ exactly. From a variation in a restricted subset of the Hilbert space, we find only an approximation $|\Phi_0\rangle$. For the calculation of an approximation $|\Phi_1\rangle$ to the first excited state $|\Psi_1\rangle$, we have to solve the variational equation (5.3) with the supplementary condition that $|\Phi_1\rangle$ is orthogonal to $|\Phi_0\rangle$:

$$\langle\Phi_1|\Phi_0\rangle = 0. \tag{5.12}$$

For the second excited state, we must have two supplementary conditions, namely:

$$\langle\Phi_2|\Phi_1\rangle = 0; \quad \text{and} \quad \langle\Phi_2|\Phi_0\rangle = 0. \tag{5.13}$$

These supplementary conditions are coupled to the problem via Lagrange parameters. We thus see that for higher excited states this method quickly gets rather complicated, therefore it has been applied mainly for the calculation of the ground state. Sometimes, however, these conditions are simply fulfilled because of symmetry properties, as, for example, is the case for states with different angular momentum quantum numbers. We will see in Chapter 7 how to calculate a whole rotational band where the determination of each level is no more complicated than that of the ground state.

So far we have shown that for a certain trial wave function, the ground state energy is always larger than or equal to the exact ground state energy and corresponds to an extremum. In actual calculations, we have to make sure that this extremum actually corresponds to a *minimum*, that is, we must calculate the second derivative of the energy functional, for example, with respect to certain parameters. In the case of the Hartree–Fock or Hartree–Fock–Bogoliubov theory, we will come back to this point (in Chapter 7).

In order to decide which of two variational approaches (i.e., two sets of trial wave functions) is the better one, we have two criteria:

(i) If one set of the trial wave functions is a subset of the other, the larger set is usually the better one, because it contains the first's set minimum.

(ii) Since the exact E_0 is a lower bound, we may hope that out of two trial wave functions, the one for which the corresponding energy is closest to E_0 is better.

Both criteria are, however, not exact statements. Pathological examples can be found which contradict them.

We finish this section with the remark that the variation principle is only valid in this form for a linear eigenvalue problem of the type (5.2). In cases where the Hamiltonian itself depends on the wave function we want to determine, we have to be very careful in applying this principle.

5.3 The Derivation of the Hartree–Fock Equation

5.3.1 The Choice of the Set of Trial Wave Functions

Using the fact that the shell model has provided a suitable approximation for the qualitative explanation of many nuclear properties, we shall assume that there is an average single-particle potential (later to be called the *Hartree–Fock potential*)

$$H^{\mathrm{HF}} = \sum_{i=1}^{A} h(i) \tag{5.14}$$

whose eigenfunction having the lowest eigenvalue E_0^{HF} is an approximation to the exact ground state function. This eigenfunction $\Phi(1 \ldots A)$ is, as we have seen in Chapter 2, a *Slater determinant*

$$|\mathrm{HF}\rangle = |\Phi(1 \ldots A)\rangle = \prod_{i=1}^{A} a_i^+ |-\rangle \tag{5.15}$$

in which the Fermion operators a_k^+, a_k correspond to the single-particle wave functions φ_k, which are themselves eigenfunctions of the single-particle Hamiltonian h, viz:

$$h(i)\varphi_k(i) = \epsilon_k \varphi_k(i), \qquad i = \{\mathbf{r}_i, s_i, t_i\}. \tag{5.16}$$

As we have seen in Section 2.5, we obtain the lowest eigenvalue of H^{HF} if one occupies the A lowest levels in the state $|\mathrm{HF}\rangle$ (Eq. 5.15). In the following, we will characterize the occupied levels in $|\mathrm{HF}\rangle$ by the letters i, j (hole states) and the empty levels by m, n (particle states). If we do not distinguish, we use the letters k, l, p, q.

The wave functions $\varphi_k(\mathbf{r}, s, t)$ are a coordinate space representation of the eigenstates $|k\rangle$ of the single-particle Hamiltonian h. Very often, we work in a configuration space based on some arbitrary complete and orthogonal set of single-particle wave functions $\{\chi_l\}$ (an example is the set of spherical harmonic oscillator wave functions). The function φ_k can be

expanded on this basis:

$$\varphi_k = \sum_l D_{lk} \chi_l. \tag{5.17}$$

If, for each wave function χ_l, we define corresponding fermion creation and annihilation operators c_l^+, c_l (see Section C.1), we can similarly express the operators a_k^+ by the operators c_l^+:

$$a_k^+ = \sum_l D_{lk} c_l^+. \tag{5.18}$$

Since both sets $\{\varphi_k\}$ and $\{\chi_l\}$ are complete and orthogonal, the transformation D has to be unitary:

$$D^+ D = D D^+ = 1. \tag{5.19}$$

This fact also guarantees that the operators (a_k^+, a_k) and (c_l^+, c_l) both obey separate Fermi commutation relations.

As discussed in Section D.2, there is no one-to-one correspondence between a Slater determinant Φ of the form (5.15) and the set of single-particle states φ_k. Any unitary transformation which does not mix particle and hole states leaves Φ unchanged (at least up to an unimportant phase).

It is therefore more convenient to represent a Slater determinant $|\Phi\rangle$ by its single-particle density matrix (D.9):

$$\rho_{ll'} = \langle \Phi | c_{l'}^+ c_l | \Phi \rangle. \tag{5.20}$$

From Eqs. (5.18) and (5.19), we get

$$\rho_{ll'} = \sum_{kk'} D_{lk} D_{l'k'}^* \langle \Phi | a_{k'}^+ a_k | \Phi \rangle = \sum_{i=1}^{A} D_{li} D_{l'i}^* \tag{5.21}$$

because ρ is diagonal in the basis a_k^+, a_k with the eigenvalues (occupation numbers) 1 for $i \leqslant A$ (holes) and 0 for $i > A$ (particles). The trace of ρ is equal to the particle number.

As we show in Appendix D.2, there is a one-to-one correspondence between the Slater determinant Φ and its single-particle density ρ. Single-particle densities ρ of Slater determinants are characterized by the fact that they have only eigenvalues 0 or 1, that is,

$$\rho^2 = \rho. \tag{5.22}$$

ρ is therefore a projector in the space of single-particle wave functions onto the subspace spanned by the hole states φ_i.

In the same way, we can define a projector σ

$$\sigma = 1 - \rho \tag{5.23}$$

onto the subspace spanned by the particle states φ_m.

The *Hartree–Fock method* [Ha 28, Fo 30] is now defined in the following way. We use the set of Slater determinants $\{\Phi\}$ of the form (5.15) consisting of A arbitrary but orthogonal single-particle wave functions φ_i as trial wave functions and minimize the energy within this set. An equivalent statement would be that we use the set of all wave functions

$\{\Phi\}$ whose single particle density (5.20) has the property $\rho^2=\rho$ and $\mathrm{Tr}\,\rho=A$.

As we will see in the following sections, this variation will give us the possibility of determining the single-particle operator H^{HF}.

5.3.2 The Hartree–Fock Energy

Before we are able to carry out the variation which allows us to determine the HF-wave function Φ, we have to calculate the HF-energy

$$E^{\mathrm{HF}}=\langle\Phi|H|\Phi\rangle. \tag{5.24}$$

We start with the many-body Hamiltonian H and represent it in second quantization by the basis operators c_l^+, c_l (see Section C.1):

$$H=\sum_{l_1l_2} t_{l_1l_2}c_{l_1}^+c_{l_2}+\frac{1}{4}\sum_{l_1l_2l_3l_4}\bar{v}_{l_1l_2,\,l_3l_4}c_{l_1}^+c_{l_2}^+c_{l_4}c_{l_3}, \tag{5.25}$$

where

$$\bar{v}_{l_1l_2,\,l_3l_4}=v_{l_1l_2l_3l_4}-v_{l_1l_2l_4l_3}. \tag{5.26}$$

Wick's theorem (Sec. C.4) allows us to calculate the energy (5.24) as a functional of the single-particle density

$$E^{\mathrm{HF}}[\rho]=\sum_{l_1l_2}t_{l_1l_2}\langle\Phi|c_{l_1}^+c_{l_2}|\Phi\rangle+\frac{1}{4}\sum_{l_1l_2l_3l_4}\bar{v}_{l_1l_2l_3l_4}\langle\Phi|c_{l_1}^+c_{l_2}^+c_{l_4}c_{l_3}|\Phi\rangle$$

$$=\sum_{l_1l_2}t_{l_1l_2}\rho_{l_2l_1}+\frac{1}{2}\sum_{l_1l_2l_3l_4}\rho_{l_3l_1}\bar{v}_{l_1l_2l_3l_4}\rho_{l_4l_2} \tag{5.27}$$

$$=\mathrm{Tr}\,(t\rho)+\frac{1}{2}\mathrm{Tr}_1\mathrm{Tr}_1(\rho\bar{v}\rho), \tag{5.28}$$

where $\mathrm{Tr}_1\mathrm{Tr}_1\ldots$ is an obvious shorthand notation. Eq. (5.28) does not depend on the basis. We can therefore use it to give an expression for the HF-energy in the HF-basis $\{\varphi_k\}$ in which ρ is diagonal with the eigenvalues 0 and 1

$$E^{\mathrm{HF}}=\sum_{i=1}^{A}t_{ii}+\frac{1}{2}\sum_{i,\,j=1}^{A}\bar{v}_{ij,\,ij}. \tag{5.29}$$

5.3.3 Variation of the Energy

To determine the HF-basis, we have to minimize the energy (5.28) for all product wave functions $|\Phi\rangle$ or for all densities ρ with the property $\rho^2=\rho$. Since a small variation $\rho+\delta\rho$ has to be a projector again, we get

$$(\rho+\delta\rho)^2=\rho+\delta\rho$$

or, up to linear terms in $\delta\rho$,

$$\delta\rho=\rho\,\delta\rho+\delta\rho\,\rho.$$

In the HF-basis, where ρ is diagonal, this means that the particle–particle (pp) and hole–hole (hh) matrix elements of $\delta\rho$ have to vanish, that is,

$$\rho\,\delta\rho\,\rho=\sigma\,\delta\rho\,\sigma=0. \tag{5.30}$$

To make sure that we stay within the set of Slater determinants, therefore, we can only allow for variations $\delta\rho_{mi}$ and $\delta\rho_{im}$ of the ph and hp matrix elements of ρ in the HF-basis.

The variation of the energy (5.27) is then given by

$$\delta E=E[\rho+\delta\rho]-E[\rho]=\sum_{kk'}h_{kk'}\delta\rho_{k'k}=\sum_{mi}h_{mi}\delta\rho_{im}+c.c., \tag{5.31}$$

where the Hermitian matrix h is defined as

$$h_{kk'}=\frac{\partial E^{\mathrm{HF}}[\rho]}{\partial\rho_{k'k}}. \tag{5.32}$$

From Eq. (5.27), we obtain

$$h=t+\Gamma \tag{5.33}$$

with the *self-consistent field*

$$\Gamma_{kk'}=\sum_{ll'}\bar{v}_{kl'k'l}\rho_{ll'}. \tag{5.34}$$

Since arbitrary values of $\delta\rho_{mi}$ are allowed, we see from Eq. (5.31), that the condition $\delta E=0$ for the HF-solution means that the ph matrix elements of h have to vanish,

$$h_{mi}=t_{mi}+\sum_{j=1}^{A}\bar{v}_{mjij}=0 \qquad (\text{for } i\leqslant A, m>A), \tag{5.35}$$

in the basis where ρ is diagonal, that is, h does not mix particle and hole states of ρ and Eq. (5.35) is equivalent to

$$[h,\rho]=[t+\Gamma[\rho],\rho]=0. \tag{5.36}$$

This is a nonlinear equation, and not easy to solve. It also states that h and ρ can be diagonalized simultaneously. Since the basis in which ρ is diagonal is determined only up to unitary transformations among the occupied levels or among the empty levels, we use this freedom and require that h shall be diagonal. This defines the *Hartree–Fock basis* and converts (5.36) into an eigenvalue problem.

$$h_{kk'}=t_{kk'}+\sum_{i=1}^{A}\bar{v}_{kik'i}=\epsilon_k\delta_{kk'}. \tag{5.37}$$

Considering the fact that this basis is given by the transformation D (5.18), we obtain the set of *Hartree–Fock equations*

$$\sum_{l'}h_{ll'}D_{l'k}=\sum_{l'}\left(t_{ll'}+\sum_{i=1}^{A}\sum_{pp'}\bar{v}_{lp'l'p}D_{pi}D_{p'i}^*\right)D_{l'k}=\epsilon_kD_{lk}, \tag{5.38}$$

which represent a Hermitian eigenvalue problem. It is nonlinear because the matrix h depends on the density ρ, that is, on the solution of the

problem. The coefficients D_{ik} found by the solution of these equations determine the single-particle wave functions φ_k [Eq. (5.17)].

We have thus derived a single-particle Hamiltonian

$$H^{\mathrm{HF}} = \sum_{kk'} h_{kk'} a_k^+ a_{k'} = \sum_{kk'} (t+\Gamma)_{kk'} a_k^+ a_{k'}$$

$$= \sum_{kk'} \left(t_{kk'} + \sum_{j=1}^{A} \bar{v}_{kjk'j} \right) a_k^+ a_{k'} = \sum_k \epsilon_k a_k^+ a_k \tag{5.39}$$

with the properties required in Section (5.3.1): The Slater determinant $|\mathrm{HF}\rangle$, where the lowest A levels are occupied, corresponds to an energy E which is stationary against small variations of the wave function.

The single-particle Hamiltonian h contains, besides the kinetic energy t, a self-consistent field Γ (Eq. (5.34)), which depends on the density of the nucleus. It is a one-body field and averages over all two-body interactions. This point will become even clearer in the coordinate representation (Sec. 5.3.4). The energy expectation value of the HF-wave function $|\mathrm{HF}\rangle$ is given by Eqs. (5.29) and (5.37):

$$E_0^{\mathrm{HF}} = \sum_{i=1}^{A} \epsilon_i - \frac{1}{2} \sum_{ij=1}^{A} \bar{v}_{ijij}. \tag{5.40}$$

It is therefore not equal to the sum of single-particle energies [compare the discussion of this point in Sec. (2.8.6)].

5.3.4 The Hartree–Fock Equations in Coordinate Space

To give a better interpretation of the structure of Eq. (5.38), we write it down in the coordinate space. Assuming a local two-body potential which does not depend on spin or isospin, that is, a pure Wigner force (see Sec. 4.2), we find instead of Eq. (5.38):

$$-\frac{\hbar^2}{2m}\Delta\varphi_k(\mathbf{r}) + \sum_{j=1}^{A} \int d\mathbf{r}'\, v(\mathbf{r},\mathbf{r}') \cdot \varphi_j^*(\mathbf{r}') \{ \varphi_j(\mathbf{r}')\varphi_k(\mathbf{r}) - \varphi_j(\mathbf{r})\varphi_k(\mathbf{r}') \}$$

$$= \epsilon_k \varphi_k(\mathbf{r}). \tag{5.41}$$

Defining the local Hartree potential

$$\Gamma_H(\mathbf{r}) = \int d\mathbf{r}'\, v(\mathbf{r},\mathbf{r}') \sum_{j=1}^{A} |\varphi_j(\mathbf{r}')|^2 = \int d\mathbf{r}'\, v(\mathbf{r},\mathbf{r}')\rho(\mathbf{r}') \tag{5.42}$$

and the nonlocal or exchange potential

$$\Gamma_{Ex}(\mathbf{r},\mathbf{r}') = -v(\mathbf{r},\mathbf{r}') \sum_{j=1}^{A} \varphi_j^*(\mathbf{r}')\varphi_j(\mathbf{r}) = -v(\mathbf{r},\mathbf{r}')\rho(\mathbf{r},\mathbf{r}'). \tag{5.43}$$

we find that $\varphi_k(\mathbf{r})$ is the solution of a nonlocal Schrödinger equation

$$\left(-\frac{\hbar^2}{2m}\Delta + \Gamma_H(\mathbf{r}) \right) \varphi_k(\mathbf{r}) + \int d\mathbf{r}'\, \Gamma_{Ex}(\mathbf{r},\mathbf{r}')\varphi_k(\mathbf{r}') = \epsilon_k \varphi_k(\mathbf{r}). \tag{5.44}$$

Equations (5.38) and (5.44) contain a self-consistency problem, since the potentials Γ, Γ_H and Γ_{Ex} depend on the local and nonlocal density $\rho(\mathbf{r})$ and $\rho(\mathbf{r},\mathbf{r}')$ of the solution. The equations can be solved by iteration,* starting with a set of phenomenological shell model wave functions to calculate Γ_H and Γ_{Ex} as a first step. Another convenient first guess is the Thomas–Fermi expression for the density (see Sec. 13.2.1). From (5.44) we then get new single-particle wave functions, and so on. This procedure is continued until convergence is obtained, that is, the potentials stay constant in two consecutive steps. In this case, Γ is the self-consistent average potential felt by one particle through interactions with all the other particles.

It should be noticed that, starting with a local two-body interaction, the Fock potential Γ_{Ex} (5.43) is nonlocal. This is caused by the Pauli principle and the antisymmetrization of the matrix element (5.26). A variation of simple product wave functions without antisymmetrization yields only the local Hartree potential. Of course, nonlocal two-body interactions give a nonlocal Hartree term, too. On the other hand, if we use a δ-force, then the Fock term is also local† [see Eq. (5.99)].

Since many of the more formal discussions on HF theory will be taken up in Chapter 7, we will not go into more detail here; we wish only to mention that we will treat there the stability of the Hartree–Fock equations, that is, the question of whether the Hartree–Fock solutions correspond to a minimum or a maximum in the energy. We will also present the so-called gradient method for the solution of the HF equations.

In order to familiarize the reader with the concept of the theory presented in this chapter, we will now present a simple model in which all equations can be solved analytically.

5.4 The Hartree–Fock Method in a Simple Solvable Model

As we will discuss in the last section of this chapter, all realistic HF calculations are very difficult numerical problems. In order to get some feeling about how this method works, we want to apply it to a very simple, exactly solvable model first proposed by Lipkin, Meshkov, and Glick [LMG 65], and which has been widely used to test all kinds of many-body theories (as we shall see later on). Let us imagine two levels in a fixed shell model potential having the same j-value, one situated just below the Fermi level, the other just above. The level below the Fermi level is filled with $2j+1$ nucleons (of one kind, for simplicity). The fixed single-particle potential can be thought of as being produced by an especially stable core formed out of the rest of the nucleons. It is then conceivable to calculate solely that part of the average potential coming from the nucleons in the last j-shell, in a self-consistent manner, such that the mutual influence of the core and the last j-shell is neglected. Of course, the idea that there is only one level with the same j above the Fermi level is very unrealistic and serves only to schematize the problem.

*For numerical methods to solve the HF-equations (5.38) or (5.41), see also [QF 78].

†In this case, however, we also have to take into account spin degrees of freedom, otherwise the exchange term cancels the direct term.

Furthermore, it is assumed that in the basis produced by the fixed potential of the core, the residual interaction of the nucleons in the two shells is of a very special form, being of the monopole–monopole type (see Chap. 4) and having essentially only one matrix element different from zero (a particle–hole matrix element of the RPA type (see Chap. 8)). The *model Hamiltonian* is then of the form

$$H = \epsilon K_0 - \tfrac{1}{2} V (K_+ K_+ + K_- K_-), \tag{5.45}$$

with

$$K_0 = \frac{1}{2} \sum_{m=1}^{\Omega} (c^+_{+m} c_{+m} - c^+_{-m} c_{-m}); \qquad K_+ = \sum_{m=1}^{\Omega} c^+_{+m} c_{-m}; \qquad K_- = (K_+)^+, \tag{5.46}$$

where $\Omega = 2j+1$ and c^+_{+m}, c^+_{-m} create a particle in the upper and lower levels, respectively, and ϵ is the energy difference between the two levels (see Fig. 5.1). The operators K_0, $K_\pm$ fulfill the commutation relations of angular momenta.

$$[K_+, K_-] = 2K_0; \qquad [K_0, K_\pm] = \pm K_\pm. \tag{5.47}$$

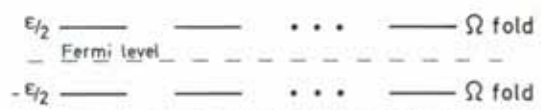

Figure 5.1. Level scheme in the schematic model.

However, it must be emphasized that the operators K_0, $K_\pm$ have nothing to do with rotations in coordinate space. They are often referred to as quasi-spin operators. In order to apply the Hartree–Fock method, we have to construct the general Slater determinant $|\Phi\rangle$. The Hamiltonian (5.45) is invariant under a permutation of the Ω levels below and corresponding levels above the Fermi surface. Therefore, in the following, we restrict ourselves to those solutions of the problem which are completely symmetric under such a permutation. In this case, there is only one possibility of exciting *ph*-pairs, and the most general Slater determinant $|\Phi\rangle$ is characterized by the complex number z:

$$|\Phi\rangle = \mathcal{N} \exp\{zK_+\}|\Phi_0\rangle = \prod_{m=1}^{\Omega} a^+_{0m}|-\rangle, \tag{5.48}$$

with

$$|\Phi_0\rangle = \prod_{m=1}^{\Omega} c^+_{-m}|-\rangle \tag{5.49}$$

and

$$a^+_{0m} = D_{-0} c^+_{-m} + D_{+0} c^+_{+m} \tag{5.50a}$$

$$a^+_{1m} = D_{-1} c^+_{-m} + D_{-1} c^+_{+m}, \tag{5.50b}$$

where we denote the new lower and upper levels by 0 and 1. With the aid of relations (5.50a) and (5.50b), we can express the Hamiltonian (5.45) in the new operators a^+_{0m}, a^+_{1m}. Then, varying $\langle\Phi|H|\Phi\rangle$ with respect to D^*_{-0} and D^*_{+0} yields* the Hartree–Fock equations in the Lipkin model (this is, in fact, just another way

* Under the subsidiary condition that the Ds are normalized [see Eq. (5.96)].

to derive the HF eqs.):

$$\begin{pmatrix} -\frac{1}{2} & -Q \\ -Q^* & \frac{1}{2} \end{pmatrix} \begin{pmatrix} D_{-0} \\ D_{+0} \end{pmatrix} = \frac{e_0}{\epsilon} \begin{pmatrix} D_{-0} \\ D_{+0} \end{pmatrix}, \tag{5.51}$$

where

$$\chi = \frac{V}{\epsilon}(\Omega - 1), \qquad Q = \chi D_{+0} D^*_{-0},$$

which is of the usual nonlinear type and can be solved by iteration. The new single-particle energies are given by

$$e_{0,1} = \mp \epsilon \sqrt{\frac{1}{4} + |Q|^2}$$

$$= \mp \frac{\epsilon}{2} \sqrt{1 + \chi^2 \sin 2\alpha}\,, \tag{5.52}$$

where we put $D_{-0} = \cos\alpha$ and $D_{+0} = \sin\alpha \cdot e^{-i\varphi}$. Solving Eq. (5.51) for D_{-0} and D_{+0} and inserting these into the expression for Q yields, with (5.52) in the case $Q \neq 0$, the following equation for the "deformation" potential Q:

$$1 = \frac{\chi}{2} \frac{1}{\sqrt{\frac{1}{4} + Q^2}}. \tag{5.53}$$

This equation has only real solutions for $\chi > 1$ corresponding to the deformed HF solution given below. (The fact that Eq. (5.53) is very similar to the gap equation of BCS theory [Eq. (6.60)] is not accidental, as will be discussed in more detail in Sec. 11.2 and Appendix F.5.)

In the coordinates α, φ, we then obtain for the ground state energy

$$E_0^{\mathrm{HF}} = -\frac{\epsilon}{2}\Omega\left(\cos 2\alpha + \frac{1}{2}\chi \sin^2 2\alpha \cdot \cos 2\varphi\right) \tag{5.54}$$

and the self-consistency condition

$$\frac{\partial E_0^{\mathrm{HF}}}{\partial \alpha} = 0 = \epsilon\Omega \sin 2\alpha (1 - \chi \cos 2\alpha \cdot \cos 2\varphi), \tag{5.55}$$

$$\frac{\partial E_0^{\mathrm{HF}}}{\partial \varphi} = 0 = \epsilon\Omega \frac{1}{2} \sin 2\alpha \cdot \sin 2\varphi.$$

From Eq. (5.55), we see that we have to distinguish two cases, depending on whether χ is greater than or smaller than one. In the latter case, we have only one solution:

$$\varphi_{\mathrm{HF}} = 0, \qquad \alpha_{\mathrm{HF}} = 0, \qquad \chi < 1. \tag{5.56}$$

For $\chi > 1$ we have a second solution,

$$\varphi_{\mathrm{HF}} = 0, \qquad \chi \cdot \cos 2\alpha_{\mathrm{HF}} = 1, \qquad \chi > 1, \tag{5.57}$$

which turns out to correspond to the minimum in the energy, the first solution having been a maximum. This can be seen from the curvature of the energy at this point:

$$\left.\frac{\partial^2 E_0^{\mathrm{HF}}}{\partial \alpha^2}\right|_{\alpha = \alpha_{\mathrm{HF}}} = 2\epsilon\Omega\left(\chi - \frac{1}{\chi}\right) > 0 \qquad \text{for} \quad \chi > 1. \tag{5.58}$$

In Fig. 5.2 we show a cut ($\varphi = 0$) through the two-dimensional energy surface (5.54) for $\chi \lesssim 1$.

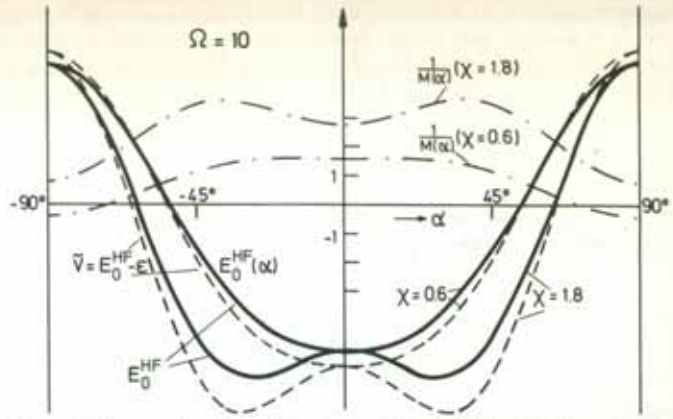

Figure 5.2. E_0^{HF} as a function of α for $\chi \lesssim 1$ (full lines). The other four curves correspond to quantities calculated within the generator coordinate method (see Sec. 10.7.5). (From [Ho 73].)

From the critical value

$$\chi_c = \frac{V_c(\Omega - 1)}{\epsilon} = 1 \tag{5.59}$$

on, the solution at $\alpha = 0$, $\varphi = 0$ becomes unstable and then we have to use a different single-particle basis. In Fig. 5.3, we show for $\chi = 6$ how the iterative solution of equation (5.51) works. Starting with $\alpha_1 = 80°$, $\varphi_1 = 30°$ we find in the subsequent steps (full lines in Fig. 5.3): $\alpha_2 = 32.01°$, $\varphi_2 = -30°$; $\alpha_3 = 39.75°$, $\varphi_3 = 30°$; $\alpha_4 = 40.19°$, $\varphi_4 = -30°$; ... . With respect to α we get a rapid convergence to the solution $\alpha_{HF} = 40.20$ [Eq. (5.57)]; with respect to the variable φ, however, we do not get convergence, the solution jumping back and forth between $+30°$ and

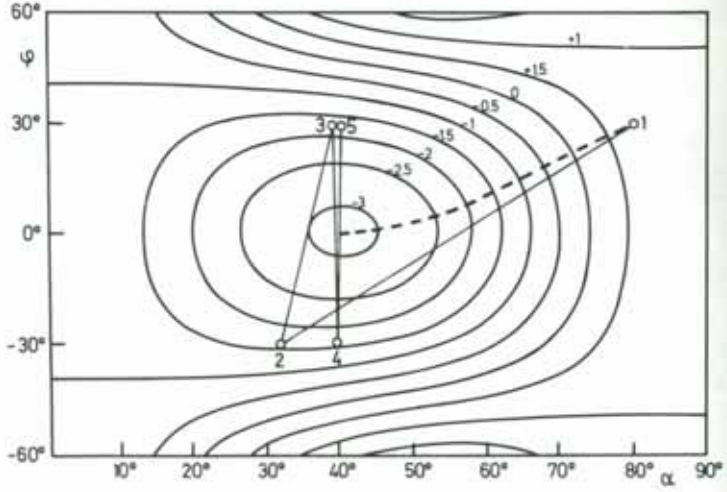

Figure 5.3. Numerical comparison of solution of the HF equations by iterative diagonalization (solid line) and the gradient method (dashed line).

$-30°$. Our model is certainly a very special case in the sense that in the general case the iterative diagonalization converges to a minimum in the energy surface. However, one sometimes also encounters in realistic calculations cases where, within a certain degree of freedom, the solution oscillates back and forth, as in our model. It is therefore preferable to use another method to find the minimum which can, in general, also give faster convergence. This is the gradient method, which will be explained in Section 7.3.3. The way in which the gradient method would converge to the minimum in our model is also indicated in Fig. 5.3 by the dashed line.

5.5 The Hartree–Fock Method and Symmetries

The HF equations (5.38) are nonlinear, which means that the self-consistent potential Γ [Eq. (5.34)] depends not only on the original Hamiltonian, but also on the solution [which is represented by its density matrix ρ (5.21)]. Therefore, this potential does not necessarily show the same symmetries as the Hamiltonian. We then say that the solution has a broken symmetry. The loss of translational invariance is one which we have already encountered, but, as we shall see, there are others—such as, for example, the rotational invariance and particle number conservation (see Chs. 6 and 7). Usually one calls a transition from a symmetry-conserving solution to a symmetry-broken solution a phase transition. The great advantage of this symmetry breaking is the fact that it allows us to take into account, in an approximate way, many-body correlations without losing the simple picture of independent particles. A more detailed discussion of this point will be given in Chapters 7 and 11 and in Appendix F, but let us give here the following argument: Let us suppose that we have a Slater determinant $|\Phi\rangle$ which consists of deformed single-particle wave functions $\{a_k^+\}$. We express them in a spherical basis $\{c_q^+\}$ through the linear transformation

$$a_k^+ = \sum_q D_{qk} c_q^+ . \tag{5.60}$$

We thus obtain a sum of Slater determinants in the spherical basis which differs in the occupation numbers of the level q:

$$a_{i_1}^+ \ldots a_{i_N}^+ |-\rangle = \sum_{q_1 \ldots q_N} d_{q_1 \ldots q_N}^{i_1 \ldots i_N} c_{q_1}^+ \ldots c_{q_N}^+ |-\rangle . \tag{5.61}$$

Here the coefficients $d_{q_1 \ldots q_N}^{i_1 \ldots i_N}$ are the corresponding minors of the matrix D_{qk}. They are of a special form; had we allowed them to be of the most general form, the ansatz (5.61) would contain the exact answer; however, this can never be the case in an independent particle (HF) description. Nevertheless, we see that a Slater determinant in one basis can be a complicated superposition of Slater determinants in another.

Of course, the exact wave function should have the symmetries of the Hamiltonian, and their violation is a matter of convenience in order to maintain the independent particle picture for as long as possible. Neverthe-

less, we should try at a later stage to restore the symmetries. How this can be achieved will be discussed in Chapter 11. However, certain symmetries are conserved in the HF theory, the so-called *self-consistent symmetries*. They depend on the symmetries of the initial density $\rho^{(0)}$ of the iteration, and are based on the property of the HF field Γ viz:

$$S\Gamma[\rho]S^+ = \Gamma[S\rho S^+] \tag{5.62}$$

for any matrix S of a unitary* symmetry operator

$$\hat{S} = \sum_{ll'} S_{ll'} c_l^+ c_{l'} \tag{5.63}$$

which commutes with the many-body Hamiltonian (5.25)

$$[H, \hat{S}] = 0.$$

The property (5.62) is easy to show for the definition (5.34) of Γ:

$$(S\Gamma S^+)_{kk'} = \sum_{ll'qq'pp'} S_{kp} S^*_{k'p'} \langle pq'|V|p'q\rangle_{as} S^*_{lq} S_{l'q'} (S\rho S^+)_{ll'} \tag{5.64}$$

$$= \sum_{ll'} \langle kl'|\hat{S}V\hat{S}^+|p'q\rangle_{as} (S\rho S^+)_{ll'} \tag{5.65}$$

From the invariance of the two-body interaction

$$\hat{S}V\hat{S}^+ = V \tag{5.66}$$

we finally get (5.62) and

$$Sh[\rho]S^+ = h[S\rho S^+]. \tag{5.67}$$

This means that if the initial density $\rho^{(0)}$ has a certain symmetry S of the Hamiltonian H, then the field $h[\rho^{(0)}]$ for the first step of the iteration has it also. The density $\rho^{(1)}$ is found by a diagonalization of $h[\rho^{(1)}]$. It therefore has to have the same symmetry again, and so on. In each step of the iteration, the symmetry S is conserved.

The existence of these self-consistent symmetries has the following implications for practical calculations [Ri 68].

(i) If we expect a certain symmetry for the solution, we can start with an initial density $\rho^{(0)}$ which has this symmetry and therefore reduce the computational effort by working in a basis consisting of eigenstates of this symmetry.

(ii) If we start with a certain symmetry, we will always stay within this symmetry, and the minimum of energy can only be found among the wave functions that have this symmetry. If, for instance, the deepest minimum is a deformed Slater determinant, we will never get to it starting with a spherically symmetric density matrix, though it may happen that small numerical errors cause small deviations, from the initial symmetry, which grow during the iteration.

*The following considerations also apply, with small modifications, for antilinear unitary symmetries [Me 61].

(iii) If we have a solution with a broken symmetry S

$$S\rho S^+ = \rho_1 \neq \rho, \tag{5.68}$$

then from Eq. (5.67) we obtain the HF-Hamiltonian $h[\rho_1]$, which belongs to the transformed density and has the form

$$h[\rho_1] = S^+ h[\rho] S. \tag{5.69}$$

This shows that ρ_1 is also a solution of the HF-equation (5.36)

$$[h[\rho_1], \rho_1] = 0. \tag{5.70}$$

In the case of a continuous symmetry, like that of translation or rotation, we therefore have, to each symmetry-breaking solution, an infinite number of degenerate solutions.

In the next section, we shall see that it is useful to do HF calculations with density dependent two-body forces. In this case, the force does not necessarily exhibit the same symmetry properties as the bare nucleon–nucleon force. Nevertheless, it is clear that the usual properties of HF solutions with respect to symmetry transformations, as previously discussed, are also retained for density dependent forces, if we require that the interaction satisfies the very plausible condition [BG 77]

$$\hat{S}V[\rho]\hat{S}^{-1} = V[S\rho S^{-1}]. \tag{5.71}$$

This means, for instance, that in the case of rotations the two-body interaction in a rotated system is the same as the interaction calculated with a rotated density. This condition is fulfilled for the Skyrme force (4.109).

5.6 Hartree–Fock with Density Dependent Forces

5.6.1 Approach with Microscopic Effective Interactions

5.6.1.1. Brückner–Hartree–Fock. One of the main obstacles to a direct application of the Hartree–Fock method, outlined in the preceding sections, is the fact that most bare nucleon–nucleon forces have an infinite or at least very repulsive core (see Chap. 4). As is easily verified, the two-body matrix elements entering the Hartree–Fock potential (5.34) all become infinite for a hard core potential. The way to solve this problem is to replace the bare interaction in (5.34) by the Brückner G-matrix discussed in Section 4.3.1. This, as a matter of fact, is not only convenient because it solves the hard core problem, but it can also be shown that it is a consistent resummation of certain higher order terms of the full many body problem. Since we do not have the technical many-body apparatus at hand here, we leave the demonstration to Appendix F.4.

The Brückner Hartree–Fock equations are given in analogy to Eq. (5.38) by (see also the review articles on the subject treated in this section by H.

S. Köhler [Kö 75] and W. Wild [Wi 77]):

$$\sum_{l'}\left\{t_{ll'}+\sum_{i=1}^{A}\sum_{pp'}G_{lp'i,l'pi}^{\epsilon_k+\epsilon_i}D_{pi}D_{p'i}^{*}\right\}D_{l'k}=\epsilon_k D_{lk}. \tag{5.72}$$

Here G is the Brückner G-matrix as defined in Eq. (4.39), written in terms of the basis of a definite single-particle potential. The corresponding ground state energies given in the basis, which are solutions of (5.72), are

$$E_0^{\mathrm{BHF}}=\sum_{i=1}^{A}t_{ii}+\frac{1}{2}\sum_{i,j=1}^{A}G_{ij,ij}^{\epsilon_i+\epsilon_j} \tag{5.73}$$

$$=\sum_{i=1}^{A}\epsilon_i-\frac{1}{2}\sum_{i,j=1}^{A}G_{ij,ij}^{\epsilon_i+\epsilon_j}. \tag{5.74}$$

For the ground state energy, it seems that we need only the hole solutions of (5.72). The particle solutions of (5.72), however, enter the Bethe–Goldstone equation (4.39) through the intermediate particle energies ϵ_n, ϵ_m. The Brückner Hartree–Fock solution then consists of a complicated doubly self-consistent procedure. It can be solved, for example, by the following iteration cycle: (i) Calculate the G-matrix via (4.39) in a suitable basis of first choice (e.g., harmonic oscillator); (ii) diagonalize once (5.72) in this basis, which gives a new basis; (iii) calculate in this new basis a new G-matrix; and so on until the convergence is achieved. In this iteration cycle there arises, however, a small ambiguity concerning the energy dependence of the G-matrix in (5.72). Since we do not know the solution a priori, we have to include the energy dependence of $G_{lp'i,l'pi}^{\epsilon_k+\epsilon_i}$ into the iteration cycle. We thus have to take for ϵ_k the energy corresponding to the basis in which we have actually written Eq. (5.72) for each step of the iteration, that is, we can take ϵ_k equal to ϵ_l or $\epsilon_{l'}$. No ambiguity arises for ϵ_i because the D_{pi} are taken to be diagonal in the iteration process. The conventional choice for the BHF potential energy matrix [see Eq. (5.34)] is (see e.g. [Ba 69a]) (of course, the final answer does not depend on any specific convention):

$$\Gamma_{kk'}^{\mathrm{BHF}}=\begin{cases}\dfrac{1}{2}\displaystyle\sum_{i=1}^{A}\left(G_{ki,k'i}^{\epsilon_k+\epsilon_i}+G_{ki,k'i}^{\epsilon_{k'}+\epsilon_i}\right) & \text{for } k,k'\leqslant\epsilon_F,\\ \displaystyle\sum_{i=1}^{A}G_{ki,k'i}^{\epsilon_k+\epsilon_i} & \text{for } \begin{matrix}k\leqslant\epsilon_F\\ k'>\epsilon_F\end{matrix},\\ \displaystyle\sum_{i=1}^{A}G_{ki,k'i}^{\epsilon_{k'}+\epsilon_i} & \text{for } \begin{matrix}k'\leqslant\epsilon_F\\ k>\epsilon_F\end{matrix}.\end{cases} \tag{5.75}$$

The particle–particle matrix elements of Γ^{BHF} are a somewhat controversial matter. For a fixed G-matrix, the particle–particle matrix elements of Γ^{BHF} do not influence the hole solutions of Eq. (5.72); they do influence, however, the particle solutions, and via (4.39) in the doubly self-consistent cycle, indirectly also the hole solutions. We can argue (see discussions in [Ba 69a, Ne 70]) that if the particle–particle matrix elements of Γ^{BHF} are equal to zero,

$$\Gamma_{kk'}^{\mathrm{BHF}}=0, \qquad \text{for} \quad k,k'>\epsilon_F, \tag{5.76}$$

three-body correlations are effectively summed, which were originally not present in our formulation (5.72) and (4.39).

Equation (5.72) is not only different from the ordinary HF equation (5.38) because the two body operator is more complicated, but also because Γ^{BHF} now depends on the energy which we want to calculate. Therefore, it is a nonlinear problem in which the solutions to different energies are, in general, no longer orthogonal (solutions with different angular momentum are, though, still orthogonal for the spherically symmetric case). However, for the iterative solution this is of no special importance.*

As we discussed in Section 4.3.1, the G-matrix sums up two-particle scattering processes in the nuclear medium. One can show that (5.74) contains all contributions of this type to the ground state energy [Ma 67b]. In Table 5.1 we show the results of Brückner–Hartree–Fock calculations for the rms radius and the binding energy per particle in the case of $^{16}_{8}$O, $^{40}_{20}$Ca, and $^{208}_{82}$Pb; the bare force was the Reid soft core potential (4.35).

Table 5.1 Results of BHF calculations with the Reid soft core potential compared with experiment (from [DMS 73])

		BHF	Experiment
$^{16}_{8}$O	$-E_0/A$ (MeV)	3.91	7.98
	rms (fm)	2.50	2.73
$^{40}_{20}$Ca	$-E_0/A$	3.88	8.55
	rms	3.04	3.48
$^{208}_{82}$Pb	$-E_0/A$	2.52	7.87
	rms	4.51	5.50

The results in Table 5.1 are deceiving. The calculations do not give even half the experimental binding energy and the rms radii are about 10–20% off. The bad result for the binding energy is not too surprising, however, in view of the fact that it is a difference between two very large numbers, that for kinetic and that for potential energy.

Nevertheless, in view of the unsatisfying result, one has to envisage taking into account more complicated processes.† Next in the hierarchy are three-particle scattering terms whose importance should depend on the density of the system. As we have seen in Section 4.3, the healing distance, which characterizes the range of the two-particle correlations, is appreciably smaller than the average interparticle distance. Thus the probability

*One should nevertheless make sure that the energy dependence of Γ^{BHF} is not too strong, otherwise the independent particle picture may no longer be valid.

†In this context, see also the hypernetted chain formalism [PB 73, FR 75, 76a, LS 77, Ri 79].

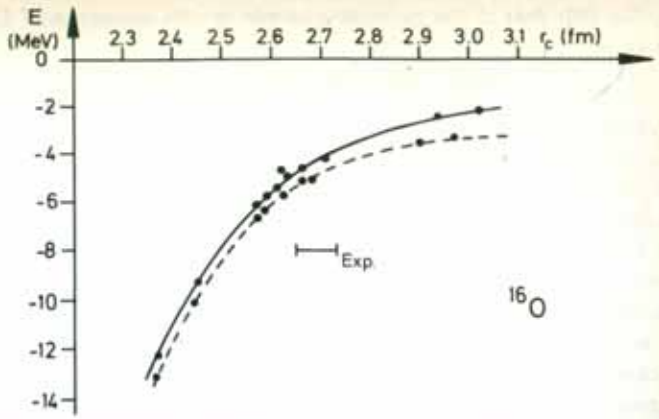

Figure 5.4. Comparison of BHF calculations with different nucleon–nucleon potentials (dots on full line) with calculations including 3-body correlations (broken line) and with experiment (from [Wi 77]).

that three particles are simultaneously within the range of the healing distance should be quite small. This is, however, a rather qualitative argument [Be 71, p. 161]. In fact, Kümmel and co-workers have been able to include three-body correlations in a completely self-consistent manner into the calculations for the gound state energy (see, e.g., [KLZ 75, 78] and further references cited therein). They also give strong arguments that four-body correlations should be negligible. Their results are very interesting in the sense that agreement with experiment is improved, though not very dramatically. For different nucleon–nucleon potentials, the results lie roughly on a smooth line in the $-E_0/A$ versus rms-radius plane, as shown in Fig. 5.4. This line is called the *Coester line*. The results of the Reid soft core potential are located approximately at the point where the curve is closest to the experimental value. In view of the claim [KLZ 75] that the results have converged, the remaining difference must be attributed to relativistic effects or to mesonic degrees of freedom.

5.6.1.2. The Local Density Approximation and the Variational Principle. In Section 4.3 we saw that the influence of a hard core potential on a two-nucleon wave function is effective over relative distances of the two nucleons ranging from 0 to about 1 fm, that is, only over very short distances, compared to the nuclear radius of about 10 fm. This means that the Brückner G-matrix is only different from the bare interaction $v(r)$ within the same range of r-values. However, in general, variations of about 1 fm in the relative variable $r=|\mathbf{r}_1-\mathbf{r}_2|$ of the two nucleons imply a similar variation in the center of mass coordinate. The nuclear density $\rho(\mathbf{R})=\rho(\frac{1}{2}(\mathbf{r}_1+\mathbf{r}_2))$ does not (at least, not in the interior of the nucleus) change very much over such a range of $\mathbf{R}$-values. It therefore seems a reasonable assumption to calculate the nuclear G-matrix at each value of $\rho(\mathbf{R})$ as if the nucleus locally around $\mathbf{R}$ were a piece of nuclear matter* with the density $\rho(\mathbf{R})$. Actually, this reasoning is

* For the theory of nuclear matter, see the reviews [Be 71, Sp 72, JLM 76].

very close to the Thomas–Fermi approximation (see Chap. 13). More explicitly, this means that in the Bethe–Goldstone equation (4.39), which can be written using (5.76) as

$$G^W=\bar{v}+\bar{v}\frac{Q_F}{W-Q_F\Gamma Q_F}G^W, \tag{5.77}$$

we replace the projector Q_F by its expression Q_F^{NM} in nuclear matter of density $\rho(\mathbf{R})$. Since Q_F (4.41) can be expressed by the nonlocal single-particle density $\rho(\mathbf{r},\mathbf{r}')=\sum_{i=1}^{A}\varphi_i(\mathbf{r})\varphi_i^*(\mathbf{r}')$,

$$\langle\mathbf{r}_1\mathbf{r}_2|Q_F|\mathbf{r}_1'\mathbf{r}_2'\rangle=[\delta(\mathbf{r}_1-\mathbf{r}_1')-\rho(\mathbf{r}_1,\mathbf{r}_1')][\delta(\mathbf{r}_2-\mathbf{r}_2')-\rho(\mathbf{r}_2',\mathbf{r}_2')], \tag{5.78}$$

this means that in (5.78) ρ has to be replaced by its nuclear matter value [see Eq. (13.20)]

$$\rho^{\mathrm{NM}}(\mathbf{r},\mathbf{r}')=\frac{3}{k_F(\mathbf{R})s}j_1(k_F(\mathbf{R})s)\rho(\mathbf{R}), \tag{5.79}$$

where $\mathbf{s}=\mathbf{r}-\mathbf{r}'$, $\mathbf{R}=\frac{1}{2}(\mathbf{r}+\mathbf{r}')$, and j_1 is a Bessel function. The $\mathbf{R}$-dependence of (5.79) comes from the fact that we have only treated the nucleus locally around $\mathbf{R}$ as nuclear matter. The relationship between k_F and ρ is given, as usual, by [see Eqs. (5.91), (13.22), and (13.23)]

$$\rho(\mathbf{R})=\frac{2}{3\pi^2}k_F^3(\mathbf{R}). \tag{5.80}$$

Numerical comparison with exact density matrices of finite nuclei have shown [Ne 75] that the nonlocal behavior of ρ is very well approximated by (5.79) in the nuclear interior, and reasonably well represented throughout the nuclear surface. We can therefore conclude that the local density approximation to the G-matrix as described here is quite good.

In principle, the G-matrix thus calculated depends on the three variables $\mathbf{r}=\mathbf{r}_1-\mathbf{r}_2$; $\mathbf{r}'=\mathbf{r}_1'-\mathbf{r}_2'$ and on $\mathbf{R}=\frac{1}{2}(\mathbf{r}_1+\mathbf{r}_2-\mathbf{r}_1'-\mathbf{r}_2')$; $G=G_{\mathbf{r},\mathbf{r}';\mathbf{R}}$. It turns out, however, that the dependence of G on the total momentum $\mathbf{P}$ (the conjugate variable to $\mathbf{R}$) is weak, and we usually put it equal to some average value [BGW 58]:

$$G_{\mathbf{r},\mathbf{r}',\mathbf{P}}\simeq G_{\mathbf{r},\mathbf{r}',\mathbf{P}_{av}}.$$

Negele [Ne 70] further simplifies the expression for G. He replaces the starting energy $W=\epsilon_i+\epsilon_j$ appearing in the G-matrix of Eq. (5.73) by an average value obtained as twice the average hole energy in nuclear matter. In this way, we get rid of the state dependence of the single-particle potential in Eq. (5.72) and the corresponding eigenfunctions form a complete orthonormal set. The next step consists of representing $G_{\mathbf{r},\mathbf{r}'}$ by an effective local operator $v^{\mathrm{eff}}(r)$; (we omit the details of how this is achieved and refer to [Ne 70]*). Furthermore, this effective interaction is renormalized phenomenologically to give the correct volume of nuclear matter [see the Bethe–Weizsäcker formula (1.4)]. In this sense, the "density dependent HF" (DDHF) method of Negele is still a semi-phenomenological procedure.

One further very important ingredient of Negele's theory we have not spoken of until now: In Table 5.1, we have seen that a pure BHF calculation does not give very good results; therefore, something better has to be invented. It turns out that

* Other applications of the 'local' density approximation can be found in [Kō 65, NV 70, CS 72, NR 72].

the intuitively appealing idea to vary the ground state energy (5.73) with G replaced by the local density approximation, with respect to the single-particle wave functions, as in the pure HF case (Eq. 5.29), yields very good results. The Hartree–Fock Hamiltonian becomes, in this case, [see Eq. (5.32)]

$$h_{kk'}^{\mathrm{HF}} = \frac{\delta E[\rho]}{\delta \rho_{k'k}} = t_{kk'} + \sum_{qq'} \bar{v}^{\mathrm{eff}}_{kq'k'q} \rho_{qq'} + \langle \Phi | \frac{\delta v^{\mathrm{eff}}}{\delta \rho_{k'k}} | \Phi \rangle, \tag{5.81}$$

where $|\Phi\rangle$ is a Slater determinant corresponding to the density ρ. For density independent forces, (5.81) just reduces to the usual HF-Hamiltonian. For density dependent forces, however, we have an additional term $\delta v^{\mathrm{eff}}/\delta\rho$, usually called the *rearrangement* or *saturation potential*. It results from the density dependence in $v^{\mathrm{eff}}(\rho)$ and plays a very important role in practical calculations. It has to be emphasized, however, that the variational method just described is not equivalent to the variation of a trial wave function minimizing the expectation value of the original many-body Hamiltonian (5.25). This implies that, at least in principle, the ground state energy calculated with (5.81) could be lower than the exact one. The method is justified in the first place by its success; theoretically, we can say that the additional term $\delta v^{\mathrm{eff}}/\delta\rho$ somehow takes into account three-body scattering terms [Ne 75] ($\delta v^{\mathrm{eff}}/\delta\rho$ has six indices in the shell model space). In Table 5.2, we show the big improvement over BHF which is obtained when using the DDHF method [Ne 70, NV 75].

Table 5.2 Binding energies (in MeV) and rms radii (in fm) with the density dependent Hartree–Fock method (DDHF)

		BHF	DDHF	Exp.
$^{16}_{8}$O	$-E_0/A$	3.91	7.59	7.98
	rms	2.50	2.75	2.73
$^{40}_{20}$Ca	$-E_0/A$	3.88	7.99	8.55
	rms	3.04	3.46	3.48
$^{208}_{82}$Pb	$-E_0/A$	2.52	7.83	7.87
	rms	4.51	5.49	5.50

The solution of the DDHF equations is a very complicated task because of the fact that the exchange term (5.43) implies that an integrodifferential equation must be solved. The fact that the nuclear force is of rather short range can, however, be exploited to simplify the problem so that the nonlocal exchange term can be expanded in powers of the nonlocality around its local value. This procedure leads in a rather natural way to a justification of the very successful HF scheme using the phenomenological Skyrme forces, which we will study next [Ne 75].

5.6.2 Hartree–Fock Calculations with the Skyrme Force

5.6.2.1. General Remarks. There have been many applications of the Hartree–Fock method over the years using different forces. It lies beyond the scope of this book to give a review of them (for a recent review, see [QF 78]). Many of them—in particular, those that do not use density dependent forces—have the shortcoming that they are not able to simultaneously produce the binding energies, the radii, and the proper single-particle spectrum for light and heavy nuclei (see, for instance, [Vo 65, MB 65, BB 67, NDK 68, PS 68, SFW 69, SP 70]).

The use of the Skyrme force (4.104) as a phenomenological interaction in HF calculations has the important merit of being able to very well reproduce binding energies and nuclear radii over the entire periodic table.* Like the Negele force, obtained from the local density approximation, the Skyrme force is density dependent and, as discussed in the last section, cannot simply be used in the variation principle (5.3), which is based on a linear Hamiltonian. Formally, this difficulty can be overcome by considering the Skyrme force as a three-particle force (4.104).

5.6.2.2. The Energy Calculated with the Skyrme Force. We start with the Skyrme force as given in Eq. (4.104) and calculate the expectation value of the corresponding Hamiltonian with respect to a Slater determinant $|\Phi\rangle$ containing the single-particle wave functions $\varphi_i(\mathbf{r}, s, t)$. For the sake of simplicity we require time reversal invariance. This is not essential [Pa 76], but simplifies the equations considerably. Furthermore, we regard only nuclei with $N = Z$ and neglect the Coulomb field.† (For the case $N \neq Z$ with Coulomb interaction, and for more details of the following derivation, see the paper of Vautherin and Brink [VB 72]).

The energy is given by:

$$\begin{aligned} E_0 &= \langle \Phi | T + V^{(2)} + V^{(3)} | \Phi \rangle \\ &= \sum_{i=1}^{A} \langle i | \frac{p_i^2}{2m} | i \rangle + \frac{1}{2} \sum_{i,j=1}^{A} \langle ij | \bar{v}^{(2)} | ij \rangle + \frac{1}{6} \sum_{ijk=1}^{A} \langle ijk | \bar{v}^{(3)} | ijk \rangle. \end{aligned} \tag{5.82}$$

Because of the δ-function character of the Skyrme force (4.104), it is possible to express E by an integral over an energy density $H(\mathbf{r})$

$$E_0 = \int H(\mathbf{r})\, d^3r, \tag{5.83}$$

in which $H(\mathbf{r})$ is an algebraic function of three quantities:

(i) the nucleon density

$$\rho(\mathbf{r}) = \sum_{i,s,t} |\varphi_i(\mathbf{r}, s, t)|^2; \tag{5.84}$$

(ii) the kinetic energy density

$$\tau(\mathbf{r}) = \sum_{i,s,t} |\nabla \varphi_i(\mathbf{r}, s, t)|^2; \tag{5.85}$$

*There is a large number of similar phenomenological density dependent forces with zero range [Mo 70, LV 71, La 72, EM 72, BJS 75, Kö 76, LB 76, TK 76, KKS 77, SM 78] or finite range [Kr 70, ZR 71, RPS 72, LMV 73, Go 75b, RBP 77] which show properties similar to the Skyrme force in HF calculations.

†For the treatment of the Coulomb field, see [Qu 72, GVL 73, Sl 51, Go 52, KS 72, TQ 74].

(iii) the so-called spin orbit densities

$$\mathbf{J}(\mathbf{r}) = (-i)\sum_{iss'} \varphi_i^*(\mathbf{r}, s, t)\left[\nabla\varphi_i(\mathbf{r}, s', t)\times\sigma_{ss'}\right]. \tag{5.86}$$

The sums are taken over all occupied single-particle states. A lengthy but straightforward calculation [VB 72] for $N=Z$ nuclei gives

$$H(\mathbf{r}) = \frac{\hbar^2}{2m}\tau(\mathbf{r}) + \frac{3}{8}t_0\rho^2 + \frac{1}{16}t_3\rho^3 + \frac{1}{16}(3t_1+5t_2)\rho\tau$$
$$+ \frac{1}{64}(9t_1-5t_2)(\nabla\rho)^2 - \frac{3}{4}W_0\rho\nabla\mathbf{J} + \frac{1}{32}(t_1-t_2)\mathbf{J}^2. \tag{5.87}$$

Besides the kinetic energy τ, we also have contributions from the two-body δ-force $\sim\rho^2$ and the three-body δ-force $\sim\rho^3$. The nonlocal p^2-terms give contributions $\sim\rho\tau$ and $\sim\nabla\rho^2$. The latter has its largest contributions at the nuclear surface. The term $\frac{1}{32}(t_1-t_2)\mathbf{J}^2$ is usually neglected because it is difficult to handle in deformed nuclei and its contribution to the spin orbit part does not reproduce the experimental spin-orbit splitting.

We could also have derived the three-body term $\sim\rho^3$ from a density dependent two-body interaction

$$\frac{1}{16}t_3\rho^3 = \frac{1}{2}\sum_{i,j<A}\langle ij|\frac{1}{6}t_3\delta(\mathbf{r}_1-\mathbf{r}_2)\rho(r_1)(1+P^\sigma)|ij-ji\rangle. \tag{5.88}$$

In Section (5.6.1.1) we saw that when using density dependent interactions we have first to calculate the energy and only afterwards vary with respect to the density. In that sense, the three-body contact force of Skyrme is equivalent to the two-body interaction (5.88). This equivalence, however, is only valid in even–even nuclei with time reversal symmetry.

Using (5.87), we are able to calculate the binding energy per particle in nuclear matter without Coulomb interaction. In this case we have translational invariance and the single-particle wave functions are given by plane waves normalized to a δ-function

$$\varphi_{\mathbf{k}st} = \frac{1}{(2\pi)^{3/2}}e^{i\mathbf{k}\mathbf{r}}\chi_s^{1/2}\chi_t^{1/2} \tag{5.89}$$

and in Eqs. (5.84)–(5.86) we have to replace

$$\sum_{i=1}^{A}\ldots \quad \text{by} \quad \int_{|k|<k_F} d^3k\ldots, \tag{5.90}$$

where all the levels with $|k|$ smaller than the Fermi momentum k_F are occupied. From (5.84), we get the usual relation between ρ and k_F [see also Eqs. (13.22) and (13.23)]

$$\rho = \frac{4}{(2\pi)^3}\frac{4\pi}{3}k_F^3 = \frac{2}{3\pi^2}k_F^3 \tag{5.91}$$

and from (5.85),

$$\tau = \frac{2}{3\pi^2}\frac{3}{5}k_F^5 = \frac{3}{5}\rho k_F^2 = \frac{3}{5}\left(\frac{3\pi^2}{2}\right)^{2/3}\rho^{5/3}. \tag{5.92}$$

Because of translational invariance, we have $\nabla\rho=\nabla\mathbf{J}=0$ and obtain for the binding energy per particle in nuclear matter

$$\frac{E_0}{A} = \frac{H}{\rho} = \frac{3}{5}\frac{\hbar^2}{2m}k_F^2 + \frac{3}{8}t_0\rho + \frac{1}{16}t_3\rho^2 + \frac{3}{80}(3t_1+5t_2)\rho k_F^2. \tag{5.93}$$

The saturation property means that there is an equilibrium density ρ_0 for which

$$\frac{\partial}{\partial\rho}\left(\frac{E_0}{A}\right)\Big|_{\rho=\rho_0} = 0 = \frac{2}{5}\frac{\hbar^2}{2m}k_F^2\rho^{-1} + \frac{3}{8}t_0 + \frac{1}{8}t_3\rho + \frac{1}{16}(3t_1+5t_2)k_F^2. \tag{5.94}$$

The incompressibility of nuclear matter K is defined as the curvature of the binding energy E_0/A with respect to the Fermi momentum k_F at this minimum:

$$K = k_F^2\frac{\partial^2(E_0/A)}{\partial k_F^2}\Big|_{\rho=\rho_0} = \frac{6}{5}\frac{\hbar^2}{2m}k_F^2 + \frac{9}{4}t_0\rho + \frac{15}{8}t_3\rho^2 + \frac{3}{4}(3t_1+5t_2)\rho k_F^2. \tag{5.95}$$

Equations (5.93)–(5.95) allow us to express the two constants t_0 and t_3 and the combination $3t_1+5t_2$ by the nuclear matter constants E_0/A, ρ_0, and K. From Eq. (5.95), we see that t_3 is strongly correlated with the incompressibility K.* From the Bethe–Weizsäcker Formula (1.4), we know that the value of $E_0/A = a_V = 15.9$ MeV. Less well determined is the equilibrium density $\rho_0 = 3/4\pi r_0^3 \simeq 0.14$ fm^{-3}. Therefore, it is not possible to adjust the force parameters of a phenomenological force to nuclear matter data alone. We first have to carry out the calculation for finite nuclei.

5.6.2.3. The Derivation of the Density Dependent Hartree–Fock Equations. According to the concept of Section 5.6.1, we have to vary the functional $E_0[\rho]$ with respect to the density in order to gain the Hartree–Fock Hamiltonian. Unfortunately, (5.95) does not have the form of a functional of ρ. It also depends on τ and $\mathbf{J}$, and it is very hard to express τ and $\mathbf{J}$ in terms of ρ. In our case, however, this is no real problem, since the HF-density is uniquely defined by the single-particle wave functions φ_k (5.84), and we can also carry out the variation with respect to φ_k under the condition that they are normalized to unity. We use Lagrange multipliers ϵ_k for these subsidiary conditions and find

$$\frac{\delta}{\delta\varphi_k}\left(E_0[\rho] - \sum_l \epsilon_l\int d^3r|\varphi_l(\mathbf{r})|^2\right) = 0. \tag{5.96}$$

The variation of the energy (5.83), after integrating by parts, can be written

$$\delta E = \int d^3r\left[\frac{\hbar^2}{2m^*(\mathbf{r})}\delta\tau(\mathbf{r}) + U(\mathbf{r})\delta\rho(\mathbf{r}) + \mathbf{W}(\mathbf{r})\delta\mathbf{J}(\mathbf{r})\right] \tag{5.97}$$

*Nuclear matter calculations give values between 150 and 250 MeV and, from recent measurements of the breathing mode in ^{208}Pb, we deduce the value $K\simeq 200$ MeV for the incompressibility of heavy, finite nuclei.

with an effective mass

$$m^*(\mathbf{r}) = m\left(1 + \frac{2m}{\hbar^2}\frac{1}{16}(3t_1 + 5t_2)\rho\right)^{-1}, \tag{5.98}$$

an average field

$$U(\mathbf{r}) = \frac{3}{4}t_0\rho + \frac{3}{16}t_3\rho^2 + \frac{1}{16}(3t_1 + 5t_2)\tau + \frac{1}{32}(5t_2 - 9t_1)\nabla^2\rho - \frac{3}{4}W_0\nabla\mathbf{J}, \tag{5.99}$$

and a one-body spin-orbit potential [we neglect the term $\frac{1}{32}(t_1 - t_2)\mathbf{J}^2$]

$$\mathbf{W}(\mathbf{r}) = \frac{3}{4}W_0\nabla\rho. \tag{5.100}$$

We now have to insert into Eq. (5.96) the variations $\delta\tau$, $\delta\rho$, and $\delta\mathbf{J}$ with respect to φ_k. From definitions (5.84)–(5.86) we get

$$\delta E = 2\sum_{i=1}^{A}\int d^3r\,\delta\varphi_i^*\left\{-\nabla\frac{\hbar^2}{2m_\tau^*}\nabla + U + \mathbf{W}\frac{1}{i}(\nabla\times\boldsigma)\right\}\varphi_i \tag{5.101}$$

and, using Eq. (5.96), we finally find the HF-equation in coordinate space viz:

$$\left\{-\nabla\frac{\hbar^2}{2m^*(\mathbf{r})}\nabla + U(\mathbf{r}) + \mathbf{W}\frac{1}{i}(\nabla\times\boldsigma)\right\}\varphi_i(\mathbf{r}) = \epsilon_i\varphi_i(\mathbf{r}). \tag{5.102}$$

The exchange term in the HF-equation (5.44) is now local and is included in the potential $U(\mathbf{r})$, so that (5.102) is a pure differential equation. The nonlocality is expressed only in the $\mathbf{r}$-dependence of the effective mass $m^*(\mathbf{r})$. In the case of spherical symmetry, we end up with a one-dimensional differential equation of second order in the radial coordinate r. In particular, the spin-orbit term (5.100) takes the form

$$\frac{3}{2}W_0\left(\frac{1}{r}\frac{\partial}{\partial r}\rho\right)\mathbf{ls} \tag{5.103}$$

and, as we have already discussed in Section 2.4, this is concentrated mainly at the nuclear surface.

5.6.2.4. Discussion of the Results. Vautherin and Brink [VB 72] originally solved the HF equation (5.102) for the spherical closed shell nuclei ^{16}O, ^{40}Ca, ^{48}Ca, ^{90}Zr, and ^{208}Pb, and were able to adjust the six parameters t_0, t_1, t_2, t_3, W_0, and x_0 so as to reproduce the radii and binding energies of these nuclei. They presented two sets of force constants (Skyrme I and II) which gave a good description of these closed shell nuclei. Both have large values of t_3, which means a strong density dependence. This is a very crucial point, because for density dependent forces the binding energy E_0^{HF} is given by (5.28) and (5.81)

$$E_0^{\mathrm{HF}} = \mathrm{Tr}\,t\rho + \frac{1}{2}\mathrm{Tr}_1\mathrm{Tr}_1\rho\bar{v}\rho = \frac{1}{2}\mathrm{Tr}\{(t+\epsilon)\rho\} - \frac{1}{2}\mathrm{Tr}\left(\langle\mathrm{HF}|\frac{\delta V}{\delta\rho}|\mathrm{HF}\rangle\rho\right) \tag{5.104}$$

which, in the case of the Skyrme force (5.88), is

$$E_0^{\mathrm{HF}} = \frac{1}{2}\sum_{i=1}^{A}(t_{ii} + \epsilon_i) - \frac{1}{32}t_3\int d^3r\,\rho^3. \tag{5.105}$$

The last term in Eqs. (5.104) and (5.105) is, as discussed in Section 5.6.1.2, called the rearrangement term. For a density independent force it vanishes, and it is not possible to simultaneously reproduce the binding energy E_0, the radii, and the experimental single-particle energies ϵ_i of a nucleus, as the last two quantities already determine (more or less) the first part of Eq. (5.105). Only the rearrangement term makes it possible to reproduce the binding energy so well. This term is always negative because of the replusion of the nuclear forces at short distances or large densities.

Later, the density dependence in many other spherical nuclei was investigated [BFG 75] and other sets of force parameters were determined (Skyrme III–VI). They differ in their density dependence, and it turns out that t_3 is not determined by the radii and binding energies alone. With rather different values of t_3, we can, in fact, reproduce these values. However, the single-particle energies ϵ_i do depend dramatically on t_3. Skyrme III [Eq. (4.108)] gives reasonable values for all these quantities.

Table 5.3 lists binding energies and root mean square radii r_c for several spherical closed-shell nuclei as calculated by the most sophisticated

Table 5.3 Experimental and calculated root mean square radii (in fm) and binding energies (in MeV) per nucleon

		Experiment	Negele [Ne 70]	Campi and Sprung [CS 72]	Nemeth et al. [NMH 73]	Skyrme III [BFG 75]
^{16}O	E	−7.98	−6.75	−7.68	−7.98	−7.96
	r_c	2.73	2.80	2.75	2.77	2.69
^{40}Ca	E	−8.55	−7.49	−8.33	−8.47	−8.54
	r_c	3.49	3.49	3.49	3.40	3.48
^{48}Ca	E	−8.67	−7.48	−8.40	−8.55	−8.71
	r_c	3.48	3.52	3.51	3.44	3.53
^{90}Zr	E	−8.71	−7.85	−8.63	−8.70	−8.71
	r_c	4.23	4.25	4.27	4.13	4.32
^{208}Pb	E	−7.87	−7.53	−7.87	−7.87	−7.87
	r_c	5.50	5.44	5.45	5.22	5.57

Hartree–Fock calculations with effective interactions derived from the bare nucleon–nucleon force and also with Skyrme III.

One has also calculated angular distributions for electron scattering and found good agreement with the experimental data. This shows that the calculations produce the proper charge distributions. For example, in Fig. 5.5(a) we show the charge distribution of ^{208}Pb compared with a phenomenological curve determined from electron scattering. Figure 5.5(b) gives the corresponding average potential U_p and U_n for protons and neutrons and the effective mass m^*/m. The HF-charge density is not completely constant in the nuclear interior, but shows some oscillations which have their origin in the shell effects. They are smaller than the oscillations that would be obtained for a shell model charge density in a phenomenological Wood–Saxon potential, but are still larger than the experimentally observed wiggles. The corresponding self-consistent fields also show deviations from a Wood–Saxon shape. For lighter nuclei, they are more important. Figure 5.5(b) also gives the ratio m^*/m, which measures the nonlocality of the Skyrme potential. It is given by the parameter combination $3t_1+5t_2$ [see Eq. (5.98)]. For Skyrme II, the nonlocality is well pronounced.

The effective mass has a strong influence on the single particle energies ϵ_i. If we assume the single-particle wave functions of the A and the $A-1$ system to be identical, that is, if we neglect the polarization of the core by the hole in the level i, then we get for the energy difference

$$E(A)-E_i(A-1)=t_{ii}+\sum_{j<A}\bar{v}^{(2)}_{ij,ij}+\frac{1}{2}\sum_{jk<A}\bar{v}^{(3)}_{ijk,ijk}. \qquad (5.106)$$

The evaluation of the right-hand side shows [VB 72] that (5.106) is exactly the single-particle energy ϵ_i, the eigenvalue of the HF-Hamiltonian. In Fig. 5.6, therefore, we compare the experimental single-particle levels in ^{208}Pb with the calculated single-particle energies ϵ_i. Essentially, we obtain the

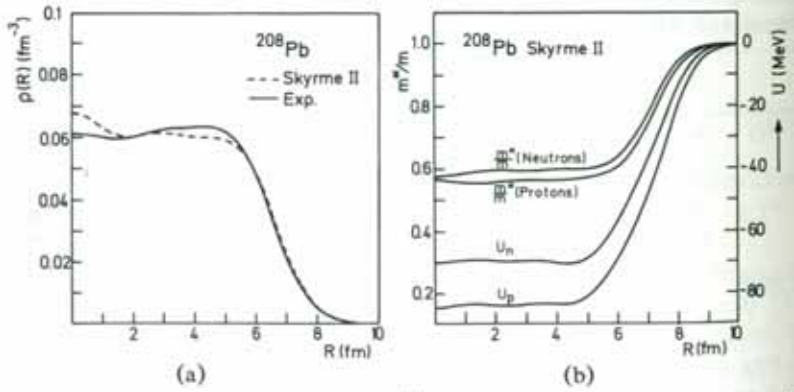

Figure 5.5. Hartree–Fock results for ^{208}Pb with the interaction Skyrme II. (a) Charge distribution. (b) Effective mass m^*/m and HF-potential $U(r)$ (the proton single-particle potential does not include the Coulomb term). (From [VB 72].)

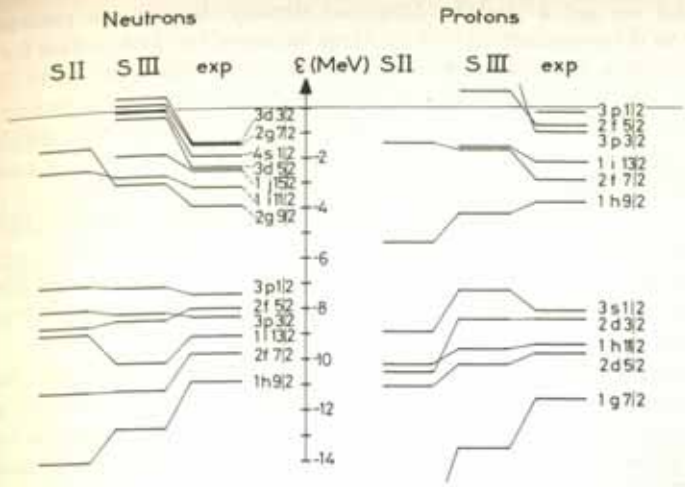

Figure 5.6. Experimental and calculated single-particle energies in the lead region. The calculated values were obtained with two different versions of the Skyrme force. With increasing effective mass, we recognize a compression of the spectrum ($m^*/m \simeq 0.6$ for SII and $\simeq 0.75$ for SIII). (From [BFG 75].)

correct ordering of the single-particle levels, although quantitatively the different sets of parameters show rather different spectra. However, it should be emphasized that we cannot expect a priori complete agreement, because polarization effects play a certain role that have not yet been taken into account [RW 73].

5.7 Concluding Remarks

Summarizing the results of this chapter, we can say that there is a microscopic foundation of the spherical shell model as discussed in Chapter 2. The Hartree–Fock method provides a tool for calculating the average potential from an effective nucleon interaction. It becomes very important to use density dependent effective interactions to get quantitative agreement. In this case, we are able to reproduce the ground state properties of spherical nuclei very well. In most cases, the calculated single-particle levels show the correct ordering; however, they deviate in detail from the experimental single-particle excitations of neighboring odd mass nuclei.

So far we discussed only applications of the HF method to nuclei with closed shells. In fact, these are the only cases where the self-consistent field can have spherical symmetry. As soon as one or several particles are put in an unfilled j-shell (*open shell* HF [Ke 63]) we have to decide which one of the orginally degenerate magnetic quantum numbers m needs to be occu-

pied and we get a slightly deformed density distribution (oblate with respect to the quantization axis for large values of $|m|$ and prolate for small values of $|m|$). This deformed density produces a deformed mean field in the next step of the iteration, which also changes the single-particle wave functions in the core. In this way, we take into account the correlations caused by the interaction of the external particle with the other nucleons. We call this effect a *polarization* of the core.

As long as we have only one or a few external particles, we can also treat this interaction in the spherical basis by a shell model configuration mixing calculation allowing for *ph excitations*. In this picture, the valence nucleons excite virtual vibrations in the core and we treat the polarization effects by a particle vibrational coupling technique (see Sec. 9.3).

In many practical applications, this effect has been taken into account only in an averaged way by distributing the external particle over all the m-quantum numbers of the next higher j-shell with equal probability $v_m^2 = 1/(2j+1)$. The wave function is then, in a sense, a HFB state (see Chap. 7) with a spherical density distribution.

In principle, the mean field approach is only justified if there is a well pronounced energy gap between the highest occupied level and the first empty level. If that is not the case (subshell closures), it is easy to excite virtual *ph*-pairs, and we can expect a more complicated wave function than a Slater determinant [see Eq. (2.36)]. From these arguments, we expect that the HF method yields a better approximation to the exact ground state for magic nuclei than for nuclei with a few particles away from the closed shell configuration. These nuclei show a small deformation in HF and have many nearly degenerate levels in the vicinity of the Fermi surface.

We call such nuclei transitional nuclei, and in the Chapters 9 and 10 we will discuss some methods for investigating their structure. For nuclei far from closed magic configurations, however, the correlation among the quasi-particles becomes so strong that they can again be treated in an extended mean field approach. Depending on the kind of correlations, we have to use a *deformed* HF *potential*—which is again a very good approximation for cases where new magic numbers develop in the deformed region (see Fig. 2.25). We will discuss these methods together with the nuclear pairing phenomenon in more detail in Chapters 6 and 7, and we will see then that nuclear deformations with density dependent forces can be explained rather nicely.

CHAPTER 6

Pairing Correlations and Superfluid Nuclei*

6.1 Introduction and Experimental Survey

In Chapter 5 we looked for a wave function describing the ground state of the nucleus. Restricting ourselves to a product ansatz and minimizing the total energy of the system has led us to the Hartree–Fock method. As we have seen, the solution of the corresponding equation yields a transformation from a given single-particle basis to a new, better one. The variational principle is equivalent to the requirement that there are no matrix elements between the ground state and the most simple excitations, the particle-hole excitations. Therefore, the Hartree–Fock method partially takes into account the particle-hole part of the interaction, that is, the long-range part of the force, as we have seen in Chapter 4. Before we turn to the excitations caused by these correlations, we want to consider the short-range part of the force which causes particle–particle correlations (cf. Chap. 4). It will turn out that this can be done formally very similarly to the particle-hole part of the force by introducing generalized product wave functions consisting of "quasi-particles."

Of course we usually have to take into account both correlations at the same time. This will be done in the next chapter within the framework of Hartree–Fock–Bogoliubov theory. Here we restrict ourselves to pure

*We are glad to see that the original version of this chapter (in the book by Baumgärtner and Schuck) [BS 68a] has partly been adopted by other authors [EG 70]. We have also incorporated some of their changes.